INFORMATION TO USERS

This manuscript has been reproduced from the microfilm master. UMI films the text directly from the original or copy submitted. Thus, some thesis and dissertation copies are in typewriter face, while others may be from any type of computer printer.

The quality of this reproduction is dependent upon the quality of the copy submitted. Broken or indistinct print, colored or poor quality illustrations and photographs, print bleedthrough, substandard margins, and improper alignment can adversely affect reproduction.

In the unlikely event that the author did not send UMI a complete manuscript and there are missing pages, these will be noted. Also, if unauthorized copyright material had to be removed, a note will indicate the deletion.

Oversize materials (e.g., maps, drawings, charts) are reproduced by sectioning the original, beginning at the upper left-hand corner and continuing from left to right in equal sections with small overlaps.

Photographs included in the original manuscript have been reproduced xerographically in this copy. Higher quality 6" x 9" black and white photographic prints are available for any photographs or illustrations appearing in this copy for an additional charge. Contact UMI directly to order.

ProQuest Information and Learning
300 North Zeeb Road, Ann Arbor, MI 48106-1346 USA
800-521-0600

Intraseasonal and Interannual Variability of Sea Ice in the Gulf of St. Lawrence

by

Yongxiang Li

A thesis submitted to the
Faculty of Graduate Studies and Research
in partial fulfilment of the requirements for the degree of

Doctor of Philosophy

Department of Atmospheric and Oceanic Sciences
McGill University
Montreal, Quebec, Canada

Abstract

Intraseasonal and interannual variability of sea-ice cover (SIC) in the Gulf of St. Lawrence, including the time of first ice presence (TFIP), time of last ice presence (TLIP), and sea-ice duration (SID), were investigated, using weekly sea ice observations from 1963-1996. For the intraseasonal variations of sea ice, it was found that SIC in different sub-regions displays contrasting features. The largest intraseasonal variations of SIC occur in the Strait of Belle Isle region and in the southwestern Gulf, where the mean SIC is largest and SID is longest. For the interannual variability of sea ice, the largest variability of SIC occurs in the area off mid-Newfoundland, where the mean SIC is small. For the TFIP and TLIP, the largest interannual variability occurs in the area off western Newfoundland and along coasts in the northeast sector of the Gulf, respectively. In addition, sea ice appeared earlier in the coastal regions and disappeared later over the entire Gulf in severe ice years; while sea ice appeared later in the central and eastern Gulf and disappeared earlier over the entire Gulf in light ice years.

Several of the forcing factors influencing sea ice variability in the Gulf of St. Lawrence were examined and mechanisms controlling this variability were discussed. It was found that surface air temperature (SAT), the eastward wind component (u-wind), sea surface temperature (SST), sea surface salinity (SSS), mixed layer depth (MLD), total river runoff, the ocean circulation pattern, and sea-ice advection from the Labrador Sea, all play important roles in explaining sea ice variability in the Gulf. However, the relative contributions of these factors to the observed sea ice variability

differ in different subregions. Quantitative relationships between sea ice variability and various forcing factors were investigated using statistical analysis and a simplified Hibler's sea-ice model. Both approaches indicated that the December-April averaged SAT, u-wind, and November SST all contribute to the variability of December-June SIC in the Gulf, with SAT playing the most important role. The analysis also indicated that the dependence of SIC on various forcing factors varies with geographical location. For example, SAT influences sea ice variability mainly in the central Gulf, while the u-wind component effects SIC mainly in the eastern Gulf. In addition, statistical analyses also suggest that SSS values present in the previous November play an important role in determining SIC variability. The linear regression between SIC and three independent variables: December-April SAT, November SST and SSS, accounts for 81% of the total SIC variance.

The statistical analysis and model study also indicated that December SAT, u-wind, November SST, and MLD control the time of first ice presence, with SAT and SST playing the dominant role. The linear regression between TFIP and three independent variables (u-wind, SST, and SSS) accounts for 76% of the total TFIP variance. For TLIP, both SAT and u-wind play an important role.

Résumé

La variabilité saisonnière et annuelle de la couverture de glace dans le Golfe du St-Laurent, comprenant le temps de première glace (TPG), le temps de dernière glace (TDG) et la durée de la période de la couverture de glace (PCG) est investiguée en utilisant des observations hebdomadaires de glace de 1963 à 1996. Pour les variations saisonnière de glace, nous trouvons que la couverture de glace dans des sous-régions du golfe démontrent des caractéristiques différentes. Les plus grandes variations saisonnières de la couverture sont observées dans la région du Détroit de Belle Isle et dans le sud-ouest du golfe, où la couverture de glace est la plus importante et le TPG le plus long. Pour la variabilité annuelle de glace, la plus grande variation de couverture de glace a eu lieu dans les secteurs longeant le centre de Terre-Neuve, où la couverture de glace est, en moyenne, petite. Pour le TPG et le TDG, la plus grande variabilité annuelle est retrouvée proche de Terre-Neuve et sur les côtes nord-est du golfe, respectivement. De plus, la glace durant les années rigoureuses apparaît plus tôt dans les régions côtières et disparaît plus tard dans le golfe en entier alors que pour les années avec peu de glace, celle-ci apparaît plus tard dans les régions centrales et orientales du golfe et disparaît plus tôt dans le golfe en entier.

Quelques-uns des facteurs influençant la variabilité de la couverture de glace dans le Golfe du St-Laurent sont examinés et les mécanismes contrôlant cette variabilité sont discutés. Nous trouvons que la température près de la surface (TPS), la composante

en direction est du vent, la température et la salinité de la surface de la mer (TSM et SSM, respectivement), la profondeur de la couche mixte (PCM), l'écoûlement total des rivières, la circulation océanique, et l'advection de glace de la Mer du Labrador, jouent tous des rôles importants dans la variabilité de la couverture de glace dans le golfe. Toutefois, les contributions relatives de chacun de ses facteurs dans la variabilité de la couverture de glace diffèrent dans certaines sous-régions. Des relations quantitatives entre la variabilité de la couverture de glace et les facteurs forçant cette variabilité sont investigués en utlitisant une analyse statisque et un modèle numérique simplifié de glace de Hibler. Les deux indiquent que les moyennes de décembre à avril de la TPS, de la composante en direction est du vent, et de la TSM en novembre contribuent tous à la variabilité de la couverture de glace entre les mois de décembre et juin dans le golfe, avec la TSM jouant le rôle le plus important. Les résultats indiquent aussi que les divers facteurs forçant cette variabilité ont une importance différente en termes de géographie sur la couverture de glace, avec la TPS influençant la variabilité de glace principalement dans le centre du golfe and la composante est du vent dans l'est du golfe. De plus, un analyse statistique suggère que la SSM présente dans le mois de novembre précédant joue un rôle important dans la variabilité de la couverture de glace. Une régression linéaire entre la couverture de glace et les trois variables indépendantes que sont la TPS de décembre à avril, la TSM et SSM de novembre explique 81% de la variabilité totale de la couverture de glace.

L'analyse statistique et la modélisation numérique indiquent aussi que la TPS de décembre, la composant est du vent, la TSM de novembre et la PCM contrôlent le temps de première présence dans le golfe, avec la TPS et la TSM étant les plus importants. Une régression linéaire entre le TPG et trois variables indépendantes que sont la composante est du vent, la TSM et la SSM, expliquent 76% de la variance totale du TPG. Pour le TDG, tous deux la TPS et la composante est du vent jouent un rôle significatif.

Table of Contents

Lists of Figures

Lists of Tables

Statement of Originality

To the author's knowledge, the original contributions to our understanding about sea ice variability in the Gulf of St. Lawrence in this thesis are as follows:

1. Spatial variations of intraseasonal and interannual variability of sea ice in the Gulf.

In the present study, I not only examined temporal variability of sea ice in the Gulf, as most of previous studies did, but also emphasized spatial variations of the temporal variability. For the intraseasonal variations of sea-ice cover, I found that sea-ice cover over different sub-regions displays contrasting features. The largest intraseasonal variations of sea-ice cover occur in the Strait of Belle Isle region and southwestern Gulf, where the mean sea-ice cover is largest and sea-ice duration is longest. For the interannual changes of sea-ice cover, I found the largest variability occurs in the area off mid-Newfoundland. I also found that the largest variability for the time of first ice presence is located in the area off Newfoundland, while for the time of last ice presence, it is along the northeast coast.

2. The characteristics of sea ice in the extreme ice years.

I examined the sea ice conditions for the extreme years (i.e., the years with severe ice or light ice), a topic not studied before, and found that sea ice in severe ice years appeared 10 days earlier in the coastal regions and disappeared 10 days later over the entire Gulf. Sea-ice duration and sea-ice cover were longer and larger than normal

over the entire Gulf, respectively, with more than 30 days longer for SID and 1/10 larger for mean SIC over December-June in the area off mid-Newfoundland. In contrast, sea ice in light ice years appeared more than 10 days later in the central and eastern Gulf and disappeared more than 30 days earlier in the eastern Gulf. Sea-ice duration and sea-ice cover were shorter and smaller than normal over the entire Gulf, respectively, with only 10 days duration and less than 1/10 in sea-ice cover in the area off mid-Newfoundland. In regard to forcing factors, surface air temperature (SAT) is lower (higher), eastward wind component (u-wind) is stronger (weaker), and both sea surface temperature (SST) and salinity (SSS) in previous November are lower (higher) for severe (light) ice years.

3. Systematic studies on the mechanisms of controlling sea ice variability in the Gulf.

Although some previous studies have been conducted to study the mechanisms of controlling sea ice variability in the Gulf, only one or two forcing factors at one or two meteorological stations were used. In this study, I examined a wide range of factors, with better spatial resolution. Some of these were distributed on more than 10 grid points and used as forcing fields. Using modern statistical methods and a model study, I investigated the relationship between sea ice variability and these forcing fields. I found that all of the forcing factors considered in this study play important roles in explaining sea ice variability. However, the different forcing factors vary in their geographic importance on sea ice variability. For example, SAT influences sea ice variability mainly in the central Gulf and u-wind mainly in the

eastern Gulf. In addition, I discussed the important physical processes controlling sea ice variability in the Gulf.

4. Systematic studies on interannual variability of the time of first ice presence (TFIP), of last ice presence (TLIP), and sea ice duration (SID) on Gulf-wide scale and the causal mechanisms.

Although Drinkwater et al. (1999) examined interannual variability of the TFIP, TLIP, and SID, they did not investigate the mechanisms to explain their variability. Drinkwater and Bugden (1994) considered interannual variability of TFIP, TLIP, and SID and their relation to surface air temperature and winds, but only in the regions seaward of Cabot Strait. In this thesis, I studied the interannual variability of TFIP, TLIP, and SID using the statistical analysis and a model study. The results indicated that both TFIP and TLIP display interannual-scale variability, with the largest variability in the area off Newfoundland for TFIP and along the northeast coast areas for TLIP, while SID has similar characteristics of variability with SIC (sea-ice cover). The results also indicated that December SAT, u-wind, November SST/SSS, and MLD (mixed layer depth) control the time of first ice presence. For TLIP, both SAT and u-wind play an important role.

5. The relative importance of the forcing factors on sea ice variability.

In this thesis, I also studied the relative importance of the forcing factors on sea ice variability. The major results are as follows. For mean SIC in December-June, SAT in December-April plays a dominant role. The u-wind in December-April and SST in

previous November also play an important role in explaining sea ice variability in the Gulf. For the TFIP, both SAT in December and SST in November contribute the most. While for the TLIP, both SAT and u-wind play an important role. In addition, this study also indicated that the v-wind component is unimportant in explaining sea ice variability in the Gulf.

Acknowledgements

I sincerely thank my thesis supervisor, Prof. R. Grant Ingram, for his continuous support and patient guidance for this thesis research. Throughout this thesis research, he has taught me a great deal about physical oceanography and climate variability. His constant encouragement and timely response to my questions have made my stay at McGill University very enjoyable. Special thanks go to Dr. Ken F. Drinkwater, for his great assistance, insight and helpful criticism. He spent considerable time with me discussing my research and frequently gave me timely guidance. He also provided the sea ice and hydrographic observations in the Gulf of St. Lawrence and river runoff data from the St. Lawrence River system. I also sincerely appreciate the encouragement and helpful comments from Prof. Lawrence A. Mysak. I would like to acknowledge the financial support provided by the Natural Sciences and Engineering Research Council, Fonds FCAR (Quebec) and the Canada Department of Fisheries and Oceans.

I am very grateful to Mr. A. Schwartz for his assistance in computer related problems and Dr. David Straub for his helpful discussions with me. Many thanks also go to Mr. Rick Danielson for his help in obtaining and using NOAA CDC meteorological data set, Dr. Francois Saucier for providing modeled winter monthly mean surface currents for 1986, Ms Ingrid Peterson and Dr. S.J. Prinsenberg for allowing me to use their sea ice observation data in the Labrador Sea, and Mr. Stephen Déry for the French version of the abstract.

Finally, I am very indebted to my wife, Shue Li, for her constant moral support and encouragement for my work.

1. Introduction

Many studies on sea ice variability in Arctic regions have been conducted over the past decades, mainly because of its important role in global climate change research. Some studies focused on sea ice variability over the entire Arctic and its relation to surface air temperature (Walsh and Johnson, 1979; Manak and Mysak, 1989; Chapman and Walsh, 1993), atmospheric circulation (Mysak et al., 1990; Mysak and Power, 1992; Power and Mysak, 1992; Fang and Wallace, 1994; Slonosky et al., 1997), and river runoff from northern Canada (Manak and Mysak, 1989; Mysak et al., 1990; Mysak and Power; 1992). Other studies examined the "Great Salinity Anomaly" (GSA) (Dickson et al., 1988) which occurred in the northern North Atlantic in 1968-1982 (Mysak and Manak, 1989; Mysak et al., 1990; Slonosky et al., 1997). Research on sea ice variability at more regional scales, especially in the Greenland-Iceland Seas, Hudson Bay, Baffin Bay, and the Labrador Sea (Mysak and Manak, 1989; Mysak et al., 1990; Wang et al., 1994; Mysak et al., 1996; Ingram et al,, 1996; Drinkwater, 1996; Drinkwater et al., 1996; Drinkwater et al., 1997; Prinsenberg et al., 1997) was also undertaken. In comparison to sea ice studies in the Arctic regions, fewer studies have been conducted on sea ice variability in lower latitude seas, such as the Gulf of St. Lawrence. This thesis presents a systematic study of intraseasonal and interannual variability of sea ice within the Gulf of St. Lawrence, using ice observations from 1963-1996. In the remainder of this Chapter, we briefly consider geographic features of the Gulf of St. Lawrence, review previous studies on sea ice variability within the Gulf, and present the objectives of the present study.

1.1 The Gulf of St. Lawrence

The Gulf of St. Lawrence combines features of an inner sea and a large estuary. It receives an annual river runoff close to 600 km^3 (Bugden, 1981). The surface area of the Gulf is about 230,000 km^2 (including the Lower Estuary) and its volume is estimated to be 34,550 km^3 (Forrester, 1964). The Gulf is connected to the Atlantic Ocean through Cabot Strait and to the Labrador Sea through the Strait of Belle Isle (Figure 1.1). Cabot Strait has a width of 104 km, a maximum depth of 480 m, and a cross-sectional area of 35 km^2. The Strait of Belle Isle is more restricted, with a width of about 15 km, a maximum sill depth of 60 m, and a cross-sectional area of about 1 km^2 (Trites, 1972).

The bathymetric features of the Gulf are shown in Figure 1.2. The Laurentian Channel, a deep trench of up to 500 m in maximum depth, extends from the mouth of the Saguenay River through Cabot Strait to the continental slope. The Esquiman Channel extends from the Laurentian Channel towards the Strait of Belle Isle, while Anticosti Channel extends towards Jacques Cartier Passage, north of Anticosti Island, from the Esquiman Channel. A large shallow area called the Magdalen Shallows, where the depths range from 50-80 m, can be found in the southwest part of the Gulf of St. Lawrence. The Northumberland Strait (length ~ 200 km, width ~ 20 km and depth ~ 20 m), separates Prince Edward Island from Nova Scotia.

1.2 Review of studies on sea ice variability in the Gulf

The Gulf of St. Lawrence is the southernmost region of eastern North America experiencing persistent sea-ice coverage. In the past decades, much attention has been

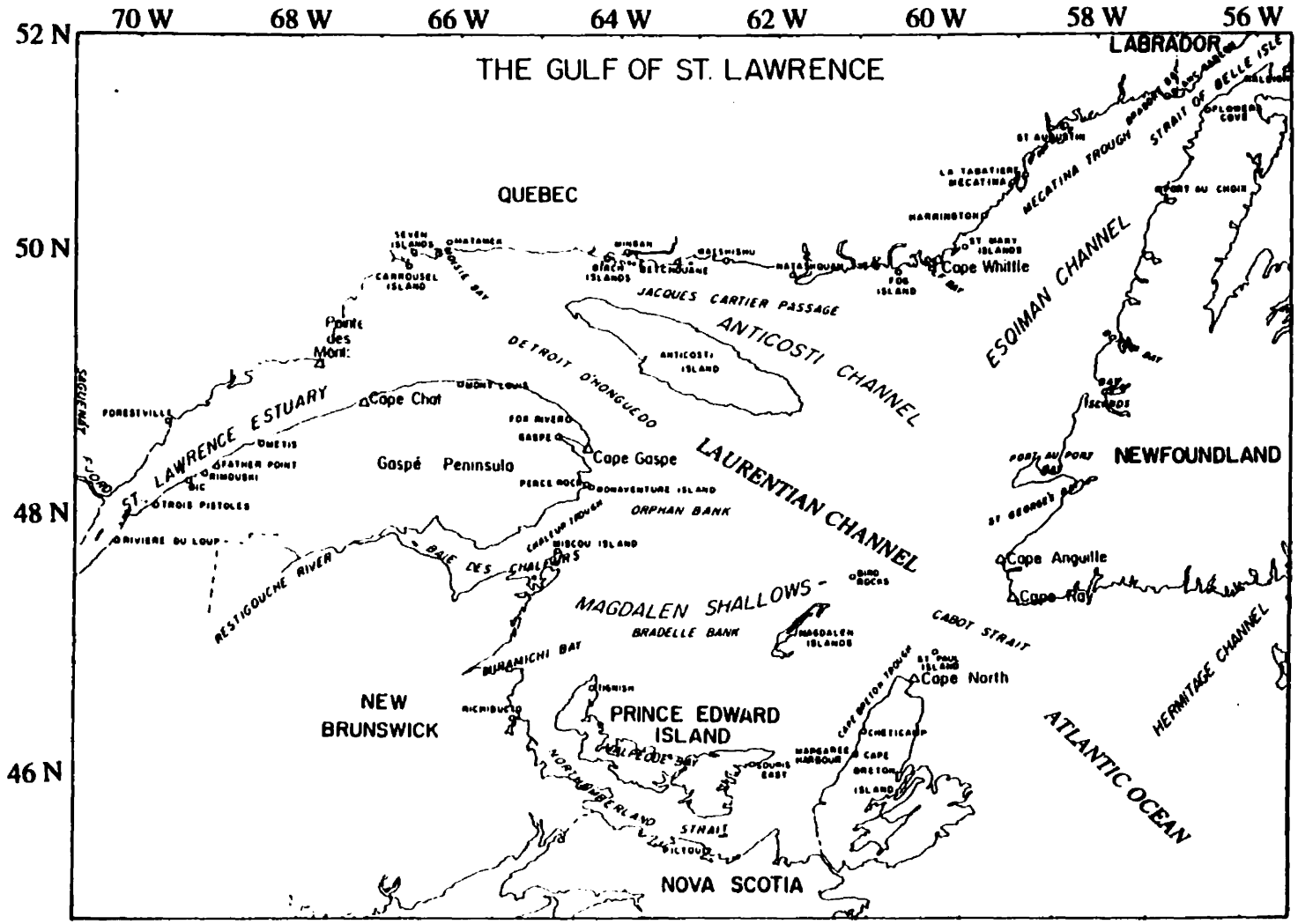

Figure 1.1 The Gulf of St. Lawrence (Adapted from Dunbar et al, 1980)

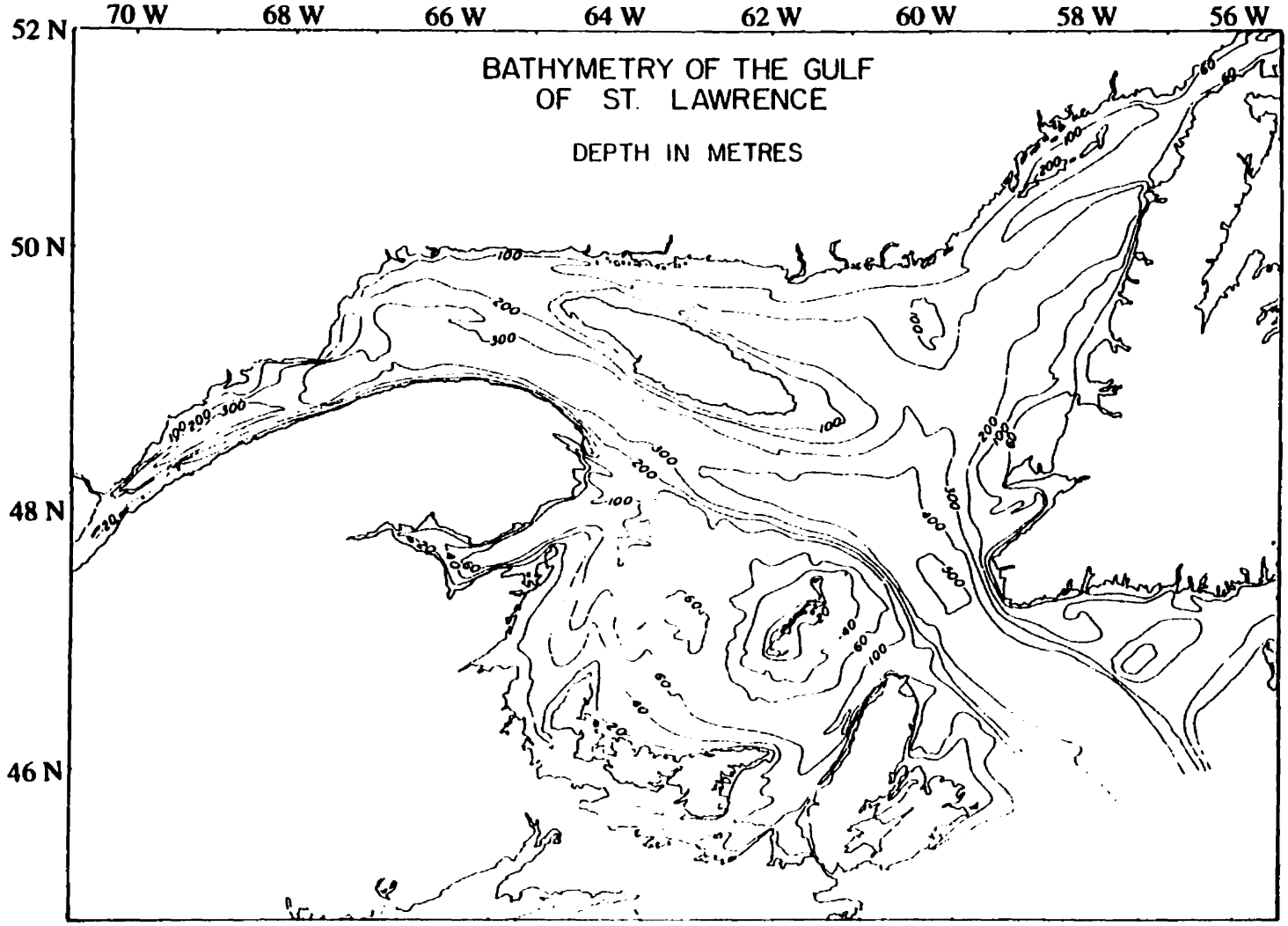

Figure 1.2 The Bathymetry of the Gulf of St. Lawrence (Adapted from Dunbar et al, 1980)

paid to sea-ice variability in the Gulf because of the following three reasons. First, many studies indicate that sea ice plays a significant role in the global climate system by affecting the surface albedo and the air-sea heat transfer through sensible and latent heat exchanges. Thus, understanding sea ice variability in the Gulf of St. Lawrence can help us understand air-sea interaction processes and their influence on the local climate system. Second, the Gulf of St. Lawrence is an important shipping route. The ice in the Gulf is a major impediment to shipping and in most winters extensive ice breaking is required to maintain open sea-lanes. Third, the Gulf of St. Lawrence is part of the marine subarctic system and yields nearly 25% of the total Canadian commercial fish catch by weight (Koutitonsky et al., 1991). A marine subarctic region, according to Dunbar (1980), is an area where the sea ice cover advances and retreats annually. This annual signal generates brine convection and vertical mixing, which helps bring nutrients to the surface. Changes in the position of ice margin can dramatically affect the fisheries and the economies of surrounding coastal populations.

Sea ice in the Gulf normally begins to form in three areas during December: the St. Lawrence Estuary, on the western shore of the Magdalen Shallows, and along the north shore of the Gulf (Coté, 1989). By late February or early March, the Gulf is typically ice-covered, extending out through Cabot Strait onto the Scotian Shelf. By April, the ice retreats, and generally disappears from the Gulf in late May or early June.

Forward (1954) noted large interannual variability of the ice cover within the Gulf during break-up from data collected from 1940-1952. He suggested that variability was mainly

caused by fluctuations in local air temperature and winds. Markham (1973) found similar results by comparing sea-ice conditions during severe winters with sea level pressure charts and surface air temperature at Grindstone Island (Magdalen Island). In addition, some studies also indicate that both mean sea-ice volume for different sub-regions of the Gulf and median positions of ice edge display year-to-year variations (Forrester, 1968; Black, 1972; Sowden and Geddes, 1980; Cote, 1989). By examining the 1960-61 and 1964-65 winter sea ice conditions, Matheson (1967) studied the influence of both atmospheric circulation and heat fluxes over the Gulf of St. Lawrence on sea-ice formation and decay. He found that the types and duration of air flows are very important on the formation and decay of sea ice.

In more recent years, Déry (1992) examined intraseasonal and interannual variability of sea-ice cover using weekly ice charts for 1963-1990. He found decadal (12-15 years) variability in sea-ice cover. Although similar variability was found in surface air temperature (SAT), sea surface temperature and salinity (SST/SSS), St. Lawrence River runoff and atmospheric circulation, no obvious link between sea-ice variability and any single forcing variable was established. Using an uncoupled Hibler sea-ice model, DeTracey (1993) simulated sea-ice conditions for three scenarios (years with maximum, minimum, and average ice cover), with input of the November SST and monthly meteorological forcing fields. Drinkwater and Bugden (1994) described the mean and interannual variability of the time of first ice presence, of last ice presence, and ice duration at three locations in the vicinity of Cabot Strait. Within the Strait, local air

temperatures and the strength of the northwesterly winds accounted for over 73% of the interannual variance in the appearance of ice.

1.3 Objectives of the present study

Although many studies have been conducted on sea ice variability in the Gulf of St. Lawrence, some uncertainties remain. First, there have been no systematic studies on intraseasonal sea-ice variations in the Gulf. Most of the previous studies on intraseasonal sea-ice variations either used scattered sea-ice observations or only presented descriptions of the changes without examining their causes. Second, there have been no systematic studies on interannual variability of the time of first ice presence (TFIP), of last ice presence (TLIP), and sea-ice duration (SID) on a Gulf-wide scale. Drinkwater et al. (1999) did examine the data, but did not consider mechanisms to explain the observed variability. Drinkwater and Bugden (1994) considered interannual variability of TFIP, TLIP, and SID, but only in the region seaward of Cabot Strait. Third, the mechanisms for intraseasonal and interannual variability of sea ice in the Gulf and the relative importance of the forcing factors on sea-ice variability are not clear. Although some of the previous studies (Forward, 1954; Markham, 1973; Déry, 1992) discussed mechanisms affecting sea-ice variability, these studies included only a few forcing factors. Furthermore, meteorological observations from only one or two stations were used in these studies. In the present study, several potential forcing factors governing sea ice variability in the Gulf of St. Lawrence are considered, their relative importance examined, and the impact of spatially varying forcing within the Gulf explored.

The objectives for present studies are as follows:

- To characterize the intraseasonal and interannual variability of sea ice in the Gulf of St. Lawrence using sea ice observations from 1963-1996.
- To understand the mechanisms and relative importance of forcing factors on sea ice variability in the Gulf using statistical analysis and a model study.

1.4 Outline of the present study

The thesis is organized as follows. Chapter 2 introduces the data and methods used in this study. Chapter 3 presents intraseasonal variations of sea-ice cover and interannual variability of sea-ice cover, time of first ice presence, time of last ice presence, and sea-ice duration in the Gulf. Chapter 4 examines the forcing mechanisms and relative importance of forcing factors on sea-ice variability from statistical approaches. Chapter 5 discusses mechanisms of sea ice variability using a simple sea ice model. Chapter 6 gives a summary of the main conclusions and discusses future work.

2. Data and Methods

2.1 Data

2.1.1 Sea-ice cover data

The sea-ice cover database consists of approximately weekly observations from January 1963 through April 1996 (see Drinkwater et al. (1999) for a detailed description of the database). The spatial resolution for the sea ice observations is 1° in longitude and 0.5° in latitude, requiring 83 grid squares to cover the Gulf (Figure. 2.1). The database includes the concentration or coverage of ice (in tenths) present in each grid and the area of open water (in tenths). The amount of ice coverage in each grid was estimated using the following formula. For grid n, the area of ice coverage (A_{in}) in tenths is estimated from $A_{in} = C_{in} * (1 - A_{wn})$, where C_{in} represents the concentration of sea ice in tenths that is present and A_{wn} is the area of open water in grid n, also in tenths. The observations generally begin in December of the previous year and end in June. However, there are some missing observations, especially in the months of December, May, and June. Sea ice generally appears in the Gulf in mid-December and disappears in May or June. No sea ice was found on either December 1 or June 30. Therefore, the sea-ice cover was set to zero on both December 1 and June 30, and linearly interpolated the weekly observations to daily values on the sea ice grid. In this way, the sea ice data on each grid are continuous from December 1 of the previous year to June 30 in the current year.

2.1.2 Meteorological data

Meteorological data (daily surface air temperature and winds) were available from the NOAA Climate Diagnostics Center (CDC) from 1958-1997, which were products of the

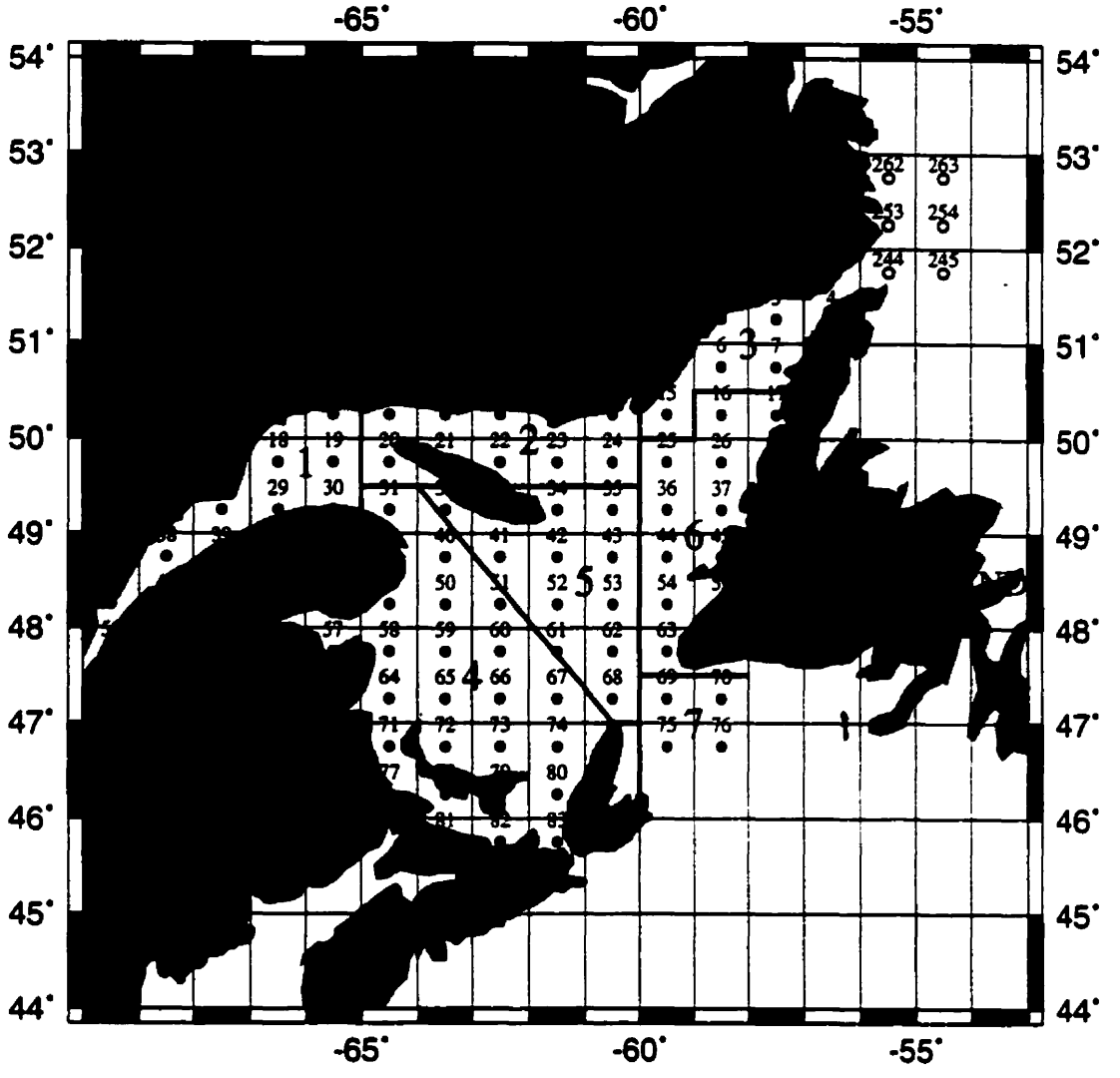

Figure 2.1 Sea ice grids and subregions in the Gulf of St. Lawrence

NCEP/NCAR 40-year (1958-1997) reanalysis project. The project was designed to produce a 40-yr record of global analyses of atmospheric fields in support of the needs of the research and climate monitoring communities. It uses a frozen state-of-the art global data assimilation system and a database as complete as possible (Kalnay et al., 1996). The system has been designed with advanced quality control and monitoring components. The database contains observations from land surface, ship, rawinsonde, pibal, aircraft, satellite, etc., provided by different countries and organizations. The spatial resolution for the data set is 2.5° in both latitude and longitude.

2.1.3 Hydrographic data

Hydrographic observations in the Gulf are not continuous in either time or space. In this study, we use November hydrographic data from the Bedford Institute of Oceanography (K. Drinkwater, personal communication), because the hydrographic conditions for this month have been shown to influence ice formation (DeTracey, 1993). Furthermore, there is a relatively large data set for this month and very few observations in winter months. Indeed, most of the hydrographic data in November were collected for the purposes of ice forecasting at the request of Canadian Ice Service (Environment Canada, Ottawa). The mean sea surface temperature and salinity in November and their anomalies from long-term means were calculated from these data.

2.1.4 River runoff from the St. Lawrence River system

Monthly river runoff observations from January 1962 to September 1995 for the St. Lawrence, Ottawa and Saguenay Rivers were obtained from Bedford Institute of

Oceanography (K. Drinkwater, personal communication) based upon data collected by the Inland Waters Directorate of the Canadian Department of the Environment. They were combined to obtain estimates of discharge from the St. Lawrence River system (called RIVSUM by Sutcliffe et al., 1976).

2.2 Methods

Several statistical methods were employed in the analysis of the sea ice data and its relationship with various potential forcing functions. These methods include Empirical Orthogonal Functions (EOFs), Singular Value Decomposition (SVD), correlation analysis, and spectral analysis.

The EOF method was used to examine the variability of a single field, i.e., a field of only one scalar variable (e.g. sea-ice cover, surface air temperature, etc.). It allows one to describe the spatial patterns of variability for a scalar field and the time variation, as well as giving a measure of the "importance" of each spatial pattern (Bretherton et al., 1992; Bjornsson and Venegas, 1997). The first step to calculate EOFs is to construct a covariance matrix from the original spatial and temporal data set, from which a set of eigenvectors and corresponding eigenvalues can be obtained. The second step is to have the eigenvectors ordered in such a way that the leading EOF (the first eigenvector) explains the most variance contained in the data set, and the second eigenvector gives the next most variance, and so on. The actual proportion of the variance explained by a given EOF is its eigenvalue. Thus, the original data set has been reduced into a series of orthogonal basis vectors. The EOF consists of both a spatial pattern and a time series

describing changes in the amplitude of that spatial pattern over the length of the record. The time series is obtained by projecting the original data matrix onto the eigenvectors.

The SVD method was used to examine the coupled variability of two scalar fields. The analysis identifies only those modes of behavior in which the variations of the two fields are strongly coupled (Bretherton et al., 1992; Wallace et al., 1992; Bjornsson and Venegas, 1997). The method is an extension to rectangular matrices of diagonalization of a square symmetric matrix. It is usually applied in geophysics to two combined data fields, such as sea-level pressure and sea surface temperature. The method identifies pairs of coupled spatial patterns and their temporal variations, with each pair explaining a fraction of covariance between the two fields. To perform SVD analysis, one needs to construct the temporal cross-covariance matrix of two fields that are dependent upon space and time. This matrix generally is not square since the two fields may be observed at different grid points. However, the variables need to span the same period of time.

The SVD of the cross-covariance matrix yields two spatially orthogonal sets of singular vectors (spatial patterns analogous to the eigenvectors in EOFs, but one for each variable) and a set of singular values associated with each pair of vectors (analogous to the eigenvalues). Each pair of spatial patterns describes a fraction of the squared covariance (FSC) between the two variables. The first pair of patterns describes the largest FSC and each succeeding pair describes a maximum FSC that is unexplained by the previous pairs. The squared covariance fraction (SCF) accounted for by the k-th pair of singular vectors is proportional to the square of the k-th singular value. The k-th expansion coefficients

for each variable are computed by projecting the k-th singular vector onto the corresponding original data field. The correlation value between the k-th expansion coefficients of the two variables indicates how strongly related the k-th coupled patterns are.

The spatial patterns corresponding to different EOF and SVD modes can be presented in several different ways. One way is to present the eigenvector itself, but the amplitudes of the contours plotted in this way are not easy to interpret in terms of useful quantities. Other ways of presenting spatial patterns, including homogeneous and heterogeneous correlation maps, could provide more information. The k-th homogeneous correlation map is defined as the vector of correlation values between the expansion coefficients of the k-th mode of a field and the values of the same field at each grid point (Wallace et al., 1992). It is used to examine the fractions of the variances of the respective field explained by the time series of the expansion coefficients of the same field. The k-th heterogeneous correlation map is defined as the vector of correlation values between the expansion coefficients of the k-th mode of a field and the grid point values of another field (Wallace et al., 1992). It indicates how well the grid point values of one field can be predicted from the knowledge of the expansion coefficients of another field. In SVD analysis, a correlation map for the k-th mode usually refers to the correlation map between the k-th expansion coefficient of one variable with the grid point values of the same variable (homogeneous map) or the other variable involved in the SVD (heterogeneous map). In both cases, the contours plotted show the distribution of correlation coefficients.

The confidence levels for any particular correlation were determined by a method suggested by Sciremammano (1979). The large-lag standard error σ between two time series X(t) and Y(t) is computed as follows:

$$\sigma^2 = \frac{1}{N} \sum_{i=-M}^{M} C_{xx}(it) C_{yy}(it)$$

where C_{xx} and C_{yy} are the autocorrelation functions of X(t) and Y(t), respectively, N is the length of both series, and M is large compared with the lag number at which both C_{xx} and C_{yy} are statistically zero. Thus, to a good approximation, the 90%, 95%, and 99% significance levels are equivalent to

$C_{90} = 1.7 * \sigma$

$C_{95} = 2.0 * \sigma$

$C_{99} = 2.6 * \sigma$

Spectral analysis was used to determine the dominant periods present in climatic time series of the variables. The spectral method used to estimate the power spectrum in this study is called the 'multi-taper' method (Thomson, 1982), which is particularly well-suited for the analysis of climatic time series (Mann and Lee, 1996). The confidence levels of spectrum relative to red noise were determined by a method described by Mann and Lee (1996).

The software package to contour the data in this study is called GMT (Generic Mapping Tools) (Wessel and Smith, 1991), which is a widely-used software package in geophysics.

3. Intraseasonal and Interannual Variability of Sea-Ice Cover in the Gulf

In this chapter, we describe the intraseasonal and interannual variability of sea-ice cover in the Gulf of St. Lawrence, including the time of first ice presence (TFIP), time of last ice presence (TLIP), and sea-ice duration (SID), using sea ice observations from January 1963 to April 1996. Spatial differences within the Gulf are emphasized. We also contrast conditions during extreme ice years (i.e., severe and light ice years).

3.1 Intraseasonal variations

Long-term mean daily sea-ice cover from December 1 through June 30 at each grid point was obtained by averaging the estimated values for the period 1963 to 1996. The sea-ice cover values from December 15 through June 1 at time intervals of half a month are shown in Figure 3.1. Sea ice begins to form in December, initially within the St. Lawrence Estuary, along the western shore of the Magdalen Shallows, and the north shore of the Gulf. The sea ice later extends offshore into the central, deeper Gulf and by early February is found over the entire Gulf. The maximum sea-ice cover exceeds 8/10, occurring along the western shore of the Magdalen Shallows in early February, within the central Gulf by early March and in the Strait of Belle Isle by early to mid-March. The sea ice usually begins to retreat by mid-March, initially in the St. Lawrence Estuary. By mid-April, sea-ice cover over most of the Gulf is less than 2/10, except over the southern Gulf and in the Strait of Belle Isle, with more ice in the latter region. By early May, sea ice disappears over the entire Gulf, except in the Strait of Belle Isle, where it persists until

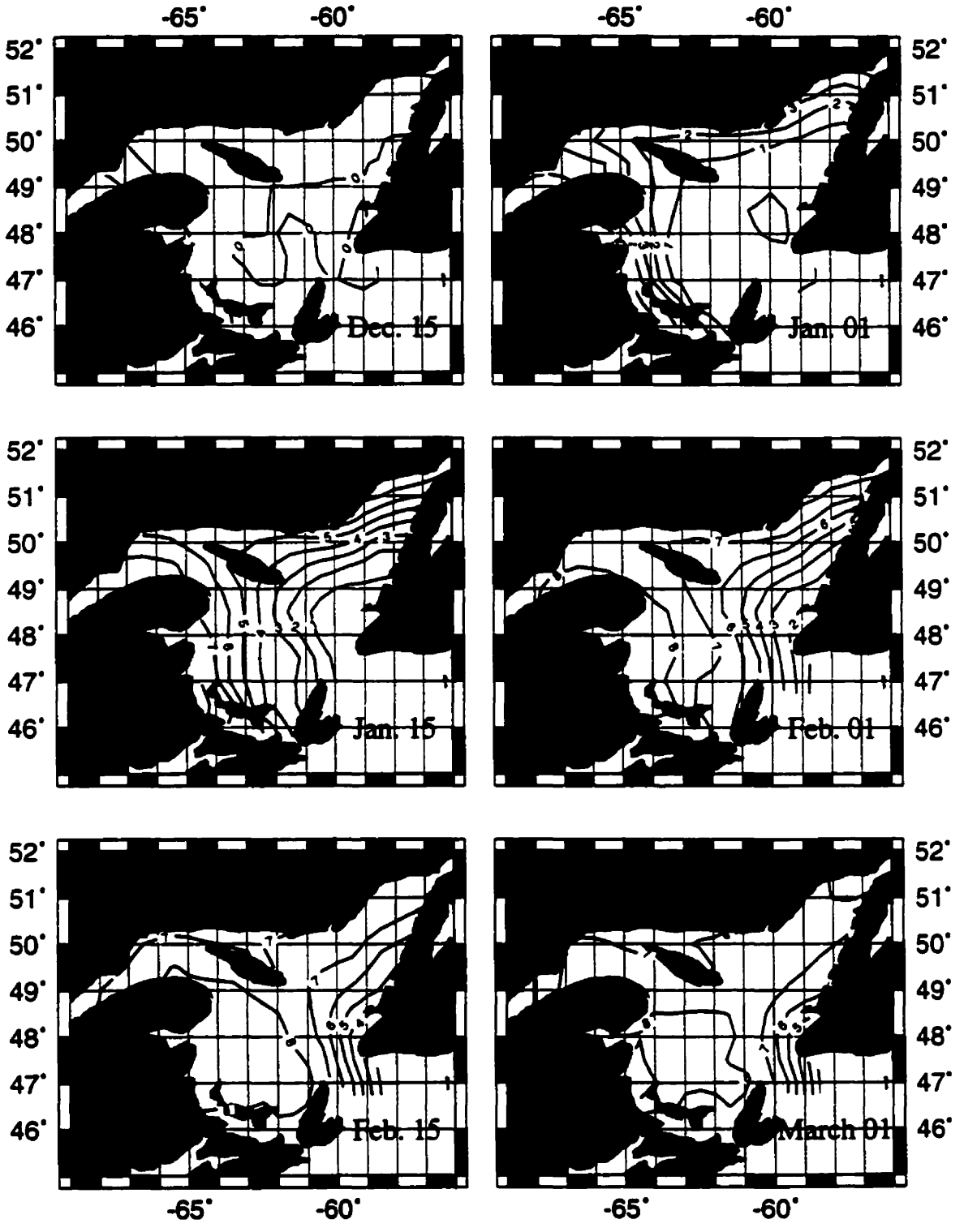

Figure 3.1 Mean daily sea-ice cover in tenths in the Gulf of St. Lawrence for 1963-96.

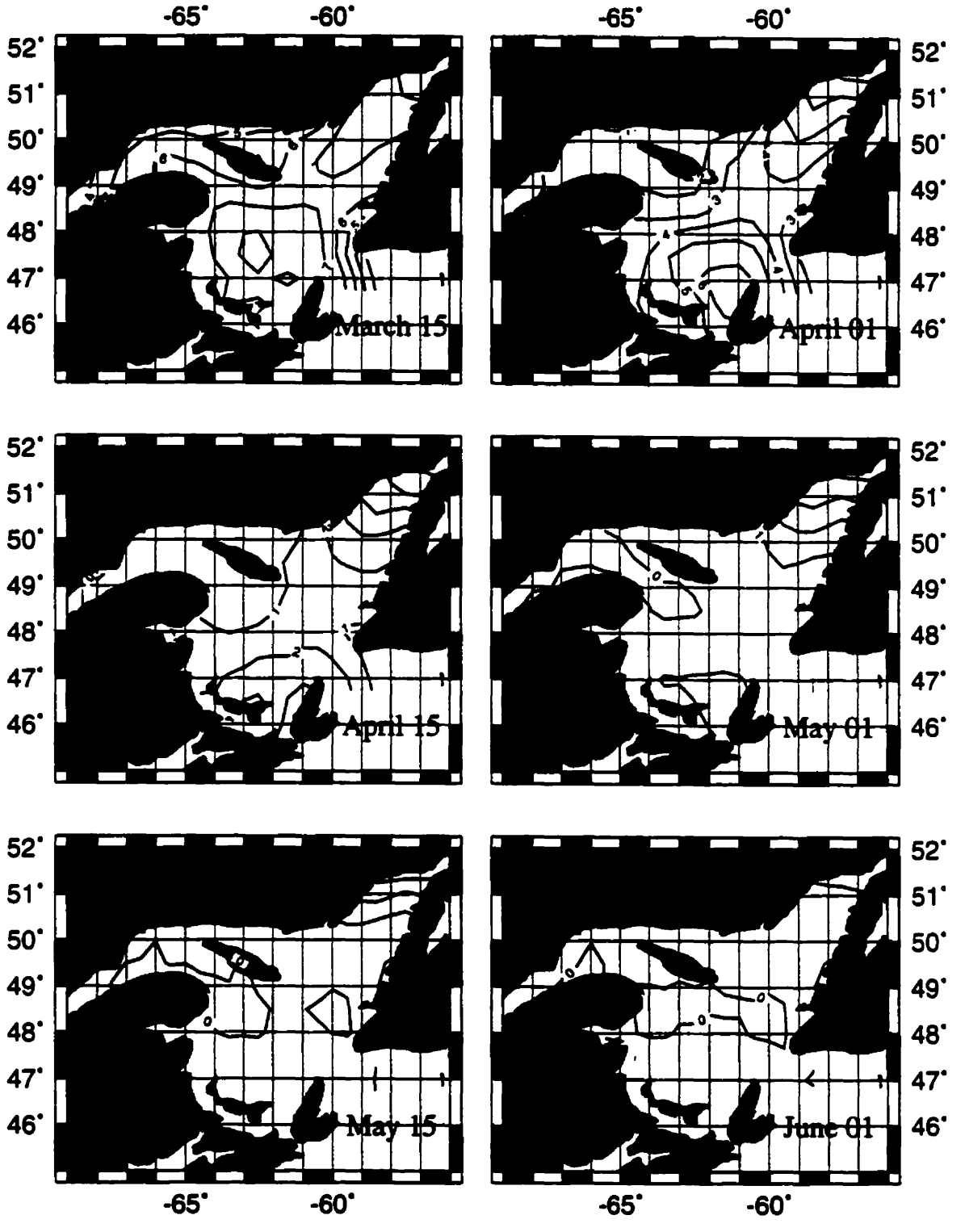

Figure 3.1 (Continued)

early June. These results are consistent with previous studies (Cote, 1989; Drinkwater et al., 1999).

To examine further the spatial differences in sea-ice coverage, we divided the Gulf into seven sub-regions (Figure 2.1). Within each sub-region, the spatial differences of mean sea-ice cover averaged over the ice season are small (Figure 3.2). Figure 3.3 shows the time series of sea-ice cover averaged over different sub-regions and for the entire Gulf. In the St. Lawrence Estuary (Region 1), the sea ice appears earlier and leaves earlier than in other regions. The maximum sea-ice cover, which is less than 8/10, occurs around the end of January. Along the northern shore of the Gulf (Region 2), the sea ice appears and disappears somewhat later than in Region 1. The maximum sea-ice cover occurs in late February to early March. In the Strait of Belle Isle (Region 3), sea-ice cover appears early and leaves late, resulting in the longest ice duration observed in the Gulf. The maximum cover exceeds 8/10. On the Magdalen Shallows (Region 4), the maximum sea-ice cover occurs during February to March. For Regions 5, 6, 7, the sea ice appears later and leaves earlier. The smallest sea-ice cover, less than 4/10, occurs in Region 7 (Cabot Strait region). The sea-ice cover averaged over the entire Gulf indicates that the maximum sea-ice cover typically occurs in late February.

The time of first ice presence, of last ice presence, and sea-ice duration in the Gulf were also examined (Figure 3.4). The presence of sea ice is defined as when sea-ice cover exceeds 1/10. Thus, sea-ice duration is not necessarily equal to the difference between the time of the first and last ice because sea ice may temporarily disappear and reappear

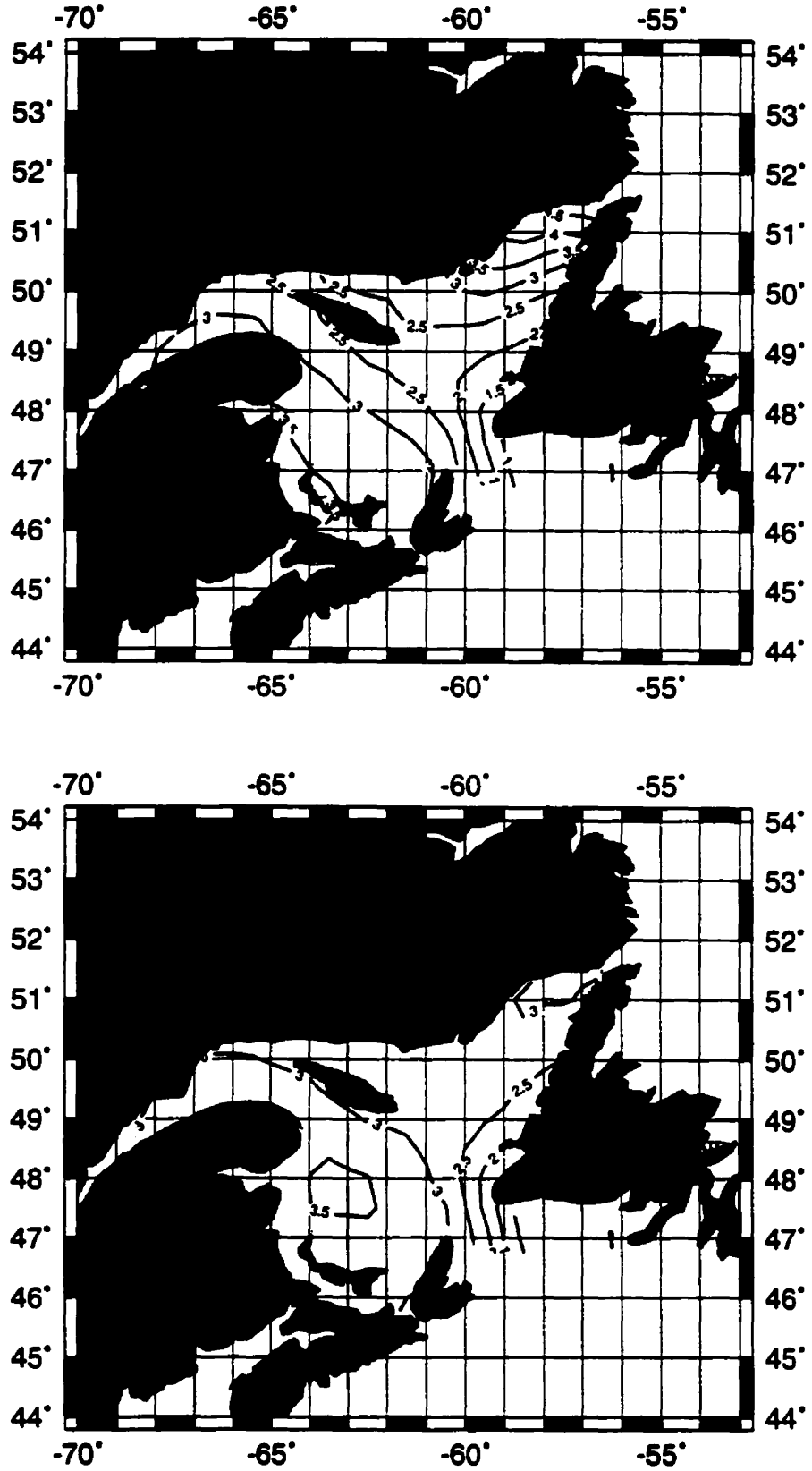

Figure 3.2 Mean December-June sea-ice cover in tenths (upper) and corresponding intraseasonal standard deviations (lower).

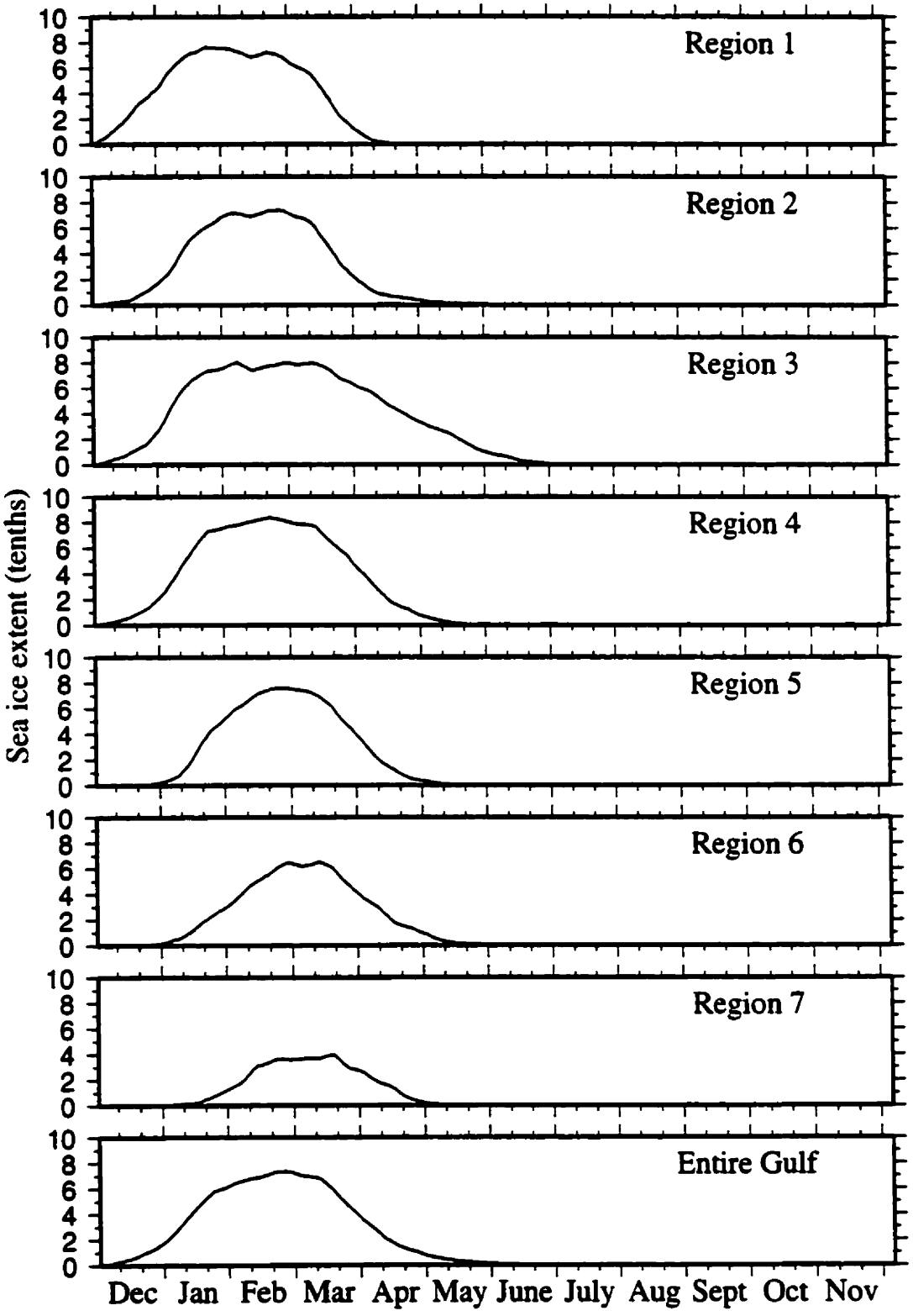

Figure 3.3 Annual sea-ice cover in tenths in different subregions.

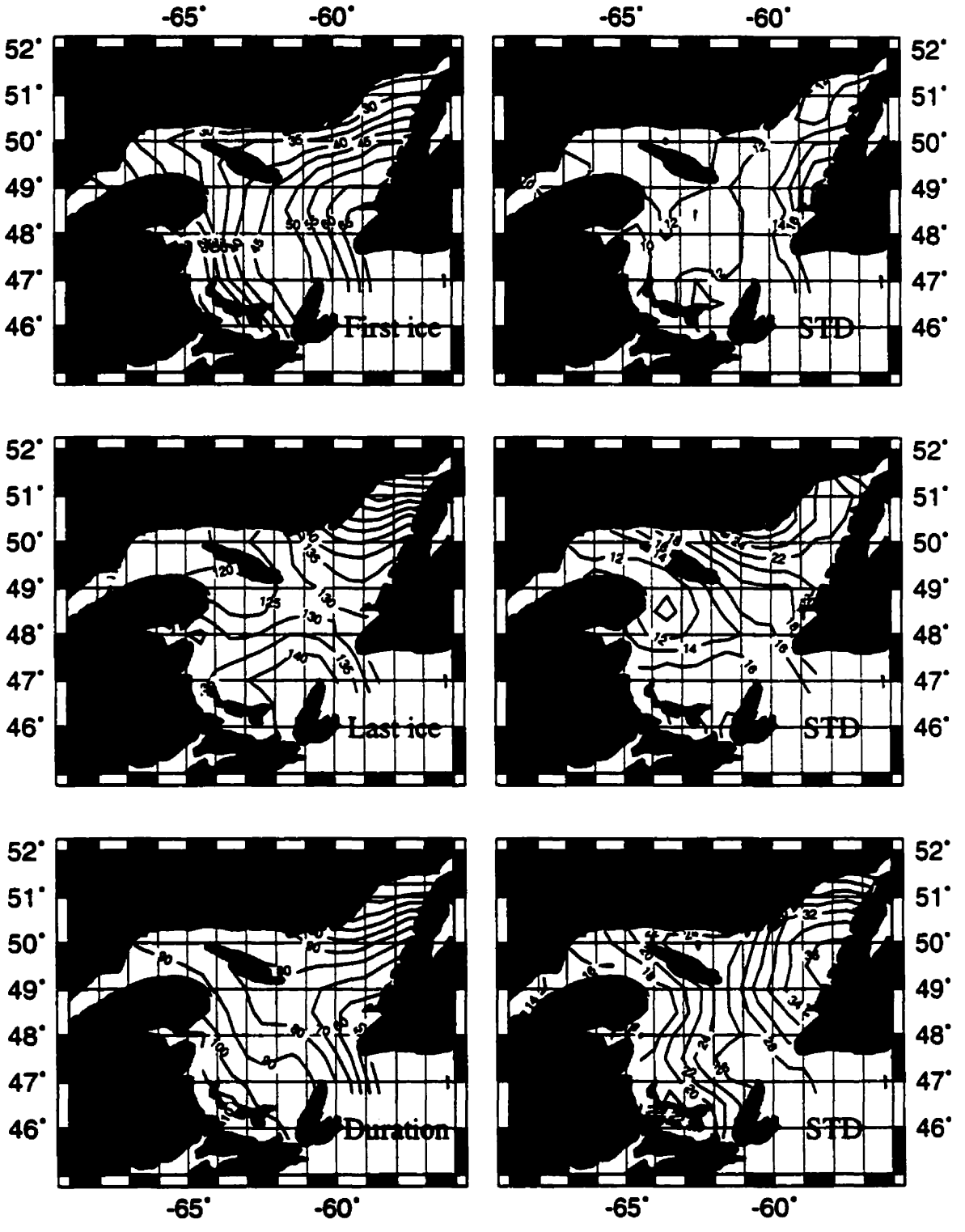

Figure 3.4 Mean dates, relative to December 1, of first ice presence (upper left) and corresponding standard deviation (upper right), of last ice presence (middle left) and corresponding standard deviation (middle right), and sea-ice duration in days (lower left) and corresponding standard deviation (lower right) in the Gulf.

at a later time. Figure 3.4 shows quantitatively the mean dates, relative to December 1, for the first and last ice presence, and sea-ice duration. These results are consistent with our previous analysis. Note that the duration of sea ice in the Strait of Belle Isle exceeds 140 days while in the southwest corner of the Gulf, it exceeds 100 days. The shortest duration (approximately 2 months) occurs off Newfoundland, near Cabot Strait. Also shown in Figure 3.4 are the standard deviation fields of TFIP, TLIP, and SID.

3.2 Interannual variability

As mentioned in Chapter 1, the Gulf of St. Lawrence is an important shipping route. Sea ice in the Gulf of St. Lawrence is a major impediment to shipping in the ice season. Thus, understanding the time of first ice presence (TFIP), time of last ice presence (TFIP), and sea-ice duration (SID) is very important to the shipping industry. Sea ice also affects fisheries. For example, the presence of heavy sea ice can restrict the geographical location of fishing and in some areas delay the opening of the lobster fishing season (Drinkwater et al., 1999). As well, the timing of the cod's return on the Magdalen Shallows is directly related to the time the sea ice disappears (Sinclair and Currie, 1994). In years when the ice retreat is delayed, the majority of the cod entering the Gulf appears later-than-normal.

In the following section, we describe the interannual variability of sea ice in the Gulf and in subsequent chapters examine the relevant forcing mechanisms.

3.2.1 SIC

Figure 3.5 shows the long-term (1963-95) mean sea-ice cover averaged over December-June and their corresponding standard deviations. The latter suggest that the largest interannual variability of sea-ice cover occurs in the area off western Newfoundland, with the smallest variability in the St. Lawrence Estuary. The standard deviations of the monthly means indicate that the largest interannual variability occurs in different regions during different months (Figure 3.6). In December, the largest sea-ice variability occurs in coastal regions, while in January, it moves to the central Gulf. In February and March, it appears in the area off Newfoundland. In contrast, the largest sea ice variability in April occurs over two regions: the Strait of Belle Isle and on the Magdalen Shallows. In May, it occurs only in the Strait of Belle Isle. In addition, the amplitudes of the interannual variability vary from month to month. The largest interannual variability, exceeding 3/10, occurs in March, the second largest in February and April.

Standard deviations (Figures 3.5 and 3.6) provide a measure of the interannual variability but do not indicate how sea-ice cover varies from year to year. Temporal variability of sea-ice cover can be examined in several ways. One way is to examine interannual variability of sea-ice cover grid by grid but this approach is tedious especially when the number of grids is large. Another way is to divide the study domain into several sub-regions, as we did to examine intraseasonal variation (Figure 3.3). This approach sacrifices spatial variability within each sub-region. These approaches generally emphasize either spatial variability or temporal variability of sea-ice cover but not both. One method that looks at both aspects simultaneously is the EOF (Empirical Orthogonal

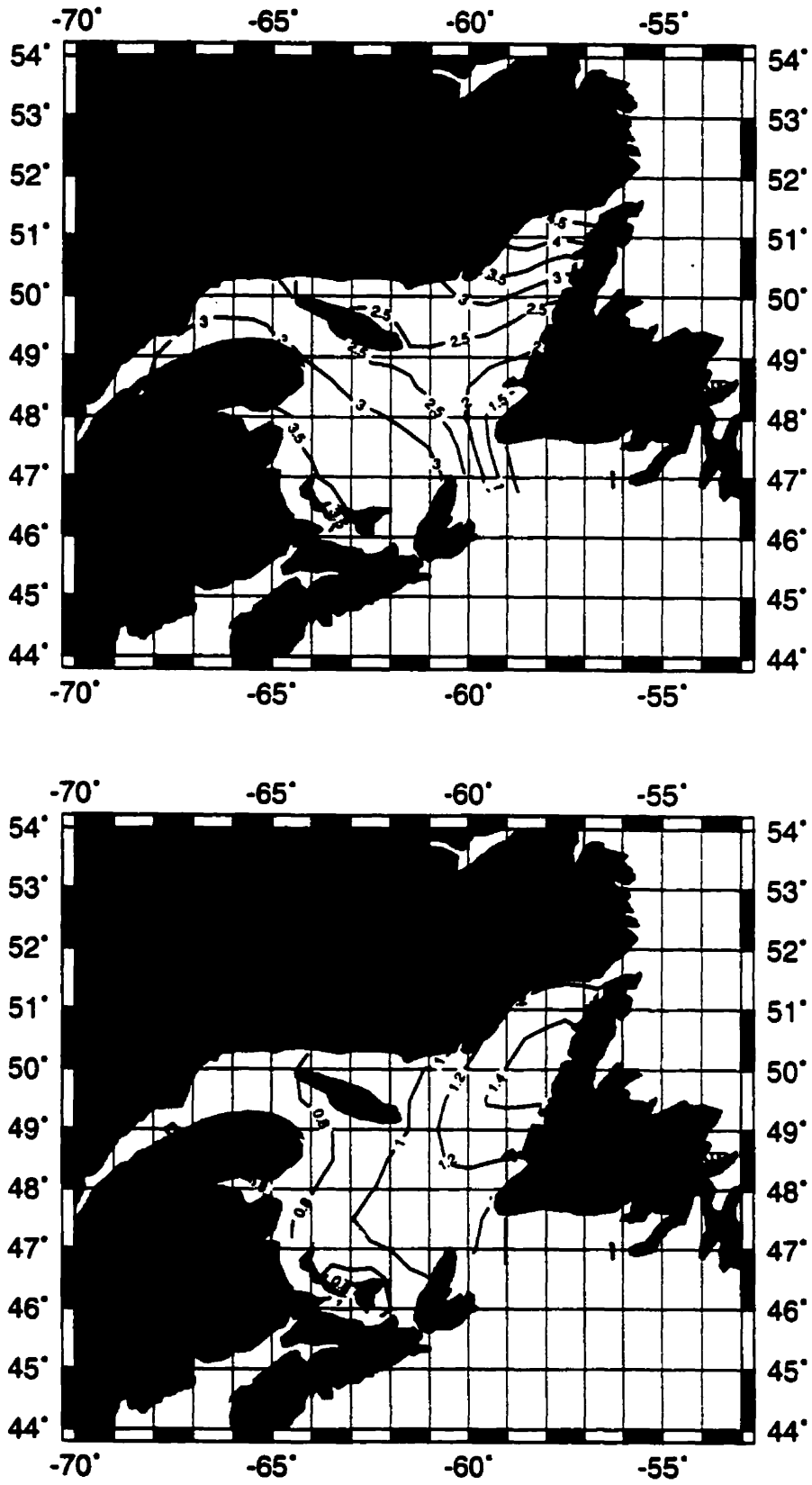

Figure 3.5 The long-term (1963-95) mean sea-ice cover in tenths averaged over December-June (top) and the corresponding standard deviations (bottom) in the Gulf of St. Lawrence

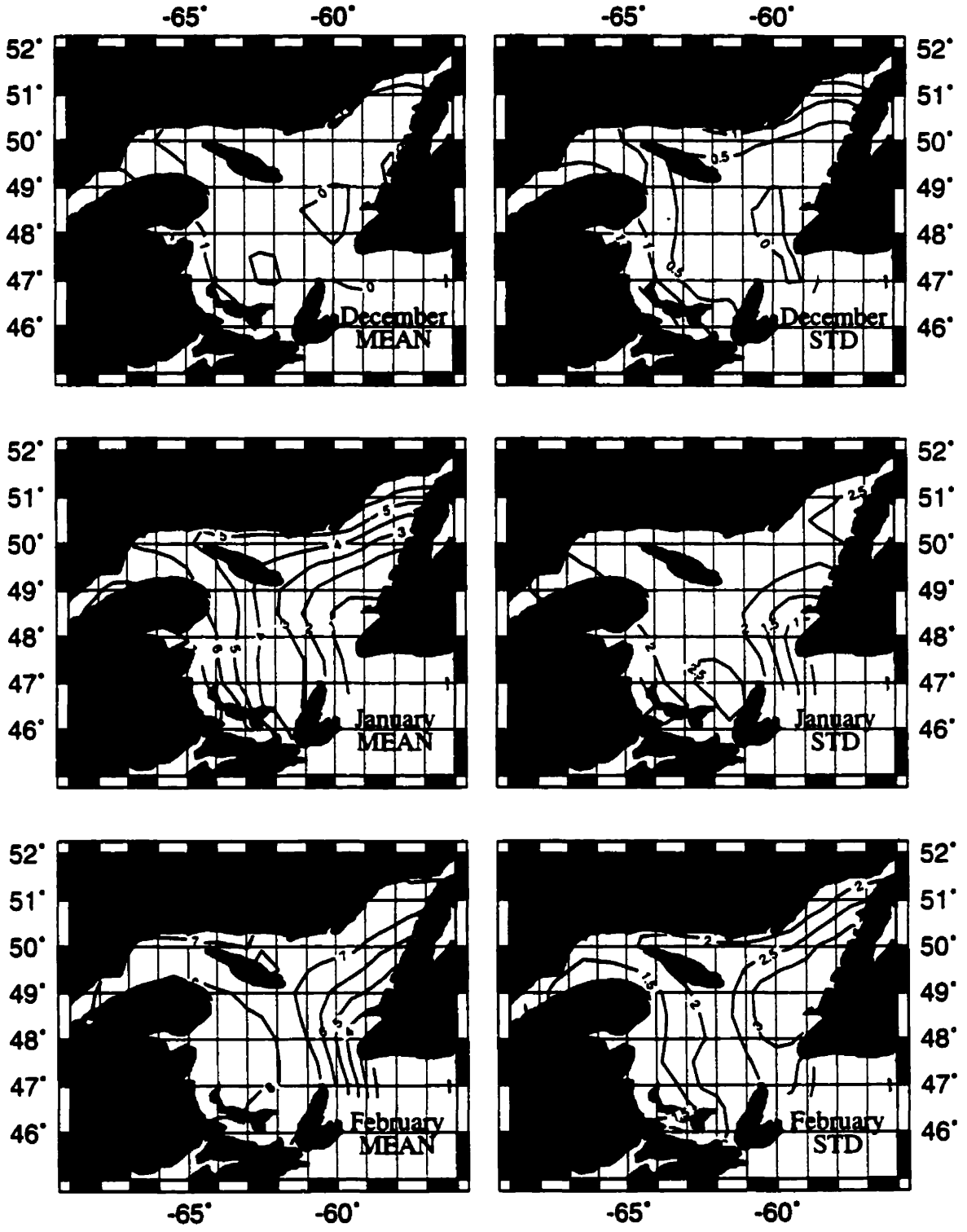

Figure 3.6 Long-term (1963-96) monthly mean sea-ice cover (left) and corresponding standard deviations (right) in the Gulf of St. Lawrence.

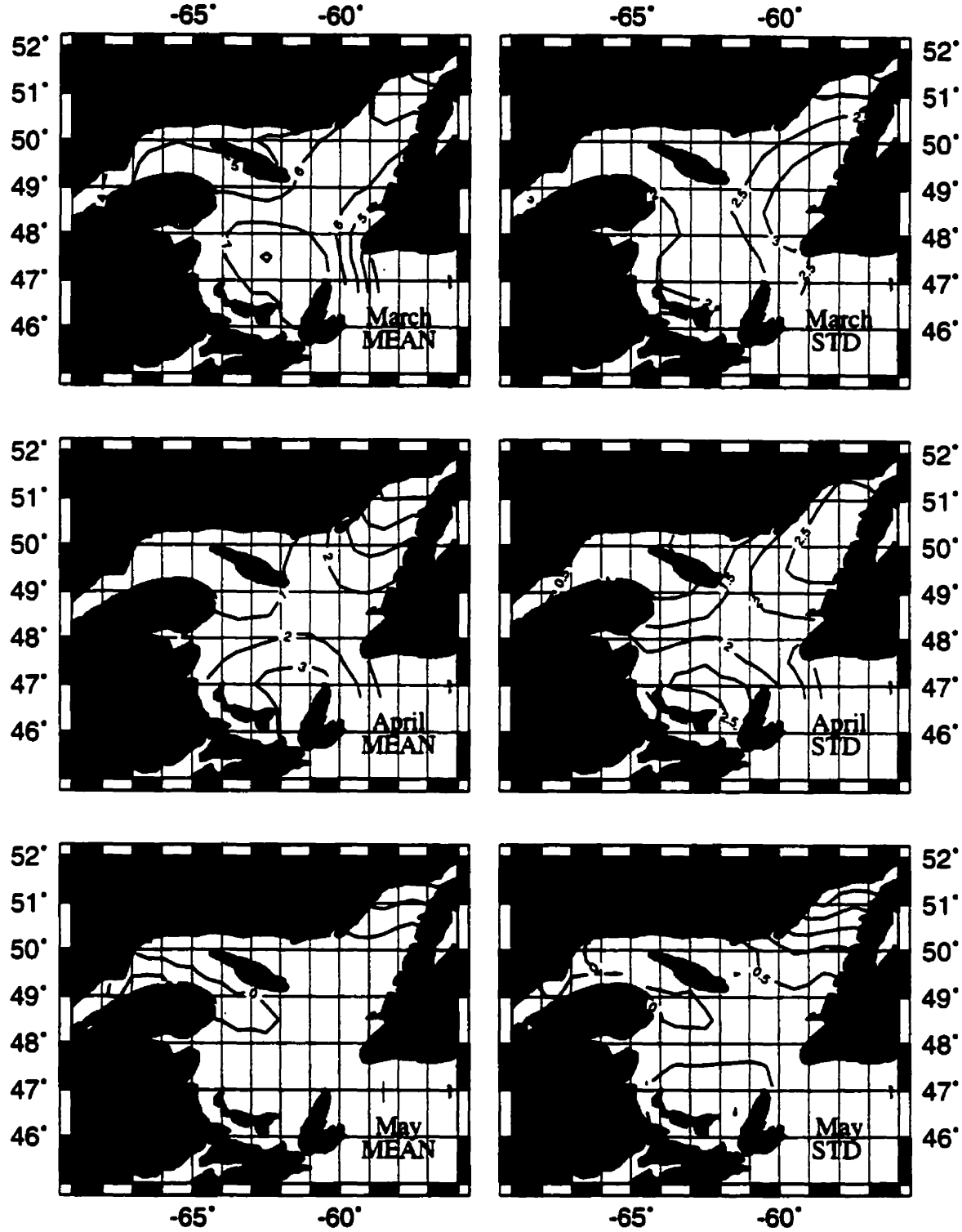

Figure 3.6 (Continued)

Functions) method. Furthermore, the EOF analysis provides a measure of the "importance" of each spatial pattern (mode).

The first EOF mode of the sea-ice cover accounts for most (70%) of the total variance (Figure 3.7). Its monopole structure indicates that the entire Gulf responds simultaneously with an increase or decrease in sea-ice coverage, but of spatially varying amplitude. This mode resembles the standard deviation field (Figure 3.5). The temporal variations of the first EOF mode are dominated by decadal-scale fluctuations, which is confirmed by spectral analysis (Figure 3.8), with a dominant period of 12.8-16 y (>95% CL, i.e. confidence level). Positive (above average) sea-ice anomalies occurred in two periods: 1972-1977 and 1984-1995, with more ice in the latter period.

The second EOF mode, accounting for 10% of the total variance of sea-ice cover in the Gulf, shows a dipole structure. Sea-ice anomalies off Newfoundland were out of phase with the rest of the Gulf. The largest amplitudes of the variation occur near the coast, off Newfoundland. The temporal variations of this mode consist of a combination of interannual and lower frequency oscillations. Spectral analysis (Figure 3.8) indicates that the dominant period for this mode is near 4 y (>95% CL).

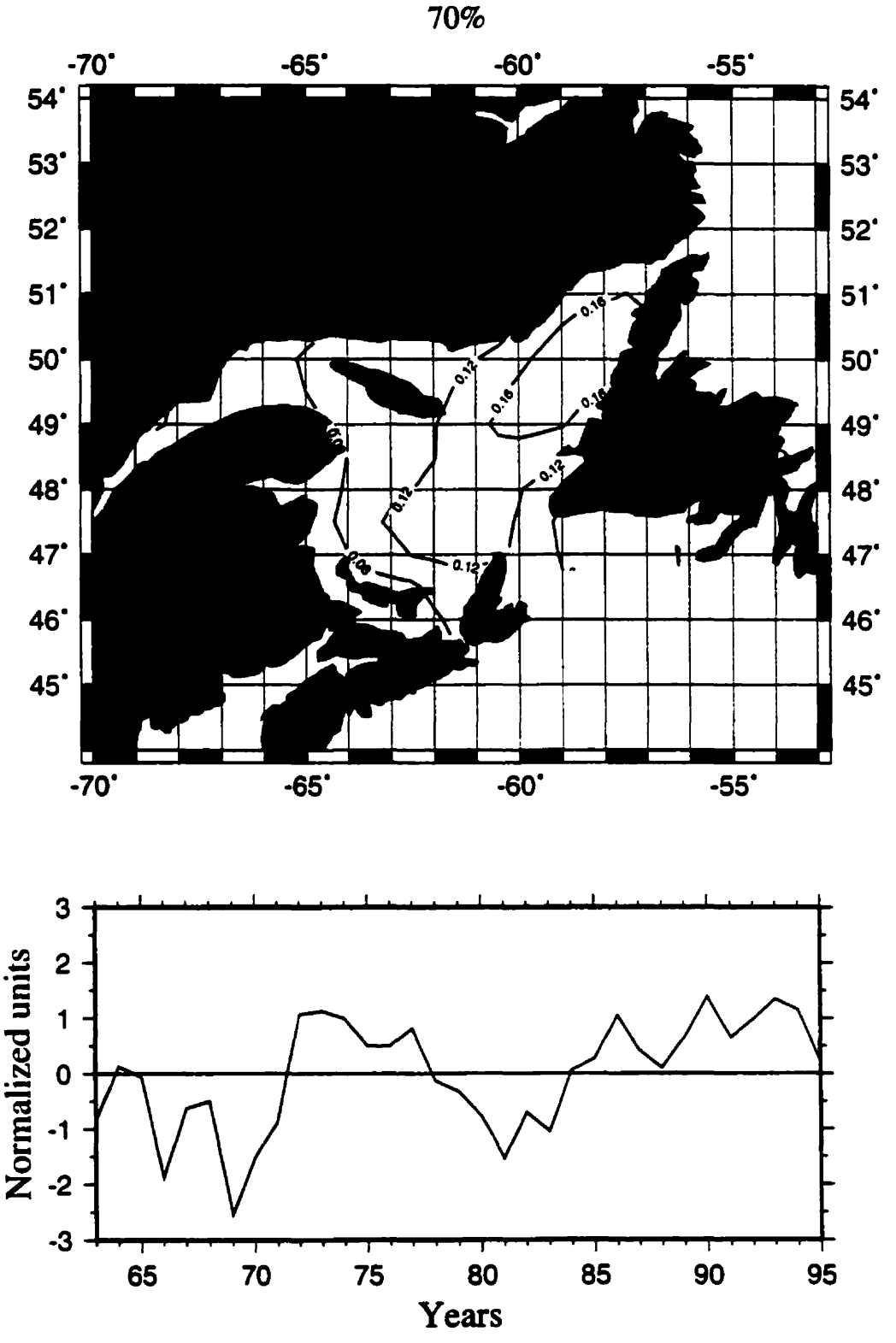

Figure 3.7 Spatial structure (top) and time series (bottom) of EOF mode 1 of mean sea-ice cover averaged for December-June for the period 1963-95 in the Gulf of St. Lawrence.

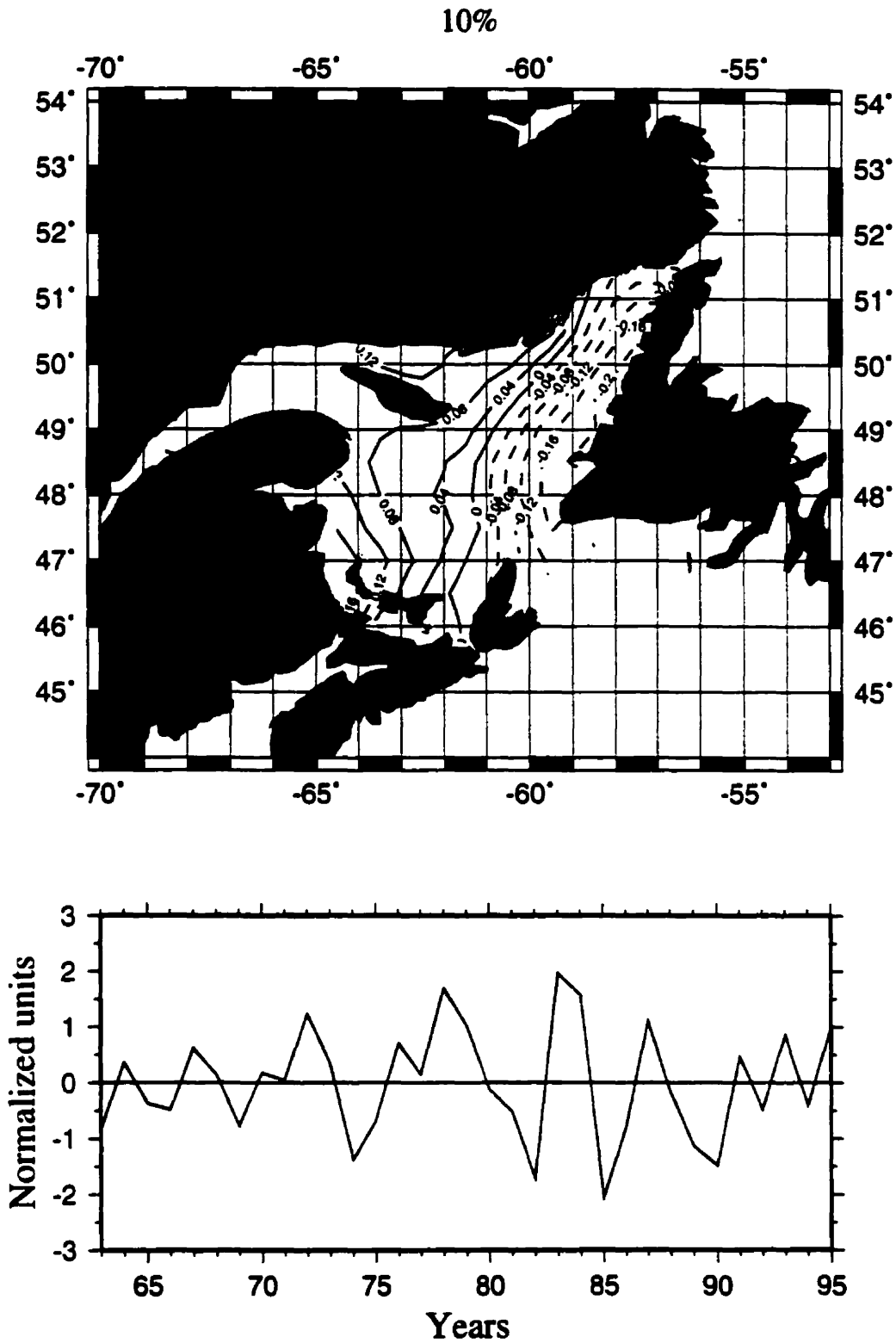

Figure 3.7(Continued). Spatial structure (top) and time series (bottom) of EOF mode 2 of mean sea-ice cover averaged for December-June for the period 1963-95 in the Gulf of St. Lawrence.

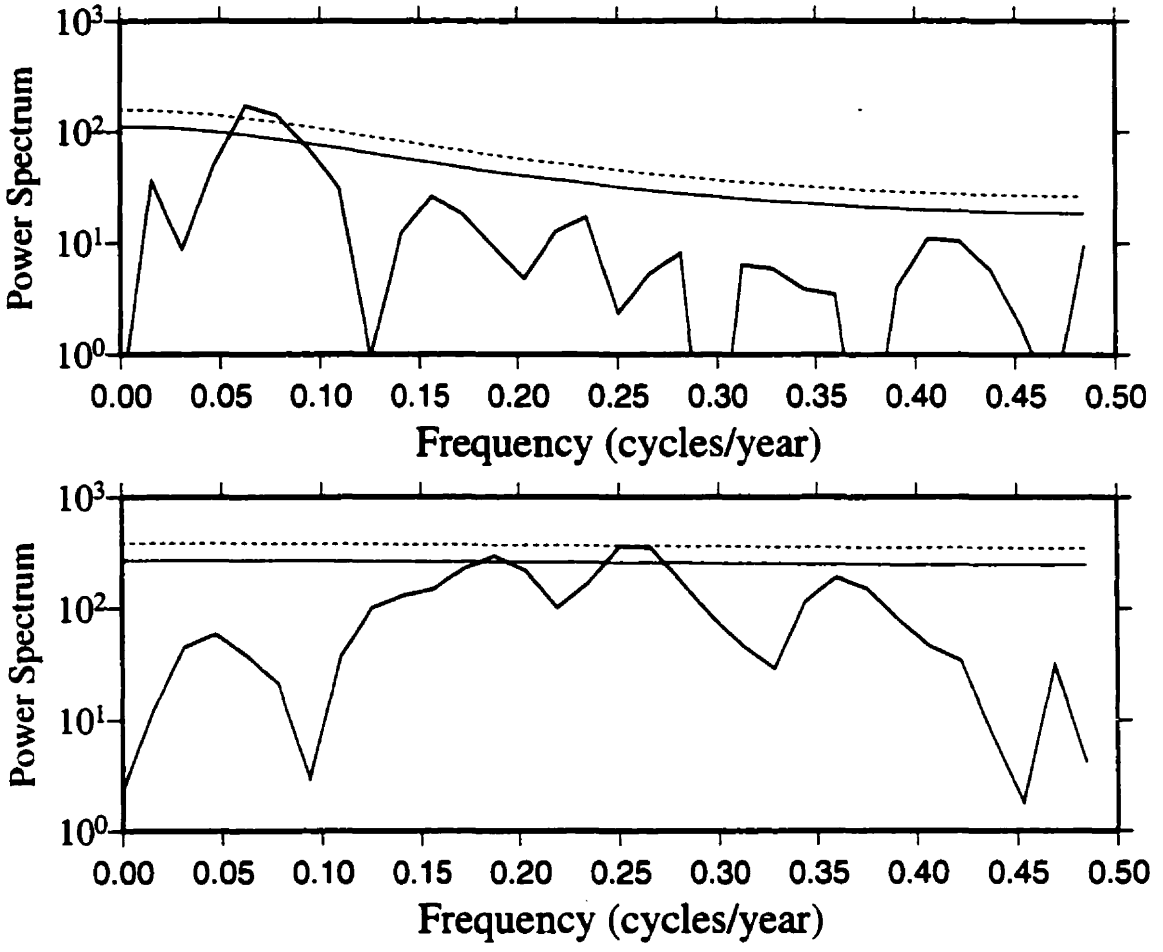

Figure 3.8. Spectra of the first (upper) and second (lower) EOF modes of mean sea-ice cover averaged for December-June for the period 1963-95 with 95% and 90% confidence levels.

3.2.2 TFIP

Compared with sea-ice cover, analysis of interannual variability of the time of first and last ice presence is more complex. Sea-ice cover has a continuous time series at every grid point and therefore is easily adapted to EOF analysis. However, the time series of time of first and last ice presence is not continuous at some grids because there is no ice in some years. In the present study, we only chose those grids with continuous time series of time of first and last sea ice presence. Because the 1968-69 winter was abnormal (to be studied in detail later), with no ice forming over most parts of the Gulf, we started the time series from the winter of 1969-70. The time series contains a 27-year (1970-1996) record.

The standard deviations (Figure 3.4) for the time of first ice range from 10 days on the western shore of the Magdalen Shallows to around 20 days in the area off Newfoundland. The first two leading EOF modes of TFIP account for 37.9% and 34.2% of the total variance, respectively (Figure 3.9). Both modes show dipole structures. The temporal variations of the first mode indicate that the sea ice appeared very late in winters of 1969-70 and 1981-82, and very early in the 1972-73 winter over most parts of the Gulf. The dominant feature in the temporal variations of the second EOF mode is the very early sea ice appearance in the 1989-90 winter. We will later look at these extreme scenarios in detail. Spectral analysis of these two modes (Figure 3.10) indicates that the first mode displays variability with dominant periods of 6.4 y (>95%CL) and 2.1 y (>95%CL) and the second mode with a dominant period of 4 y (>95%CL).

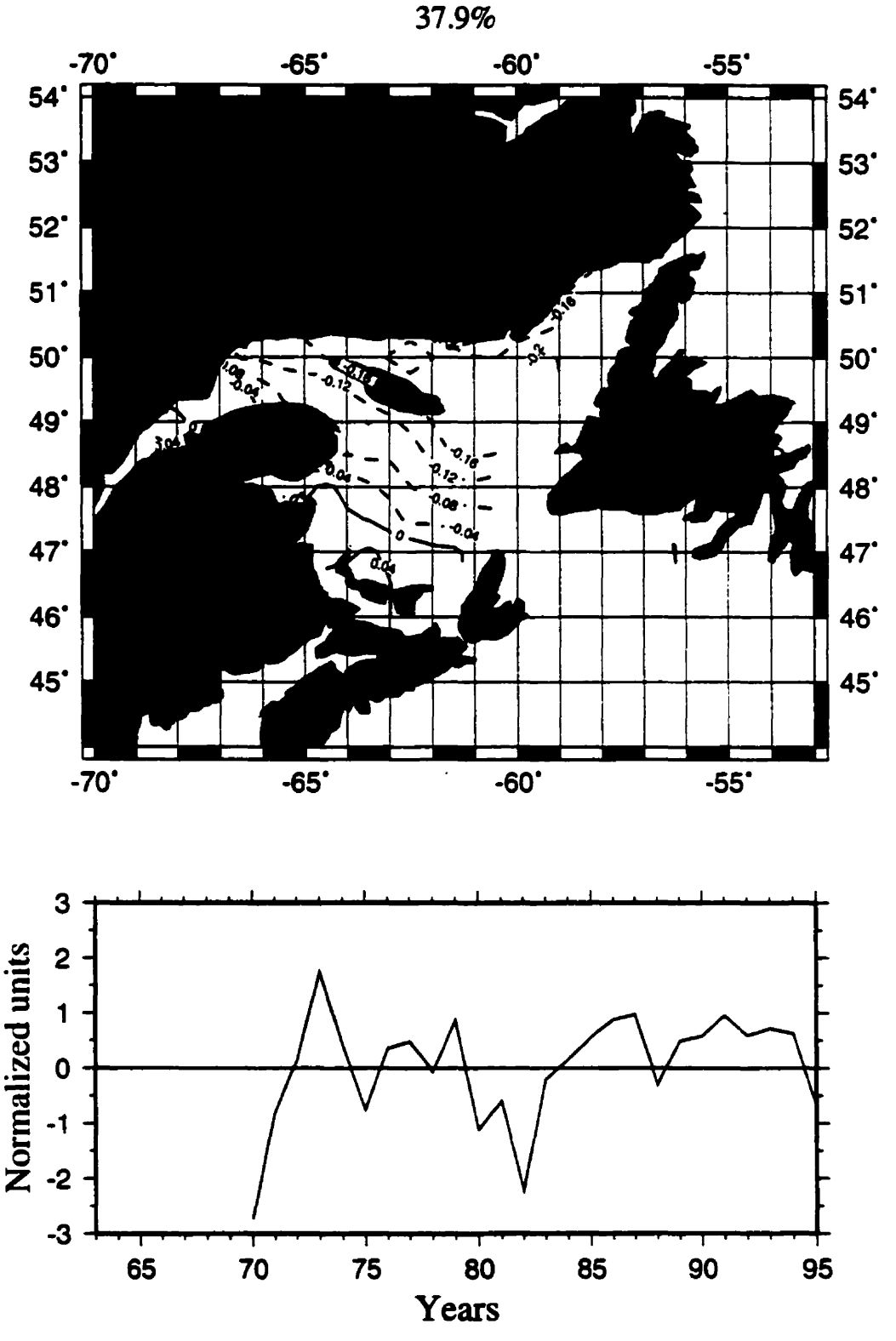

Figure 3.9. Spatial structure (top) and time series (bottom) of EOF mode 1 of time of first ice presence for the period 1970-96 in the Gulf.

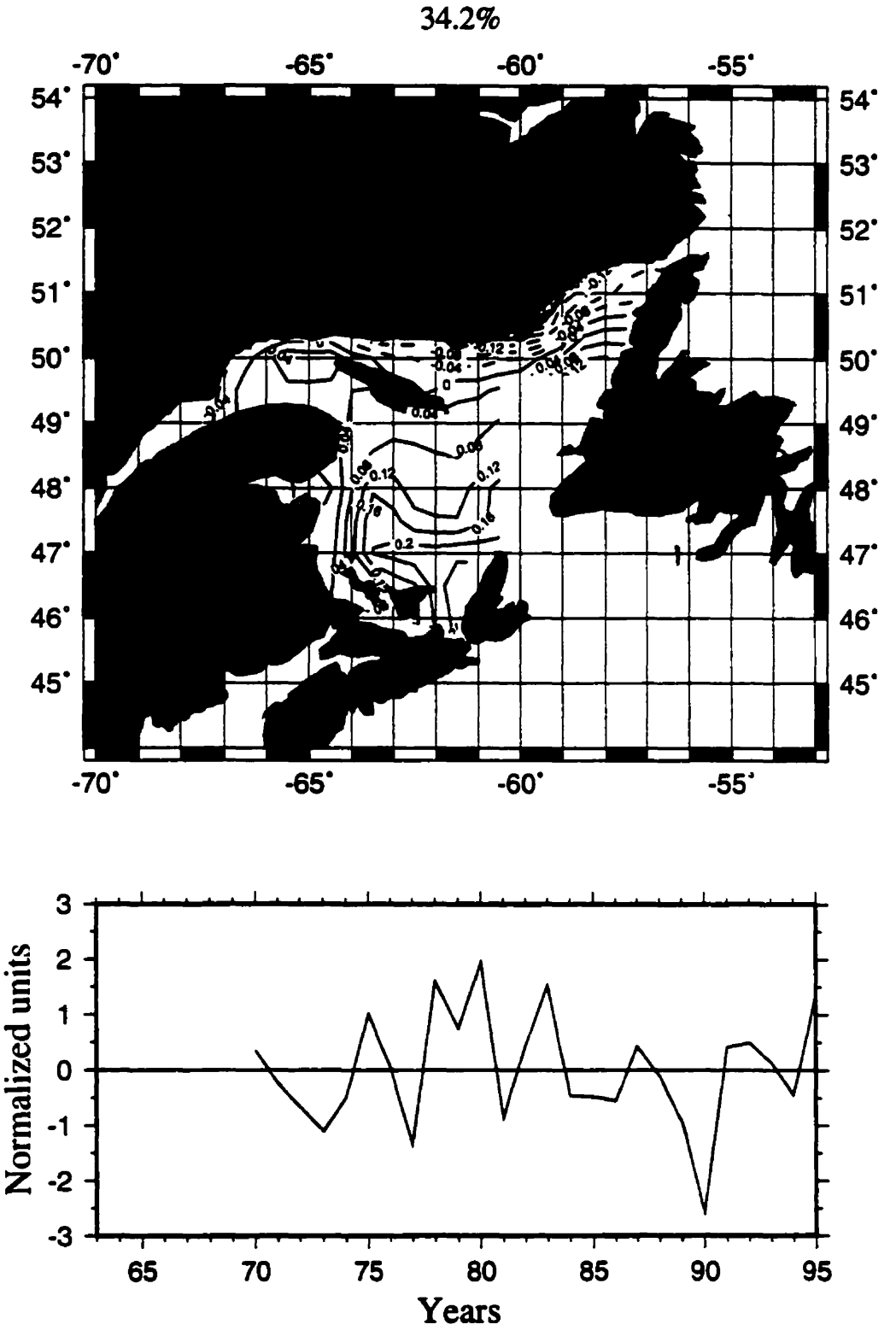

Figure 3.9 (Continued). Spatial structure (top) and time series (bottom) of EOF mode 2 of time of first ice presence for the period 1970-96 in the Gulf.

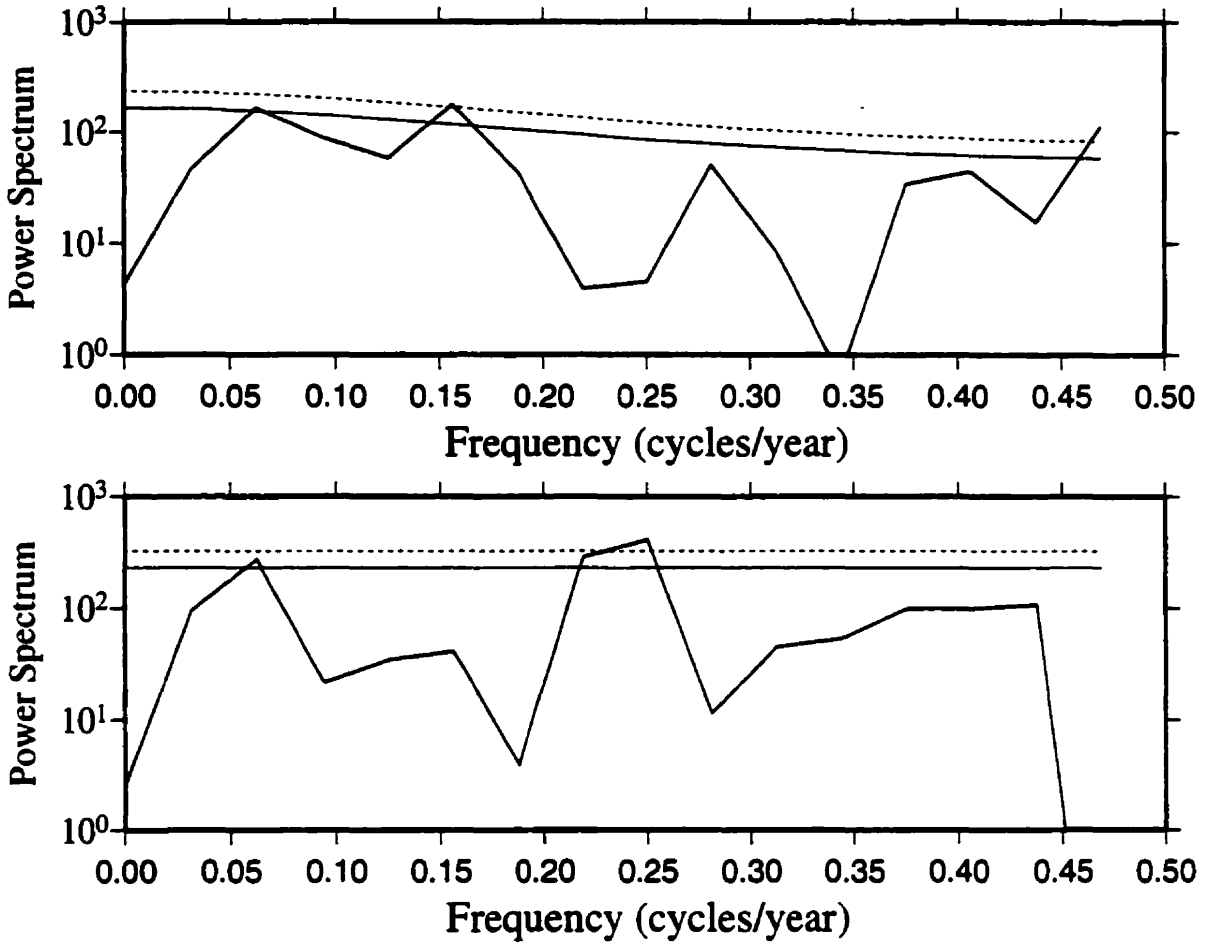

Figure 3.10 Spectra of the first (upper) and second (lower) EOF modes of time of first ice presence for the period 1970-96 with 95% and 90% confidence levels.

3.2.3 TLIP

The standard deviations of the TLIP (Figure 3.4) range from 10-12 days in the St. Lawrence Estuary to around 26 days in the northeast coastal regions. Similar to the analysis on TFIP, we undertook an EOF analysis for TLIP using 1970-95 data on those grids with a continuous time series. The first two leading EOF modes account for 55.3% and 22.7% of the total variance, respectively (Figure 3.11). Both modes show weak dipole structures with an out-of-phase relationship between the anomalies on the western shore and the rest of the Gulf for the first mode and between the Strait of Belle Isle region and the rest of the Gulf for the second mode. The first EOF mode shows the largest amplitude of TLIP variability in the northeast Gulf. Spectral analysis (Figure 3.12) shows that the first mode displays variability with dominant periods of 16 y (>90%CL), 4 y (>90%CL), and 2.1 y (>95%CL) and the second mode displays no dominant periods above the 90% confidence level.

3.2.4 SID

The standard deviations of sea-ice duration (Figure 3.4) range from 16-18 days in the St. Lawrence Estuary to around 36 days in the area off mid-Newfoundland. Not surprisingly, the spatial pattern of the sea-ice cover averaged over December-June (Figure 3.5) is similar to the sea-ice duration (Figure 3.4). Their standard deviations exhibit a similar relationship. The correlation between SIC for December-June and SID by grid point was estimated, then the correlation coefficients averaged over all grids to obtain a mean correlation. The mean correlation is 0.92, indicating December-June SIC

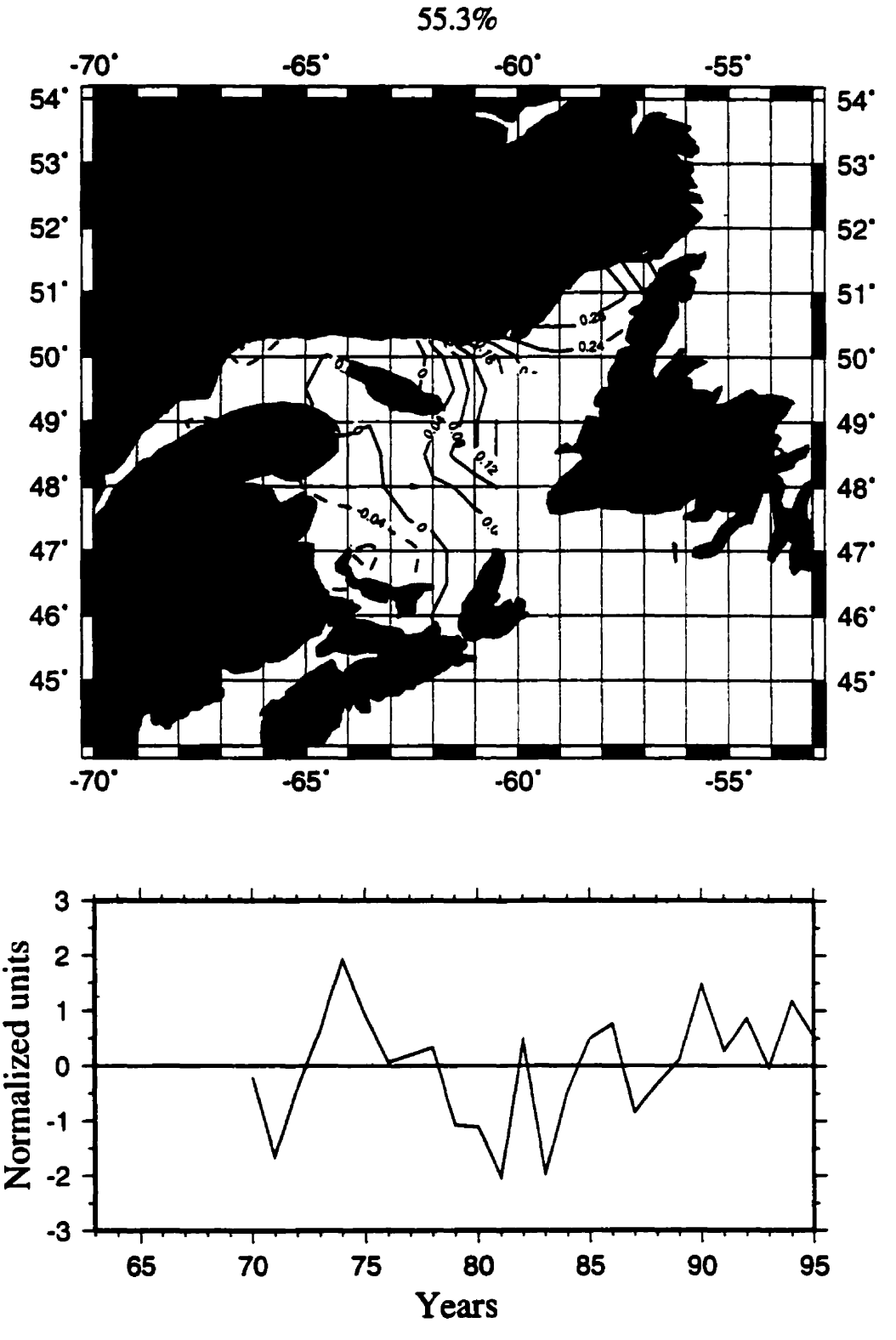

Figure 3.11. Spatial structure (top) and time series (bottom) of EOF mode 1 of time of last ice presence for the period 1970-95 in the Gulf.

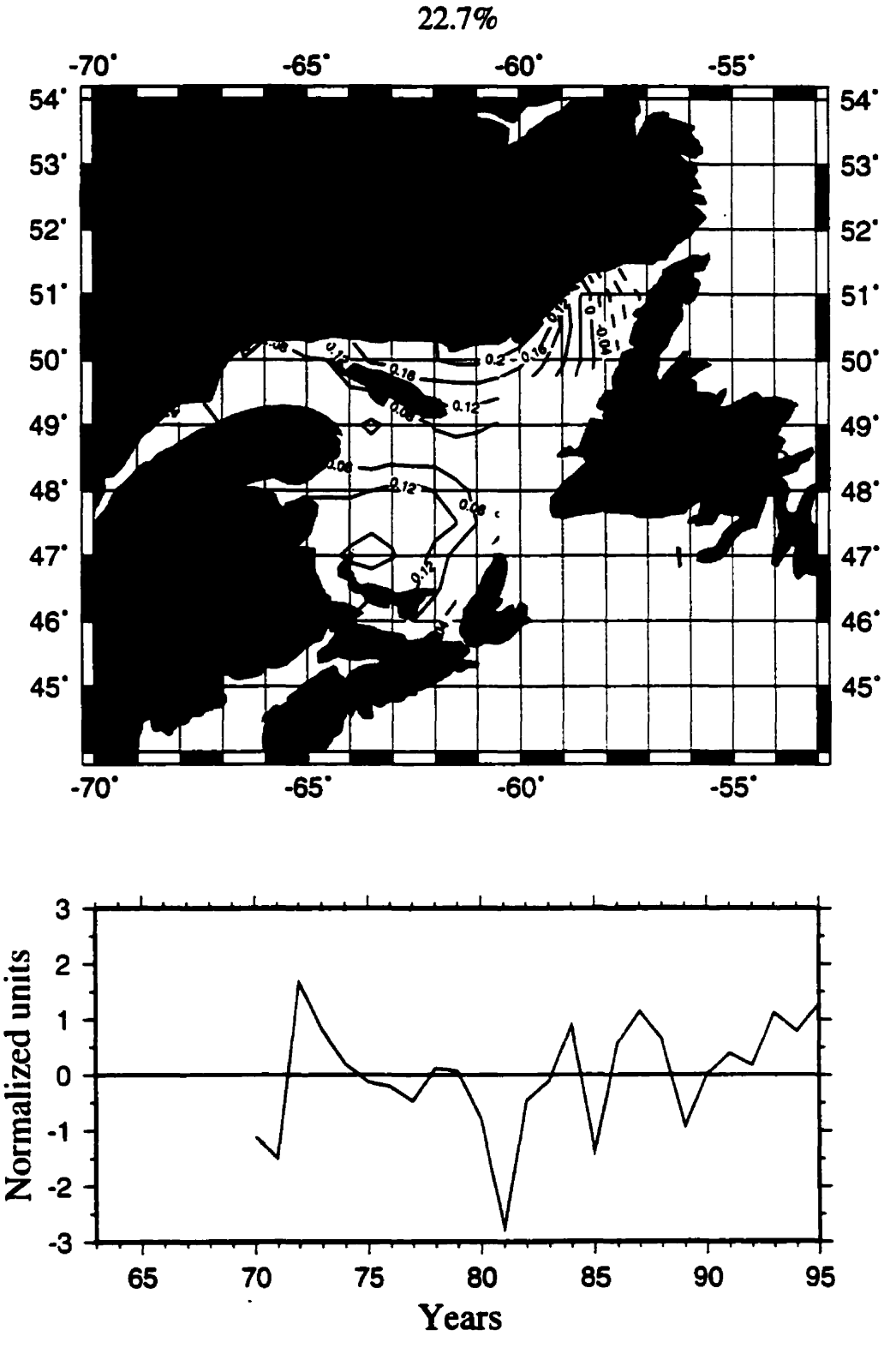

Figure 3.11 (Continued). Spatial structure (top) and time series (bottom) of EOF mode 2 of time of last ice presence for the period 1970-95 in the Gulf.

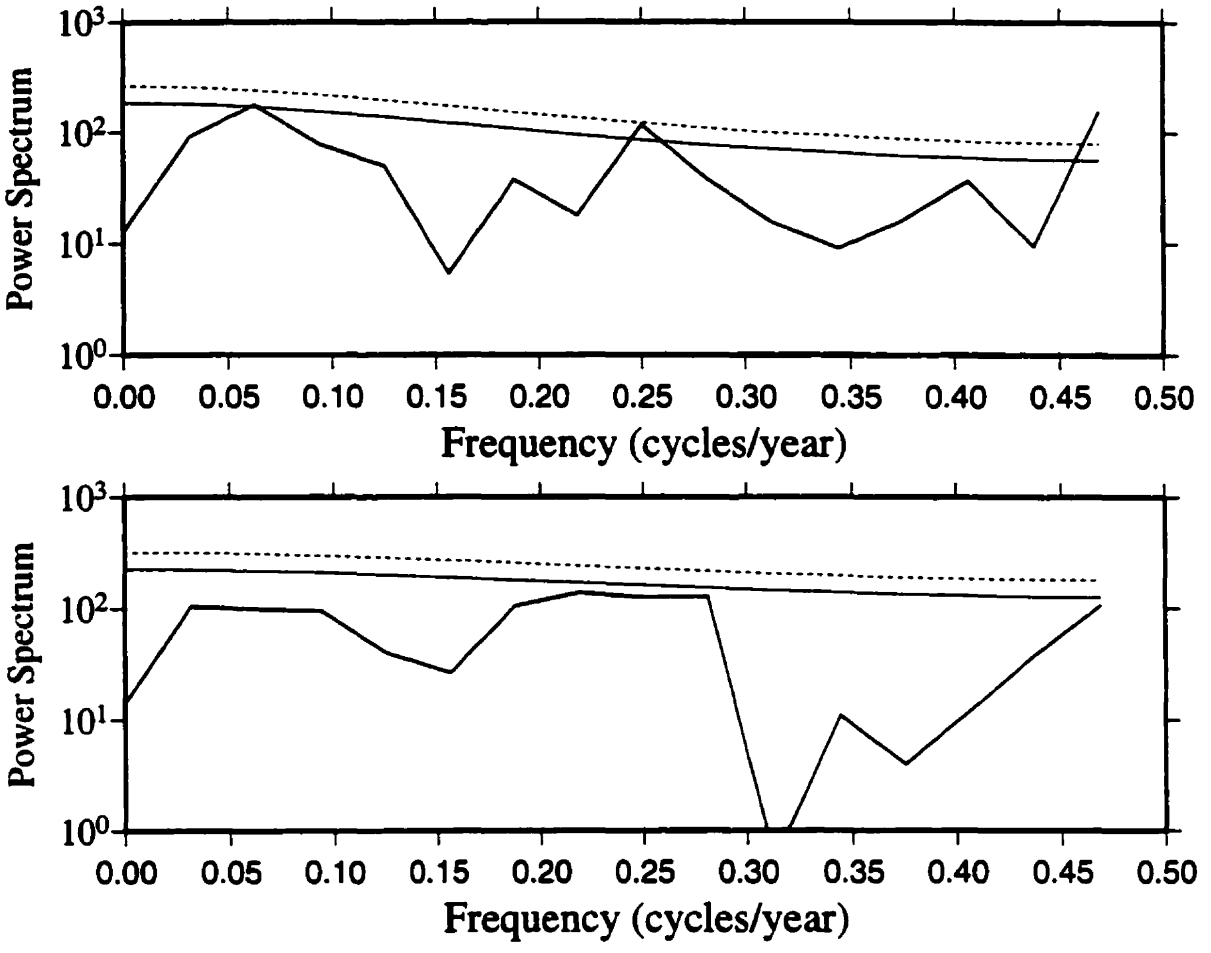

Figure 3.12 Spectra of the first (upper) and second (lower) EOF modes of time of last ice presence for the period 1970-95 with 95% and 90% confidence levels.

is strongly correlated with SID. The results of the EOF and spectral analysis (not shown) of sea-ice duration are similar with those of mean sea-ice cover averaged over December-June (Figures 3.7 and 3.8).

3.2.5 Extreme sea ice scenarios

In this subsection, we describe extreme sea ice scenarios: years with severe ice or light ice.

3.2.5.1 Years with severe ice

Figure 3.13 shows monthly sea-ice cover and its anomalies from the long-term means (1963-96) during the winter of 1989-90, the most severe ice season on record. The anomalies in most parts of the Gulf were positive throughout the winter, but the regions of the largest sea ice anomalies differed monthly. In December, the largest sea ice anomalies occurred in the southwest, while in January, the largest anomalies (> 5/10) were located in the southern part of the Gulf. In contrast, the largest sea ice anomalies in February (> 5/10) appeared in the area off Newfoundland, near Cabot Strait. In March, although the largest anomalies were still present, their intensities were weaker. However, at this time, ice anomalies in the St. Lawrence Estuary and the southwest Gulf were negative, or less ice than normal. In April, the largest positive sea ice anomalies (> 5/10) occurred off mid-Newfoundland. Negative sea ice anomalies were observed in the southern Gulf. In May, the largest sea ice anomalies were found in the Strait of Belle Isle region. During the entire ice season, the largest sea ice anomalies occurred in January.

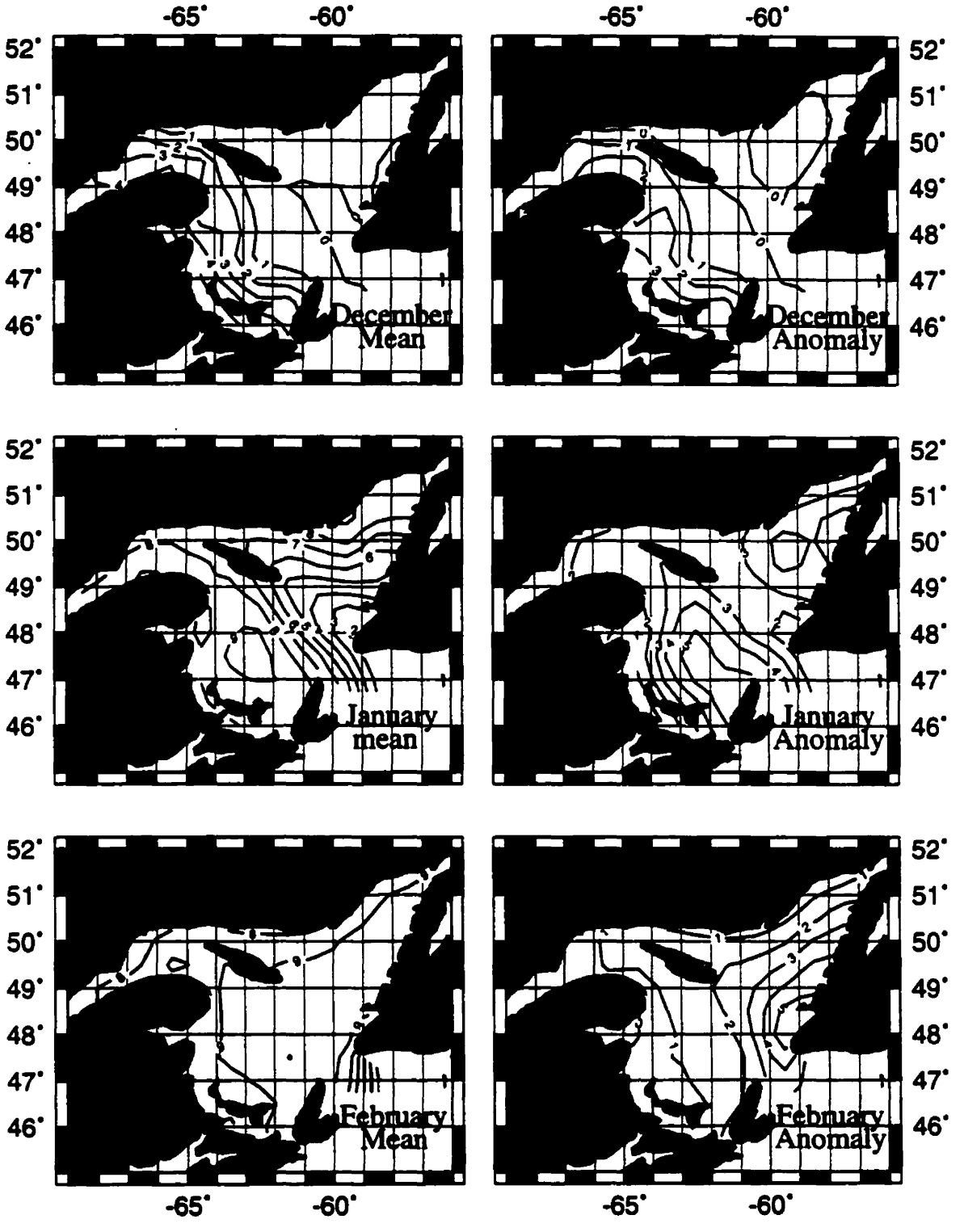

Figure 3.13 Monthly sea-ice cover in the 1989-90 sea ice season (left) and its anomalies (right) from long-term means (1963-96).

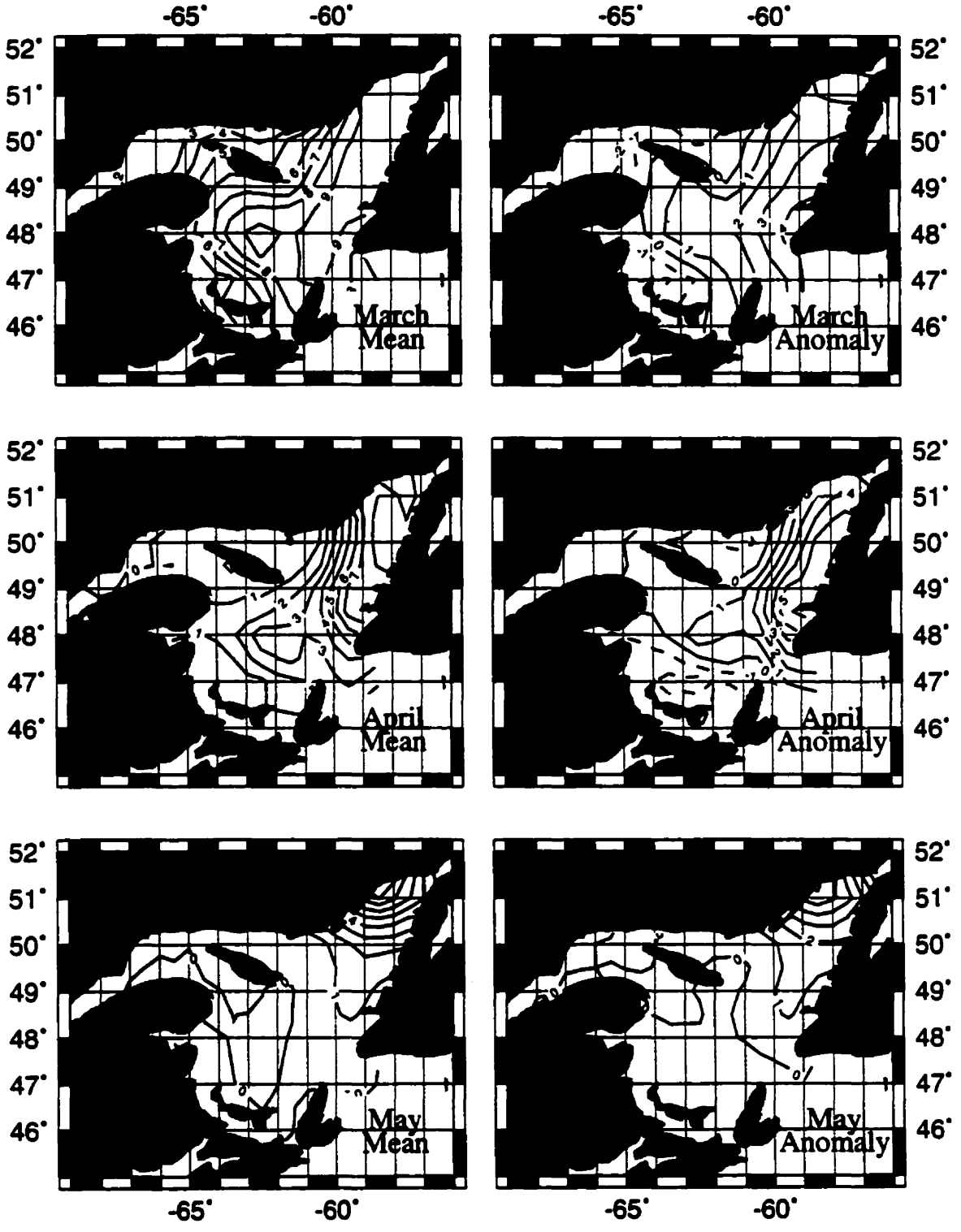

Figure 3.13 (Continued)

In addition, sea-ice cover in February shows the entire Gulf is basically covered by sea ice (> 8/10) for this month.

Sea ice in the winter of 1989-90 appeared earlier than normal over the entire Gulf, and earlier by more than 20 days in the southern Gulf (Figure 3.14). Over most of the Gulf, sea ice disappeared later than normal, with a maximum delay of 20 days off mid-Newfoundland. However, on the southern Magdalen Shallows, sea ice disappeared earlier than normal. As expected, the anomalies of sea-ice duration and mean sea-ice cover averaged over December-June were positive with the largest anomalies (nearly two months longer-than-normal for sea-ice duration and 2/10 larger-than-normal for sea-ice cover) in the area off mid-Newfoundland.

We conducted composite analysis for the years with severe ice, defined as those years when the time expansion coefficients of the first EOF mode of mean sea-ice cover over December-June (Figure 3.7) were positive and greater than one standard deviation. With this definition, the 1971-72, 1972-73, 1985-86, 1989-90, 1992-93, and 1993-94 winters were years with severe ice. Figure 3.15 shows the composite monthly sea-ice cover and its anomalies from long-term means (1963-96) for those extreme ice years. The anomalies of sea-ice cover were positive throughout the Gulf during the entire ice season. In December, the largest anomalies were near the western shore region, while in January they (>2/10) were found in the central Gulf. In February and March, the largest sea ice anomalies (>3/10) were located in the area off mid-Newfoundland. In April, the largest sea ice anomalies (>3/10) were in the central Gulf again. In May, they were located in

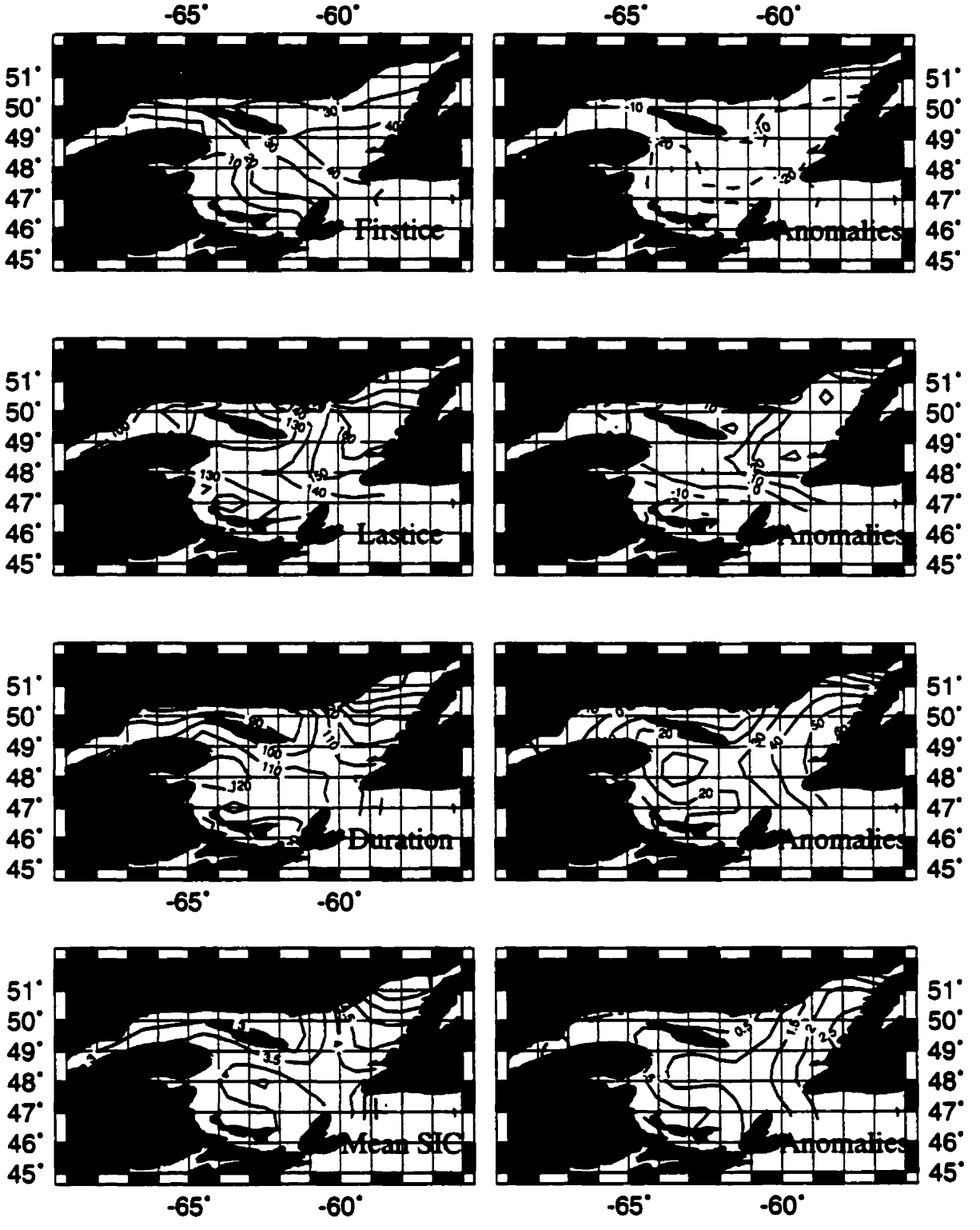

Figure 3.14 The dates of first ice and last ice, duration, and mean sea-ice cover averaged over December-June in the winter 1989-90 and their anomalies with respect to long-term means in the Gulf of St. Lawrence.

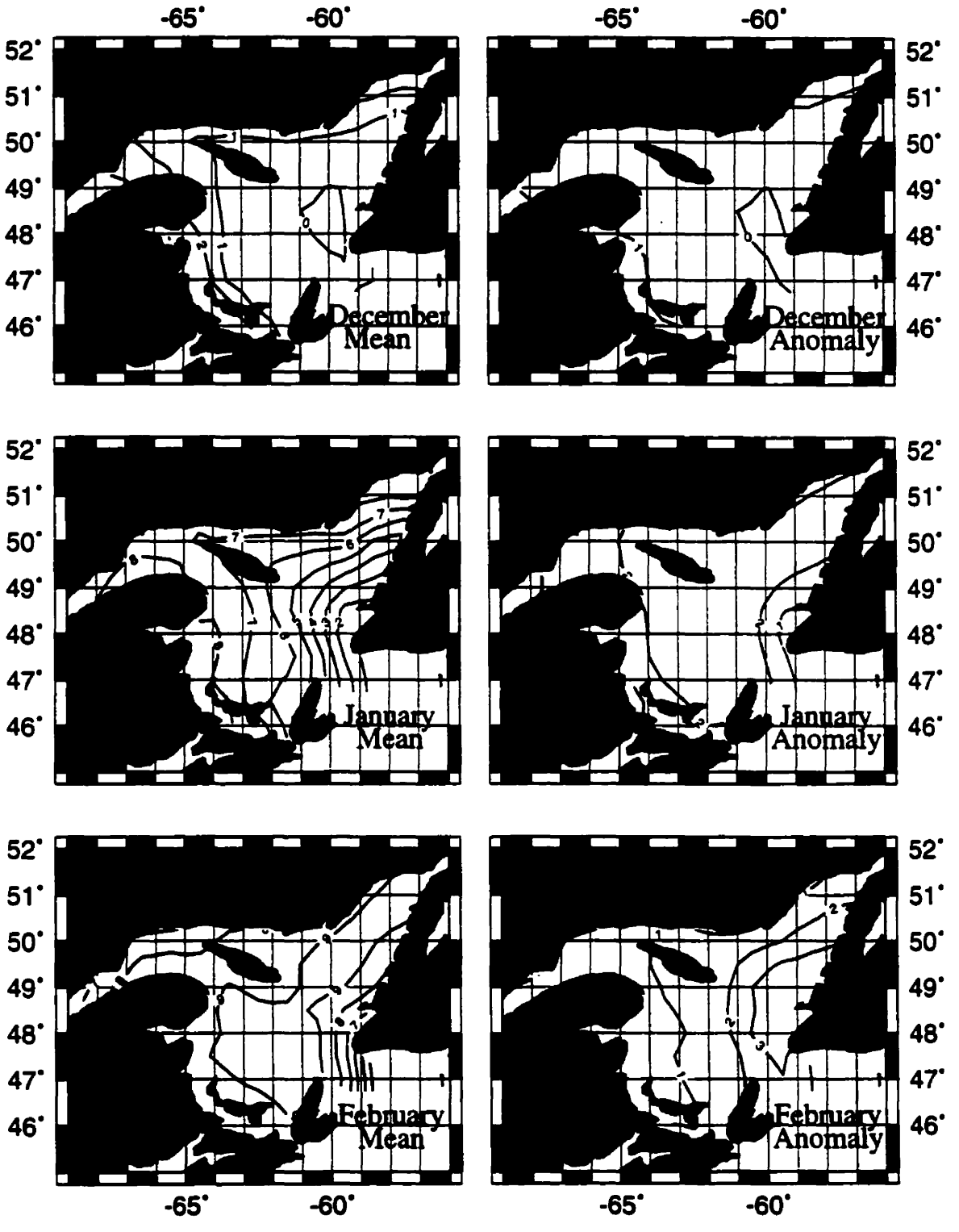

Figure 3.15 Composite monthly sea-ice cover (left) and its anomalies (right) from long-term means (1963-96) for sea ice seasons of 1971-72, 1972-73, 1985-86, 1989-90, 1992-93, and 1993-94 in the Gulf of St. Lawrence.

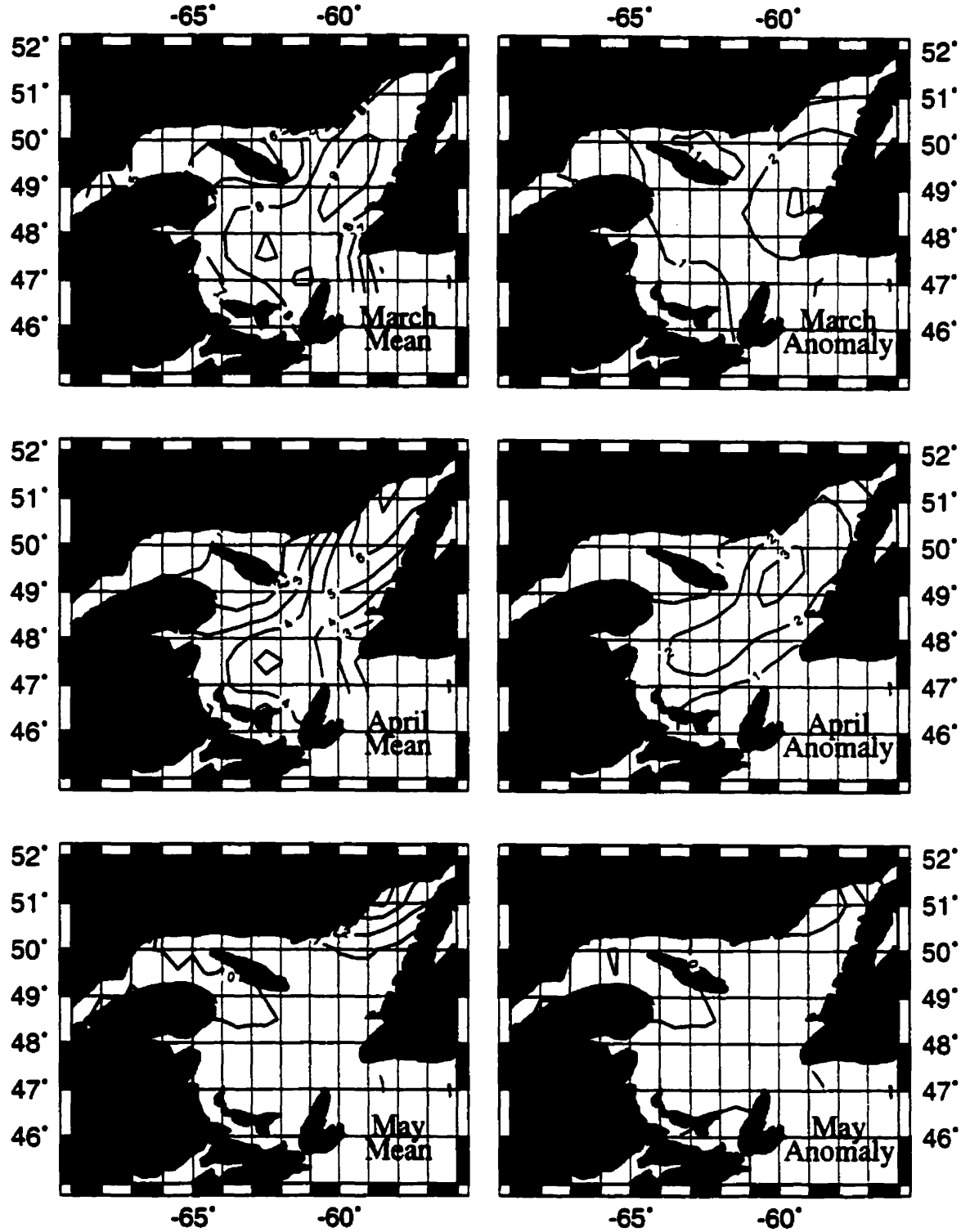

Figure 3.15 (Continued)

the Strait of Belle Isle region. On the Gulf-wide scale, the largest sea ice anomalies occurred in January and April, i.e., sea ice formation and melting times in the central and eastern Gulf.

The anomalies of the TFIP, TLIP, SID, and mean SIC over December-June (Figure 3.16) indicate that the sea ice appeared 10 days earlier than normal in coastal areas for those winters and disappeared more than 10 days later over the entire Gulf. The anomalies of sea-ice duration and mean sea-ice cover are all positive with the largest anomalies (one month longer for SID and 1/10 larger for SIC) located in the area off mid-Newfoundland.

3.2.5.2 Years with light ice

Figure 3.17 shows monthly sea-ice cover and its anomalies in the winter of 1968-69, the lightest ice season in the period of 1963-96. The anomalies in the entire Gulf were negative throughout the whole ice season. No ice appeared in the central and eastern Gulf during this winter and there was much less ice in the coastal regions. Furthermore, sea ice was only present from January to March. The largest negative anomalies of sea-ice cover (> 8/10) occurred in central Gulf in February and March. The ice, which did form, appeared late, left early and was there for only a short duration (Figure 3.18).

Similar to the severe ice years, light ice years were defined as those when the time expansion coefficients of the first EOF mode of mean sea-ice cover over December-June (Figure 3.7) were negative, with the amplitudes greater than one standard deviation. With this definition, the 1965-66, 1968-69, 1969-70, 1980-81, and 1982-83 winters were

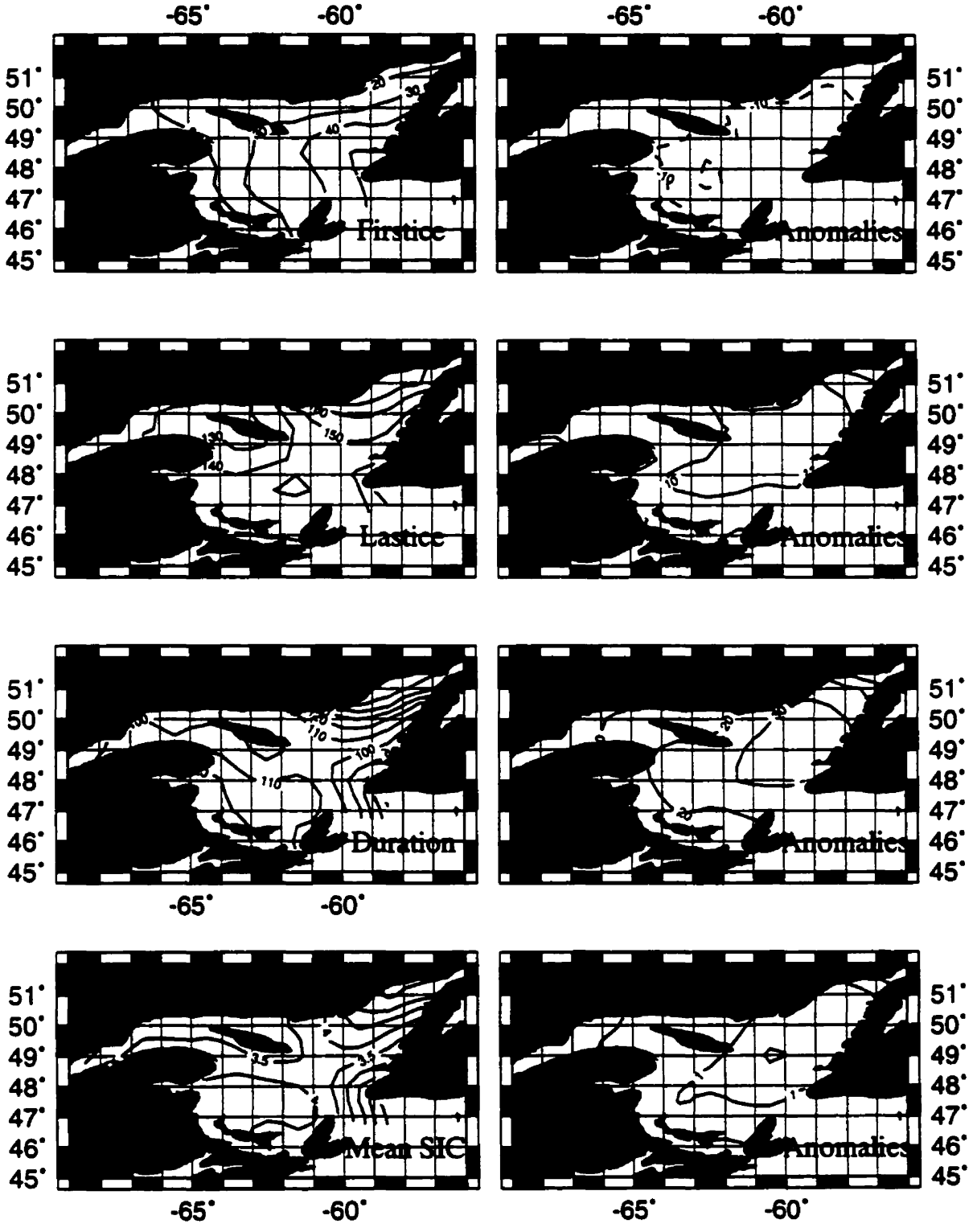

Figure 3.16 The mean dates of first ice and last ice, duration, and mean sea-ice cover averaged over December-June for 1971-72, 1972-73, 1985-86, 1989-90, 1992-93, 1993-94 winters and their anomalies, from respective long-term means in the Gulf of St. Lawrence.

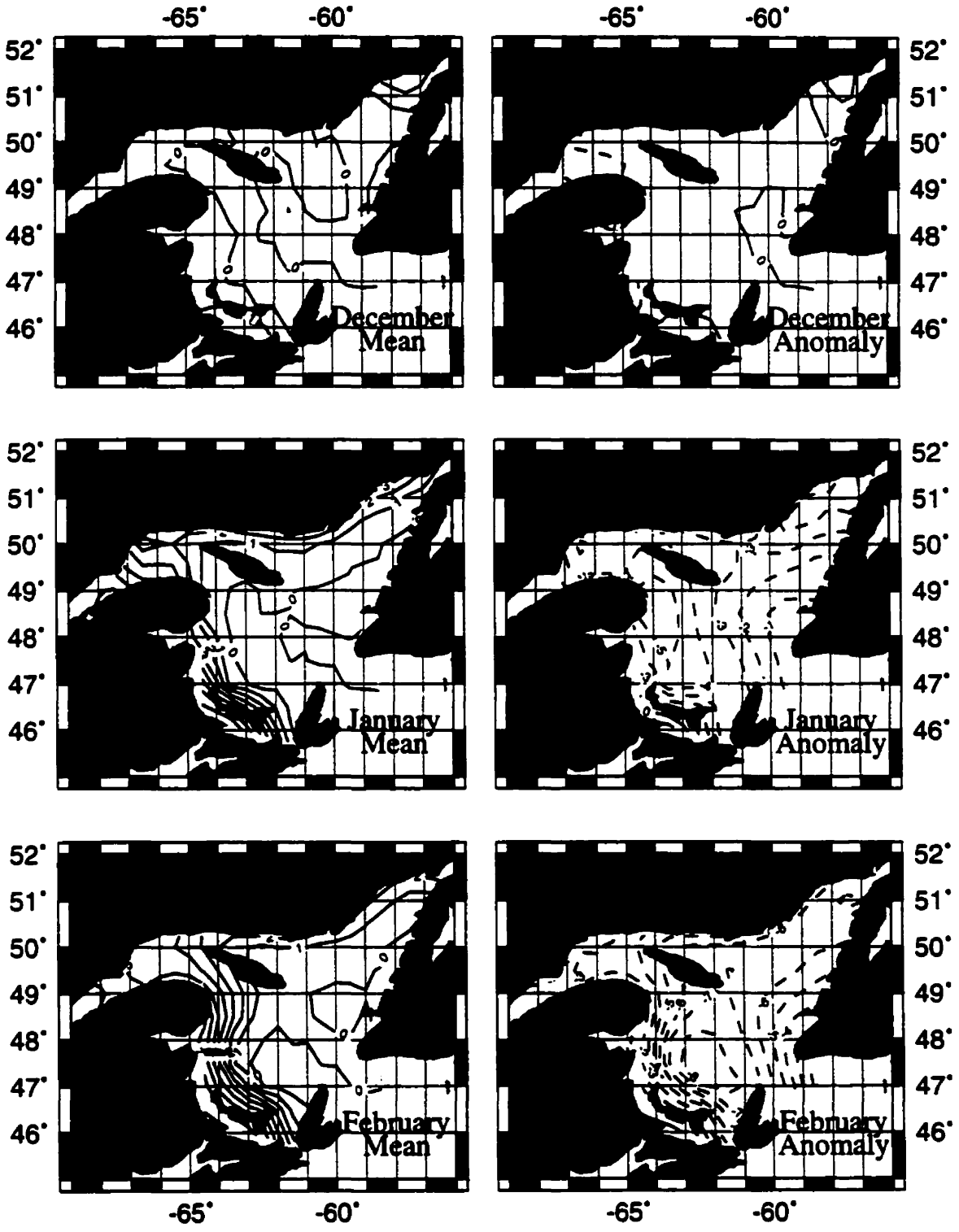

Figure 3.17 Monthly sea-ice cover (left) and its anomalies (right) from the long-term means (1963-96) for the 1968-69 ice season in the Gulf of St. Lawrence.

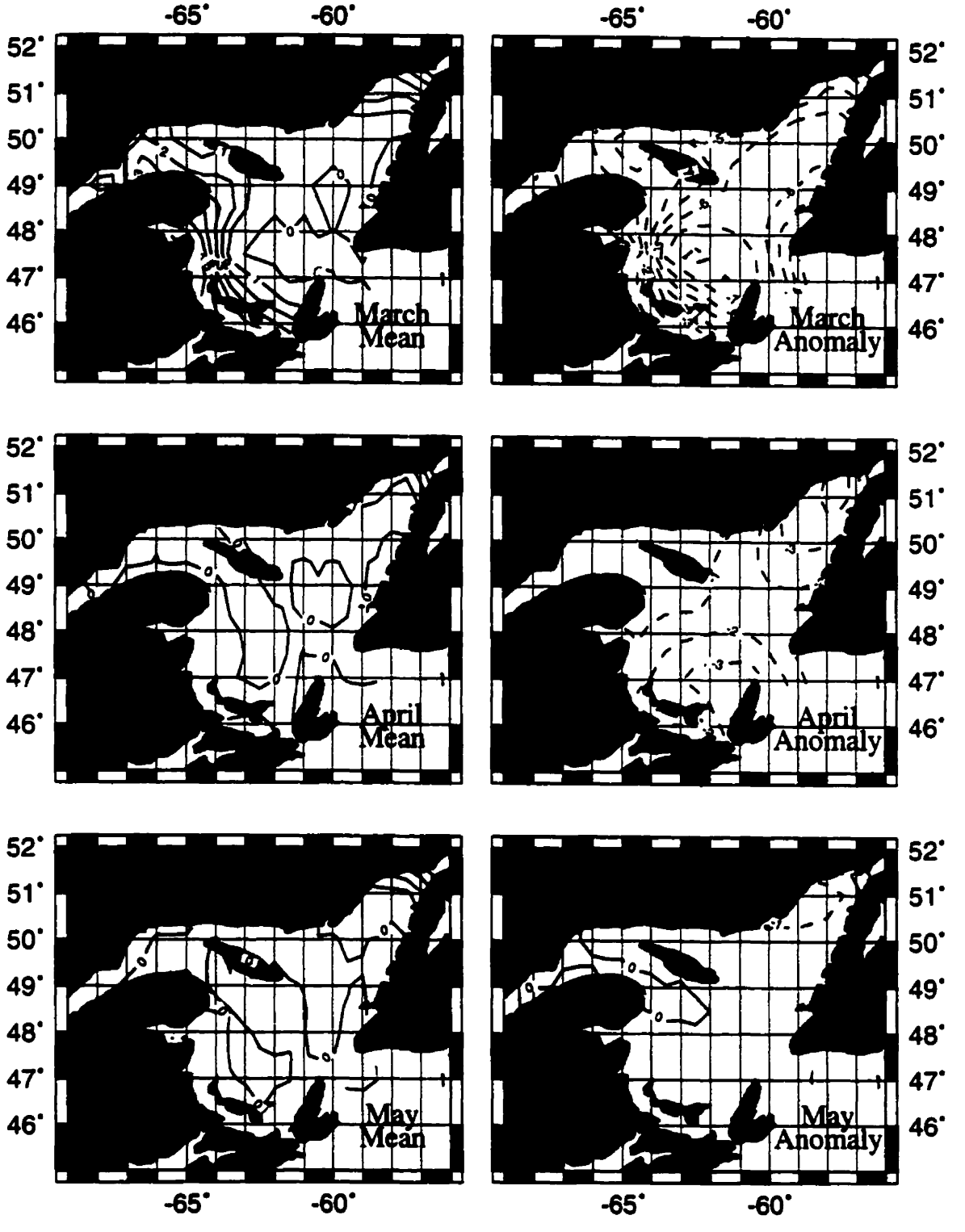

Figure 3.17 (Continued)

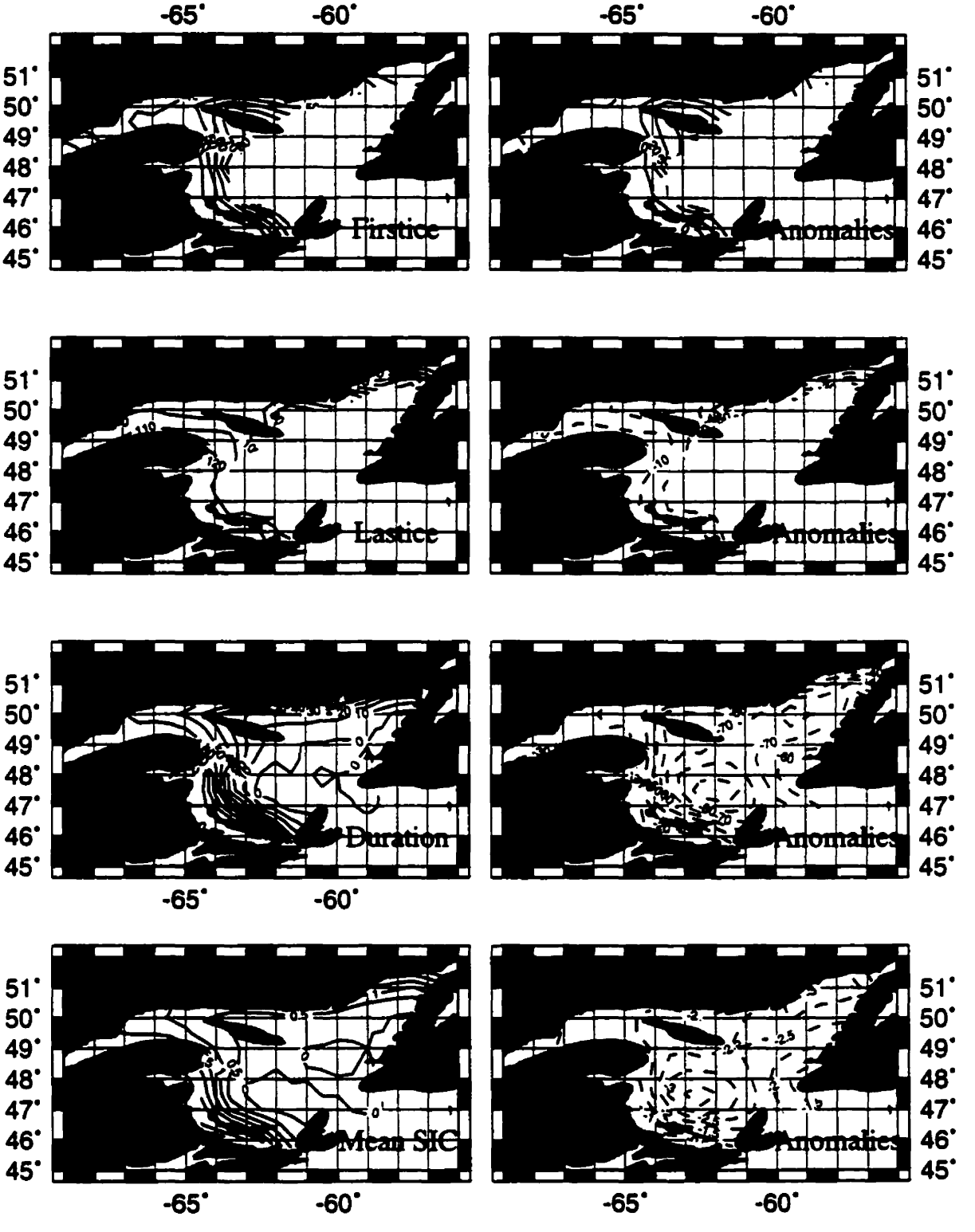

Figure 3.18 The dates of first ice and last ice, duration, and mean sea-ice cover averaged over December-June in the winter 1968-1969 and their anomalies with respect to long-term means in the Gulf of St. Lawrence.

classified as light ice years. Figure 3.19 shows the composite monthly sea-ice cover and anomalies from long-term means (1963-96) for those winters. The anomalies of sea-ice cover were all negative throughout the Gulf from January. The largest anomalies were in the central Gulf in February (> 4/10) and in the area off mid-Newfoundland in March (> 5/10). The anomalies of TFIP, TLIP, SID, and mean SIC over December-June (Figure 3.20) indicate that the sea ice appeared more than 10 days later than normal in the central and eastern Gulf and left 10-30 days earlier over the entire Gulf. In April, sea ice was found only in the Strait of Belle Isle region and a small area in the southwestern Gulf. The anomalies of TLIP, SID, and mean SIC were all negative with the largest values in the area off mid-Newfoundland, where sea ice disappeared 30 days earlier, SID is 50 days shorter (only around 10 days), and SIC is 2/10 less (only 0.5/10).

3.3 Summary

Using long-term (1963-96) sea ice observations, we analyzed intraseasonal and interannual variability of sea-ice cover in the Gulf of St. Lawrence. For the intraseasonal variations, sea-ice cover over different sub-regions displayed contrasting features. The largest intraseasonal variations of sea-ice cover occur in the Strait of Belle Isle region and southwestern Gulf, where the mean sea-ice cover is largest and sea-ice duration is longest, exceeding 140 days in the former region. For the interannual variability of sea-ice cover, the sea-ice cover averaged over December-June and sea-ice duration were found to display both interannual and decadal-scale variability, with the latter accounting for a large part of the total variance. The largest variability occurs in the area off mid-Newfoundland. The time of first ice presence and time of last ice presence displayed

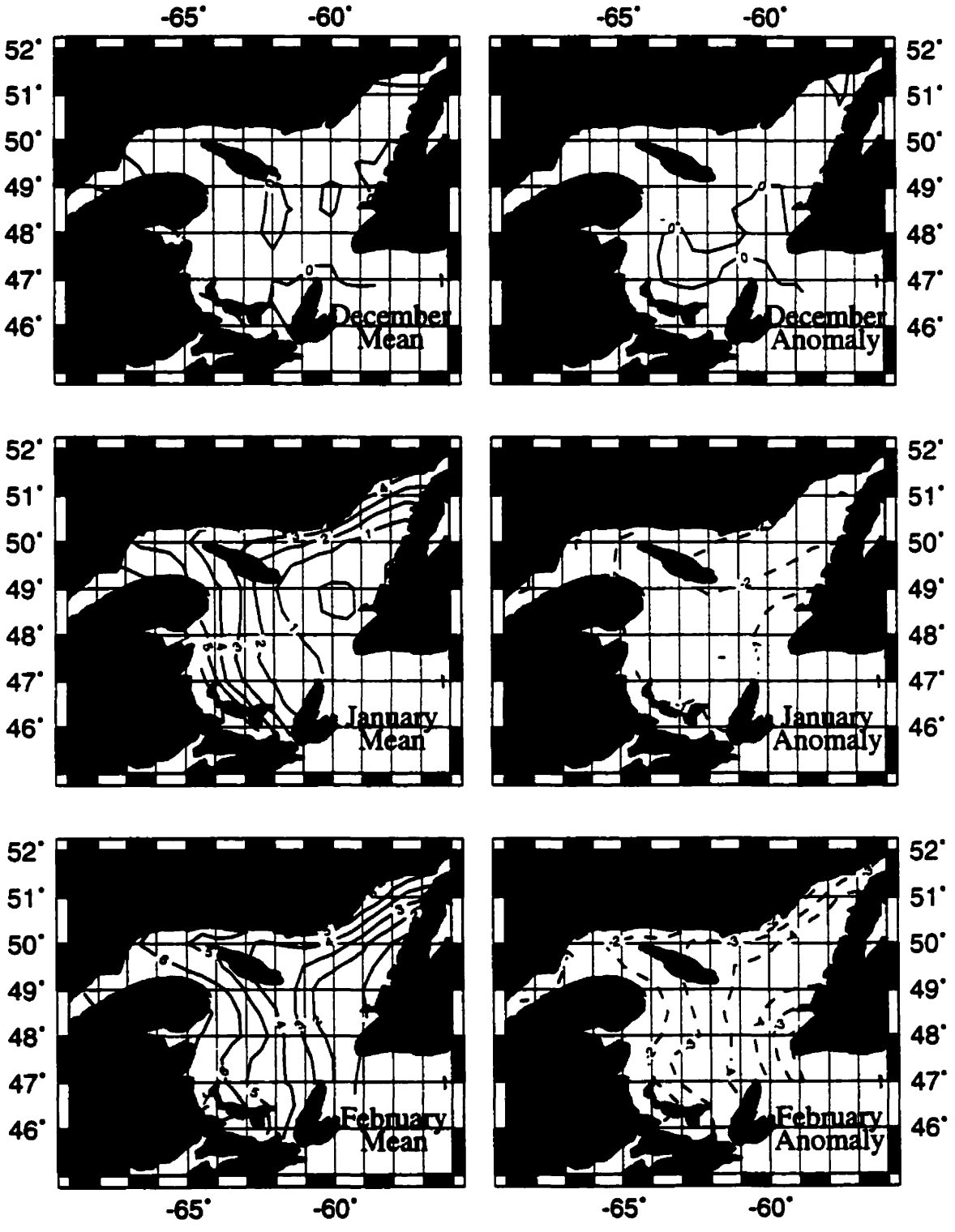

Figure 3.19 Composite monthly sea-ice cover (left) and its anomalies (right) from long-term means (1963-96) for 1965-66, 1968-69, 1969-70, 1980-81, and 1982-83 ice seasons in the Gulf of St. Lawrence.

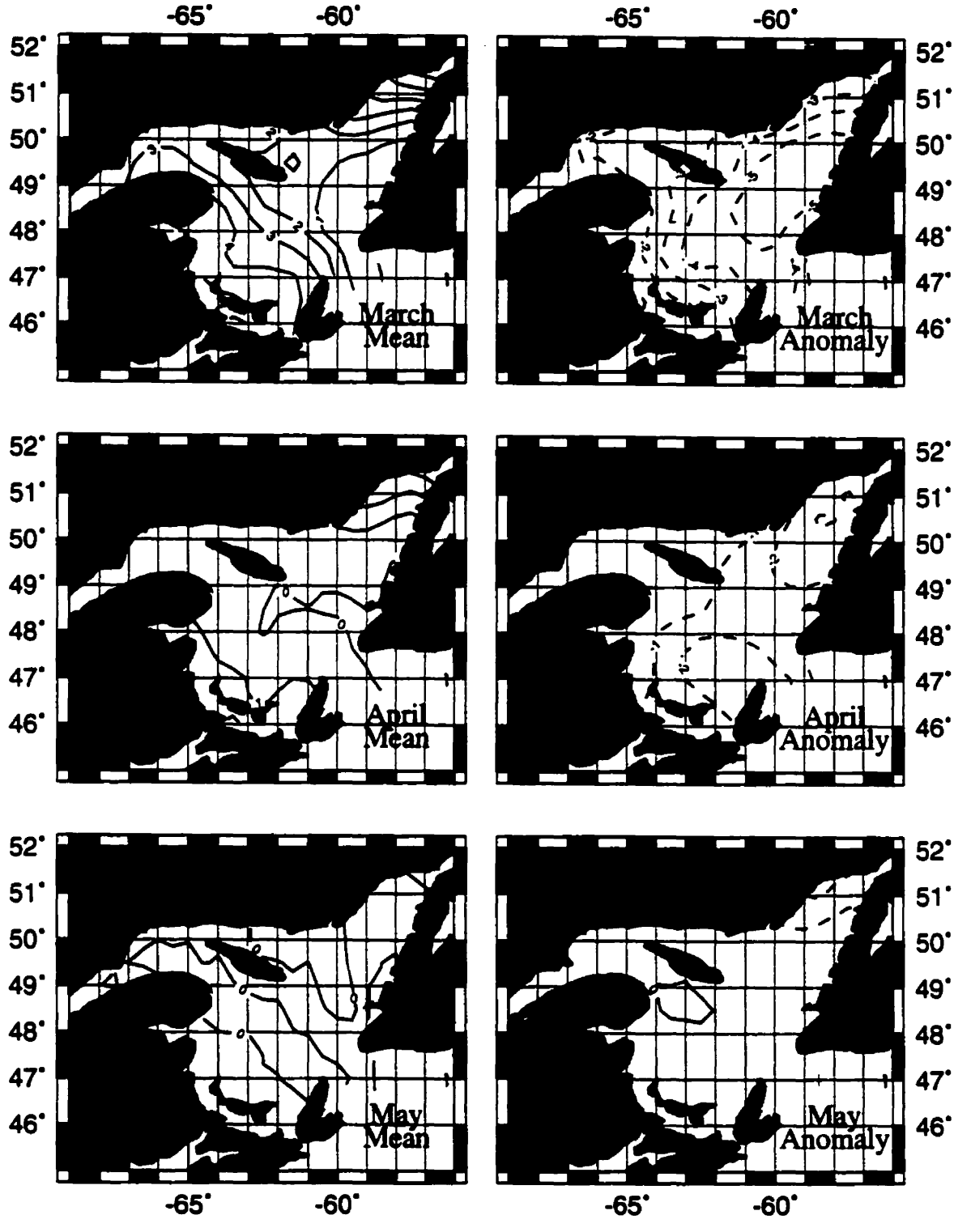

Figure 3.19 (Continued)

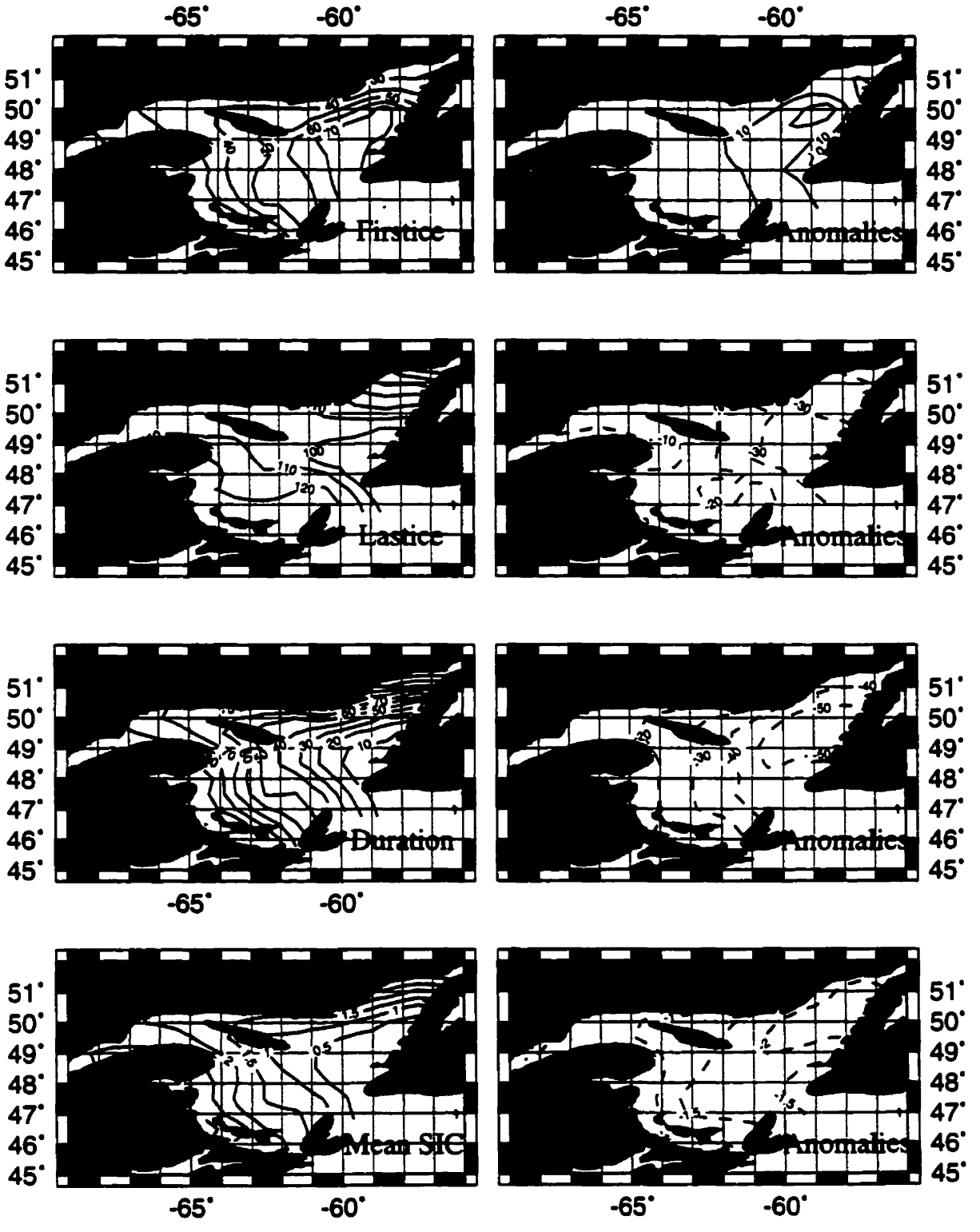

Figure 3.20 The mean dates of first ice and last ice, duration, and mean sea-ice cover averaged over December-June for 1965-66,1968-69,1969-70,1980-81,1982-83 winters and their anomalies, from respective long-term means in the Gulf of St. Lawrence.

interannual-scale variability, with the largest variability in the area off Newfoundland for TFIP and along the northeast coasts for TLIP.

Sea ice conditions in extreme ice years were examined. In severe ice years, sea ice appeared 10 days earlier in coastal regions and disappeared 10 days later over the entire Gulf. Sea-ice duration and sea-ice cover were longer and larger than normal over the entire Gulf, respectively, with more than 30 days longer for SID and 1/10 larger for mean SIC in December-June in the area off mid-Newfoundland. In the 1989-90 winter, sea ice in February almost covered the entire Gulf. The sea-ice duration in the area off Newfoundland was almost two months longer than usual. In light ice years, sea ice appeared 10 days later in the central and eastern Gulf and disappeared more than 30 days earlier in the eastern Gulf. Sea-ice duration and sea-ice cover were shorter and smaller than normal over the entire Gulf, respectively, with only 10 days duration and 0.5/10 in sea-ice cover in the area off mid-Newfoundland. In the 1968-69 winter, sea ice was only present in the coastal regions during January-March, with no ice present in the central and eastern Gulf for the whole winter.

According to Drinkwater et al. (1999), sea-ice cover in the Gulf of St. Lawrence is a good proxy for the estimated ice volumes during most of the ice season. Indeed, because of the limited information on sea-ice thickness, we do not expect to get better results on sea ice volumes than they did. Thus, the results of intraseasonal and interannual variability of sea-ice cover in the Gulf in the present study can also, to some extent, be applied to the intraseasonal and interannual variability of sea ice volume.

4. Discussions on Mechanisms of Sea Ice Variability – Statistical Analysis

In this and the following chapter, the possible mechanisms controlling sea ice variability in the Gulf of St. Lawrence are discussed using statistical and dynamical analysis. In this chapter, the potential forcing factors are first described and the statistical relationships (including regression analysis) between sea ice variability and several possible forcing factors are then examined. Although some previous studies have been conducted to study the relationship between sea-ice cover and forcing factors (Forward, 1953; Markham, 1973; Dery, 1993), only one or two factors at one or two meteorological stations were used. In this study, a wide range of factors, with better spatial resolution, are examined. Some of these are distributed over more than 10 grid points and thus form forcing fields. Moreover, the relationships between the time of first and last ice presence and the forcing factors are examined, an issue not studied before. A more recent modern statistical method – SVD (Singular Value Decomposition) is used to examine the relationship between two coupled fields. The relative importance of forcing factors on sea ice variability in the Gulf is also explored.

4.1 Forcing factors

Sea ice variability is controlled by both thermodynamic and dynamic processes (Hibler, 1979, 1980). Surface winds and surface currents are responsible for dynamic processes while the major component of the thermodynamic processes is the air-sea surface heat flux. Thus, it would be advantageous to directly use surface heat flux to study its effect

on sea ice variability. However, there are some limitations using this approach. First, heat flux, consisting of short-wave radiation, long-wave radiation, sensible heat flux, and latent heat flux, is calculated using empirical formulas from other measured parameters, such as, surface air temperature, surface winds, sea surface temperature, etc., rather than measured directly. Some coefficients used in the formulas are empirical. Second, from the prediction point of view, it would be advantageous to use measured parameters directly. Third, and most importantly, the available wintertime measurements of sea surface temperature in the Gulf of St. Lawrence are very limited for the period of 1963-96. Since sea surface temperature is indispensable to calculate long-wave radiation, sensible and latent heat fluxes, it was not possible to obtain surface heat fluxes without sea surface temperature measurement.

In this study, the following forcing factors were examined: surface air temperature (SAT), surface winds, sea surface temperature (SST) and salinity (SSS), river runoff from St. Lawrence River System, sea surface circulation, and ice advection into the Gulf from the Labrador Sea. Surface air temperature and surface winds were selected because of their importance in sea ice variability, as suggested by earlier studies (Forward, 1954; Markham, 1973; DeTracey, 1993; Drinkwater and Bugden, 1994) and by research in the Arctic (Walsh and Johnson, 1979; Manak and Mysak, 1989; Chapman and Walsh, 1993). Runoff was included because of its importance to sea ice formation in other regions (Manak and Mysak, 1989; Mysak et al., 1990; Mysak and Power, 1992) and expected importance in the Gulf. The St. Lawrence River runoff has been shown to influence seasonal and interannual salinity changes of the waters in the Gulf, at least over the

Magdalen Shallows (Lauzier, 1957; Sutcliffe et al., 1976). Available sea surface temperature and salinity data were also used to examine their influence on sea ice variability. Their importance was suggested by earlier studies (Matheson, 1968; De Tracey, 1993). In addition, Forward (1954) proposed the importance of sea ice advection from the Labrador Sea to the Gulf.

Related studies have also shown that atmospheric pressure changes parameterized by the North Atlantic Oscillation (NAO) (Hurrell and Van Loon, 1997) influence sea ice variability in the Greenland-Iceland Seas, Hudson Bay, and the Labrador Sea (Mysak and Manak, 1989; Mysak et al., 1990; Wang et al., 1994; Mysak et al., 1996; Drinkwater, 1996; Ingram et al., 1996; Prinsenberg et al., 1997, Slonosky et al., 1997). In this study, these effects on sea ice variability in the Gulf were examined.

4.1.1 Surface air temperature

Surface air temperature plays an important role in exchange of heat between the atmosphere and ocean by affecting long-wave radiation, sensible heat flux, and latent heat flux. Colder air early in the season causes greater heat loss from the ocean through higher sensible and latent heat losses, which leads to greater ice formation. In the middle of the ice season, continuous colder air promotes further ice formation resulting in increased sea-ice coverage and thickness. Late in the ice season, cold air delays melting through related sensible heat transport, thereby resulting in later disappearance and longer sea-ice duration. Figure 4.1a shows the climatological mean surface air temperatures at the beginning and middle of the month for the period December 1 to May 15. The

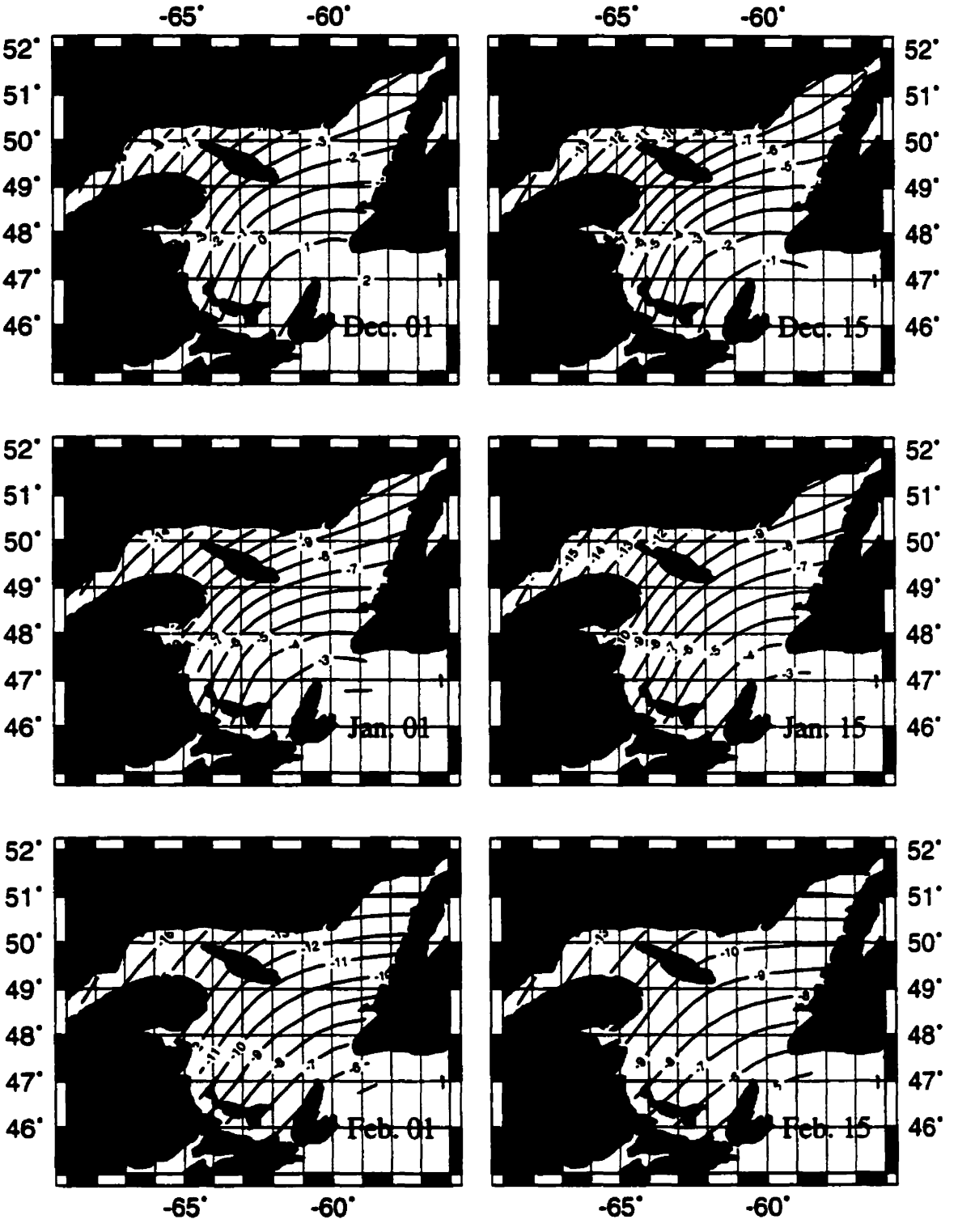

Figure 4.1a Annual surface air temperature (°C) over the Gulf of St. Lawrence

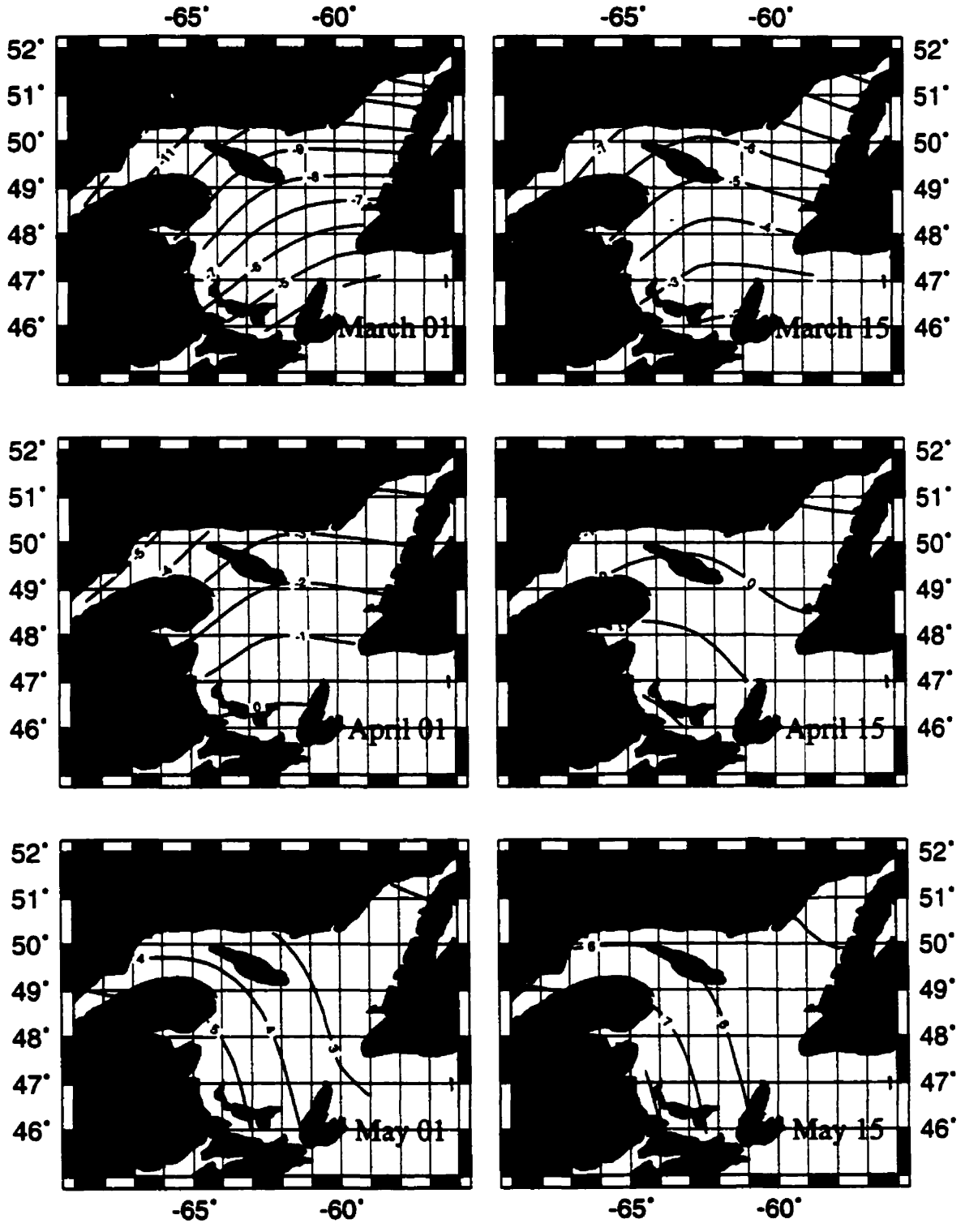

Figure 4.1a (Continued)

isotherms are basically oriented northeast-southwest with the coldest temperatures in the northwest Gulf from December 15 through March 1. This is most likely due to the prevailing northwesterly winds, which advect cold air over the Gulf (see subsection 4.1.2). The coldest temperatures are reached in mid-January to early February in the northwest Gulf and in early February in the northeast Gulf. By early March, the isotherms tend to run east-west with colder air to the north. From mid-April on, temperatures exceed 0°C. In May, the warmest temperatures are in the western regions.

The mean and standard deviations of the surface air temperature averaged between December and April (December 1 – April 15) were constructed (Figure 4.1b). Surface air temperature was examined only in December-April, because very little sea ice is left in May and June. The standard deviation field shows that the largest intraseasonal variation of the surface air temperature occurs in the northwest Gulf, where the mean temperatures are lowest.

The interannual variability of mean surface air temperatures was examined in three periods: December-April (December 1 – April 15), December (December 1-31), and March-April (March 15 –April 15) (Figure 4.2), in an attempt to examine their effect on sea-ice cover averaged over December-June, time of first ice presence, and time of last ice presence, respectively. Mean December-April SAT and December SAT have similar spatial patterns with the coldest temperatures in the northwest Gulf. However, surface air temperatures in December are lower than the December-April average in the northwest Gulf, but higher in the northeast Gulf. In contrast to the other two periods, the isotherms

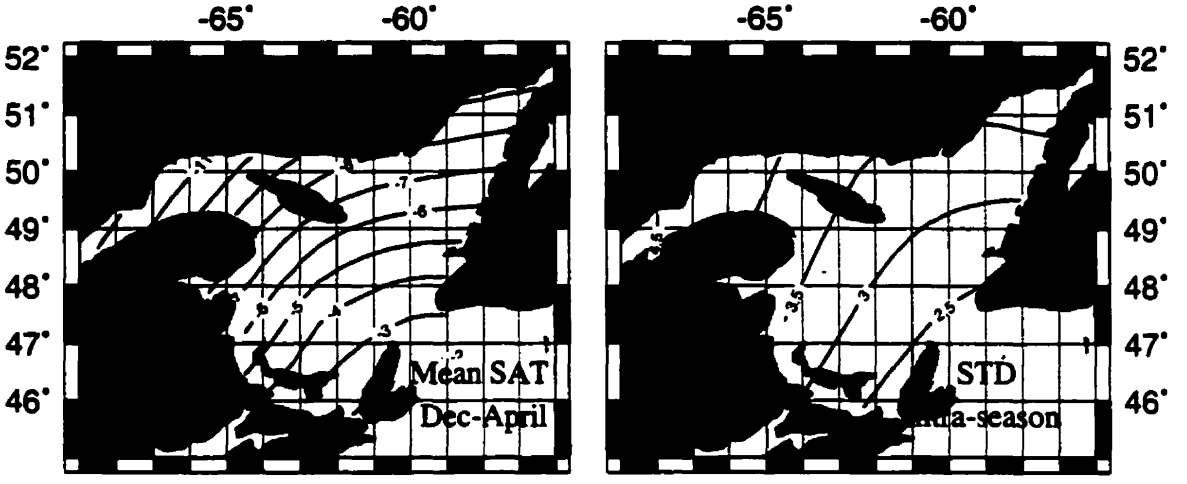

Figure 4.1b Averaged daily climatology of surface air temperature (°C) and corresponding standard deviations (intraseasonal).

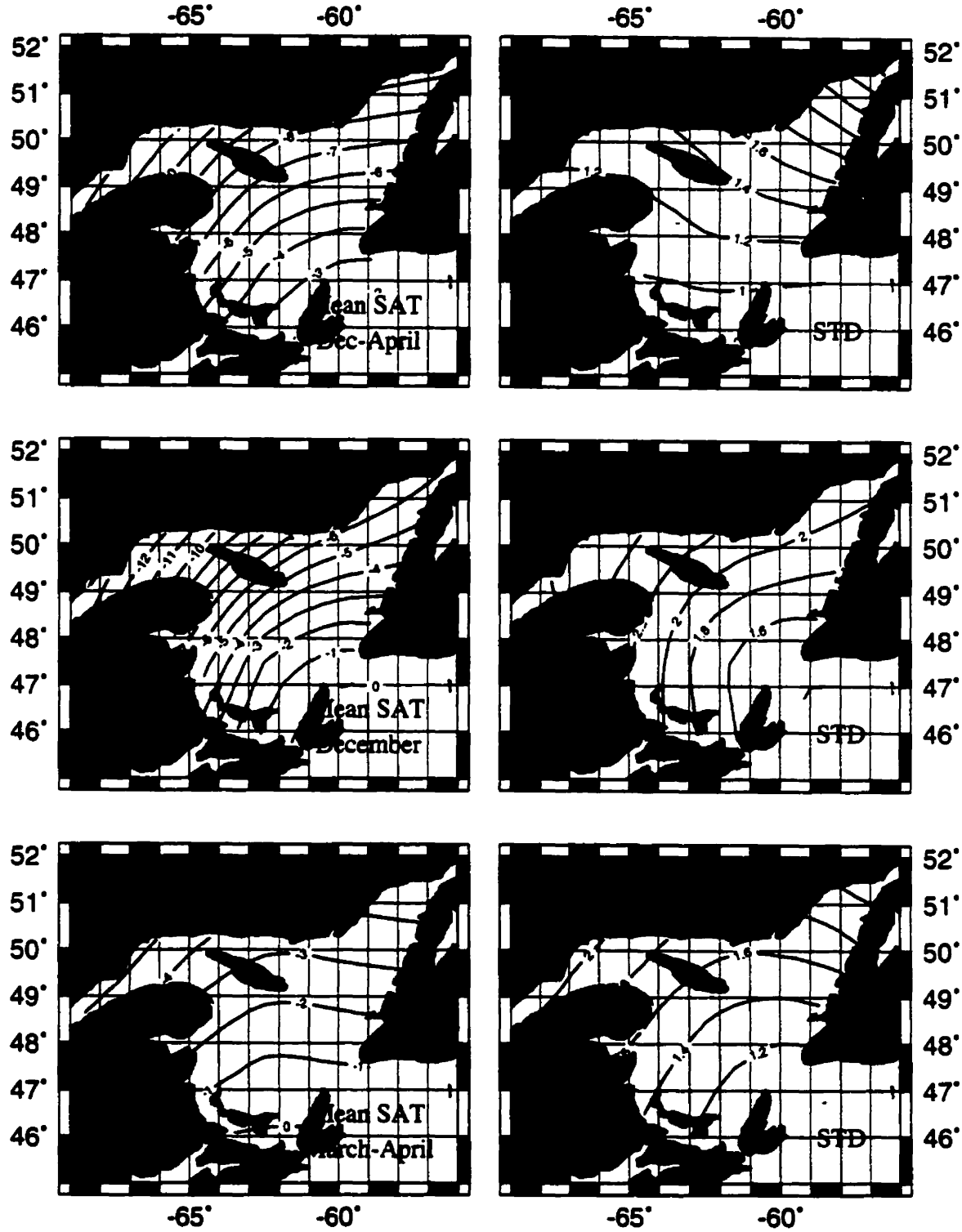

Figure 4.2 Long-term (1962-1996) mean surface air temperature (°C) averaged over December-April (upper), in December (middle), and in March-April (bottom), and corresponding standard deviations.

of SAT in March-April are more oriented in a west-east direction. The largest interannual variability of SAT for December-April is in the northeast Gulf, for December in the northwest Gulf, and for March-April in both the northwest and northeast Gulf (Figure 4.2).

4.1.2 Surface winds

Surface winds influence sea ice formation and distribution in several ways. First, stronger winds increase sensible and latent heat fluxes between atmosphere and ocean. Second, winds and wind-induced currents can advect sea ice from one place to another, which may change the spatial distribution of sea ice. A third, but indirect effect, is that stronger winds from land to the ocean, in early to mid ice season, can transport colder air over the ocean.

The climatological mean surface winds at the beginning and middle of the month for the period from December 1 through May 15 (Figure 4.3a) indicate the strongest winds occur in December-February. Spatially, the winds are stronger in the southern areas during December-February, but weaker in later months, when the winds are highly variable in direction. The means and standard deviations of the winds averaged over December-April are shown in Figure 4.3b. The mean field shows the winds are northwesterly in the northern Gulf and westerly in the southern Gulf. However, the standard deviation fields indicate that the u-wind has a larger variability than the v-wind, with the highest variability in the southeastern Gulf.

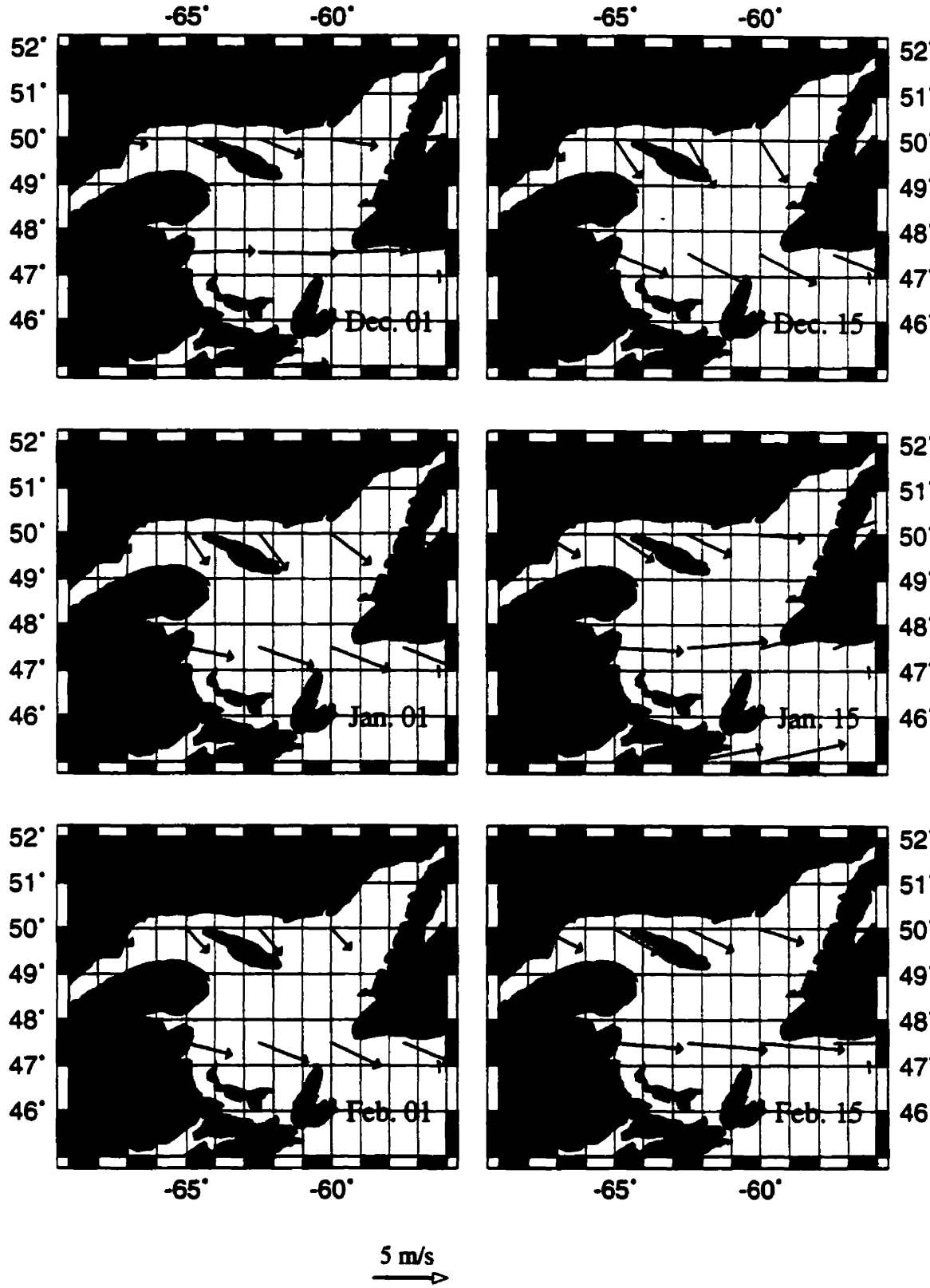

Figure 4.3a Average surface winds (m/s) over the Gulf of St. Lawrence for dates indicated.

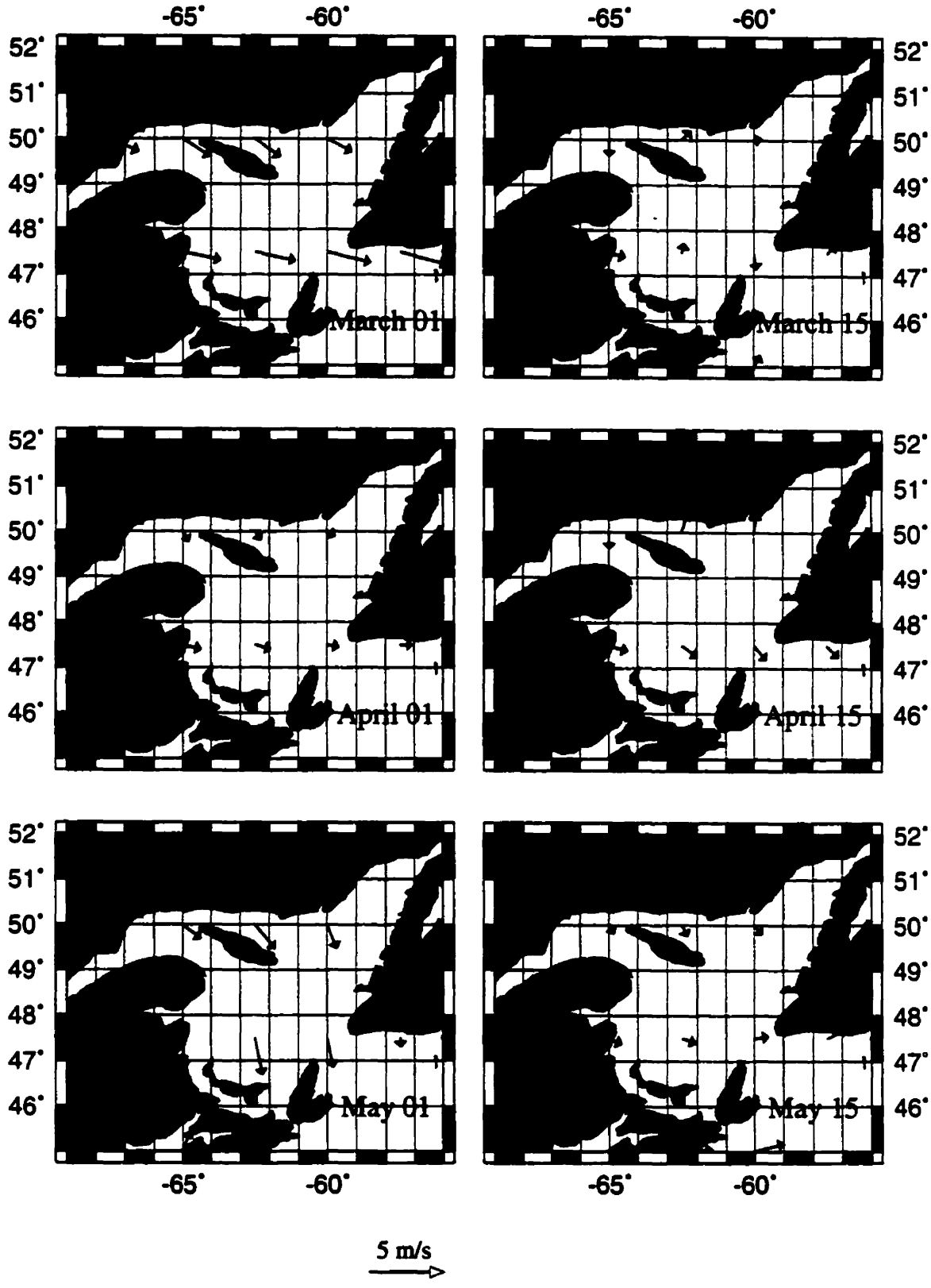

Figure 4.3a (Continued)

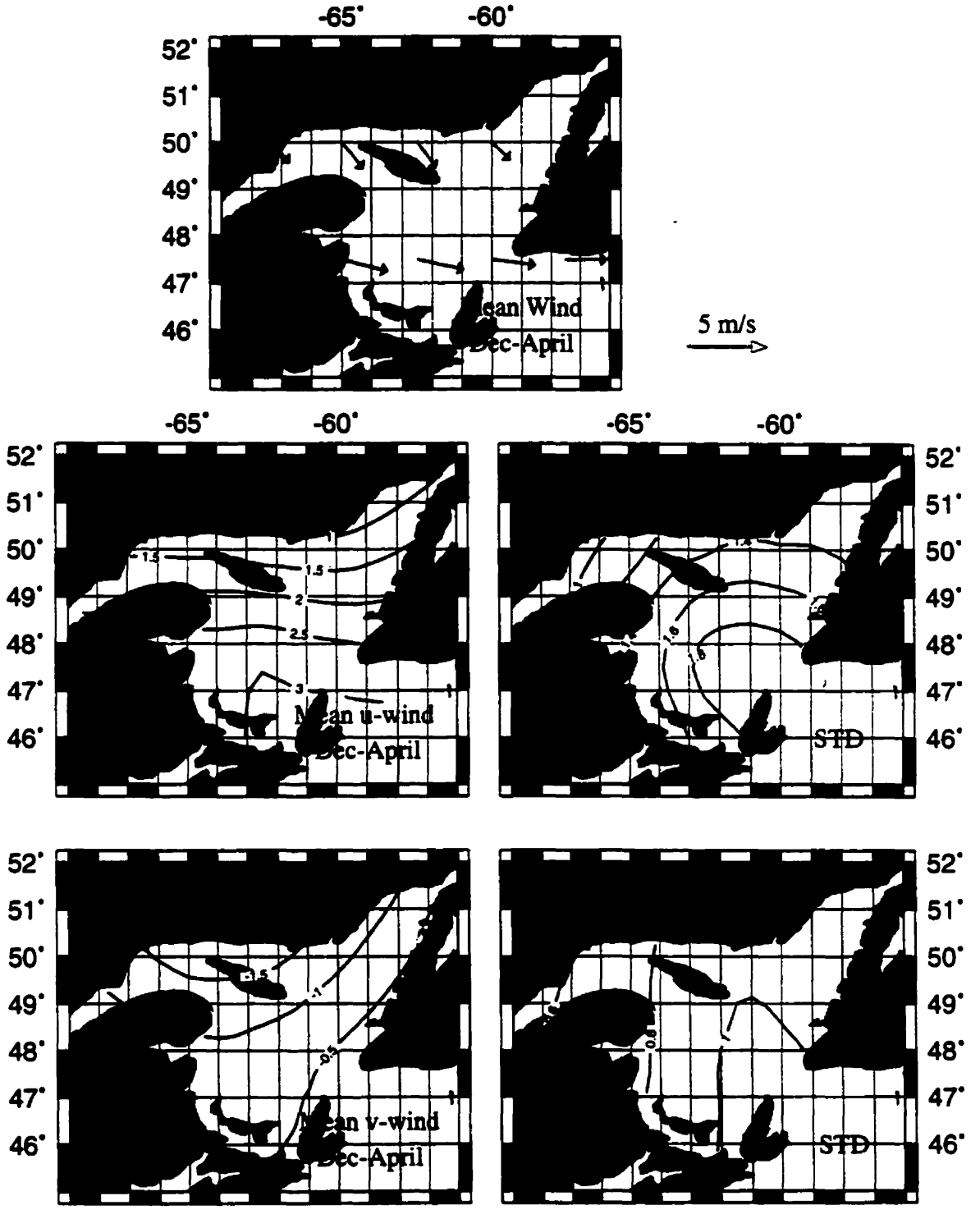

Figure 4.3b Means and standard deviations of wind fields (m/s) in December-April (intraseasonal)

The long-term means of the surface winds averaged over December-April, for December, and for March-April are shown in Figure 4.4a, with means and standard deviations for their components (u, v) in Figures 4.4b and 4.4c. The mean wind fields in December-April and in December show a similar spatial pattern, with northwesterlies in the northern Gulf and westerlies in the southern Gulf. The intensity is larger in December. In contrast, the surface winds in March-April are weaker. In the southern Gulf, winds are westerly, while in the northern Gulf, winds are southerly in the central area and northerlies elsewhere. The standard deviations of the surface winds in March-April and December are comparable and larger than in December-April. The largest standard deviations occur in the eastern Gulf for the period of December-April and in the southeast for the other two periods.

4.1.3 Hydrographic fields in November

Sea surface temperature, like surface air temperature, affects the long-wave radiation, as well as sensible and latent heat fluxes. Furthermore, sea surface temperature and salinity influence sea ice formation in a very direct way. Lower SSTs can reach the freezing point more rapidly. Thus, less heat loss is required from the ocean in order to form ice. With lower SSSs, the surface reaches the freezing point at higher temperatures.

DeTracey (1993) showed that colder sea surface temperatures in November result in earlier ice formation in the Gulf of St. Lawrence. There is a relatively large hydrographic data set in this month, which was collected for the purpose of ice forecasting at the request of Canadian Ice Service of Environment Canada in Ottawa, and very few

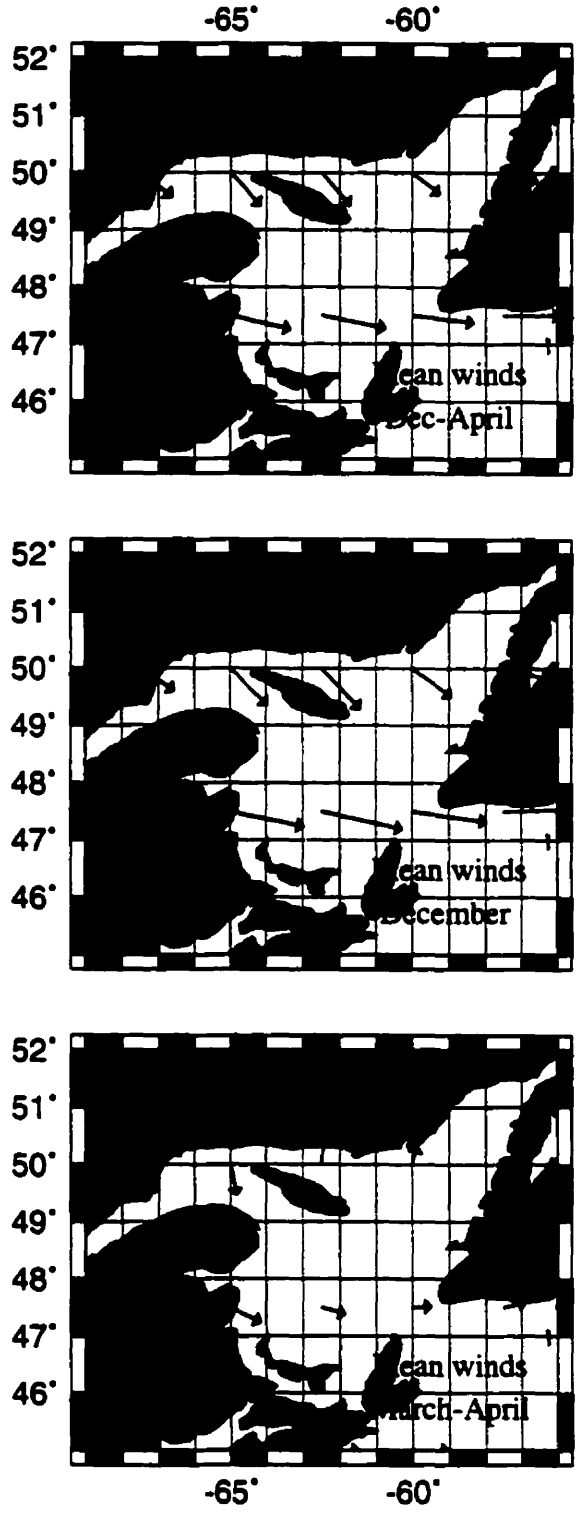

Figure 4.4a Long-term (1962-1996) mean surface winds (m/s) averaged over December-April (upper), in December (middle), and in March-April (bottom).

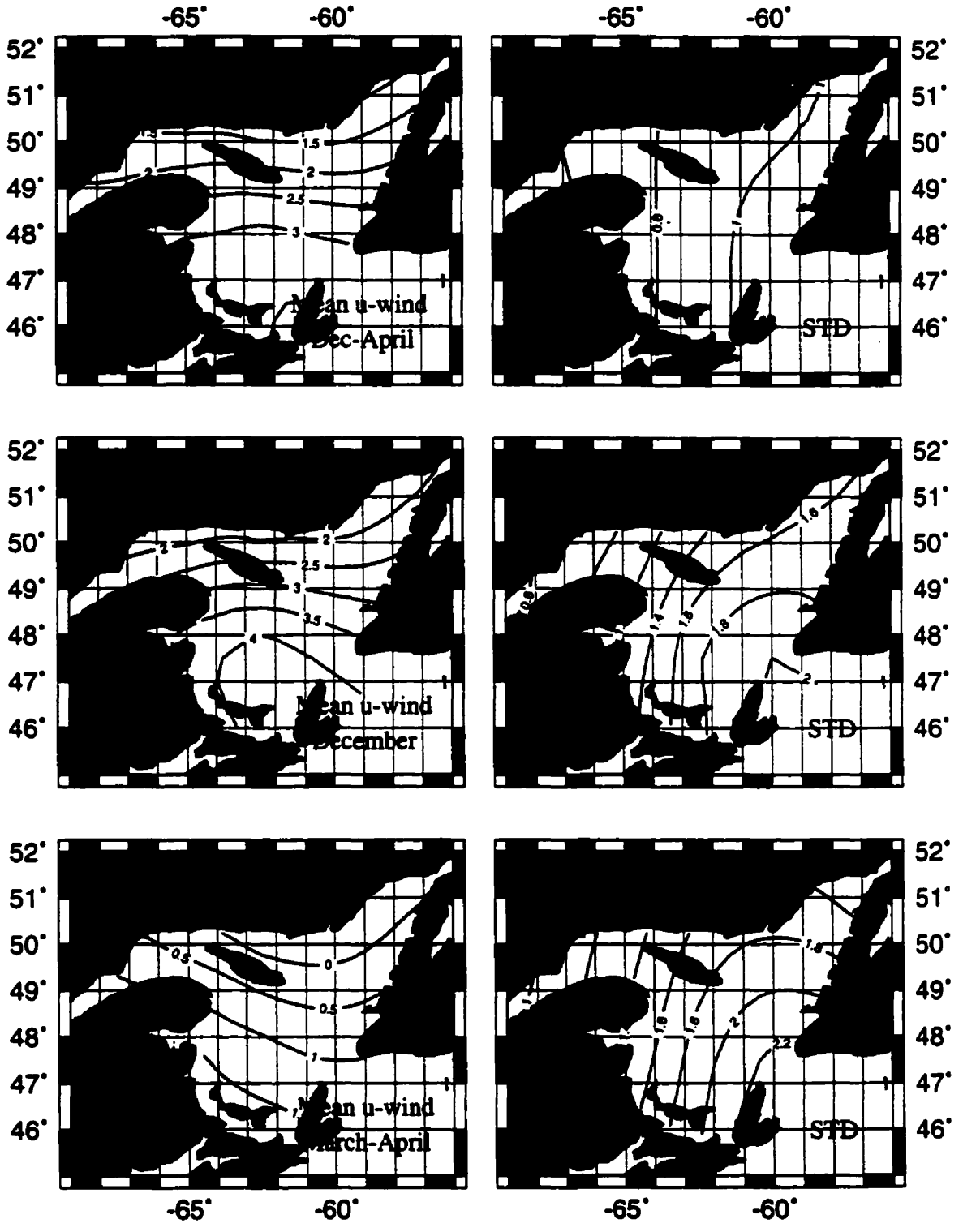

Figure 4.4b Long-term (1962-1996) mean u-wind (m/s) averaged over December-April (upper), in December (middle), and in March-April (bottom), and corresponding standard deviations.

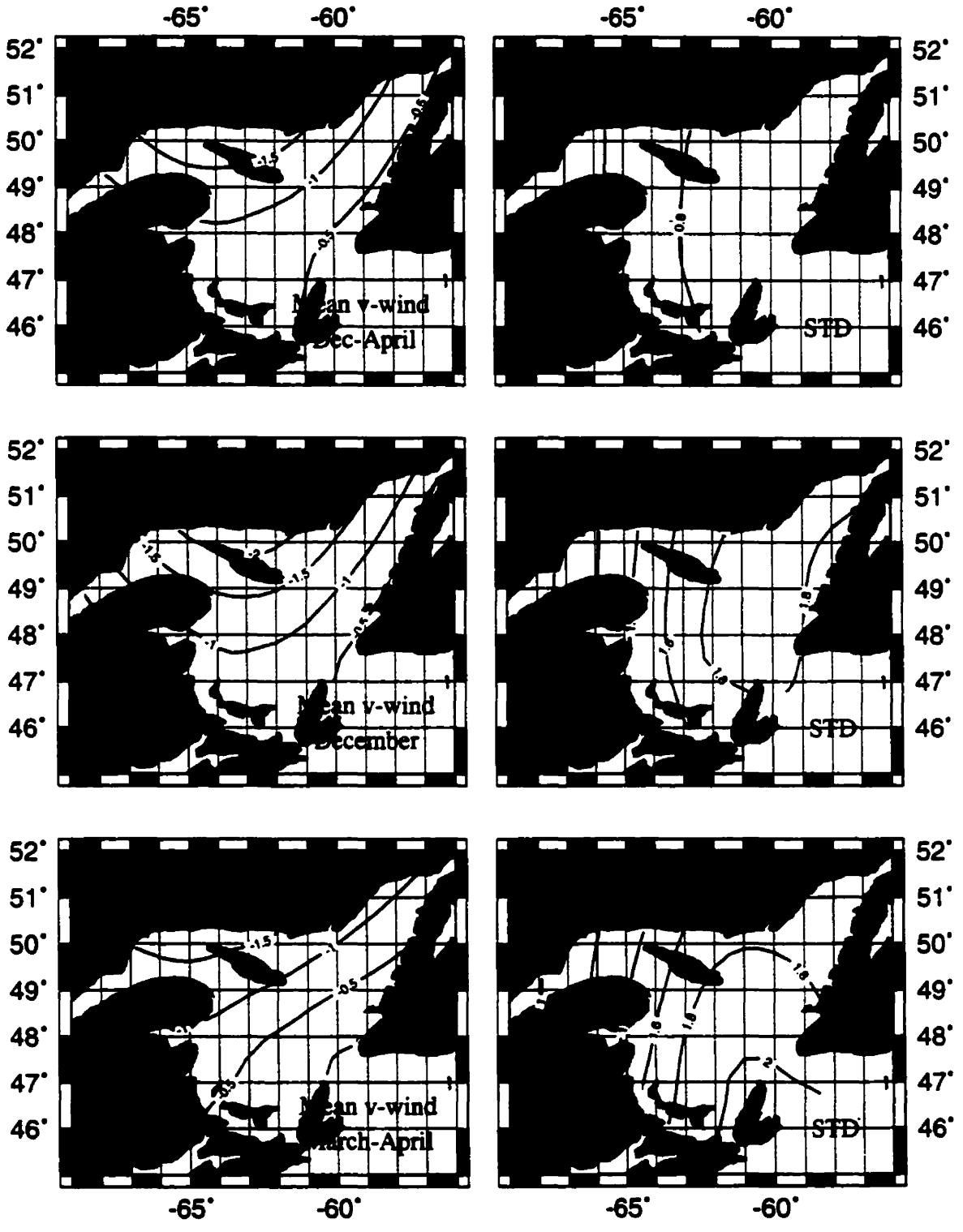

Figure 4.4c Long-term (1962-1996) mean v-wind (m/s) averaged over December-April (upper), in December (middle), and in March-April (bottom), and corresponding standard deviations.

observations in the winter months in the Gulf. In this study, the November data from 1962-96 were used, although there were no observations for some years. A climatology of sea surface temperature and salinity in November was prepared with the corresponding standard deviations (Figures 4.5a and 4.5b). The lowest temperatures occur in the St. Lawrence Estuary and Strait of Belle Isle region. The isotherms are basically oriented in northeast-southwest direction. The largest interannual variability occurs in the Strait of Belle Isle region and southwestern Gulf. The lowest salinities are located in the southwestern Gulf, where the largest interannual variability occurs, and in the Estuary. The isohalines are oriented in a northwest-southeast direction.

Mixed layer depth also influences sea ice formation. It is believed that sea ice can form only when the temperature of the entire mixed layer approaches the freezing point. Deeper mixed layers need to lose more heat for ice to form while shallower mixed layers lose comparatively less heat to form sea ice. The climatology for the mixed layer depth in November is shown in Figure 4.5c, which was prepared by DeTracey (1993) by examining climatological sigma-t profiles for the Gulf (Petrie et al., 1990). The shallowest mixed layer depths are located in the southwest Gulf.

4.1.4. River runoff from St. Lawrence River system

River runoff from the St. Lawrence River system to the Gulf influences sea surface salinity distribution and thereby affects sea ice formation. Figure 4.6 shows the 34-year (1962-95) monthly mean river runoff, the time series for the May runoff, and the time series of yearly runoff from the St. Lawrence River system. May was chosen because it

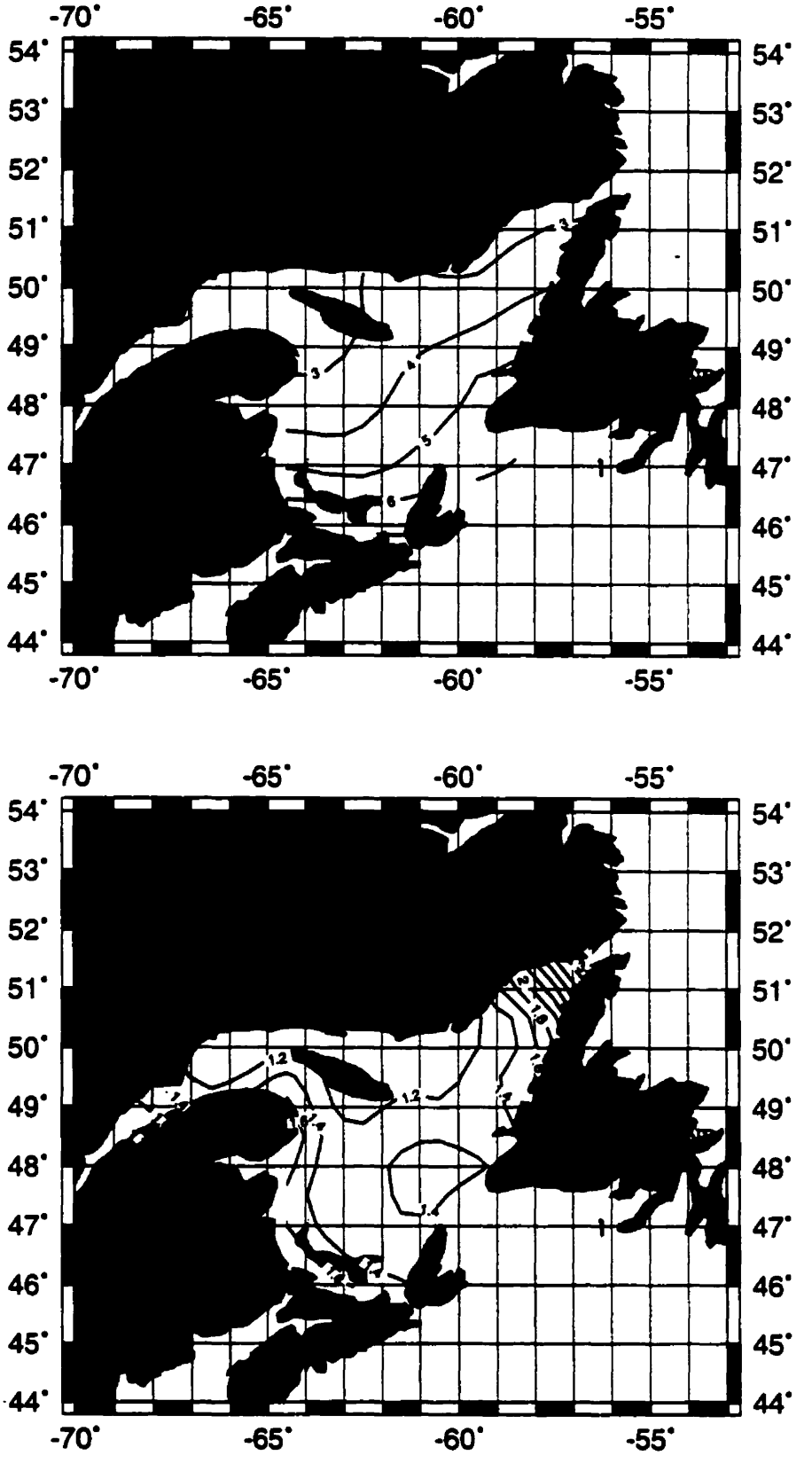

Figure 4.5a Mean November sea surface temperature (upper) (°C) and corresponding standard deviations (lower) in the Gulf of St. Lawrence

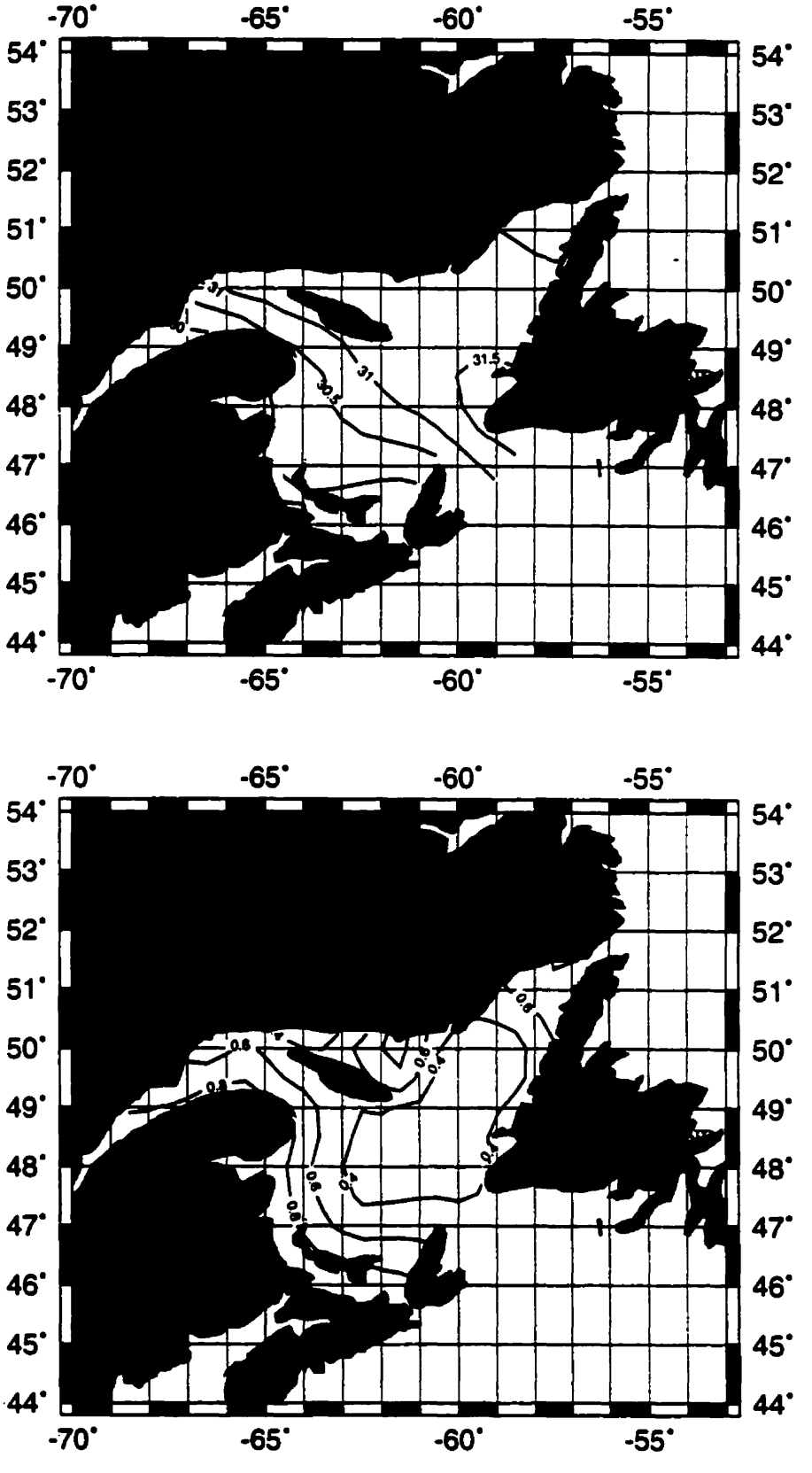

Figure 4.5b Mean November sea surface salinity (upper) and corresponding standard deviations (lower) in the Gulf of St. Lawrence

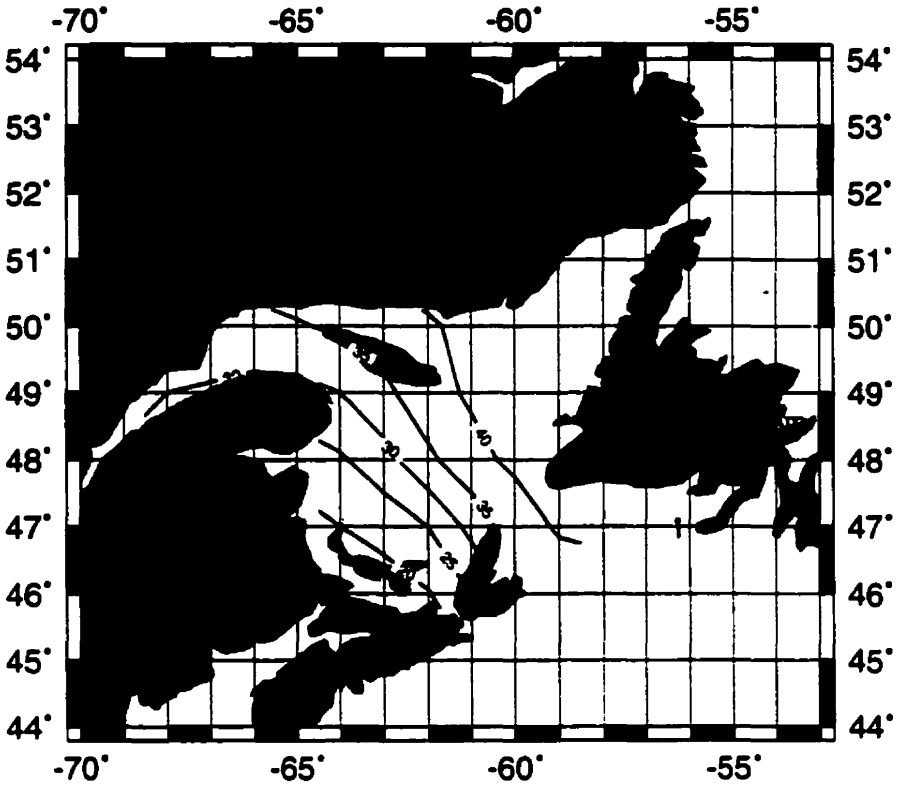

Figure 4.5c Climotology of mixed layer depth (m) in November in Gulf of St. Lawrence (Adapted from DeTracey, 1993).

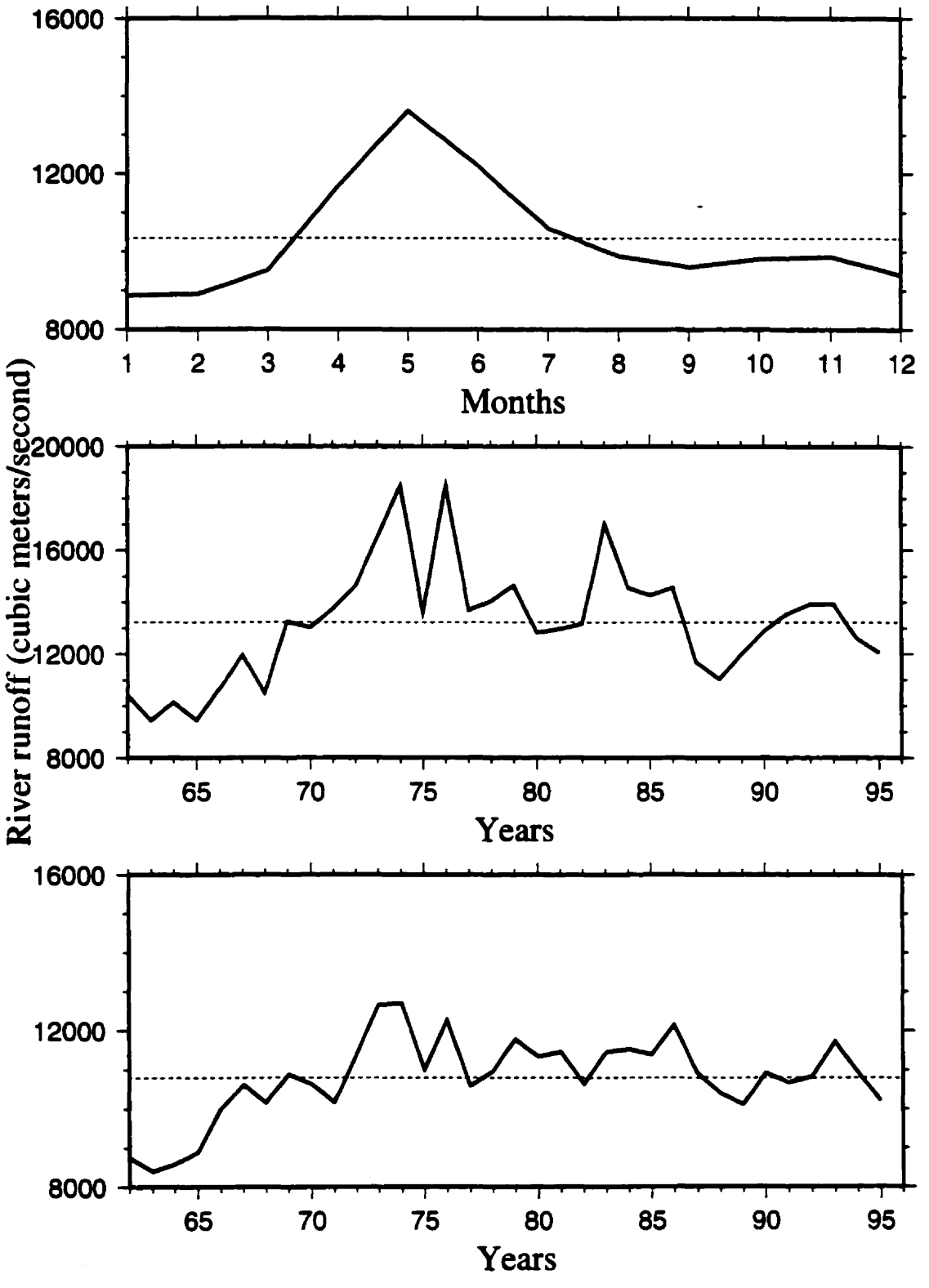

Figure 4.6 The long-term (1962-95) monthly mean river runoff (top), the time series of May runoff (middle), and the time series of yearly averaged runoff (bottom) from the St. Lawrence River system.

has the highest monthly runoff and had the highest correlation with sea-ice cover. May runoff was above normal from 1970 to 1986 and below normal for the remaining years. The lowest May runoff occurred in the early 1960s. Yearly runoff was used in examining its relationship to the time of first ice and time of last ice. It also indicates that the lowest runoff values occurred in the early 1960s.

4.1.5 North Atlantic Oscillation (NAO)

The North Atlantic Oscillation (NAO) is associated with changes in the surface westerlies across the Atlantic onto Europe. The NAO index is defined as the difference of normalized pressures between Lisbon, Portugal and Stykkisholmur, Iceland (Hurrell and Van Loon, 1997). The time series of NAO index during the period of 1963-95 and its power spectrum indicate strong oscillation with a period of 7-8 years (Figure 4.7). Variability of the NAO could influence sea ice variability in the Gulf of St. Lawrence in two ways. First, NAO changes could indicate varying meteorological conditions over the Gulf associated with large-scale atmospheric circulation, which in turn influences hydrographic conditions and sea ice variability in the Gulf. Second, large scale atmospheric changes could cause sea ice variability in the Labrador Sea and thereby influence sea ice variability over the Gulf by sea ice advection through the Strait of Belle Isle.

4.1.6 Circulation patterns in the Gulf

Ocean circulation can re-distribute sea-ice coverage by advecting it from one place to another. Using hydrographic data available before 1975, El-Sabh (1976) calculated the

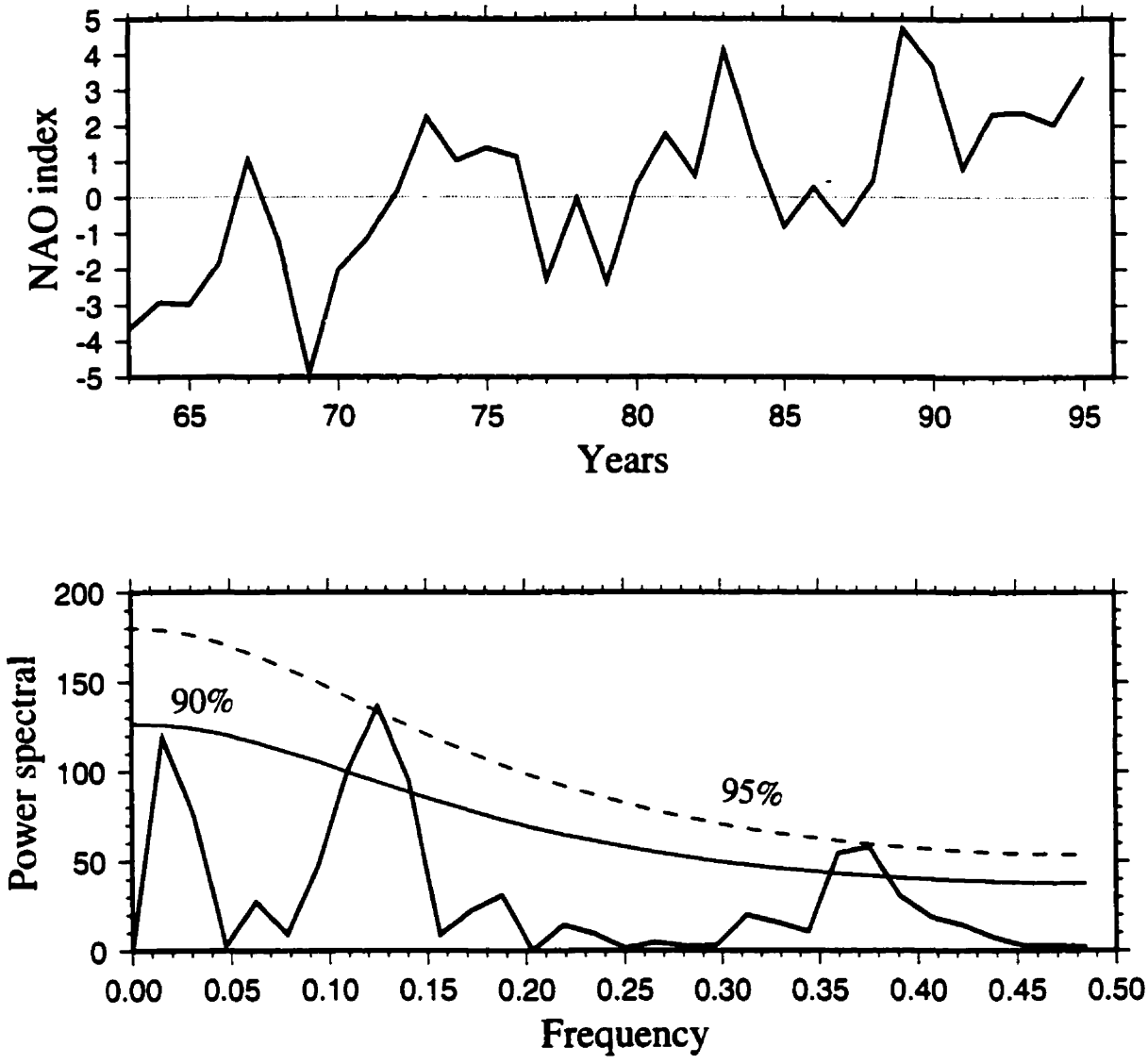

Figure 4.7 Time series (top) and power spectrum (bottom) with 95% and 90% confidence levels of NAO (North Atlantic Oscillation) index

surface geostrophic currents in the Gulf. The circulation in June, July, August, and November indicate a strong Gaspe Current and a cyclonic gyre in the Gulf (Figures 7-10 of El-Sabh's paper). The geostrophic circulation pattern in winter (Figure 11 of El-Sabh's paper), calculated using hydrographic data in February and March, shows a weaker Gaspe Current and no cyclonic gyre. However, there were no data in the southwestern and northeastern Gulf. Currents are mostly southeastward, except in the middle of Cabot Strait, where the currents are northwestward. Recently, Dr. Francois Saucier at the Maurice Lamontagne Institute (1999, personal communication) kindly provided monthly mean surface currents for January – May 1986, which were the output from his coupled three-dimensional ocean-ice model. In that particular year, surface currents in January-March period were southeastward over most of the Gulf, except in the northeastern Gulf and upper St. Lawrence Estuary. In the northeastern Gulf, currents varied from month to month but were primarily eastward or southeastward. Currents in the Strait of Belle Isle were into the Gulf for all winter months.

4.1.7. Sea-Ice advection through the Strait of Belle Isle

Forward (1954) suggested that sea-ice advection from the Strait of Belle Isle could play an important role on sea ice conditions in the Gulf of St. Lawrence. To test this hypothesis, we used sea ice observations on six grid points (244, 245, 253, 254, 262, and 263 in Figure 2.1) in the Labrador Sea to represent sea ice conditions near the entrance to the Strait of Belle Isle. The long-term (1963-95) means of sea-ice cover averaged over these grid points and averaged over the Strait of Belle Isle region (Region 3 in Figure 2.1) in the Gulf of St. Lawrence are shown in Figure 4.8. Sea ice observations in the Labrador

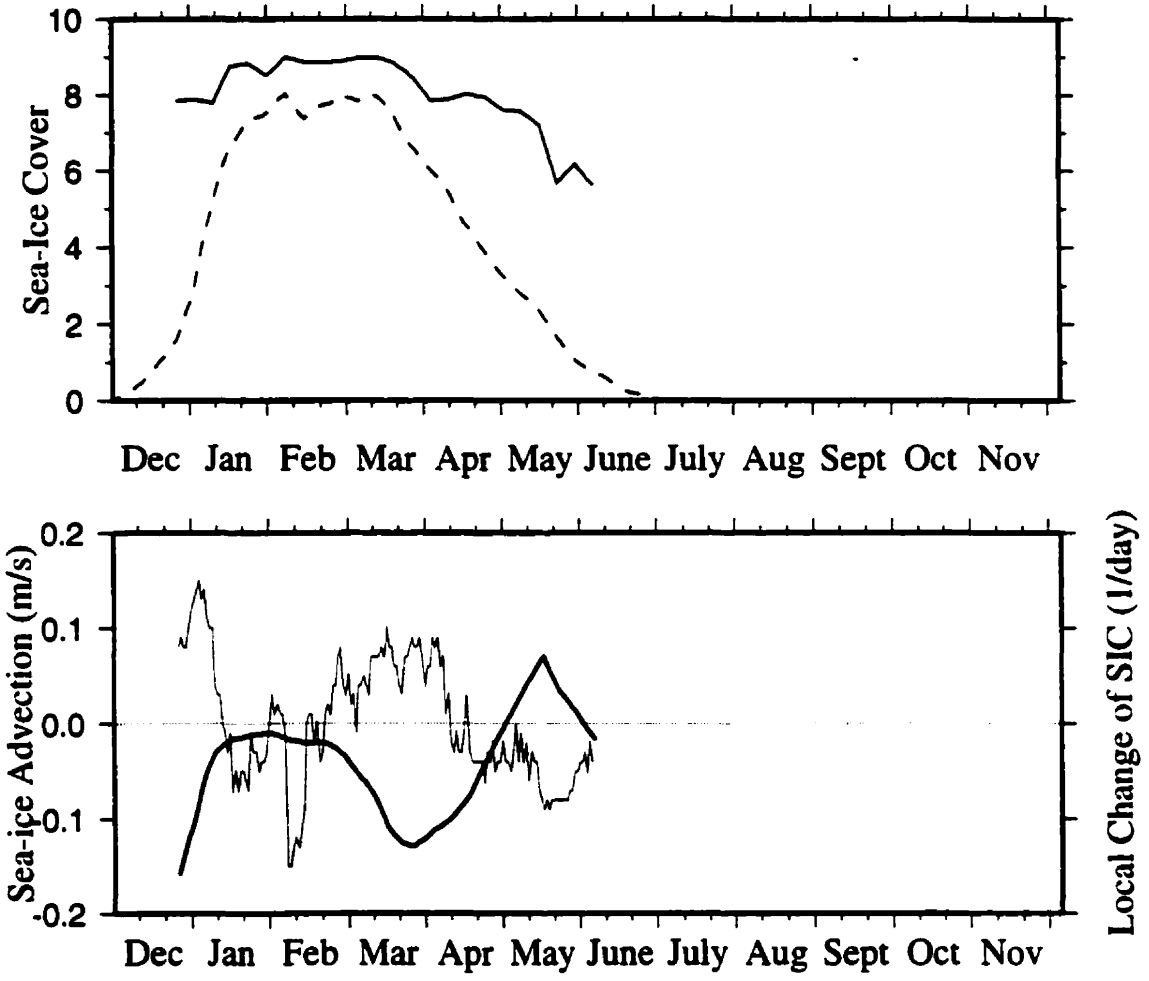

Figure 4.8 The long-term means (1963-95) of sea-ice cover (in tenths) outside of the Strait of Belle Isle in the Labrador Sea (-) and inside of the Strait over the Gulf (-.-) (Region 3 in Figure 2.1)(top) and sea-ice advection in the Strait (thick curve) and local change of average sea-ice cover (thin curve) in Region 3.

Sea generally begin at the end of December. The most striking feature is that sea-ice cover in the Labrador Sea is always larger than that in the Gulf. By the end of December, the sea-ice cover in the Labrador Sea reaches 8/10, while the sea-ice cover in the Gulf is only about 4/10, providing a strong sea-ice gradient between the Labrador Sea and the Gulf. In February-March, the sea-ice cover in the Labrador Sea reaches 9/10 while in the Gulf it is around 8/10. From early April, sea-ice cover in both regions begins to decrease but at different rates, being faster in the Gulf. Thus, the sea-ice gradient between the two regions increases again.

The relationship between sea-ice cover in Region 3 (Figure 2.1) and sea-ice advection from the Labrador Sea to the Gulf will now be discussed. Specifically, we estimate the correlation between local time change of sea-ice cover $\partial C/\partial t$ in Region 3, where C is sea-ice cover and t time, and sea-ice advection $u\partial C/\partial x$, where u is the along-strait current and $\partial C/\partial x$ is sea-ice gradient between the Labrador Sea and Region 3. Garrett and Petrie (1981) estimated monthly surface flow along the Strait of Belle Isle from sea level measurements in 1970-77 under the assumption that 1963, the year the current measurements were made, was an average year. These data were interpolated linearly to daily values and then sea-ice advection was calculated by multiplying daily surface flow with the differences between the average sea-ice cover near the entrance of the Strait in the Labrador Sea and Region 3 in the Gulf. In order to examine the effects of sea-ice advection from the Labrador Sea under an assumption of no clogging of ice in the Strait, sea ice anomalies in Region 3 were calculated by removing the spatial means over the entire Gulf, attempting to eliminate the effects of other forcing factors. The local time

change rate of the sea ice anomalies was then calculated. The time series of sea-ice advection from the Labrador Sea and the local change rate of sea ice anomalies in Region 3 are shown in Figure 4.8. Negative sea-ice advection means that the sea ice is advected into the Gulf from the Labrador Sea. A positive local change rate of the sea-ice cover means the sea-ice cover increases with time. The two time series are opposite in sign, except in January and February, suggesting that the sea-ice cover increases with time when sea ice is advected from the Labrador Sea and vice versa. The lagged-correlation between the two times series indicates the maximum correlation is –0.72, occurring when SIC was lagged two days behind sea-ice advection. The correlation is significant at the 90% confidence level, based on the method described by Sciremammano (1979). The inconsistency for the two time series in January and February could be related to other factors, like ocean circulation, which advects sea ice from this area.

4.2 Relationship between sea ice variability and forcing factors

In this section, the quantitative relationship between sea ice variability and some of the aforementioned forcing factors is considered. We first look at some forcing factors in the extreme sea ice scenarios (i.e., in years with severe and light ice).

In Chapter 3 we found sea-ice cover in severe ice years during December-June is larger than normal, sea-ice duration is longer, sea ice appears earlier and disappears later. In light ice years, the opposite situation occurs. Figures 4.9-4.12 show composite anomalies of surface air temperature and surface winds averaged in December-April, December, and March-April, respectively, and sea surface temperature and salinity in November for

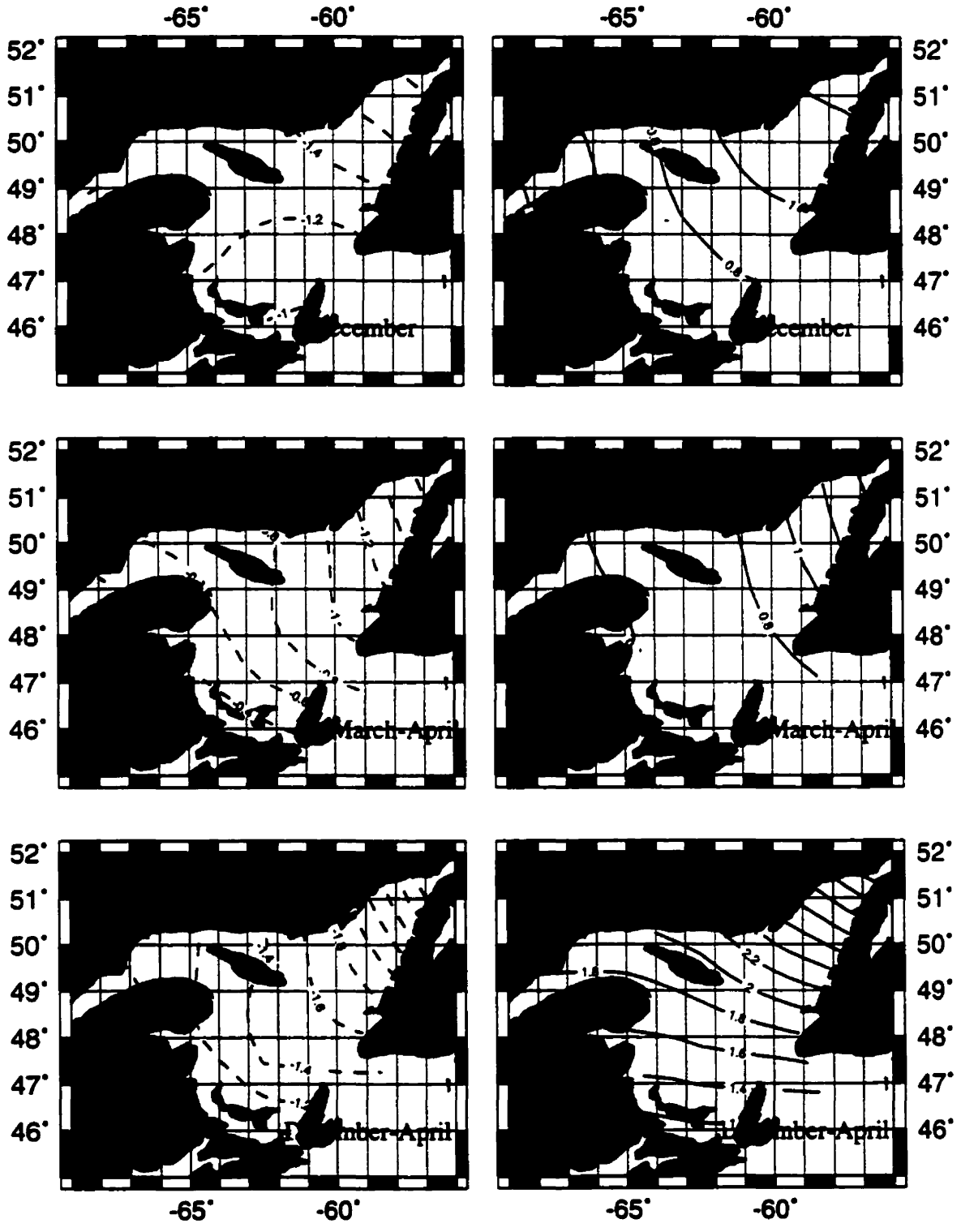

Figure 4.9 Composite anomalies of surface air temperature for six most severe ice years (left panels) and for five lightest ice years (right panels) in different periods.

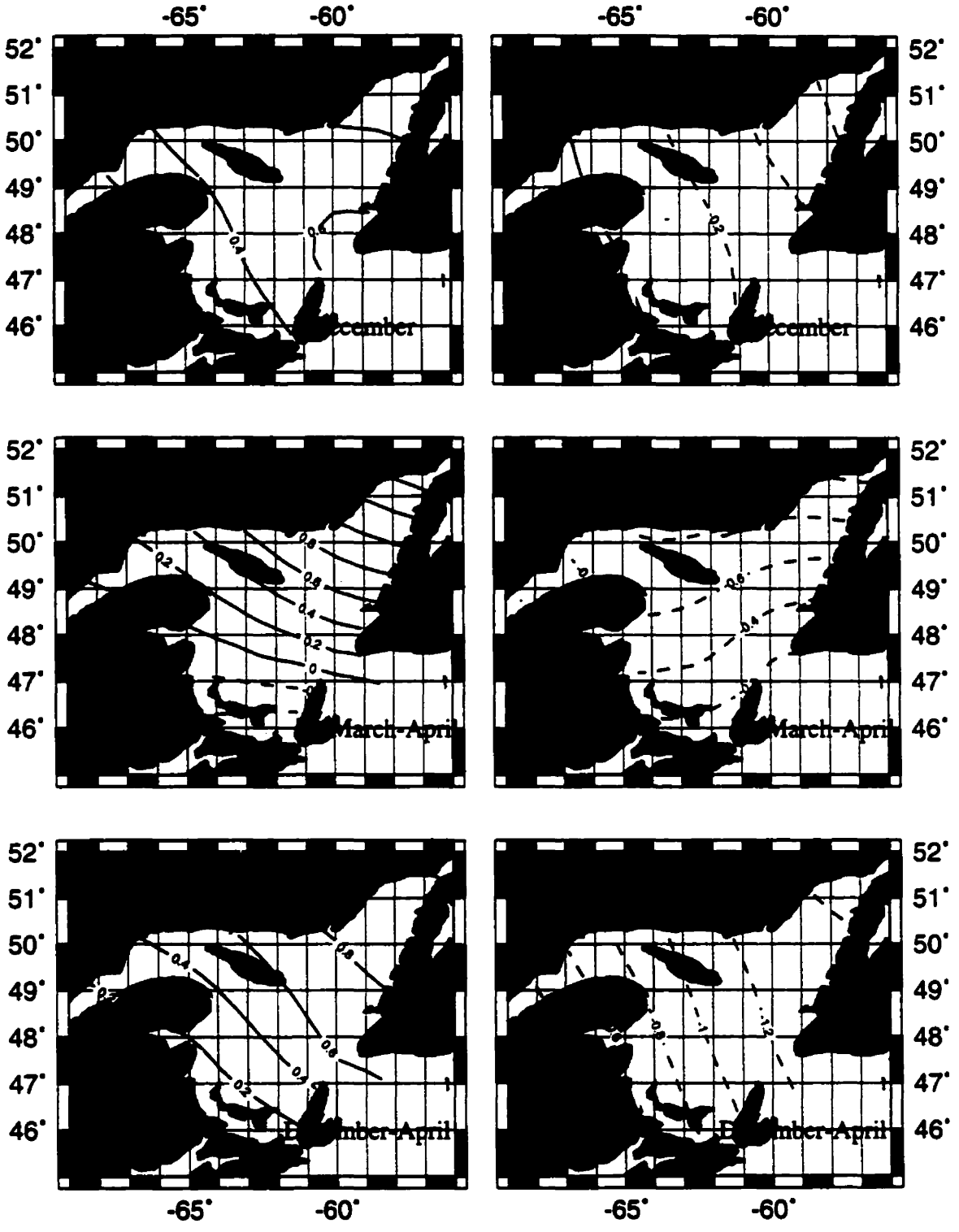

Figure 4.10 Composite anomalies of u-wind for six most severe ice years (left panels) and for five lightest ice years (right panels) in different periods.

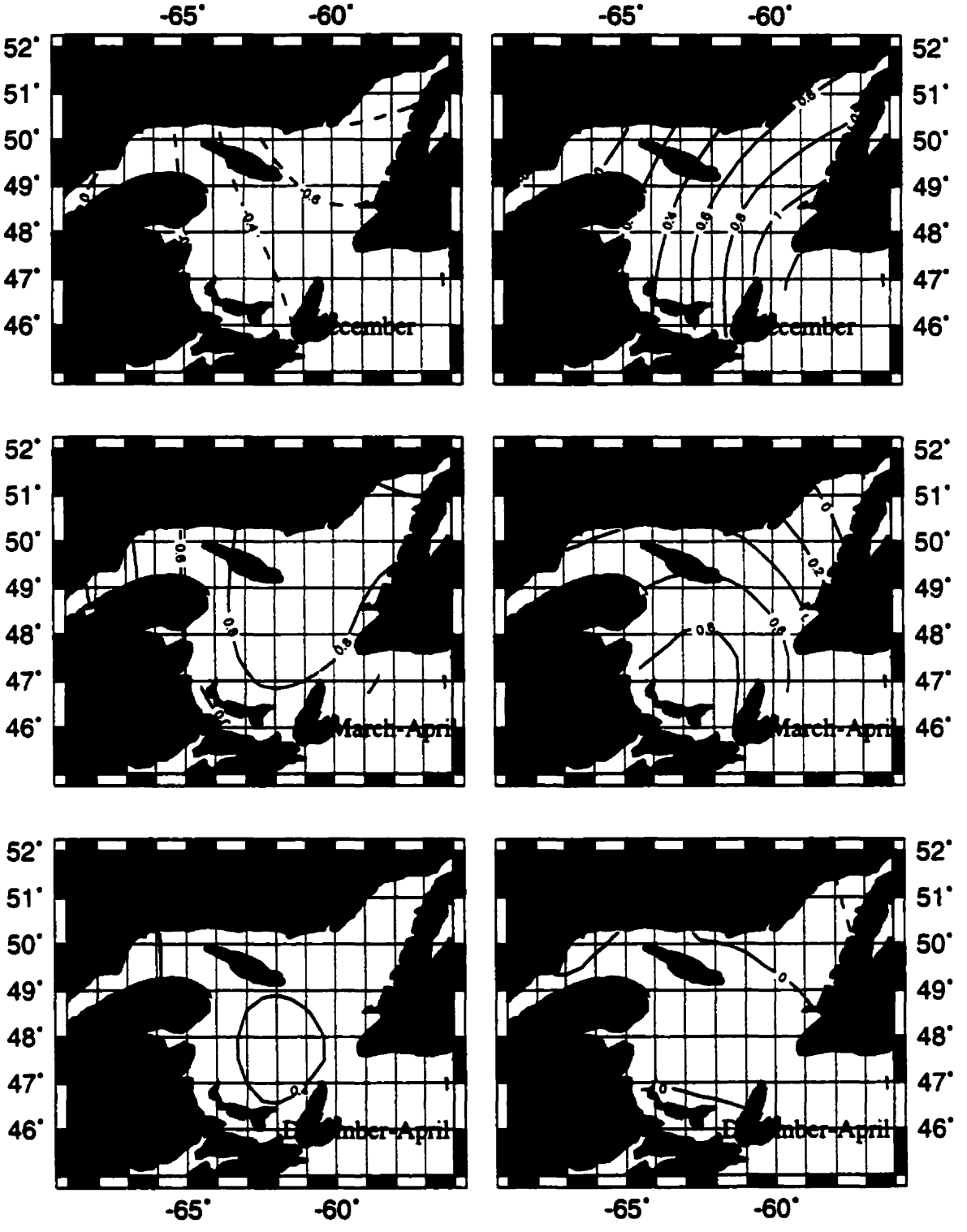

Figure 4.11 Composite anomalies of v-wind for six most severe ice years (left panels) and for five lightest ice years (right panels) in different periods.

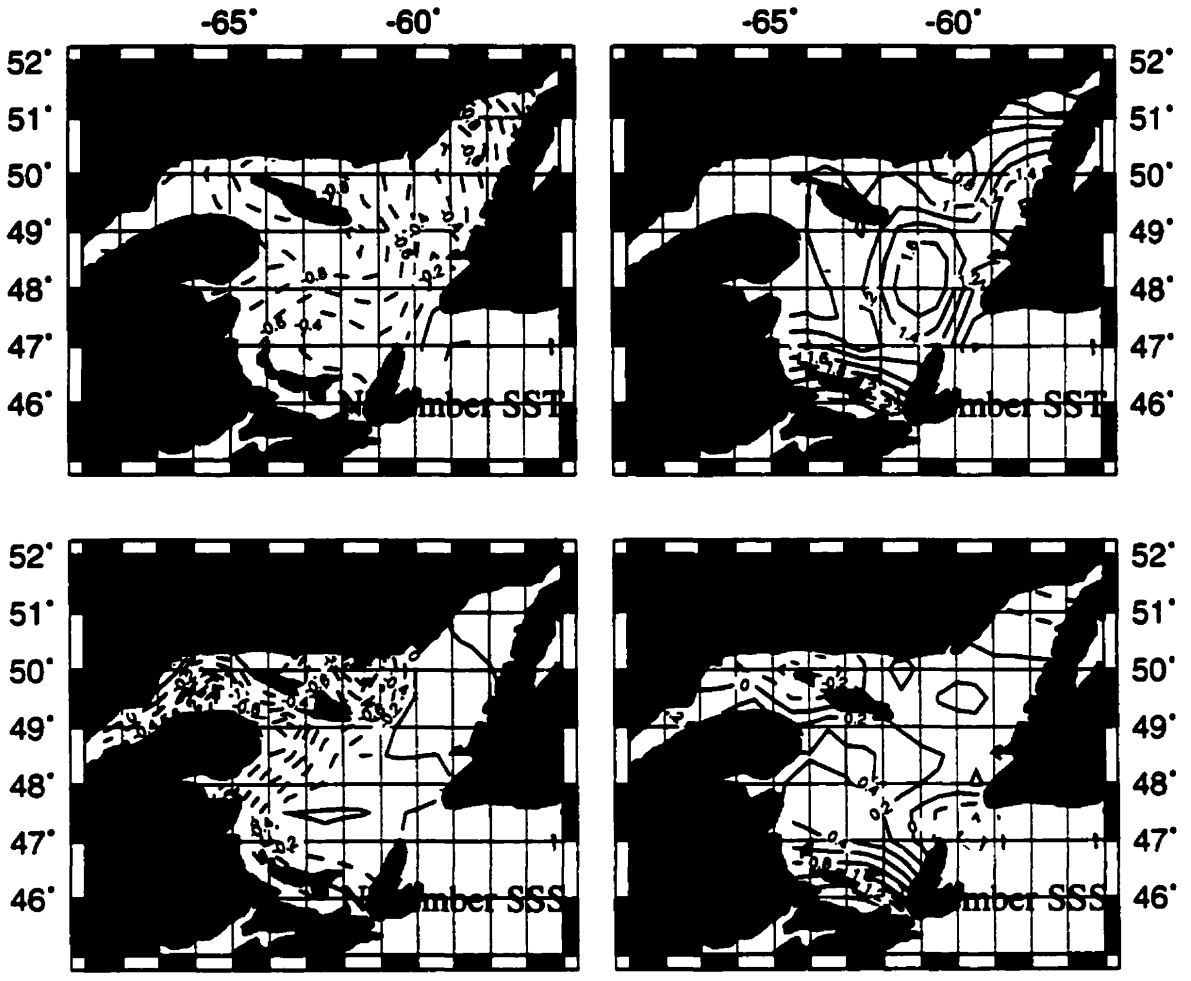

Figure 4.12 Composite November SST and SSS anomalies for six most severe ice years (left panels) and for five lightest ice years (right panels).

the six most severe ice years and for the five lightest years. As might be expected, surface air temperatures, in the most severe ice years, are lower than normal and the u-wind component is stronger for all three periods. Both sea surface temperature and salinity in November are lower. In the lightest ice years, SAT is higher and u-wind is weaker. Both SST and SSS are higher. These results are consistent with our analysis in last section for forcing factors and also suggest a possible relationship between sea ice variability and forcing factors. For the v-wind (Figure 4.11), the situation is different. Since the long-term mean December v-wind is northerly (Figure 4.4c), negative (positive) anomalies indicate stronger (weaker) northerlies, which would advect colder air over the Gulf. Thus, it is expected that in the most severe (lightest) ice years the northerlies are stronger (weaker), which is the case. However, the anomalies of the v-wind component averaged in December-April and March-April are positive for both the most severe ice years and the lightest ice years. This might suggest that the v-wind component is unimportant for interannual variability of sea-ice cover in December-June and the time of last ice presence.

We now examine the quantitative relationship between sea ice variability and different forcing factors, using SVD (Singular Value Decomposition) and correlation methods. As suggested by the mean dates of first and last ice presence (Figure 3.4), sea ice generally appears in the coastal regions of the Gulf during late December. This suggests that the meteorological fields in December would play an important role in determining

the time of first ice presence. Thus, meteorological fields in December were chosen to determine their influence on TFIP. Since sea ice generally begins to retreat from the St. Lawrence Estuary in early April and then later in the central Gulf, we selected the meteorological fields in the period from March 15 to April 15 to study their effects on TLIP. In addition, as mentioned earlier, we chose meteorological fields in December-April to examine their influences on mean sea-ice cover in December-June. Meteorological fields for this period were also used to study their influence on TLIP. Although sea ice begins to retreat in the early part of April, sea ice in this period is the product of accumulation since the previous December. The amount of sea ice created in this period would affect the time it takes for sea ice to disappear. As will be seen later, mean sea-ice cover in December-June is related to SAT and u-wind in December-April. Thus, it is worthwhile to examine the relationship between SAT and u-wind in December-April and TLIP.

4.2.1 Relationship between mean sea-ice cover in December-June and forcing factors

In this subsection, we examine the quantitative relationship between mean sea-ice cover in December-June and the different forcing factors: mean SAT and winds in December-April, SST and SSS in previous November, river runoff from the St. Lawrence River system, and NAO. Since winds are vectors, we examine the effect of the two components, u and v, on sea ice variability separately.

4.2.1.1 Relationship between SIC and forcing factors: SAT, winds, SST, and SSS

The homogeneous correlation maps and time series of expansion coefficients of the first SVD modes for SIC and forcing factors SAT, u-wind, v-wind, SST, and SSS are shown in Figures 4.13 – 4.17, respectively. The main results of these SVD analyses are summarized in Table 4.1.

The squared covariance fraction (SCF) represents how much of the total covariance of two coupled fields can be accounted for by a specific mode (the first mode in this case). The correlation coefficient of the two time series of expansion coefficients indicates the degree of coupling between the first mode of SIC and the first mode of the forcing factor. According to Sciremammano (1979), the strength of the correlation of two time series can be judged by the ratio (values in parentheses in Table 4.1) of the correlation coefficient of the two time series and their 95% confidence value (values in square brackets). The larger the ratio, the stronger the correlation between the two time series. The SIC variance accounted for by the first mode is calculated by taking the spatial average of the square of the correlation coefficients in S1 (SIC) (Wallace et al., 1992), which represents how much of the total SIC variance over the entire Gulf can be explained by this mode. The regions where the correlation coefficients are largest in homogeneous maps are the areas the largest variance is explained (because variance is the square of correlation coefficients).

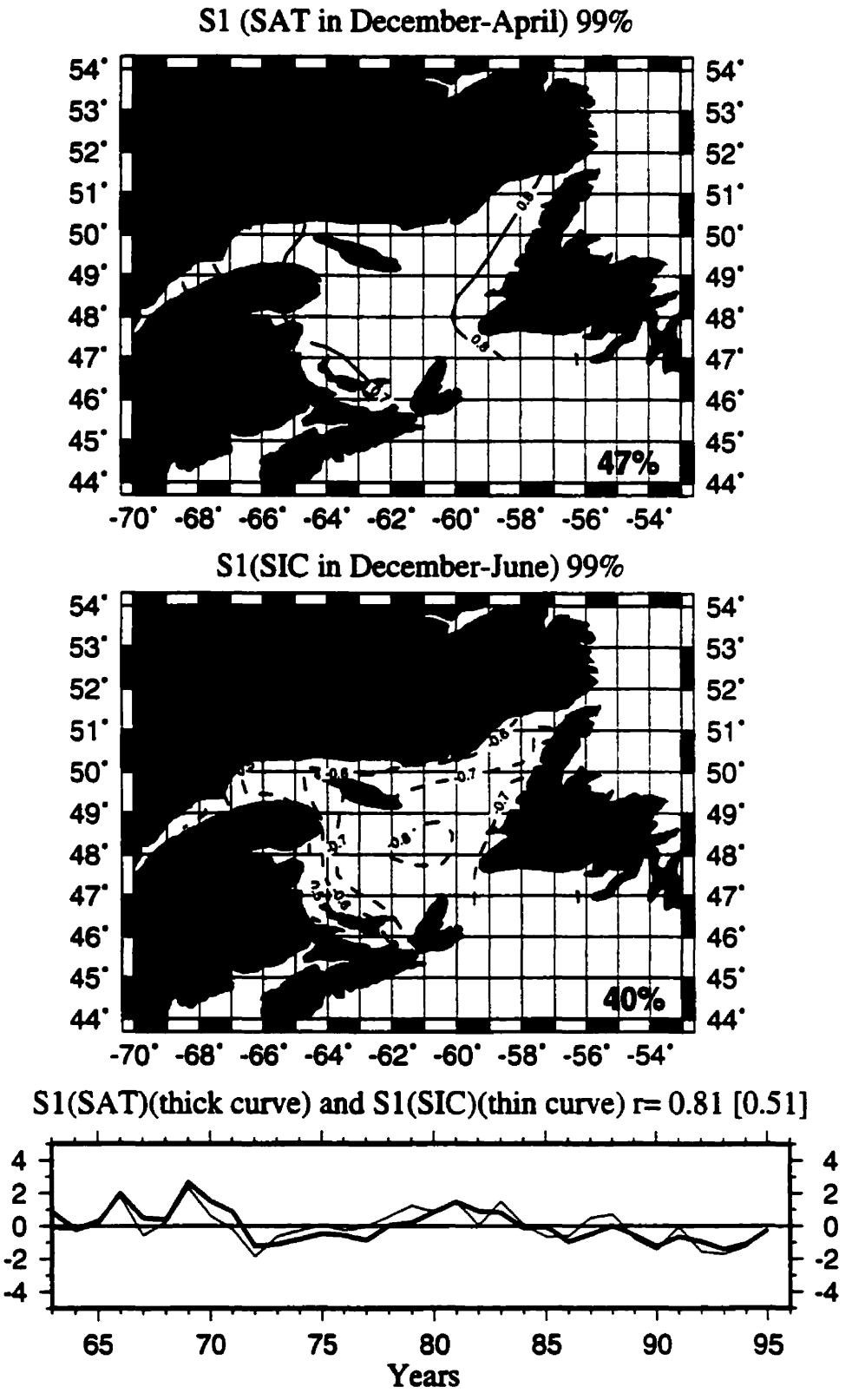

Figure 4.13 Spatial patterns (S1) presented as homogeneous correlation maps and time series of expansion coefficients of the first SVD modes of SAT and SIC

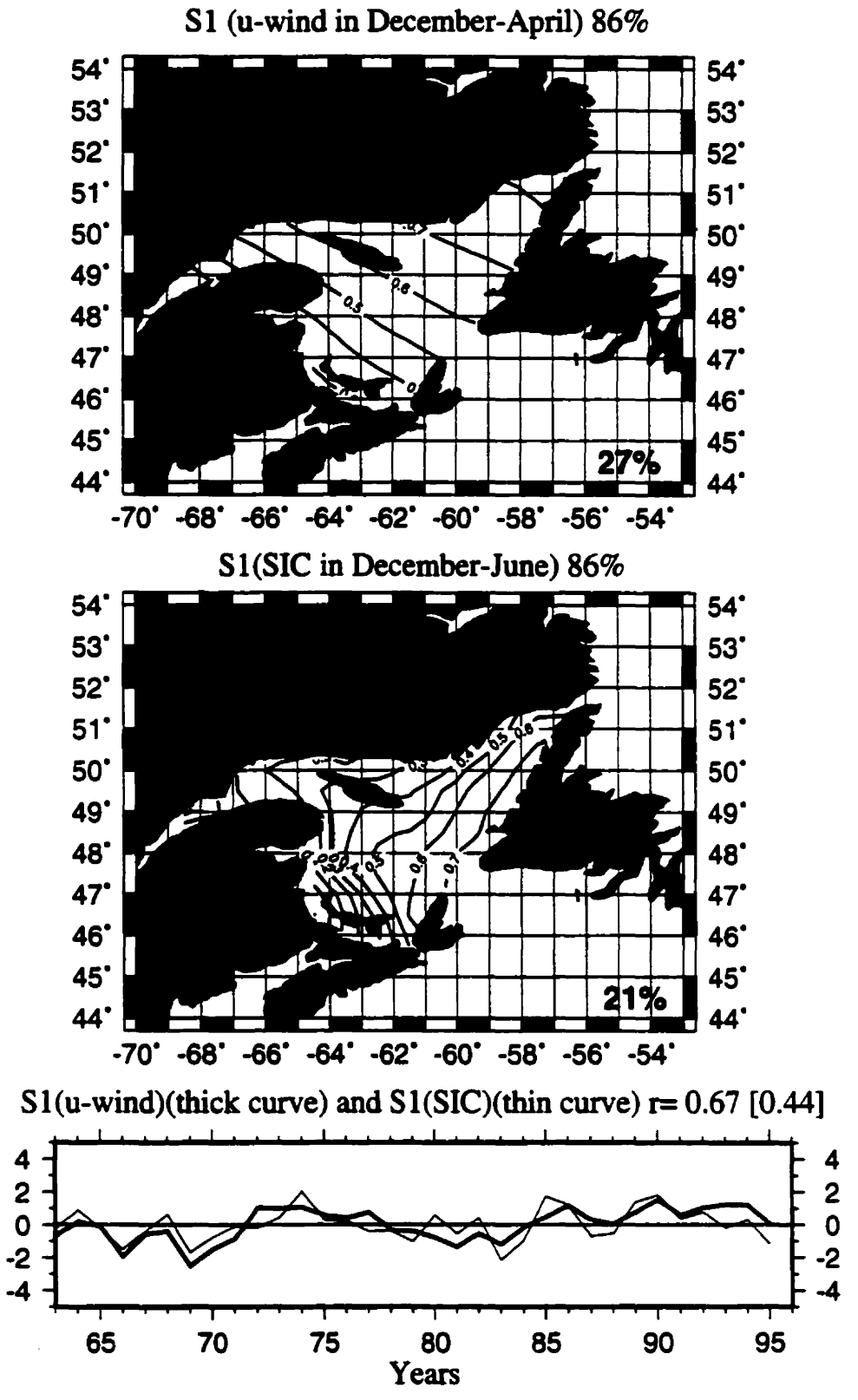

Figure 4.14 Spatial patterns (S1) presented as homogeneous correlation maps and time series of expansion coefficients of the first SVD modes of u-wind and SIC

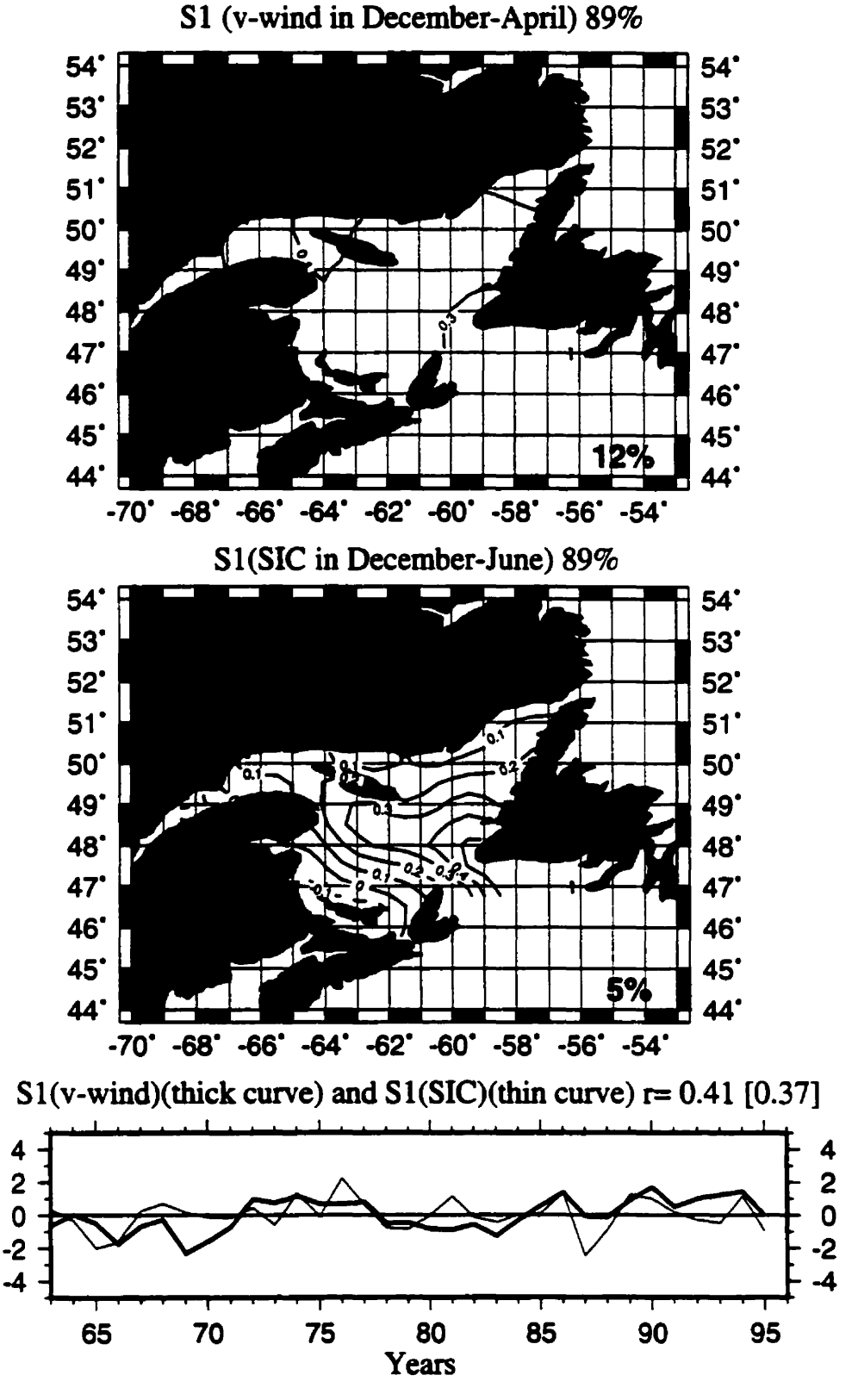

Figure 4.15 Spatial patterns (S1) presented as homogeneous correlation maps and time series of expansion coefficients of the first SVD modes of v-wind and SIC

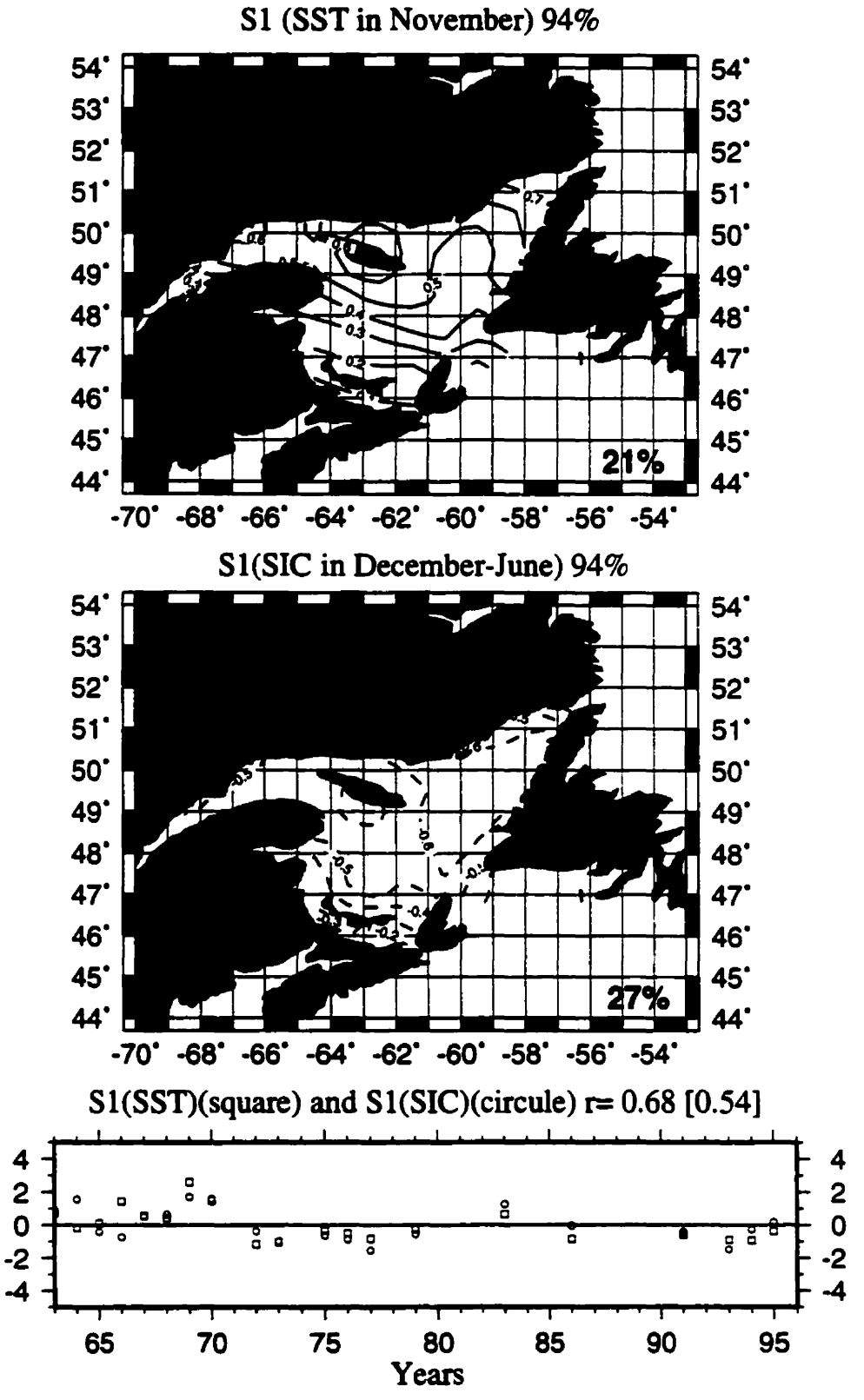

Figure 4.16 Spatial patterns (S1) presented as homogeneous correlation maps and time series of expansion coefficients of the first SVD modes of SST in November and SIC.

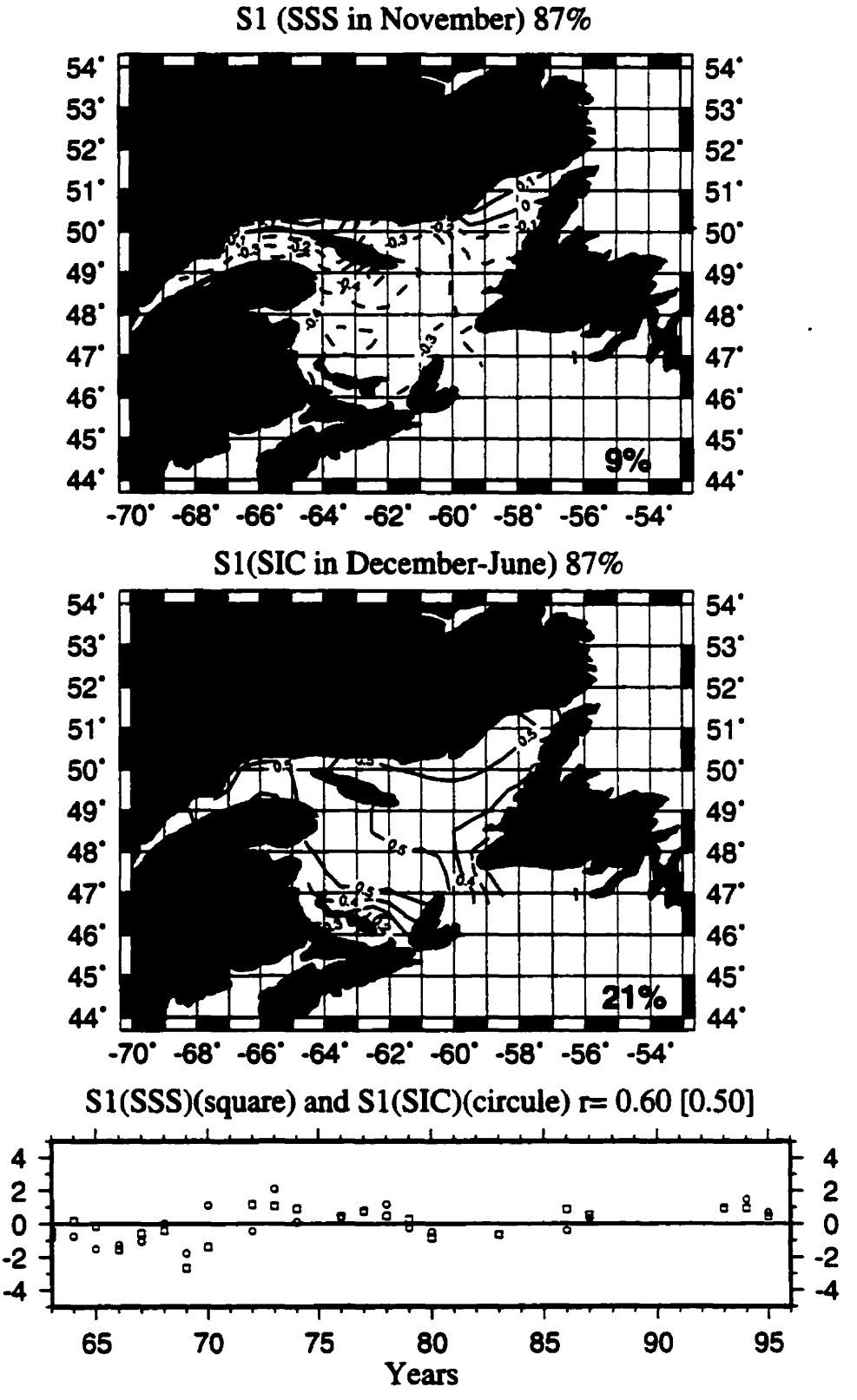

Figure 4.17 Spatial patterns (S1) presented as homogeneous correlation maps and time series of expansion coefficients of the first SVD modes of SSS in November and SIC

Table 4.1. The results of SVD analyses for the relationship between SIC and SAT, winds, SST, and SSS.

	SAT (Dec–April)	u-wind (Dec–April)	v-wind (Dec-April)	SST (November)	SSS (November)
SCF	99%	86%	89%	94%	87%
Correlation Coefficient	-0.81[-0.51] (1.59)	0.67 [0.44] (1.52)	0.41 [0.37] (1.11)	-0.68 [-0.54] (1.26)	-0.60 [-0.50] (1.20)
SIC Variance Accounted	40%	21%	5%	27%	21%
Regions where the Largest Variance Explained	Most Gulf, except coastal regions.	Eastern Gulf	Southeastern Gulf	Northeastern Gulf	Magdalen Shallows

The first SVD modes for SIC and all the forcing factors (Table 4.1) account for the majority of the covariance, the largest SCF being between SIC and SAT (99%) and the least between SIC and u-wind (86%). We thus assume that these are strong enough to examine the relationship between them. The SIC and all the forcing factors all strongly coupled, the most strongly coupled fields being between SIC and SAT and the least between SIC and v-wind. Among the forcing factors, SAT and SST account for the largest part of the total SIC variance (40% and 27%, respectively). In contrast, the v-

wind component accounts for very little of the total SIC variance (5%). This suggests that v-wind is relatively unimportant in explaining the variability of SIC, consistent with our inference from examining extreme sea ice conditions. Regional differences occurred for the relationship between SIC variance and forcing factors. SAT accounts for the largest variance of SIC in most of the Gulf, except for coastal regions. The largest variance in SIC accounted for by the u-wind is in the eastern Gulf, by SST in the northeast Gulf, and by SSS on the Magdalen Shallows.

As expected, the SIC and SAT are strongly correlated in a negative sense, indicating that colder SAT results in more SIC. Figure 4.2 indicates that the mean surface air temperatures are lower in the northern and western coastal regions, and that standard deviations are relatively uniform and small compared with mean values over the entire Gulf. This might suggest that the variability of SAT have little influence on surface heat flux in the northern and western coastal regions, but a relatively larger influence in the central Gulf, which in turn influences sea-ice cover in the central Gulf. This could explain the strong link between SAT and SIC in the central Gulf.

The correlation between SIC and the u-wind component is positive, indicating that with stronger westerlies, sea ice concentrations increase over the Gulf. This can be understood if we examine the mean field of the sea-ice cover (Figure 3.5). Higher concentrations of ice appear in the western Gulf. The stronger westerlies, by themselves and related surface ocean currents, would push ice to the east and lead to greater coverage over the Gulf. We also calculated the correlation between the mean u-wind and SAT in

December-April (averaged over the entire Gulf), and found that they are negatively correlated (–0.63), suggesting that u-wind can advect colder air from land to the Gulf. This colder air would contribute to the positive correlation between u-wind and SIC. In addition, the larger interannual variability of u-wind in the eastern Gulf (Figure 4.4b) would lead to the larger variability of sea-ice cover in this region. The similarity between the standard deviations of sea-ice cover (Figure 3.5) and the first SVD mode of SIC coupled with u-wind (Figure 4.14) supports the fact that the sea ice variability influenced by the u-wind occurs mainly in the eastern Gulf.

Although the SIC and v-wind component are statistically correlated, the v-wind accounts for a negligible amount (only 5%) of the total SIC variance. This is believed to be due in large part to the smaller mean values and weaker variability compared with u-winds (Figures 4.4b and 4.4c). We also calculated the correlation between the mean SAT and v-wind averaged over the entire Gulf and found no significant correlation between them. This suggests that the weak v-winds, northerly in winter, do not bring a significant amount of cold air from the north, so as to affect SIC variability.

The SIC and SST fields are strongly negatively correlated, indicating that that lower SST in November leads to more sea-ice cover in the Gulf. The prerequisite condition for sea ice formation is that the SST must reach the freezing point. Higher SST requires more energy from the atmosphere to remove heat from the ocean and therefore it takes a longer time for sea water to reach the freezing point. The largest variability of November SST occurs in the northeastern Gulf (Figure 4.5a), which would explain why the largest

variance of SIC accounted for by SST occurs in this region.

The SIC and SSS are also strongly negatively coupled, indicating that lower SSS in November causes greater sea-ice cover in the Gulf. As pointed out earlier, the freezing point of sea water drops with high SSS. The lower mean SSS and larger standard deviations in the southwestern region (Figure 4.5b) explain why the largest variance of SIC is accounted for by SSS in this region.

From the variance accounted for by the first SVD modes of SIC and forcing factors SAT, winds, SST, and SSS (Table 4.1), it seems that the SAT is the most important forcing factor (40% of the total SIC variance), followed by SST (27% of the total variance), u-wind (21% of the total variance), and SSS (21% of the total variance). The v-wind is relatively unimportant for sea ice variability. However, because there is an important correlational link between SAT and u-wind, the portion of the SIC variance accounted for by SAT that is caused by the u-wind component is unknown. In Chapter 5, a dynamical model will be used to demonstrate that SAT is the most important forcing factor on sea ice variability in the Gulf.

4.2.1.2 Relationship between SIC and forcing factors: river runoff and NAO

The correlation between SIC and river runoff for each month of the previous year was calculated. The highest correlation occurred with May runoff. The correlation map between SIC and river runoff in May, for which the correlation coefficients are above 90% confidence limits (Figure 4.18 upper), shows the most significant correlation occurs

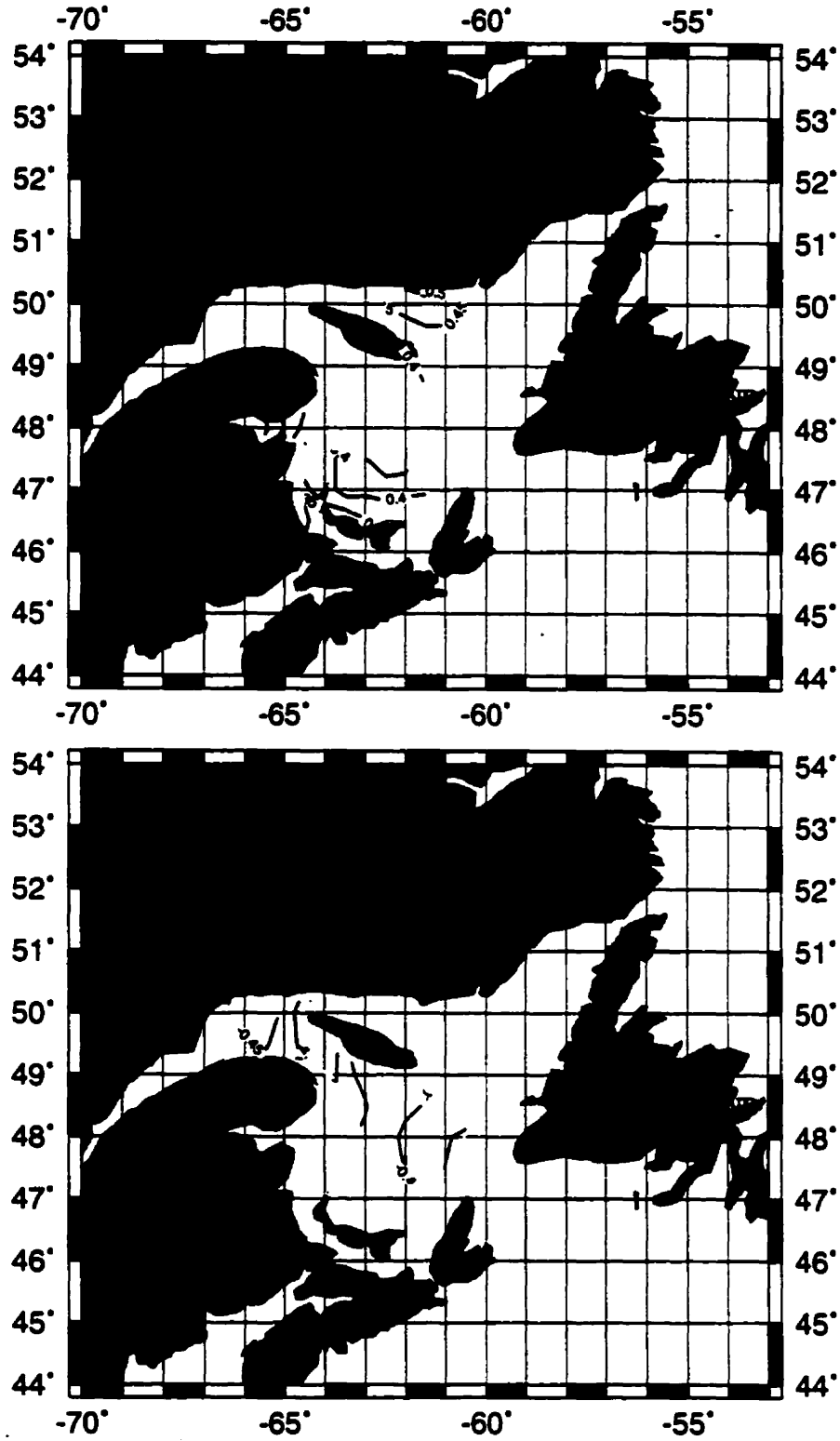

Figure 4.18 Correlation maps (above 90% confidence levels) between sea-ice cover in December-June and May river runoff from the St.Lawrence River system (top) and between the time of first ice presence and yearly runoff (bottom)

in the southwestern Gulf and in a small area near the northern coast. The correlation is positive, indicating higher river runoff generates increased sea-ice cover. The good correlation between SIC and river runoff in the southwestern Gulf is consistent with the lower salinities in that region during November. However, the high correlation near the northern coast is most likely caused by river runoff from local rivers. It might be expected that precipitation values are correlated over wide areas of eastern Canada. In addition, 14% of the total SIC variance can be explained by river runoff.

We also calculated the correlation values between SIC and the North Atlantic Oscillation index (Figure 4.19 upper). The correlation map shows that SIC and NAO are correlated over most of the Gulf. The positive correlation between them indicates that a stronger NAO index is associated with greater sea-ice cover. As pointed out in Section 4.1.5, NAO could influence sea ice variability in the Gulf by influencing meteorological conditions over the Gulf through large-scale atmospheric circulation. We calculated the correlation between NAO and SAT and found they were negatively correlated (–0.45). This implies that stronger values of the NAO index would lead to lower SAT over the Gulf of St. Lawrence, which in turn leads to more sea-ice cover. In Section 4.1.7, we found that there is good correlation between sea ice advection via the Strait of Belle Isle and sea ice anomalies in Region 3 in the Gulf. Previous studies also indicate that NAO fluctuations can be linked to sea ice variability in the Labrador Sea. Thus, NAO can indicate changes of sea ice conditions in the Gulf through sea ice advection from the Labrador Sea to the Gulf and lower SATs at large spatial scales

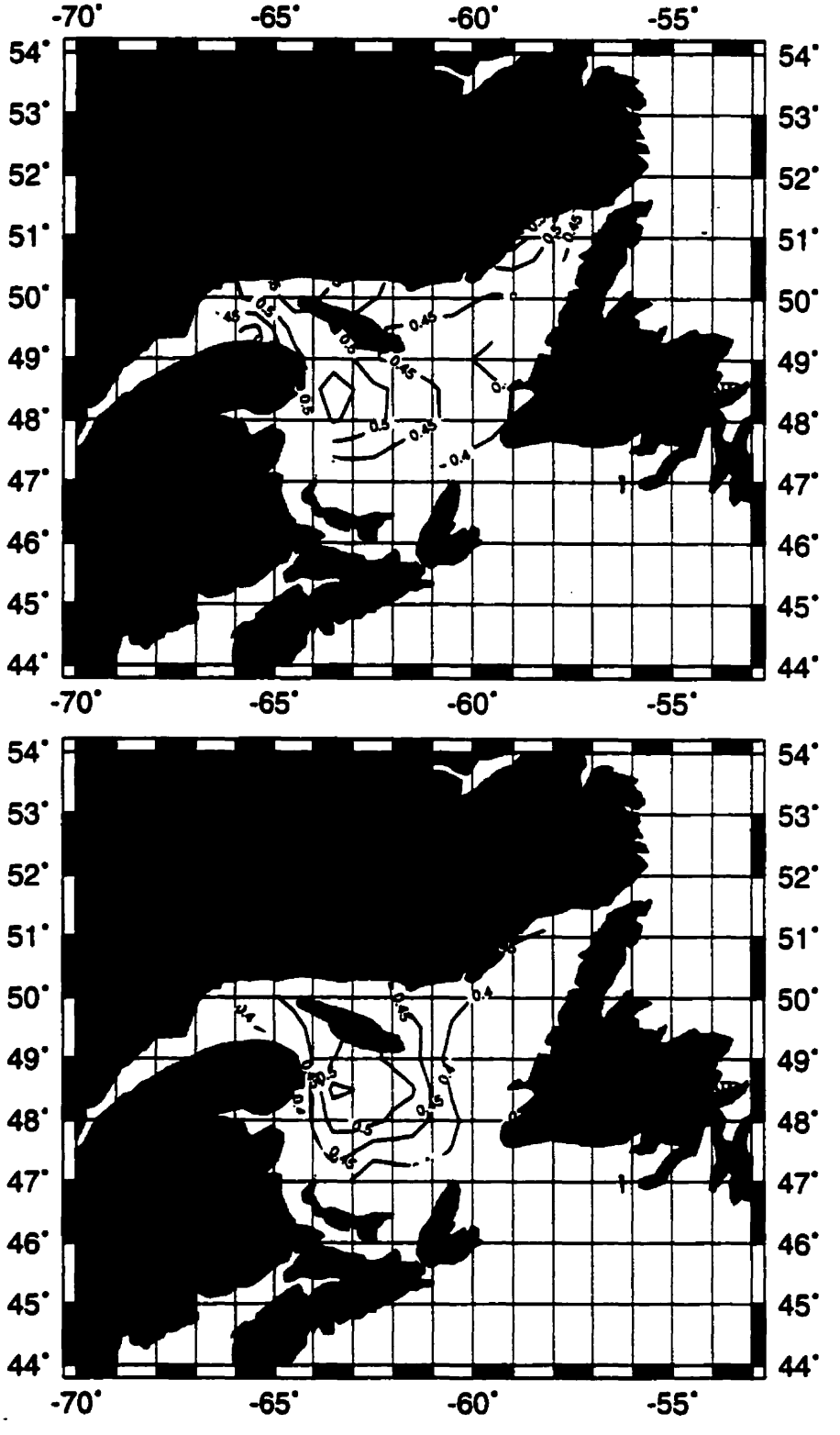

Figure 4.19 Correlation maps (above 90% confidence levels) between sea-ice cover in December-June and North Atlantic Oscillation (NAO) (top) and between the time of last ice presence and NAO (bottom).

4.2.1.3 Regression between SIC and forcing factors

In order to further examine the relative importance of the forcing factors, we ran multiple regressions between SIC and all the forcing factors discussed above. Initially, SIC and each forcing factor (excluding the river runoff and NAO) were averaged for corresponding periods over the entire Gulf. The correlation coefficients were then calculated between SIC and each forcing factor. Figure 4.20a shows the time series of normalized spatially averaged overall mean SIC, overall mean forcing factors (river runoff and NAO are single variables), and the correlations between them. The correlations between SIC and December-April SAT, u-wind, November SST/SSS, and NAO are all significant at the 95% confidence levels. The correlation between SIC and May river runoff is significant at the 90% confidence level. No significant correlation was found between SIC and v-wind. Linear regressions were then calculated for normalized overall mean SIC with overall mean forcing factors SAT, u-wind, SST, SSS, NAO, and river runoff as independent variables. The following relationship was determined.

$$SIC=-0.55*SAT+0.19*u\text{-}wind-0.25*SST-0.08*SSS+0.18*NAO+0.30*RIV_{May} \quad (4.1)$$

This regression accounts for 89% of the total SIC variance over the entire Gulf. However, since some of the independent variables, SAT and u-wind, SSS and river runoff, NAO and SAT, in above regression are correlated, the coefficients before each independent variable may not reflect its contribution margin to the SIC correctly. By removing this co-linearity and keeping only three independent variables: SAT, SST, and SSS, the regression was recalculated as follows:

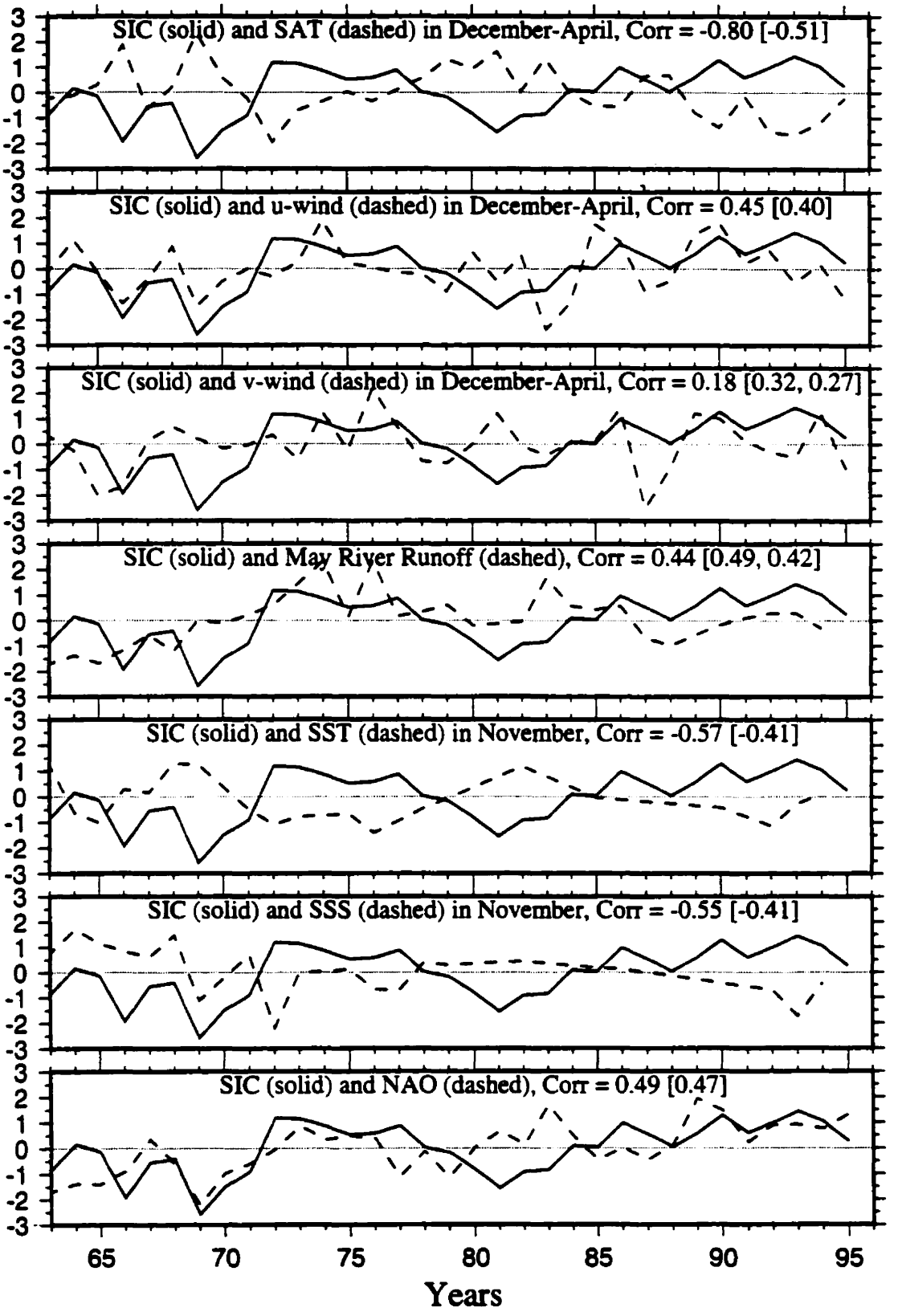

Figure 4.20a Time series of normalized sea-ice cover (SIC) in December-June, forcing factors with SAT and winds in December-April, and correlation between them

$$SIC = -0.68 * SAT - 0.41 *SST - 0.14 *SSS. \quad (4.2)$$

This regression accounts for 81% of the total SIC variance over the entire Gulf. Although simple, it clearly indicates the relationship between SIC and forcing factors SAT, SST, and SSS. SIC and these three forcing factors are negatively correlated, consistent with our previous SVD analysis. This regression also indicates the relative importance of these forcing factors on SIC variability. Since all the variables are normalized, the coefficients represent their relative importance, i.e., the SAT, SST, and SSS are ranked at first, second, and third, respectively. In addition, this regression can also be used to estimate the SIC conditions once SAT in December-April, November SST and SSS are known.

In the following, we explore the possibility of predicting SIC when November SST, SSS, May river runoff, December SAT and December winds are available. Figure 4.20b shows the time series of normalized SIC, forcing factors with SAT and winds in December, and the correlation between them. The correlation between SIC and December SAT is significant above the 95% confidence level. However, no significant correlation was found between SIC and both u-wind and v-wind in December. A linear regression was calculated for normalized overall mean SIC with overall mean forcing factors: December SAT, November SST and SSS, and river runoff as independent variables. The regression is as follows:

$$SIC=-0.35*SAT_{DEC}-0.33*SST-0.19*SSS+0.38*RIV_{May} \quad (4.3)$$

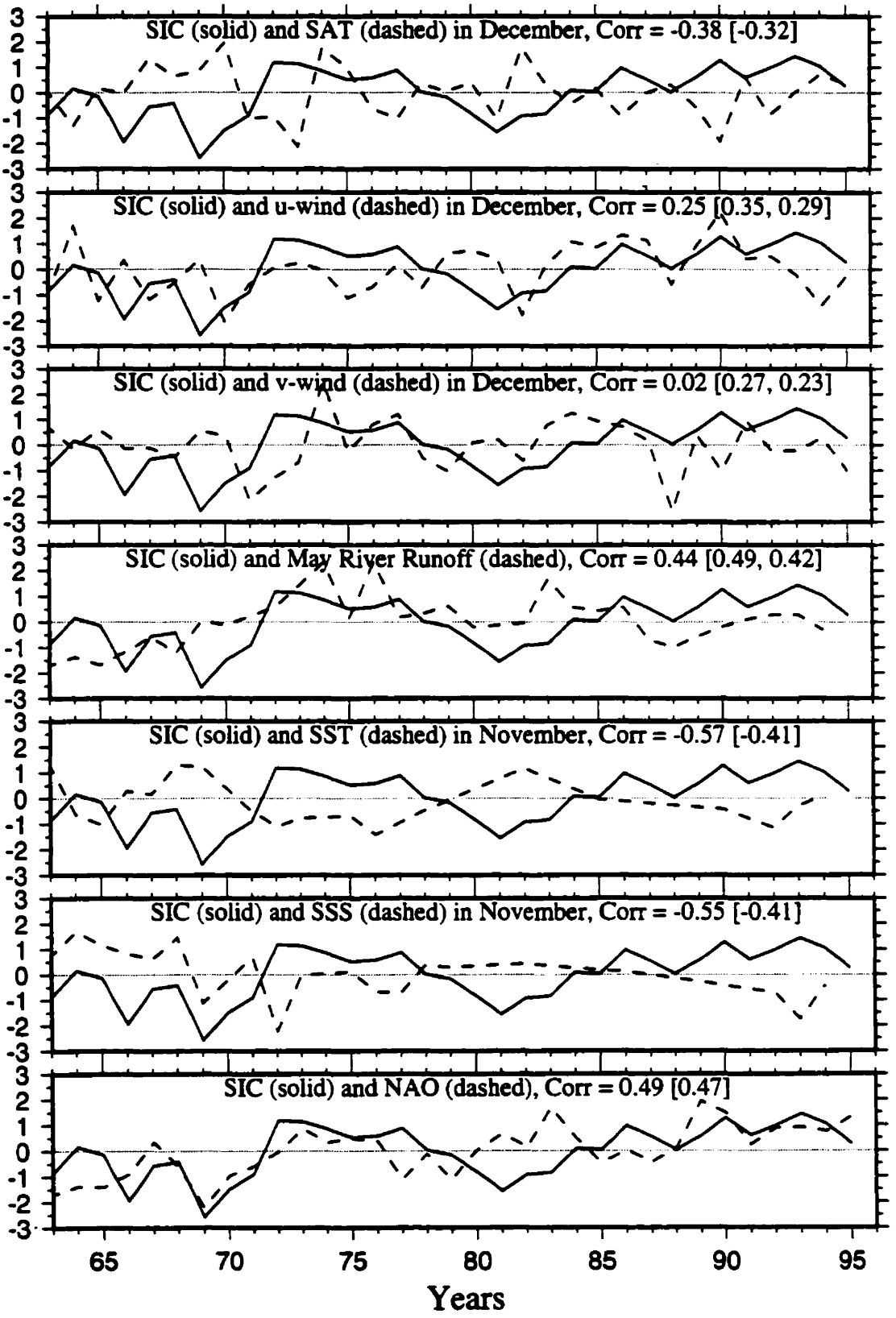

Figure 4.20b Time series of normalized sea-ice cover (SIC) in December-June, forcing factors with SAT and winds in December, and the correlation between them

This regression accounts for 60% of the total SIC variance over the entire Gulf. By removing co-linearity from the forcing factors, we have the following regression:

$$SIC = -0.28*SAT_{DEC}-0.52*SST-0.40*SSS \quad (4.4)$$

This regression accounts for 55% of the total SIC variance over the entire Gulf. From this regression, we can predict SIC conditions once December SAT, November SST and SSS are available although the total SIC variance accounted for by this formula is not very high.

4.2.2 Relationship between the time of first ice presence and forcing factors

4.2.2.1 Relationship between TFIP and forcing factors SAT, winds, SST, SSS, and river runoff

Similar to the analysis of the relationship between SIC and different forcing factors, we also examined the relationship between both TFIP and TLIP and the same forcing factors as before. The homogeneous correlation maps and the time series of expansion coefficients of the first SVD modes of TFIP and forcing factors: December SAT, December u-wind, December v-wind, November SST, and November SSS are shown in Figures 4.21 – 4.25, respectively. The main results are summarized in Table 4.2.

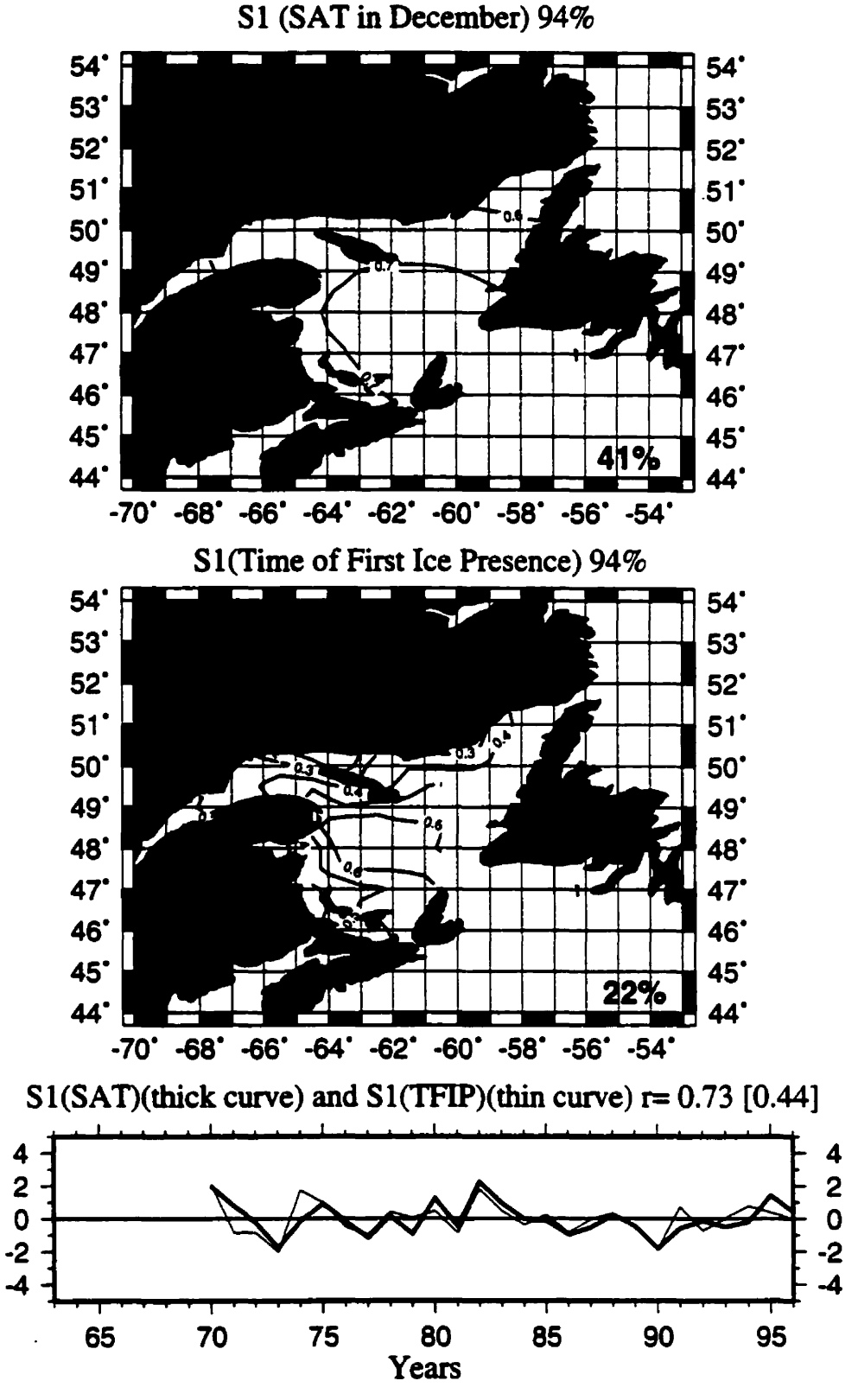

Figure 4.21 Spatial patterns (S1) presented as homogeneous correlation maps and time series of expansion coefficients of the first SVD modes of SAT in December and TFIP

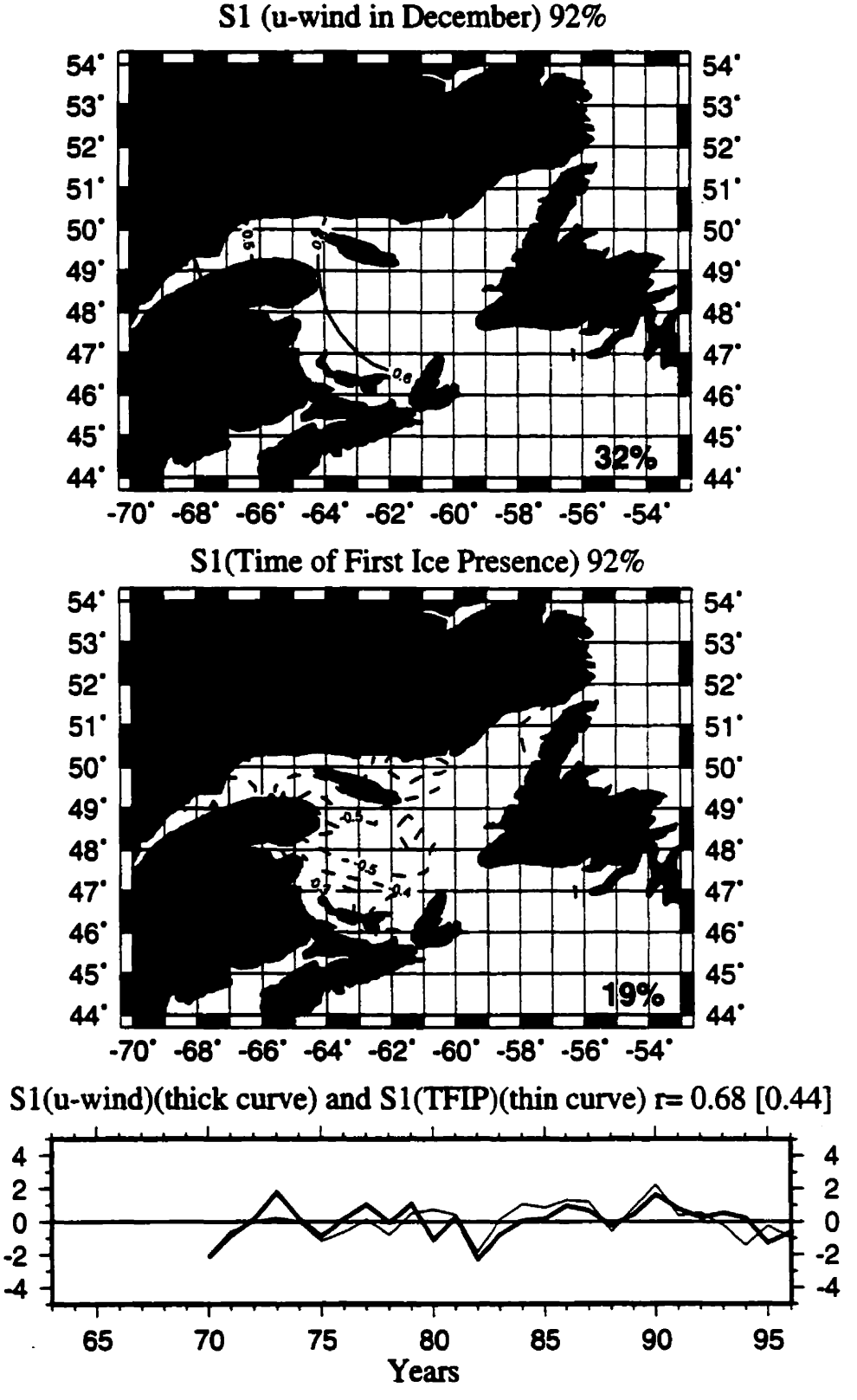

Figure 4.22 Spatial patterns (S1) presented as homogeneous correlation maps and time series of expansion coefficients of the first SVD modes of u-wind in December and TFIP

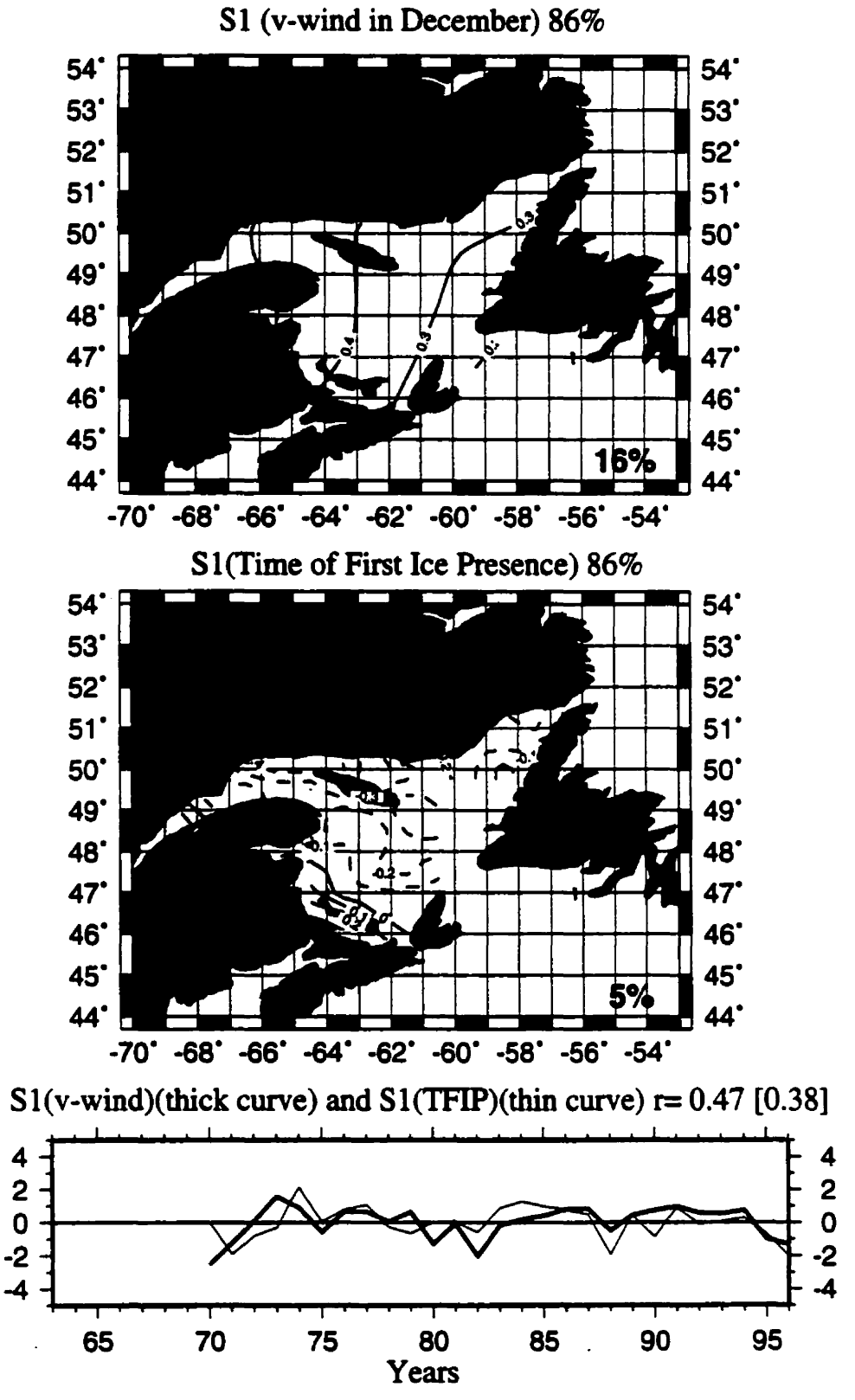

Figure 4.23 Spatial patterns (S1) presented as homogeneous correlation maps and time series of expansion coefficients of the first SVD modes of v-wind in December and TFIP.

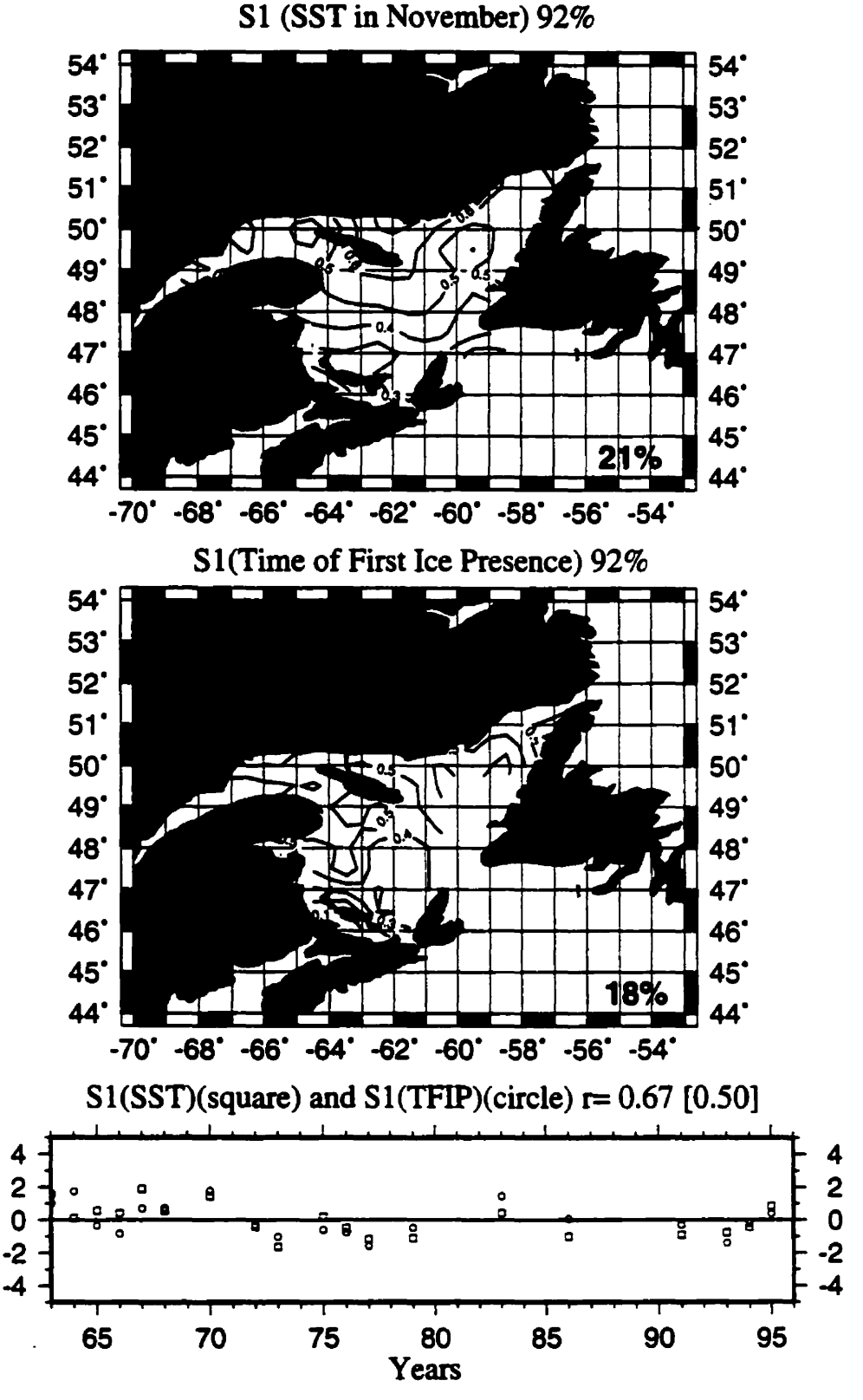

Figure 4.24 Spatial patterns (S1) presented as homogeneous correlation maps and time series of expansion coefficients of the first SVD modes of SST in November and TFIP.

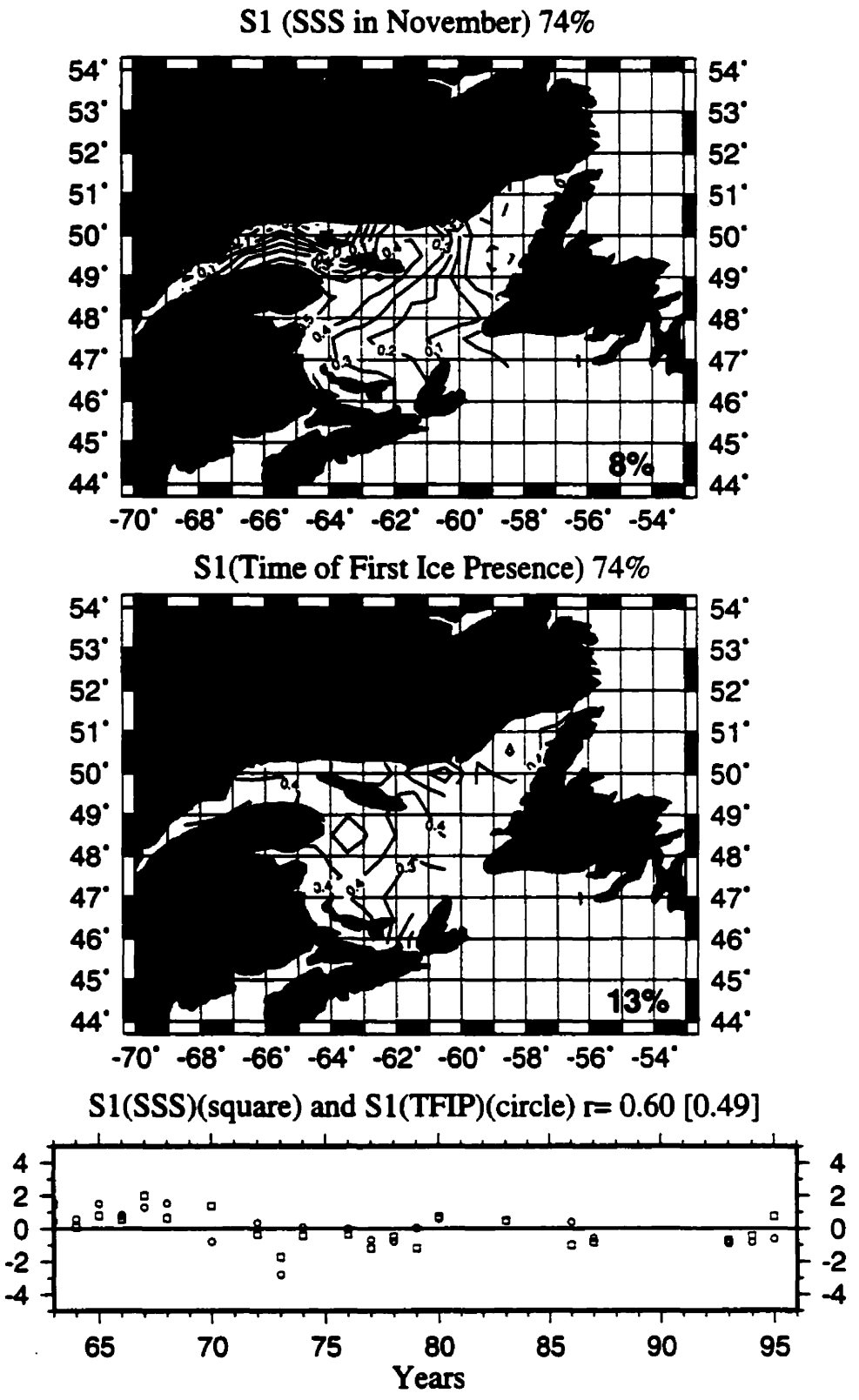

Figure 4.25 Spatial patterns (S1) presented as homogeneous correlation maps and time series of expansion coefficients of the first SVD modes of SSS in November and TFIP.

Table 4.2. The results of SVD analyses for the relationship between TFIP and SAT, winds, SST and SSS.

	SAT (December)	u-wind (December)	v-wind (December)	SST (November)	SSS (November)
SCF	94%	92%	86%	92%	74%
TFIP Variance Accounted	22%	19%	5%	18%	13%
Correlation Coefficient	0.73 [0.44] (1.66)	-0.68 [0.44] (1.55)	-0.47 [0.38] (1.24)	0.67 [0.50] (1.34)	0.60 [0.49] (1.22)
Region where the Largest Variance Explained	Central Gulf	Central Gulf	St. Lawrence Estuary	St. Lawrence Estuary	St. Lawrence Estuary

The December SAT accounts for the largest part of the total TFIP variance (22%) among all the forcing factors. As expected, TFIP and SAT are strongly positively correlated, indicating that colder surface air temperature in December results in earlier sea ice appearance. The largest variance of TFIP accounted for by December SAT in the central Gulf is most likely explained as follows. Although the largest standard deviations of December SAT are in the northwest Gulf, the mean SAT there is very low (Figure 4.2).

Thus, the mean SAT plus one standard deviation is still much lower than the freezing point. In contrast, in the central Gulf, the mean SAT plus one standard deviation is close to the freezing point. Thus, sea ice formation there would be expected to vary more than in the other regions.

The u-wind accounts for 19% of the total TFIP variance. The correlation between TFIP and the u-wind is negative, indicating that stronger westerlies cause earlier sea ice appearance. This is most likely caused by the following three processes. First, u-wind and its related ocean currents can transport sea ice from the St. Lawrence Estuary and the western coast to the central and eastern Gulf, which leads to earlier sea ice formation in these regions. Second, as pointed out earlier, u-wind can advect colder air from land to the Gulf, which in turn leads to earlier sea ice formation. Third, the stronger u-wind, by increasing sensible and latent heat, leads to more heat loss from the ocean and therefore also provokes earlier sea ice appearance. The largest variability of TFIP accounted for by u-winds in the central Gulf can be explained by the larger variability of u-winds in the central and eastern Gulf (Figure 4.4b).

The variance of the total TFIP field accounted for by v-wind is very small, only 5%of the total, suggesting that v-winds are again unimportant in explaining TFIP. SST accounts for 18% of the total TFIP variance. The TFIP and SST are strongly positively correlated, indicating that lower SSTs lead to earlier sea ice formation. The largest variance accounted for by SST is in the St. Lawrence Estuary, which could be caused by the lower mean SST values in that region (Figure 4.5a) since sea water there can reach the freezing

point faster than in other regions. The SSS accounts for 13% of the total TFIP variance. The positive correlation between SSS and TFIP indicates that lower SSS leads to earlier sea ice formation. The largest variance attributable to SSS is found in the St. Lawrence Estuary, which is most likely related to the lower mean SSS and larger standard deviations in that region (Figure 4.5b). Among all the forcing factors, SAT accounts for the largest part of the total TFIP variance, followed by u-wind, SST, and SSS in that order.

We also calculated the correlation between TFIP and yearly-mean river runoff from the St. Lawrence River system (Figure 4.18 lower). A significant correlation (above 90% confidence limits) occurs in the St. Lawrence Estuary and the Magdalen Island region. This is believed to be related to the fresher water and its larger variability in these regions (Figure 4.5b). In regard to total TFIP variance, 9% can be explained by river runoff.

4.2.2.2 Regression between TFIP and forcing factors

We also examined the relationship between the overall mean TFIP for the entire Gulf and overall mean forcing factors. Figure 4.26 shows the time series of normalized TFIP, forcing factors, and correlation between them. The correlations between TFIP and December SAT, u-wind, and November SST/SSS are all significant, above the 95% confidence level. No significant correlation was found between TFIP and v-wind or between TFIP and river runoff. Because u-wind and SAT are correlated, we chose only one factor as an independent variable. In this case, we chose u-wind because it yields a larger variance in regression analysis. The regression equation for normalized overall

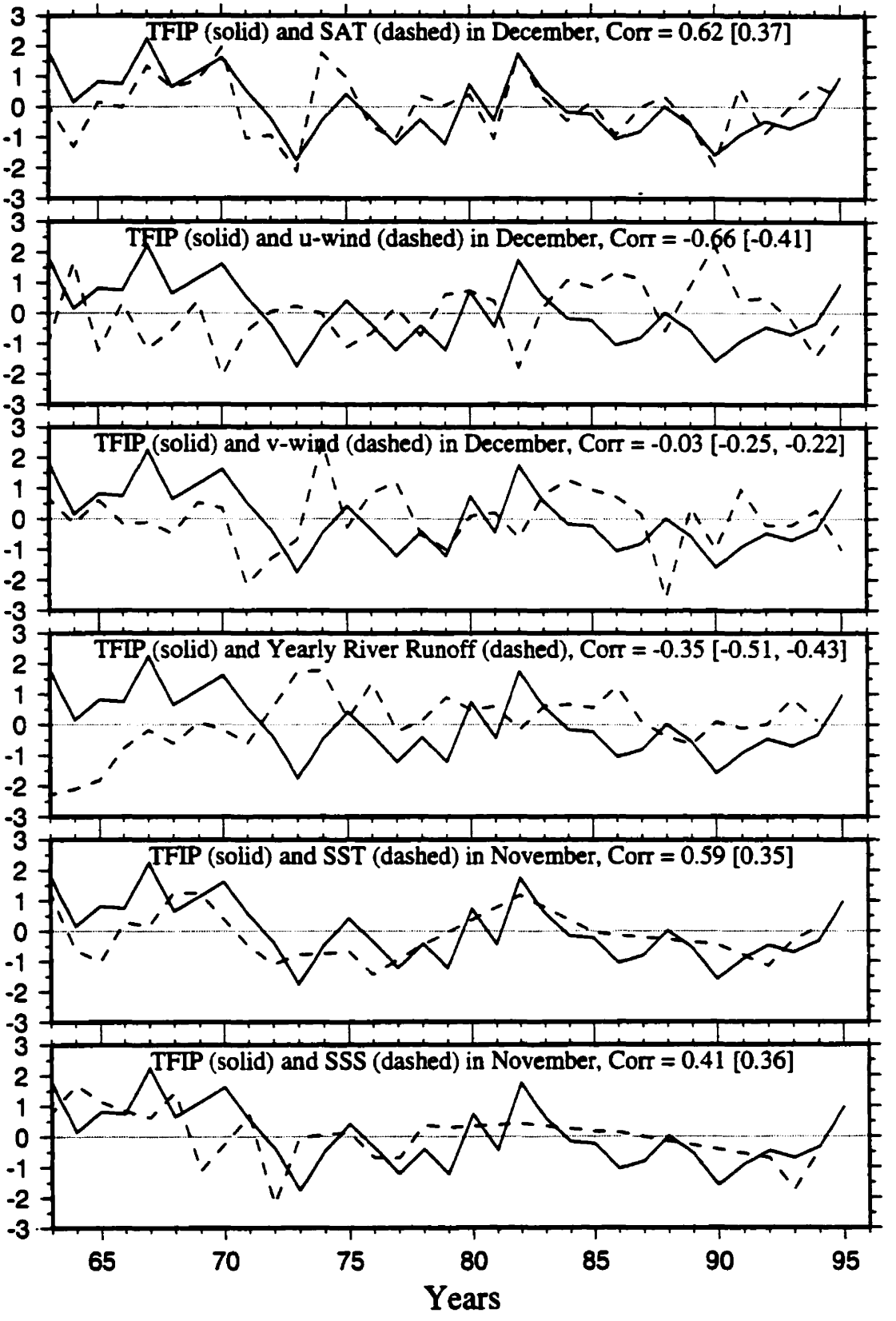

Figure 4.26 Time series of normalized time of first ice presence (TFIP), forcing factors, and the correlation between them.

mean TFIP with overall mean forcing factors u-wind, SST, and SSS as independent variables is:

$$TFIP = -0.56 * \text{u-wind} + 0.54 * SST + 0.43 * SSS. \quad (4.5)$$

This regression accounts for 76% of the total TFIP variance over the entire Gulf. It indicates that TFIP is negatively correlated with u-wind and positively correlated with SST and SSS, consistent with the SVD analysis. This regression also indicates that u-wind and SST are of same importance to variability of TFIP. SSS is less important. The regression equation can be also used to estimate the TFIP over the entire Gulf, assuming SAT in December, and November SST and SSS are available.

4.2.3 Relationship between time of last ice presence and forcing factors

The homogeneous correlation maps and the time series of time expansion coefficients of the first SVD modes for TLIP and the following forcing factors: March-April SAT, u-wind, and v-wind are shown in Figures 4.27-4.29, respectively. The main results are summarized in Table 4.3.

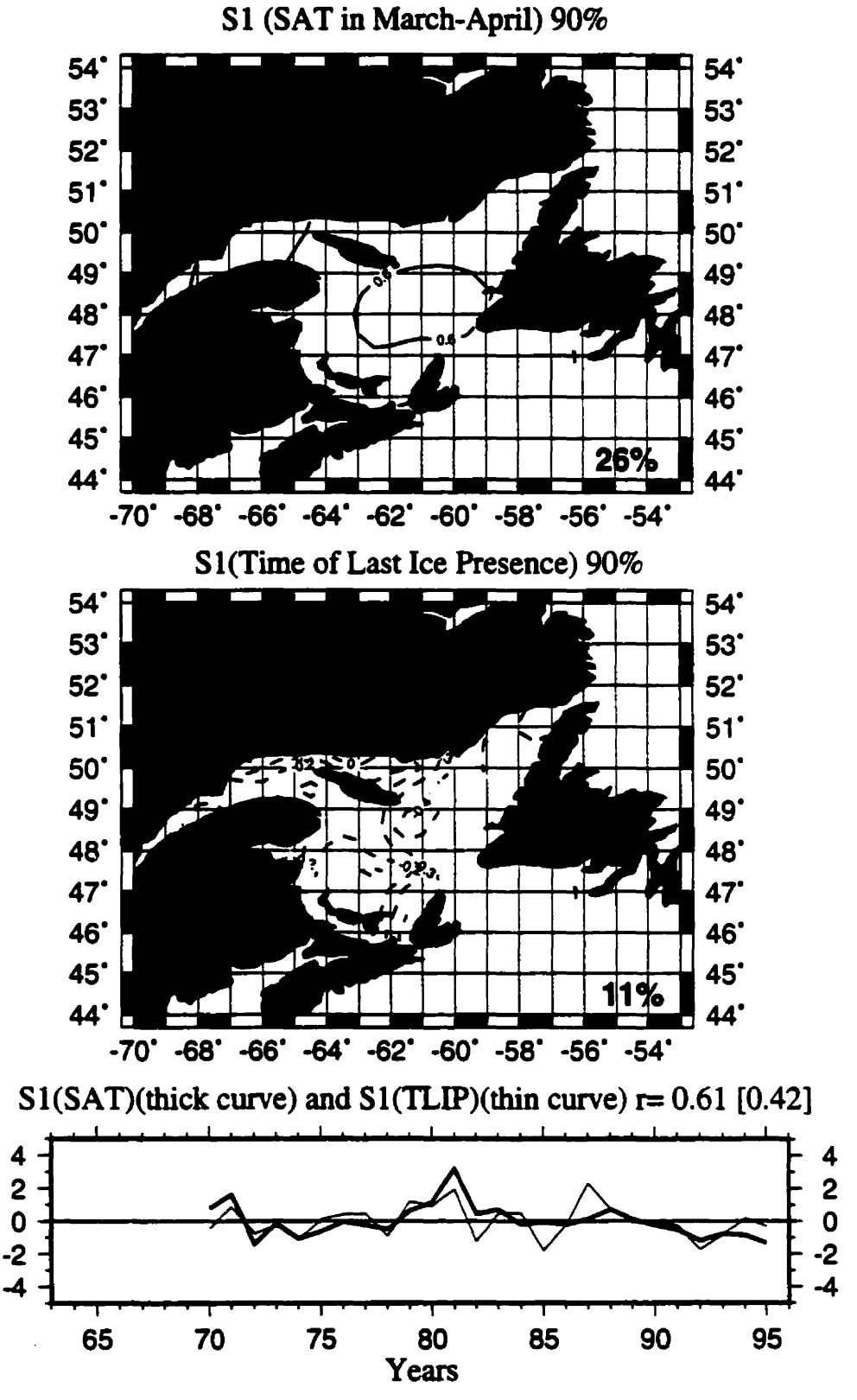

Figure 4.27 Spatial patterns (S1) presented as homogeneous correlation maps and time series of expansion coefficients of the first SVD modes of SAT in March-April and TLIP.

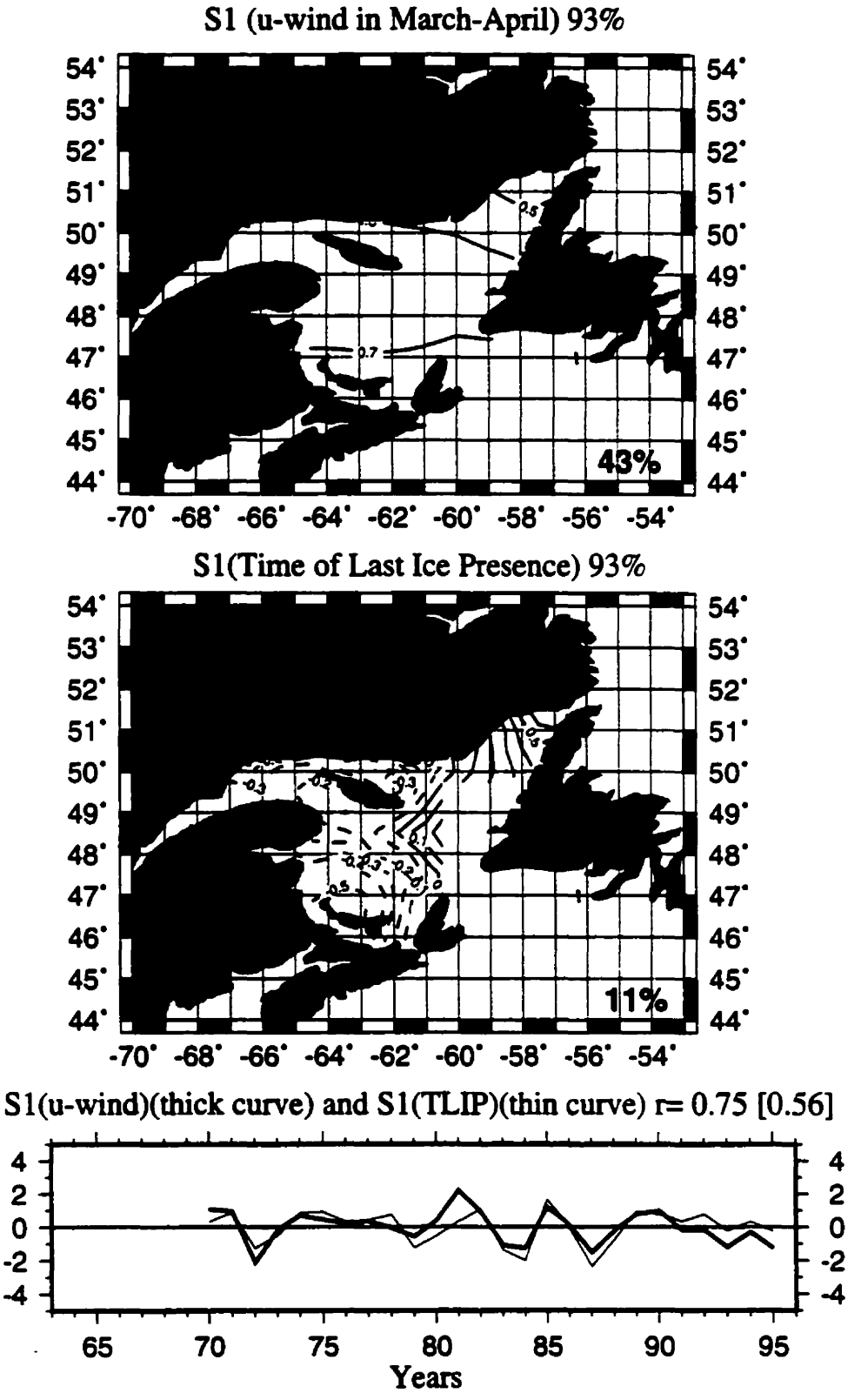

Figure 4.28 Spatial patterns (S1) presented as homogeneous correlation maps and time series of expansion coefficients of the first SVD modes of u-wind in March-April and TLIP.

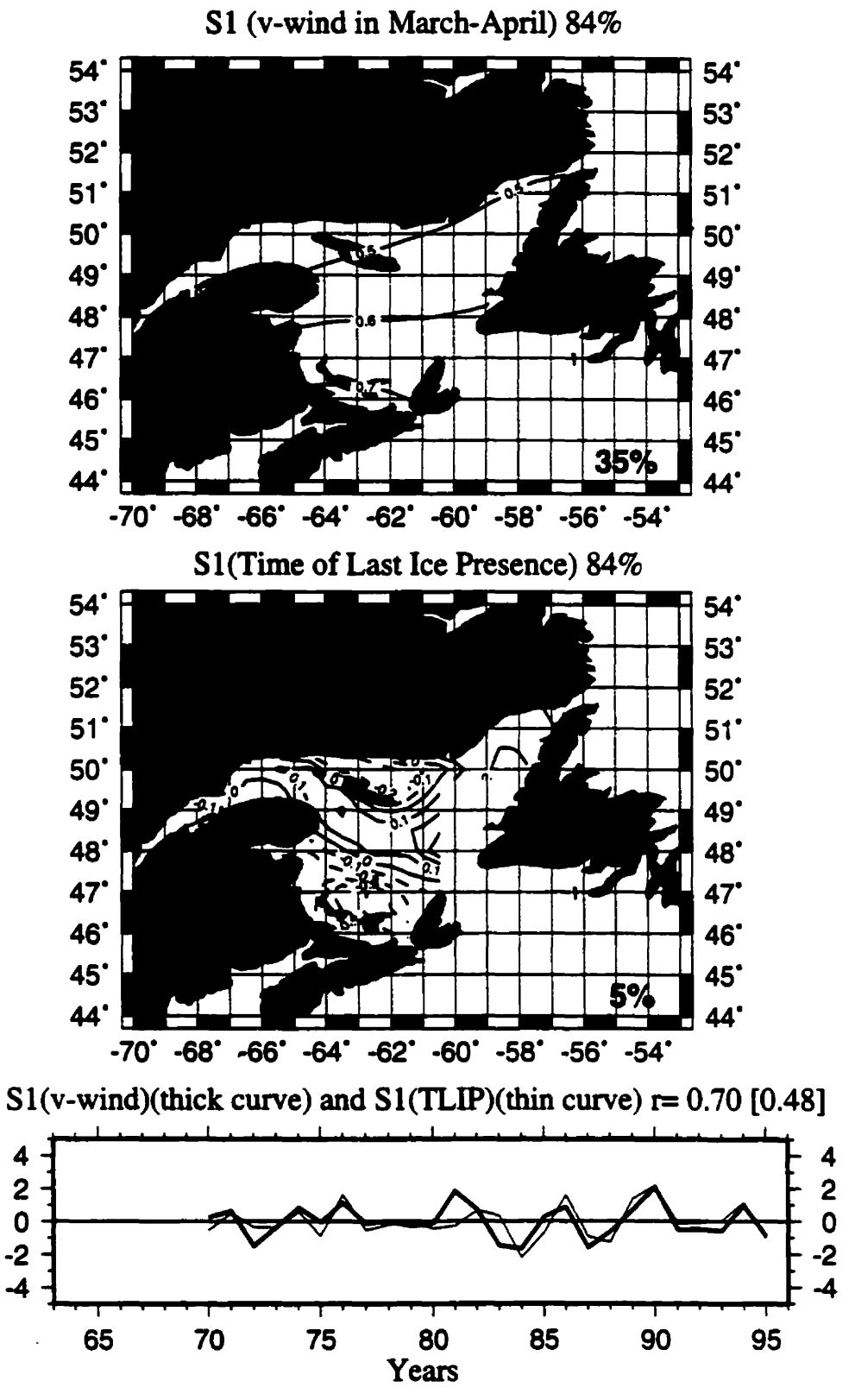

Figure 4.29 Spatial patterns (S1) presented as homogeneous correlation maps and time series of expansion coefficients of the first SVD modes of v-wind in March-April and TLIP.

Table 4.3. The results of SVD analyses for the relationship between TLIP and SAT, and winds.

	SAT (March–April)	u-wind (March–April)	v-wind (March-April)
SCF	90%	93%	84%
SIC Variance Accounted	11%	11%	5%
Correlation Coefficient	-0.60 [0.42] (1.43)	±0.75 [0.55] (1.36)	±0.70 [0.48] (1.46)
Regions where the Largest Variance Explained	Central Gulf	Western and Eastern Coasts	Southern and Northern Coasts

The first SVD modes of March-April SAT, u-wind, and v-wind account for a majority of the total TLIP variance and they are all coupled with the TLIP field. However, the variance of TLIP accounted for by these forcing factors is not large, only 11% for the SAT and u-wind and 5% for the v-wind. As expected, the TLIP and SAT are negatively correlated. Again, the largest variance of TLIP is explained by SAT in the central Gulf

region. This is believed to be related to the mean March-April SAT plus one standard deviation being close to the freezing point in the central Gulf (Figure 4.2). However, the largest variance of TLIP explained by the u-wind occurs in the western and eastern Gulf. Moreover, u-wind and TLIP are negatively correlated in the western Gulf but positively correlated in the eastern Gulf. This is most likely due to the fact that u-wind and its related currents transport sea ice from the western Gulf to the eastern Gulf. Since in most years sea ice lasts longer on the western Gulf, increased westerly winds would tend to push ice out of the western region and into the east. Once again, the v-wind component seems unimportant to the variability of TLIP.

We also examined the relationship between TLIP and November SST, SSS, river runoff, but could find no significant correlation between them. Figure 4.19 (lower) shows the correlation map for which correlation coefficients are greater than 90% confidence levels between TLIP and NAO. The highest correlation occurs near the St. Lawrence Estuary. No significant correlation was found between NAO and SAT in March-April and between NAO and u-wind. However, there is a significant correlation between NAO and SAT in December-April. Thus, the highest correlation between TLIP and NAO could be caused by the December-April SAT. By examining the relationship between TLIP and SAT and winds in December-April (Figures 4.30-4.32), the larger variance of TLIP (19%) was explained by the December-April SAT (Figure 4.30). However, December-April u-wind does not increase the explained variance of TLIP. The December-April v-wind has little influence compared with that explained by SAT.

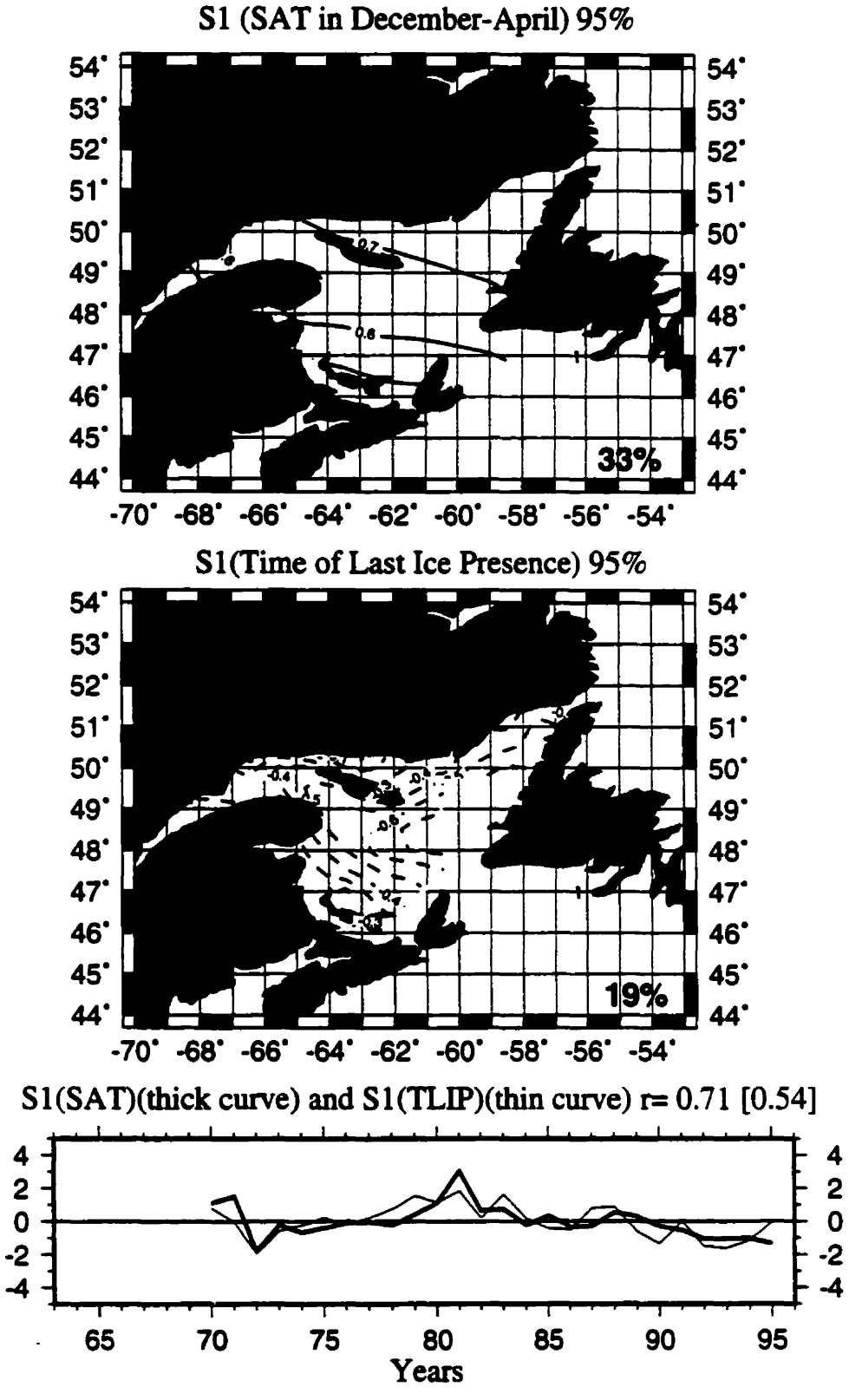

Figure 4.30 Spatial patterns (S1) presented as homogeneous correlation maps and time series of expansion coefficients of the first SVD modes of SAT in December-April and TLIP.

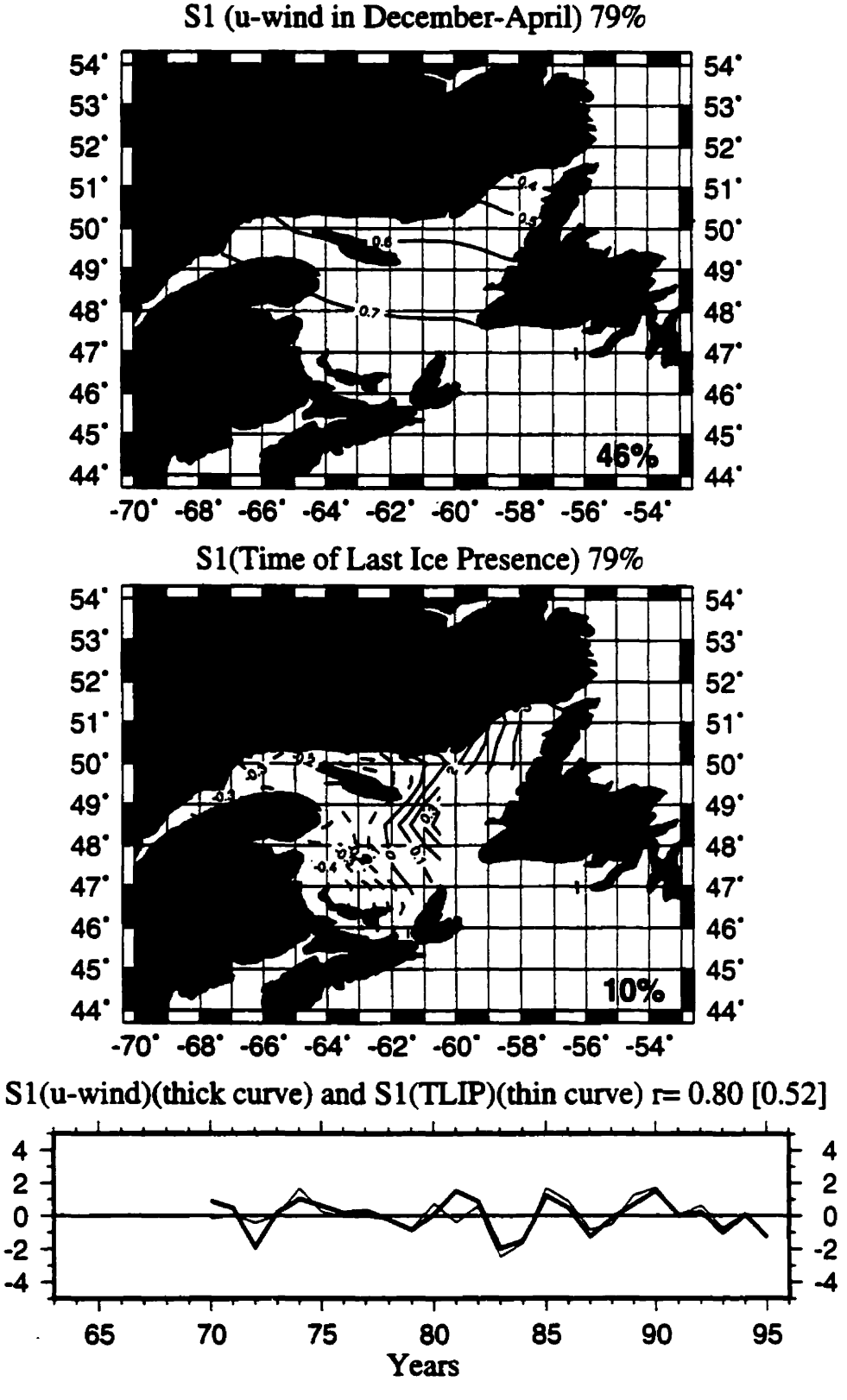

Figure 4.31 Spatial patterns (S1) presented as homogeneous correlation maps and time series of expansion coefficients of the first SVD modes of u-wind in December-April and TLIP.

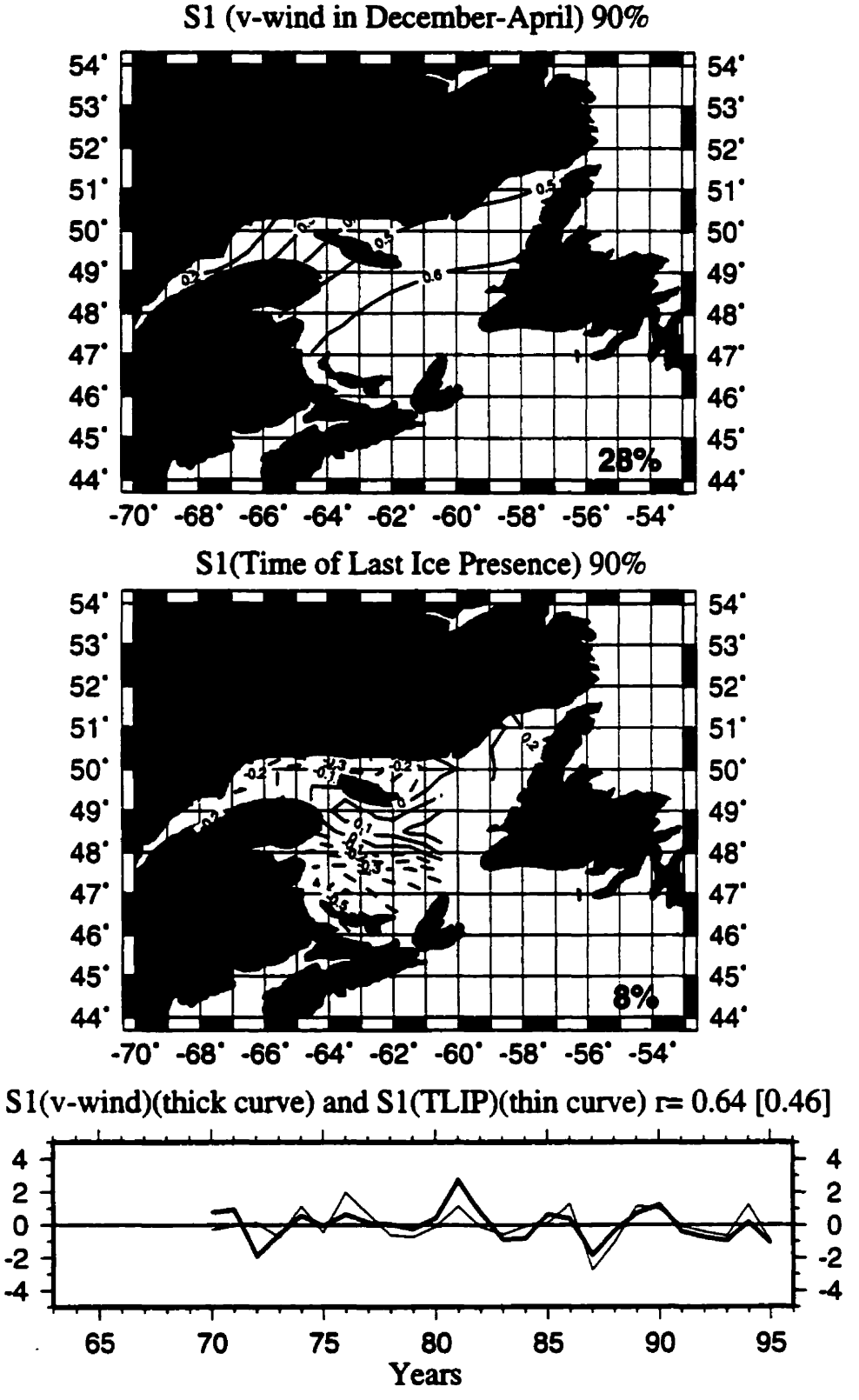

Figure 4.32 Spatial patterns (S1) presented as homogeneous correlation maps and time series of expansion coefficients of the first SVD modes of v-wind in December-April and TLIP.

Figure 4.33a and Figure 4.33b show time series and the correlation between the overall mean TLIP and forcing factors with SAT and winds in March-April and in December-April, respectively. Over the Gulf-wide scale, only SAT is useful in explaining variability of TLIP. However, the correlation between TLIP and SAT is not high, -0.50 for TLIP and SAT in March-April and –0.64 for TLIP and SAT in December-April. Thus, an explanation of the forcing factors controlling variability of TLIP needs study.

4.3. Discussions and summary

4.3.1 Intraseasonal variability

Sea ice begins to form in the St. Lawrence Estuary, the western shore of the Magdalen Shallows, and the Strait of Belle Isle region in mid to late December. For these different regions, the mechanisms responsible for the early sea ice formation are not the same. In the St. Lawrence Estuary, both lower SST in November (Figure 4.5a) and lower SAT in early December (Figure 4.1a) contribute to the early formation of sea ice. Lower salinities (Figure 4.5b) in this region would also play a role. For the Strait of Belle Isle region, similar to the St. Lawrence Estuary, both lower SST and lower SAT play a role in the early sea ice formation. However, because both have higher values in this region than in the St. Lawrence Estuary, the most probable forcing factor causing the early formation of the sea ice is sea-ice advection from the Labrador Sea (Figure 4.8). Since there are strong sea-ice gradients and strong surface inflow (Garrett and Petrie, 1981) in the Strait of Belle Isle in December, the sea-ice advection is presumed to be large (Figure 4.8). For the Magdalen Shallows, the mechanisms governing sea ice formation are different. Since the SST in November (Figure 4.5a) and SAT in December (Figure 4.1a) are relatively

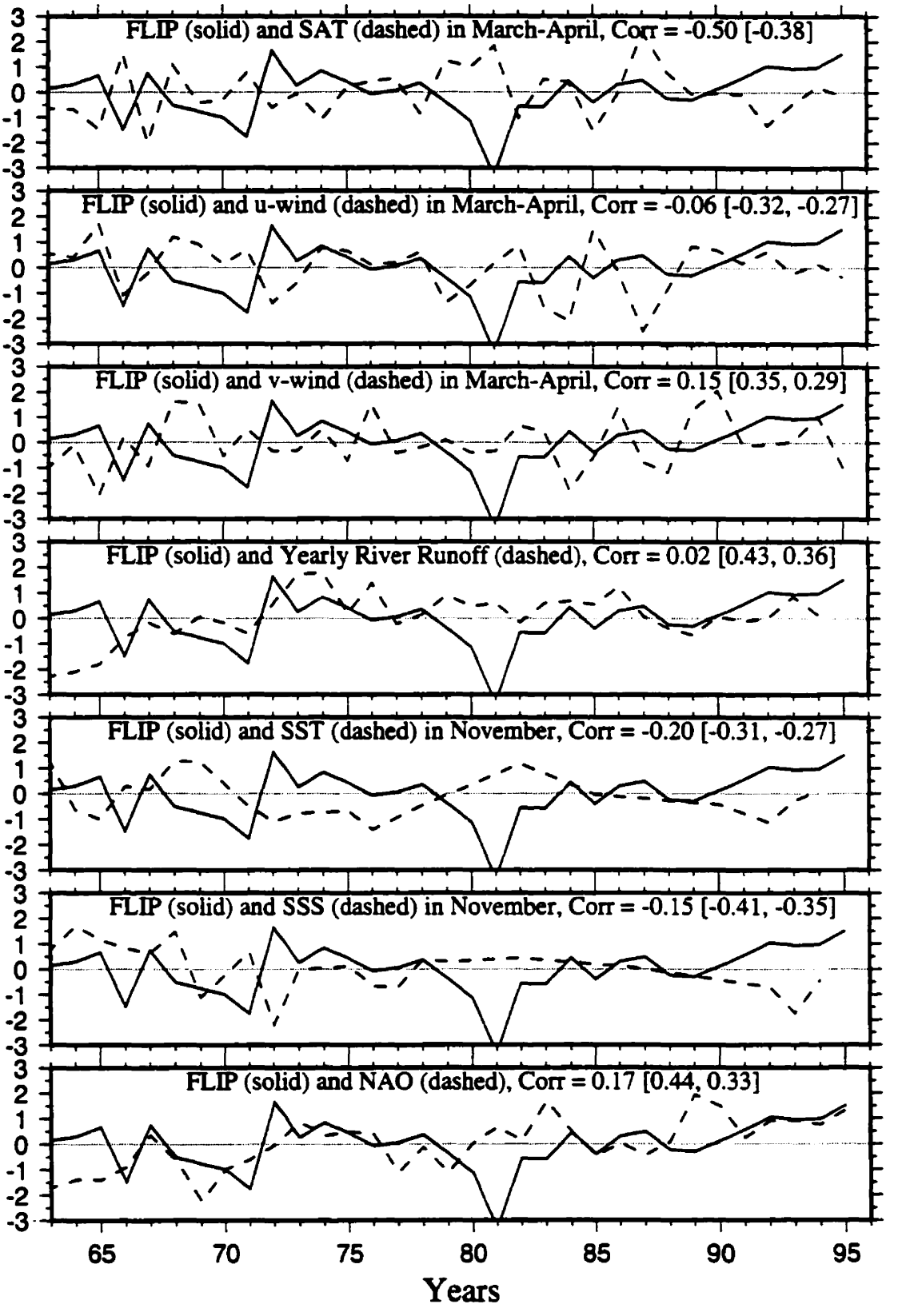

Figure 4.33a Time series of normalized time of last ice presence (TLIP), forcing factors with SAT and winds in March-April, and the correlation between them.

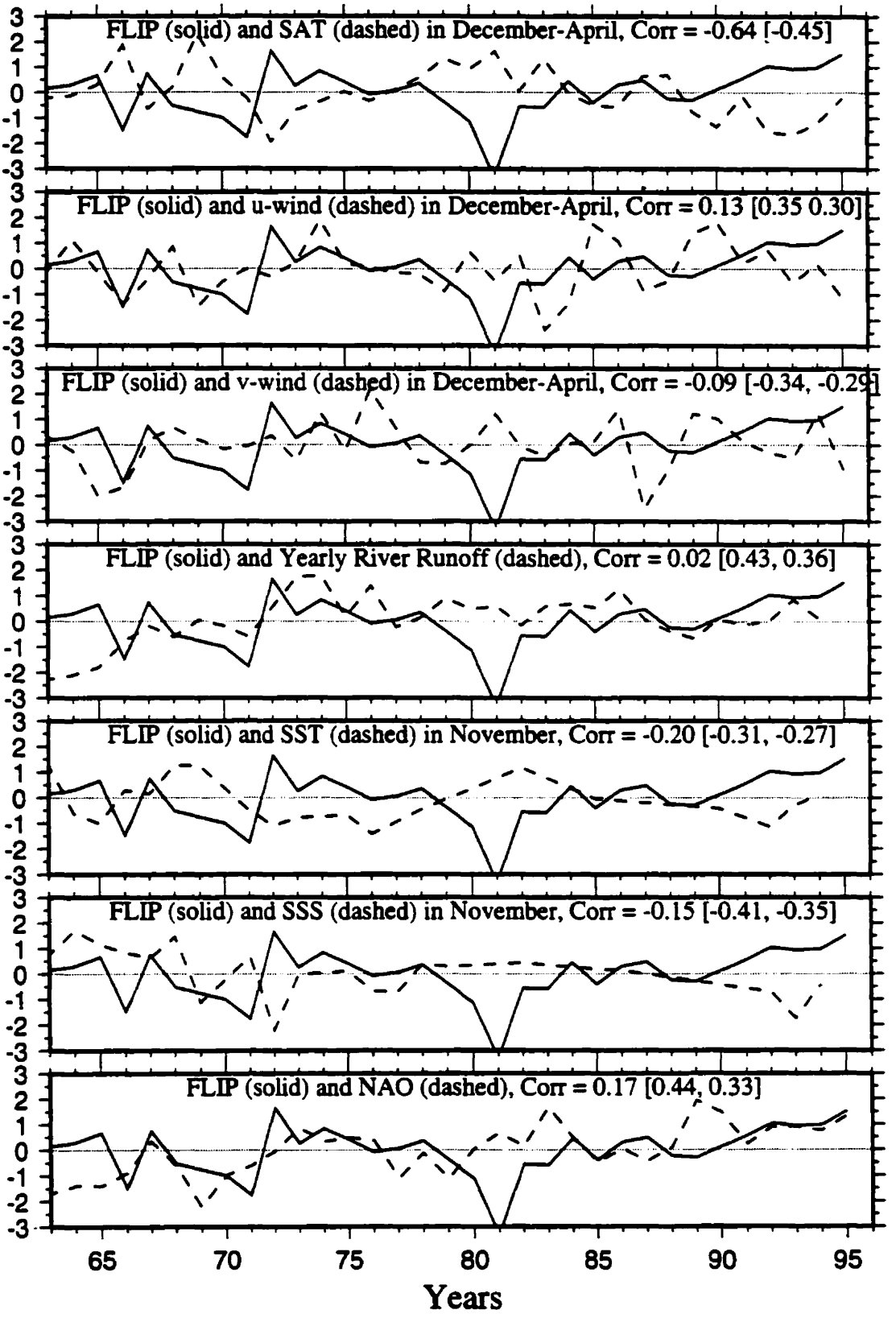

Figure 4.33b Time series of normalized time of last ice presence (TLIP), forcing factors with SAT and winds in December-April, and the correlation between them.

higher in this region than in other two regions, these two factors could not play as important a role in the early formation of the sea ice. But the mixed layer depths (MLD) in this region (Figure 4.5c) are shallower. Thus, the upper layer can reach the freezing point more quickly with continuous heat loss from the surface. Another important factor responsible for the early formation of sea ice in this region could be the lower sea surface salinity (Figure 4.5b).

Sea ice appears in the deeper Gulf later than in the coastal regions. This can be explained by the distribution of SST and MLD in November. For the deeper Gulf areas, the SST is higher (Figure 4.5a) and MLD deeper (Figure 4.5c). In order for SST to reach the freezing point, more heat needs to be lost from the ocean and hence delays sea ice formation. This fact also partly explains why the maximum of sea-ice cover in different sub-regions is reached at different times.

We noted in Chapter 3 that the regions with the longest sea-ice duration are located in the southwest part of the Gulf and the Strait of Belle Isle region. Lower mean SAT averaged over December-April is found in the Strait of Belle Isle region (Figure 4.1b). Probably the most important factor, however, is sea-ice advection from the Labrador Sea (Figure 4.8). This occurs because sea-ice cover in the Labrador Sea is always higher than that in Region 3 of the Gulf and surface currents in this region flow mainly into the Gulf from September to June (Garrett and Petrie, 1981). For the southwest region of the Gulf, the long sea-ice duration could be attributed to the shallower MLD in November, northwesterly winds, and the winter Gulf circulation from December to February. The

shallower MLD in November causes sea ice to form earlier. The northwesterly winds (Figure 4.1a) and southeastward currents (El Sabh, 1976) in the southwest Gulf can advect the sea ice from the St. Lawrence Estuary and western coast regions to this area. In addition, the concave shape of coasts in southern Gulf promotes sea ice convergence and retards ice transport out of this region.

The smallest sea-ice extent in the area off southwest Newfoundland (Figure 3.2) can be explained by the combination of higher SST (Figure 4.5a), higher SAT (Figure 4.1a and b), and a deeper MLD (Figure 4.5c). The most important reason is probably the southeastward surface flow in this region (El Sabh, 1976), which advects the locally formed sea ice away from this region.

Finally, reasons for the early sea ice retreat from the St. Lawrence Estuary are discussed. This is unexpected since the local SAT is the lowest over the entire Gulf between December and April (Figure 4.1b). The early retreat of sea ice in the Estuary may be attributed to the wind forcing and the winter circulation pattern. Both the northwesterly winds (Figure 4.2a) and surface current regime (El Sabh, 1976) combine to advect sea ice away from this region to the other downstream areas.

4.3.2 Interannual variability

We examined the forcing fields in extreme ice years and found that in years with severe ice, SAT is lower and the u-wind component stronger during three periods: December-April, December, and March-April. SST and SSS in the previous November are also

lower. This corresponds to a larger mean sea-ice cover (longer sea-ice duration), earlier sea ice formation, and later sea ice disappearance. In years with light ice, the opposite occurs, i.e., higher SAT, weaker u-wind, and higher SST and SSS correspond to less sea ice, later ice formation, and earlier ice disappearance.

The quantitative relationship between SIC and forcing factors was investigated using SVD and correlation analysis. On a Gulf-wide scale, SAT is the most important factor influencing sea ice variability in the Gulf amongst all the forcing factors. SST in the previous November, u-wind, and SSS are also very important. However, v-wind is unimportant in explaining SIC variability. We also found that different forcing factors have different geographic importance on sea ice variability. For example, SAT influences sea ice variability mainly in the central Gulf and u-wind mainly in the eastern Gulf. We ran the linear regression between SIC and three independent variables SAT, SST, and SSS. The regression accounts for 81% of the total SIC variance.

In Chapter 3 we concluded that the largest interannual variability of sea-ice cover occurs in the area off Newfoundland, where the mean sea-ice cover is the small. There are several possible reasons responsible for this. First, the MLD in this region is deeper (Figure 4.5c) and has a large interannual variability (Doyon, 1996; Petrie et al., 1996). Deeper MLD leads to a longer time to form the ice and large interannual variability of MLD leads to large interannual variability of sea ice in this region. Second, the predominate westerlies can advect the sea ice from the western Gulf to the eastern Gulf. The large interannual variability of the u-wind component in this region (Figure 4.4b) can

cause higher interannual variability of sea ice (Figure 4.14). Third, the large interannual variability of SST (Figure 4.5a) can also contribute to increased sea ice variability in this region (Figure 4.16). Fourth, SAT may also play a role in explaining the greater sea ice variability in this region (Figure 4.13).

The quantitative relationship between both TFIP and TLIP and various forcing factors was also examined. For Gulf-wide scales, SAT in December plays a dominant role on TFIP, followed by the u-wind in December and SST for the previous November. The SSS also plays a role. Again, v-wind is unimportant for TFIP. The linear regression between TFIP and the three independent variables (u-wind, SST, and SSS) accounts for 76% of the total TFIP variance. For TLIP over the Gulf-wide scale, only SAT plays an important role. The SAT in December-April accounts for the largest part of the total TLIP variance. The u-wind produces an opposite effect on TLIP in the western and eastern Gulf. Stronger u-winds in March-April lead to earlier sea ice disappearance in the western Gulf and later sea ice disappearance in the eastern Gulf.

Similar to the SIC, the largest interannual variability of TFIP (off Newfoundland) can also be explained by the deeper and large interannual variability of MLD in this region, u-wind, SST, and SAT. The large interannual variability of TLIP along the northeast coast can be explained by the large variability of SAT in this region and sea ice advection from the Labrador Sea.

5. Discussions on Mechanisms of Sea Ice Variability - A Simple Model Study

In this Chapter, we develop a simplified sea-ice model, based upon a dynamic thermodynamic sea ice model (Hibler, 1979, 1980), in an attempt to increase our understanding of the mechanisms controlling sea ice variability in the Gulf of St. Lawrence. The outline for this Chapter is as follows. In the next section, we briefly describe the sea ice model, then discuss the external (atmospheric and oceanic) forcing, model parameters, and numerical methods (Section 5.2). In Section 5.3, we discuss the model results for the seasonal cycle of sea-ice extent and compare them with the observations. The response of sea ice extent to changes of some external forcing (SAT, winds, SST, etc.) and the comparison of results with observed sea ice variability are presented in Section 5.4. In the final section, a summary and conclusions are provided.

5.1 Description of the model

The sea ice models proposed by Hibler (1979, 1980) have been applied successfully to the Arctic Ocean. The sea ice extent simulated by these models compares well with the observations. The equations for Hibler's models and a discussion of some of the simplifications made for the present study are now presented.

5.1.1 Momentum equation

The two-dimensional momentum equation for sea-ice motion is as follows:

$$m\frac{D\vec{u}}{Dt} = -mf\vec{k}\times\vec{u} + \vec{\tau}_a + \vec{\tau}_w - mg\nabla\xi + \vec{F} \tag{5.1}$$

where m is the ice mass per unit area, D/Dt = $\partial/\partial t+u\partial/\partial x+v\partial/\partial y$ is the substantial time derivative, $\vec{u}$ the horizontal ice velocity, f the Coriolis parameter, $\vec{k}$ the vertical normal unit vector, and $\vec{F}$ the internal ice stress. $\vec{\tau}_a$ and $\vec{\tau}_w$ are the stresses caused by air and water, respectively, and $mg\nabla\xi$ is the gradient force due to the sloping sea surface.

The air and water stresses are determined from simple nonlinear drag laws as follows (Brown, 1979; McPhee, M., 1975):

$$\vec{\tau}_a = \rho_a C_a |\vec{U}_a| [\vec{U}_a\cos(\varphi) + \vec{k}\times\vec{U}_a\sin(\varphi)] \tag{5.2}$$

$$\vec{\tau}_w = \rho_w C_w |\vec{U}_w - \vec{u}| [(\vec{U}_w - \vec{u})\cos(\theta) + \vec{k}\times(\vec{U}_w - \vec{u})\sin(\theta)] \tag{5.3}$$

where $\vec{U}_a$ is the surface wind; $\vec{U}_w$ the surface ocean current; C_a and C_w are the air and water drag coefficients, respectively; ρ_a and ρ_w are the air and water densities, respectively; and φ and θ are the air and water turning angles, respectively. Both turning angles were set to zero because measured winds were used rather than geostrophic winds. In the present model, the effects of surface currents were not considered because of the

lack of wintertime current observations. It is expected that they do have an important role on the distribution of sea-ice cover.

We now consider the orders of magnitude of the various terms in the momentum equation.

$$m\frac{\partial \vec{u}}{\partial t} + m(\vec{u} \bullet \nabla)\vec{u} = -mf\vec{k} \times \vec{u} + \vec{\tau}_a + \vec{\tau}_w + \vec{F} \qquad (5.4)$$

The gradient force term is not included because we did not have access to surface current data. The typical order of ice velocity $\vec{u}$ in the Gulf is around 0.2 m/s (DeTracey, 1993). The grid size used in the model is 0.25 degrees in both latitude and longitude. This corresponds to around 20 km in the longitudinal direction and 28 km in the latitudinal direction. The order of the Coriolis parameter f is 10^{-4}. The ice mass per unit area is the product of ρ_{ice} h, where ρ_{ice} is density of sea ice (910 kg/m^3) and h is the equivalent sea-ice thickness (see Section 5.1.2 for details) in a grid (assumed to be 0.3 m). The typical order of both wind stress and water stress is 10^{-2} N/m^2. The internal ice stress term $\vec{F}$ is calculated from the viscous-plastic constitute law (Hibler, 1979, 1980). The order of $\vec{F}$ can be estimated from $\frac{\partial(P/2)}{\partial x}$, where P/2 is the ice pressure and P=P*h exp[-C(1-A)), P* and C are empirical constants (Hibler used P* = 5.0 x 10^3 and C = 20 in his studies) and A is sea-ice compactness (sea-ice cover). We assigned A = 8/10 as the typical order of sea-ice cover in the Gulf (Figure 3.1). In addition, we assigned the typical order of

time as one day (86400 s). Using these values, we obtained the following order of magnitude for each term in the momentum equation:

$$m\frac{\partial \vec{u}}{\partial t} + m(\vec{u}\bullet\nabla)\vec{u} = -mf\vec{k}\times\vec{u} + \vec{\tau}_a + \vec{\tau}_w + \vec{F}$$

$$O(10^{-4}) \quad O(10^{-4}) \quad O(10^{-3}) \quad O(10^{-2}) \quad O(10^{-2}) \quad O(10^{-4})$$

Keeping terms of order 10^{-3} and larger, the momentum equation reduces to:

$$-mf\vec{k}\times\vec{u} + \vec{\tau}_a + \vec{\tau}_w = 0 \tag{5.5}$$

5.1.2 Ice compactness and thickness equations

The sea ice in any grid cell is characterized by two variables: the compactness A, defined as the areal fraction covered by ice, and the equivalent ice thickness h, defined as the ice thickness if the ice is spread uniformly over the entire grid cell (Hibler, 1979). The ice is assumed uniformly distributed between 0 and 2h/A in thickness, with an average ice thickness h/A. Continuity equations, with added thermodynamic source/sink terms, are used to describe the evolution of A and h as follows,

$$\frac{\partial h}{\partial t} = -\nabla.(\vec{u}h) + S_h + Diff \tag{5.6}$$

$$\frac{\partial A}{\partial t} = -\nabla.(\vec{u}A) + S_a + Diff \tag{5.7}$$

where A is sea-ice compactness ($A \leq 1$) and h is an equivalent ice thickness; $\vec{u}$ is sea-ice velocity; S_h and S_a are the thermodynamic forcing or source terms; and *Diff* is the horizontal diffusion term, which is small compared to the advection term according to Hibler (1979).

The thermodynamic source terms, S_h and S_a, are given by the equations

$$S_h = g(h/A)A + (1-A)g(0) \tag{5.8}$$

$$S_a = \begin{cases} (g(0)/h_0)(1-A), & \text{if } g(0) > 0 \\ 0, & \text{if } g(0) < 0 \end{cases} + \begin{cases} 0, & \text{if } S_h > 0 \\ (A/2h)S_h, & \text{if } S_h < 0 \end{cases} \tag{5.9}$$

where g(h) is the growth rate of ice of thickness h, and g(0) is the growth rate of ice in open water. The net ice growth is given by S_h, which is the sum of the ice growth over the fraction of grid cell covered with ice and the growth of new ice over the remaining fraction of open water. If g(0) is negative, no ice forms on the open water and the excess heat is assumed to melt ice remaining in the grid cell, while the mixed layer temperature remains at the freezing point.

The growth/decay of ice compactness is given by S_a. The first term in the equation (5.9) indicates that if the growth of ice over open water g(0) is positive then the area of open

water (1-A) decays exponentially with a time constant $h_0/g(0)$. The term h_0 is an adjustable parameter. If g(0) is negative, it does not contribute to a change in A, but as previously mentioned, contributes to lateral melting. The second term in equation (5.9) describes the change in ice compactness under melting conditions.

For open water, the ice growth rate is given by

$$g(0) = -(Q_{surf} + Q_{sea})/L_f \qquad (5.10),$$

where Q_{surf} is the net incoming atmospheric heat flux at the surface of the open water, or leads, due to short-wave solar radiation, long-wave radiation, sensible and latent heat flux; Q_{sea} is the oceanic heat flux transported into the oceanic mixed layer from the deep ocean or the heat flux due to the heat content of the basin; and L_f is the volumetric heat of fusion of sea water. The total heat gained or lost by the mixed layer is the sum of the surface heat flux and the deep ocean heat flux.

In the ice–covered grid cell fraction, the ice growth rate is given by

$$g(h/A) = -(Q_{cond} + Q_{sea})/L_f \qquad (5.11)$$

where Q_{cond} is the conductive heat flux through the ice into the ocean. It is calculated from:

$$Q_{cond} = \frac{k_{ice}}{h/A}(T_{surf} - T_B) \qquad (5.12)$$

where k_{ice} is the conductivity of the ice, T_B is the bottom temperature of the ice slab, and T_{surf} is the surface temperature of the ice. T_B is set to the freezing point. Sea ice tends to grow (melt) when $S_h > 0$ (<0), since the ice loses (gains) heat.

The model was initialized with the SST and mixed layer depth in November (Figures 4.5a and 4.5c). In the absence of an ice cover, the mixed layer temperature is calculated from the following equation

$$\rho_w C_{p,w} \, h_{mix} \frac{\partial T_{mix}}{\partial t} = Q_{surf} + Q_{sea} \qquad (5.13)$$

where ρ_w is the water density, $C_{p,w}$ the specific heat of sea water, h_{mix} the mixed-layer thickness, T_{mix} the mixed layer temperature, Q_{surf} the net surface energy flux, and Q_{sea} the deep ocean heat flux. If equation (5.13) results in a temperature below the freezing point, it is set to a constant value of –1.7°C, which is equivalent to a water salinity of 31 PSU, following DeTracey (1993). The temperature is maintained at the freezing point and ice is formed.

5.2 External forcing, model parameters, and numerical methods

The external forcing for the model is the surface heat flux, the deep-sea heat flux, surface wind, November SST and mixed layer depth. The November SST (Figure 4.5a) was taken as the climatology, calculated from all available hydrographic cruises collected during the ice forecasting program. A striking feature is the lower temperatures in the St. Lawrence Estuary and the Strait of Belle Isle regions, as discussed in Chapter 4. The mixed layer depth is based on climatology calculated by Petrie et al. (1990), using November sigma-t profiles for the Gulf (Figure 4.5c, DeTracey, 1993). The most notable feature of the mixed layer depth distribution is the shallower range of values over the Magdalen Shallows.

Surface wind was taken as the daily output from the NOAA-CDC data set. The surface heat flux is the sum of short-wave radiation, long-wave radiation, sensible heat, and latent heat fluxes. It was calculated as follows.

For the short-wave radiation, we used the NOAA-CDC values multiplied by (1-α), where α is the albedo for open water or ice, depending on whether sea surface is open water or ice-covered. The long-wave radiation is calculated from:

$$Q_B = 0.985\sigma T_S^4(0.39 - 0.05\sqrt{e_a})(1 - 0.6N^2), \quad (5.14)$$

where σ is the Stefan-Boltzman constant, T_S the water surface temperature, N the cloud cover, and e_a the water vapor pressure in mb (Gill, 1982).

The sensible and latent heat fluxes were calculated, following Bunker (1976) as follows:

$$Q_S = \rho_a C_{p.a} C_H (T_S - T_A) U_a \quad (5.15)$$

$$Q_L = \rho_a L C_E (q_s - q_A) U_a \quad (5.16)$$

where

$$q_S = 0.622 e_s(T_s) / P_a \quad (5.17)$$

$$q_A = 0.622 r e_s(T_A) / P_a \quad (5.18)$$

where ρ_a is the air density, $C_{p.a}$ the specific heat of air at constant pressure, and U_a the wind speed at a height of 10 m; r the relative humidity, P_a the surface air pressure, and L is the latent heat of evaporation. C_H and C_E are the empirical bulk exchange coefficients, 1.75×10^{-3} being used for both coefficients in this study. The saturation vapour pressure e_s was determined following Bolton's formula (Rogers and Yau, 1989),

$$e_s(T) = 6.112\exp(17.67T/(T+243.5)), \quad (5.19)$$

where e_s is in mb and T in °C.

Using daily climatologies (1958-1997) of surface air temperature, wind, relative humidity, and cloud cover from the output of NOAA-CDC, we calculated the total annual surface heat flux ($Q_{Total} = Q_{sw} + Q_B + Q_s + Q_L$) over the Gulf of St. Lawrence (Figures 5.1 and 5.2). Note, the heat fluxes shown in Figure 5.2 were averaged over the entire Gulf. The largest heat loss from the ocean occurs in early January. The heat flux reaches zero around mid-March and from then on the heat flux is positive, indicating that the ocean begins receiving heat from the atmosphere.

Among the four components of heat flux, long-wave radiation dominates in winter followed in order by the sensible and latent heat terms. From March onwards, the total heat flux is mainly controlled by short-wave solar and long-wave radiation. Solar radiation reaches a minimum in December-January. Long-wave radiation (Q_B) is relatively constant during the winter and increases slightly in spring. This is because Q_B is mainly determined by sea surface temperature, which is close to the freezing point in winter but increases in spring. Sensible and latent heat reach a maximum in early to mid winter and decrease to very small values by March. This is because sensible heat is determined by the difference of air-sea temperatures and winds, whereas latent heat was calculated using the difference of water vapor pressure and saturated water vapor pressure and winds. The winds are strong in winter months (Figure 4.3) and the

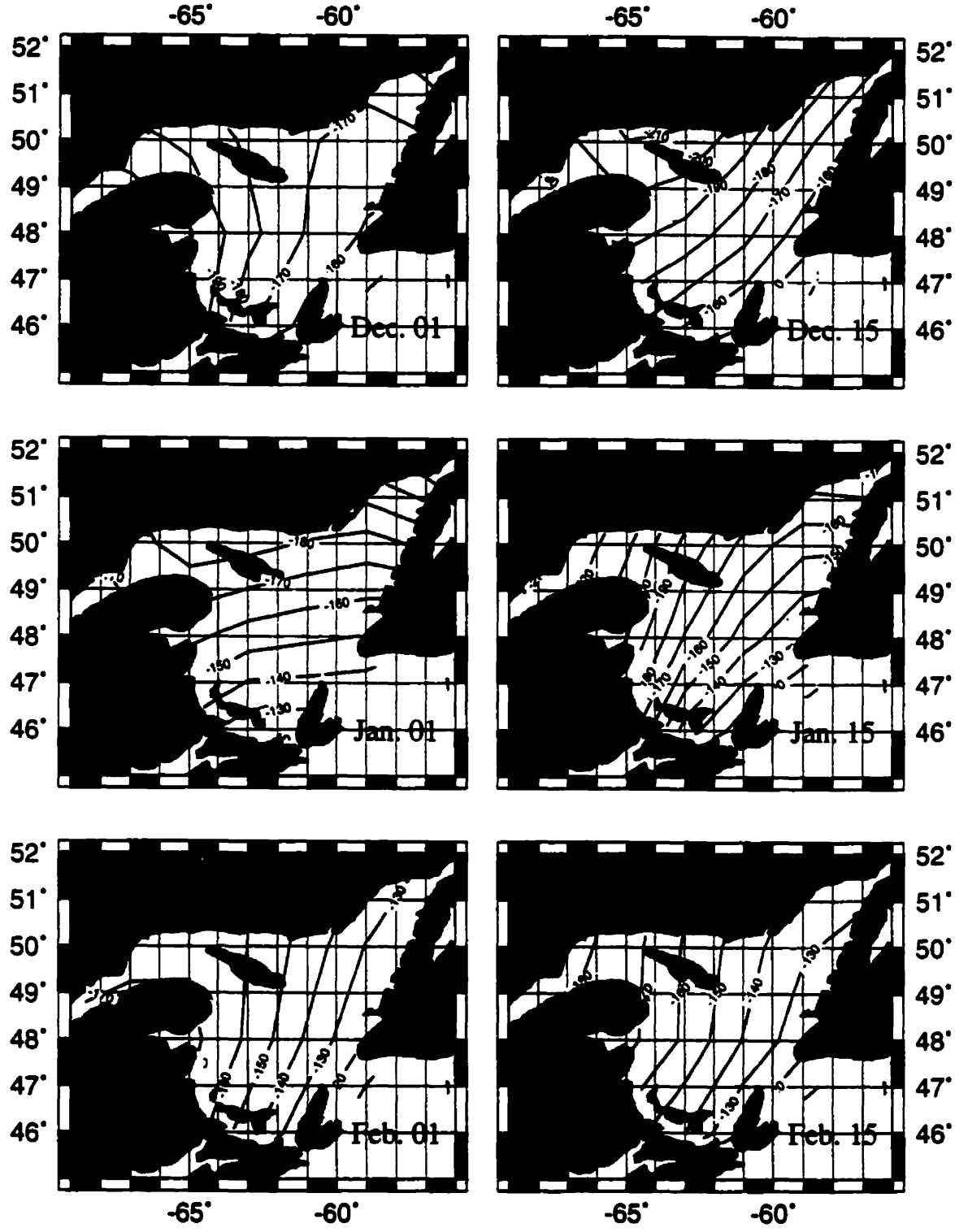

Figure 5.1 Annual surface heat flux (W/m^2) over the Gulf of St. Lawrence calculated using NOAA-CDC data set from the period 1958-97.

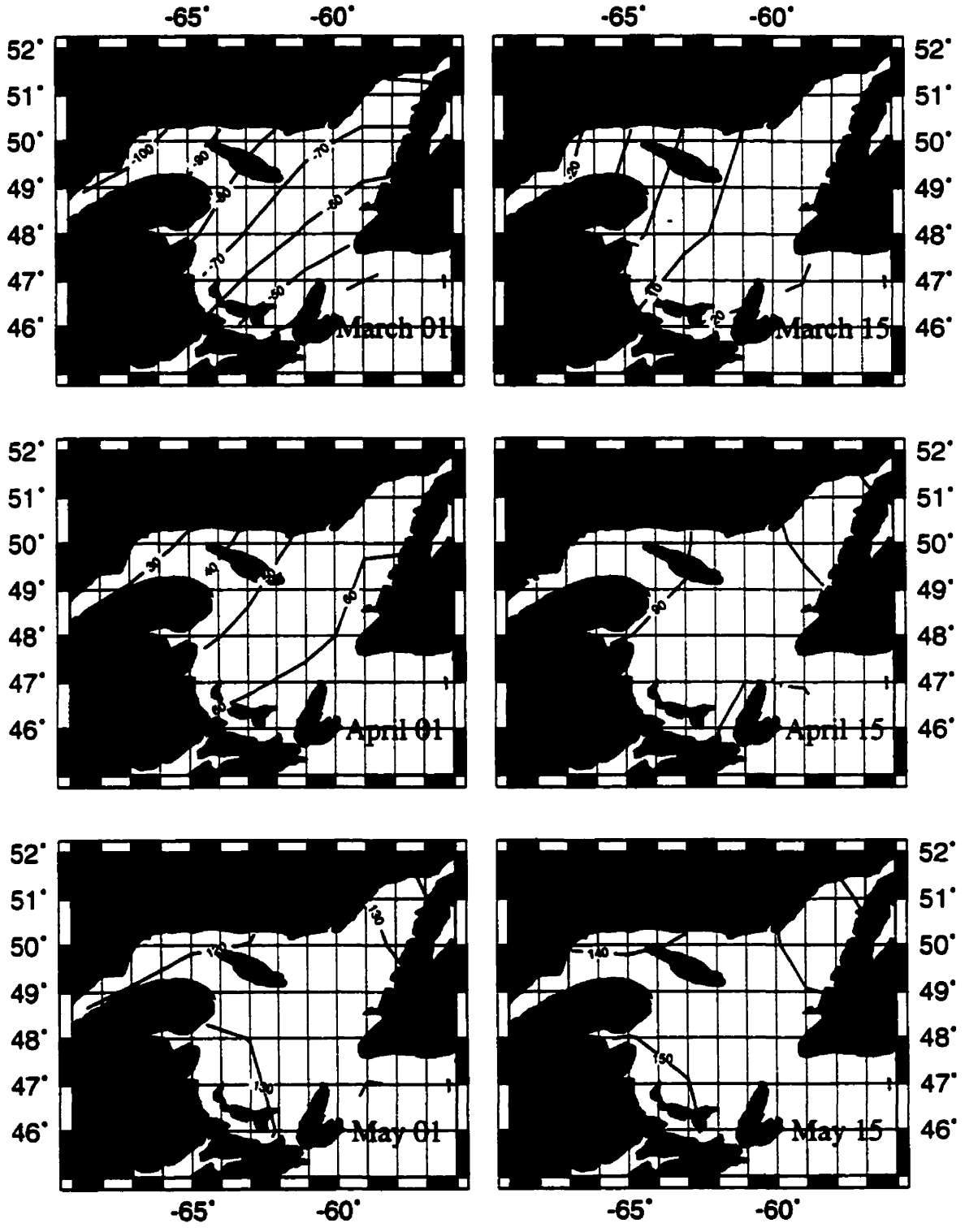

Figure 5.1 (Continued)

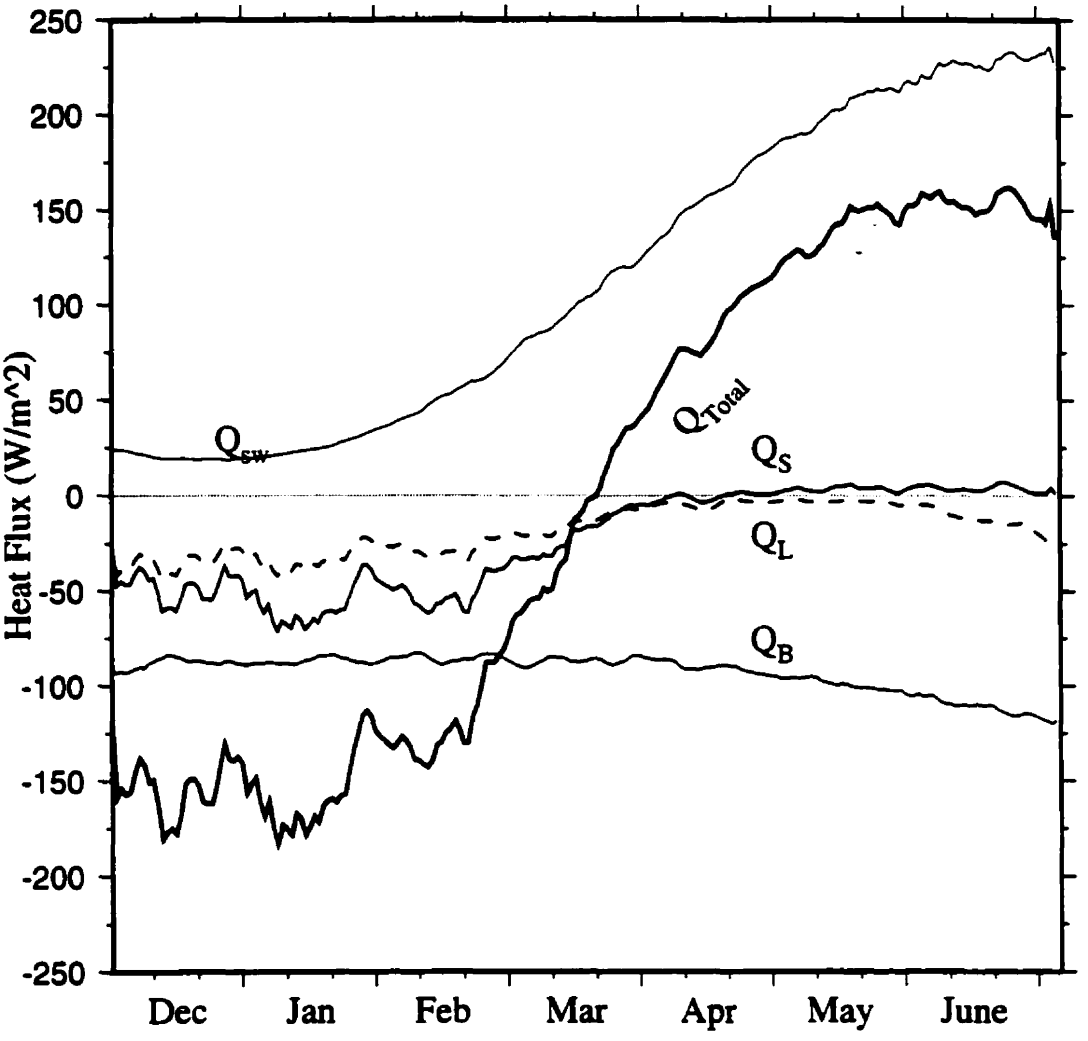

Figure 5.2 Climatology (1958-97) of the total heat flux (Q_{Total}) and each component averaged over the entire Gulf from December to June.

difference of air-sea temperatures and difference of water vapor pressure and saturated water vapor pressure are also large in the winter months.

The parameter values used in present study are given in Table 5.1.

Table 5.1. Model parameters used in the present study

Air Drag Coefficient	C_a =0.0012
Water Drag Coefficient	C_w = 0.015
Water Specific Heat	$C_{p.w}$ = 3930 J $kg^{-1}K^{-1}$
Coriolis Parameter	f = 1.081 x 10^{-4} s^{-1}
Ice Conductivity	k_{ice} = 2 W $m^{-1}K^{-1}$
Latent Heat Fusion	L_f = 3.3 x 10^8 Jkg^{-1}
Air Density	ρ_a = 1.3 kgm^{-3}
Ice Density	ρ_i=910 kg m^{-3}
Water density	ρ_w=1025 kg m^{-3}
Grid Spacing	dx (dy) = 0.25 Longitude (Latitude)
Time Step	dt = 1 day
Wind and Current Turning Angles	0

The model grid is shown in Figure 5.3. All the external forcing fields were interpolated onto the model grid points using the interpolation scheme called "minimum curvature with a tension factor" (Smith and Wessel, 1990). The sea ice velocity was calculated on

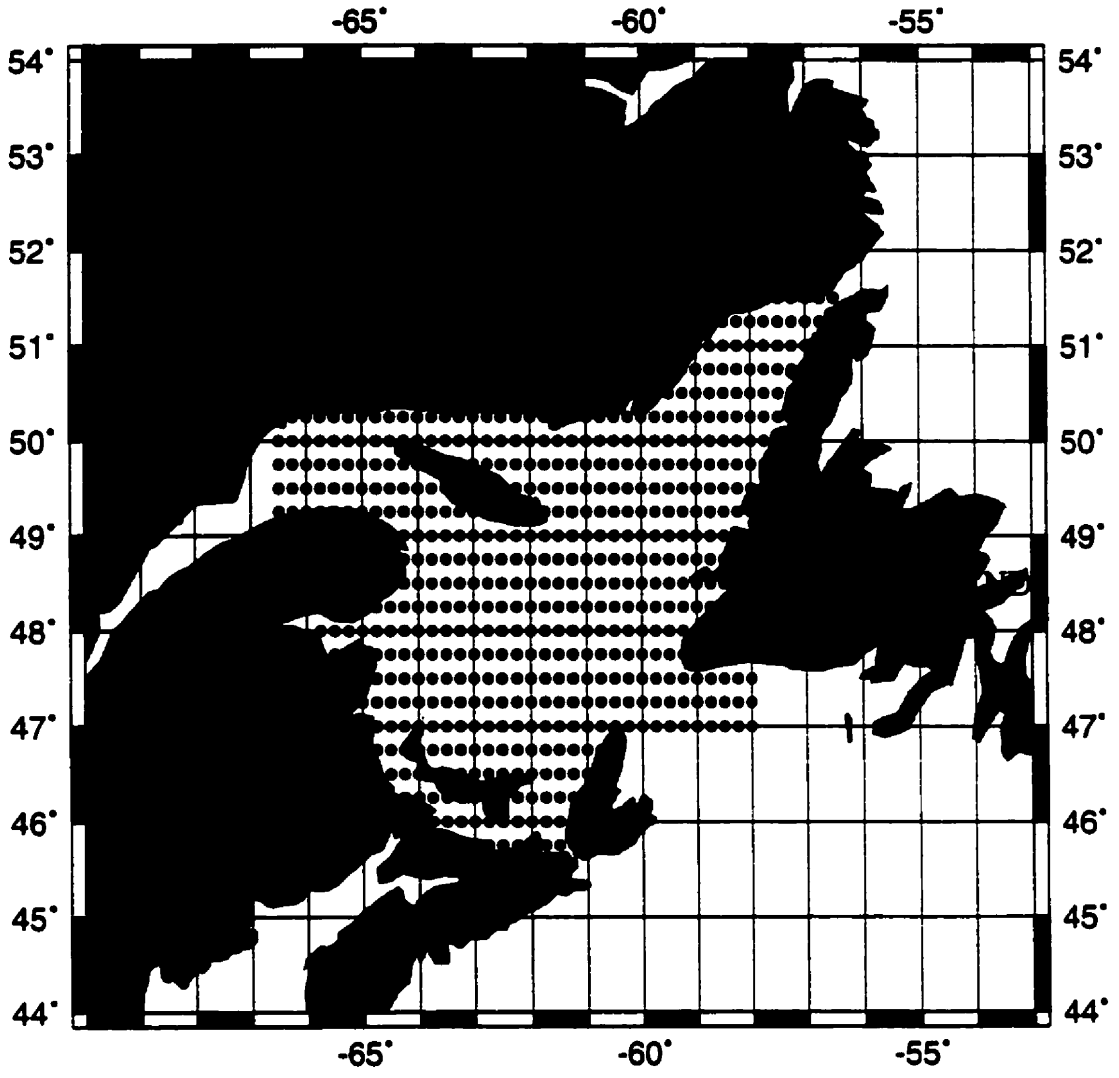

Figure 5.3 Model grid for the Gulf of St. Lawrence. Grid spacing is 0.25° latitude by 0.25° longitude.

these grid points from the momentum equation (5.5) and the sea ice compactness and thickness were calculated at the center points of the grid as shown below.

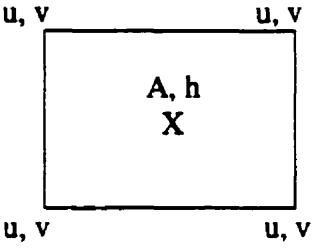

Because there was no time derivative term in the momentum equation (5.5), we calculated sea ice velocity using an iterative approach. The continuity equations were integrated explicitly using a forward Euler scheme. For the boundary conditions, we set ice velocities to zero on coastlines. For the St. Lawrence estuary, Strait of Belle Isle, and Cabot Strait, a zero-gradient boundary was prescribed.

In the following sections, we first model the annual variability of sea ice and compare the results with observations. We then use the model to study the variability of sea-ice cover under different scenarios and compare these results with those from previous data analysis in order to increase our understanding of the mechanisms controlling sea ice variability in the Gulf.

5.3 Model results of annual variation of the sea ice

Using the climatological atmospheric and oceanic forcing described previously, we simulated annual sea ice variations using our simple sea ice model. Figure 5.4 shows the simulated annual variations of sea-ice cover in tenths and thickness in centimeters with

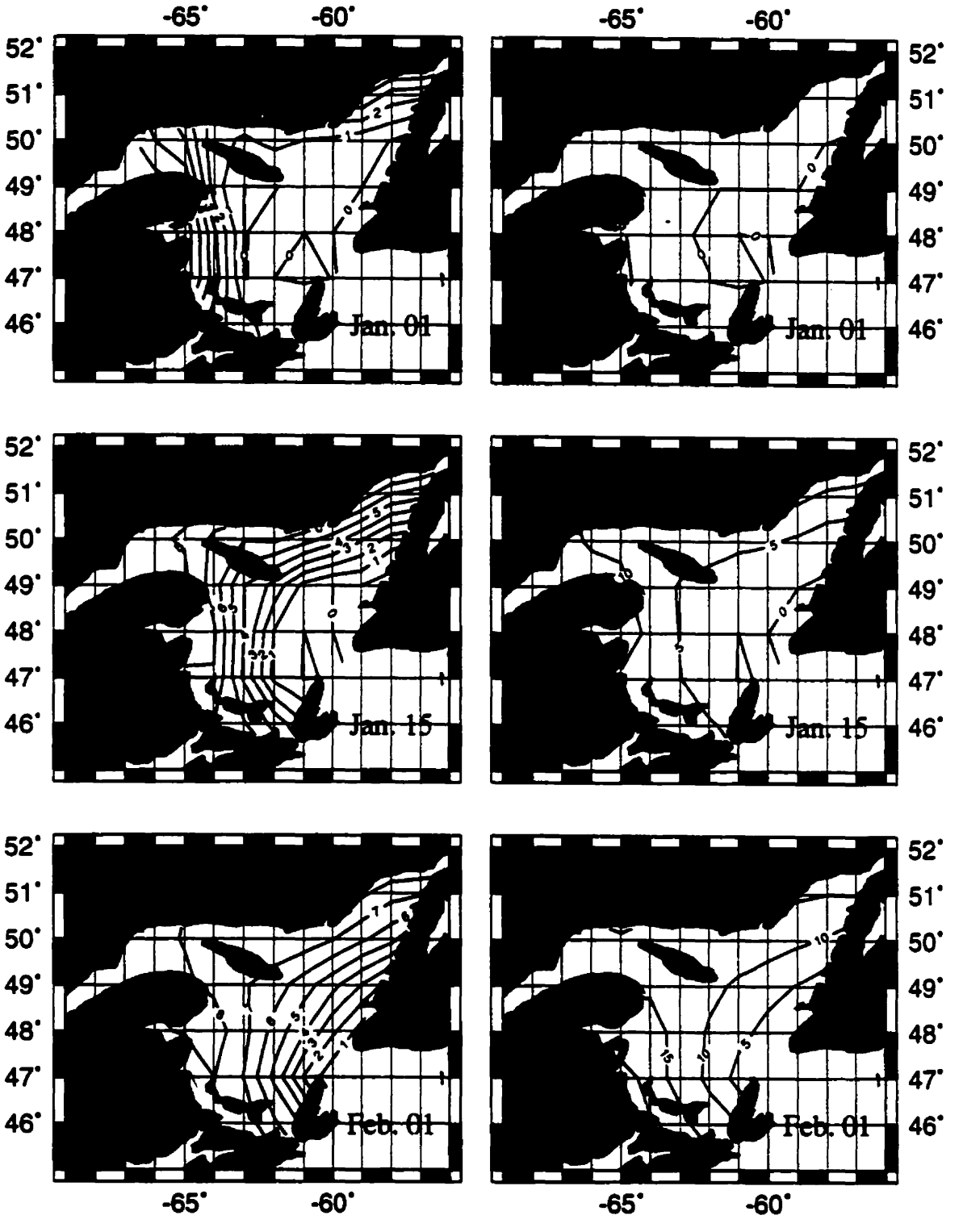

Figure 5.4 Modelled sea-ice extent climatology in tenths (left) and thickness (right) in centimeters in the Gulf of St. Lawrence

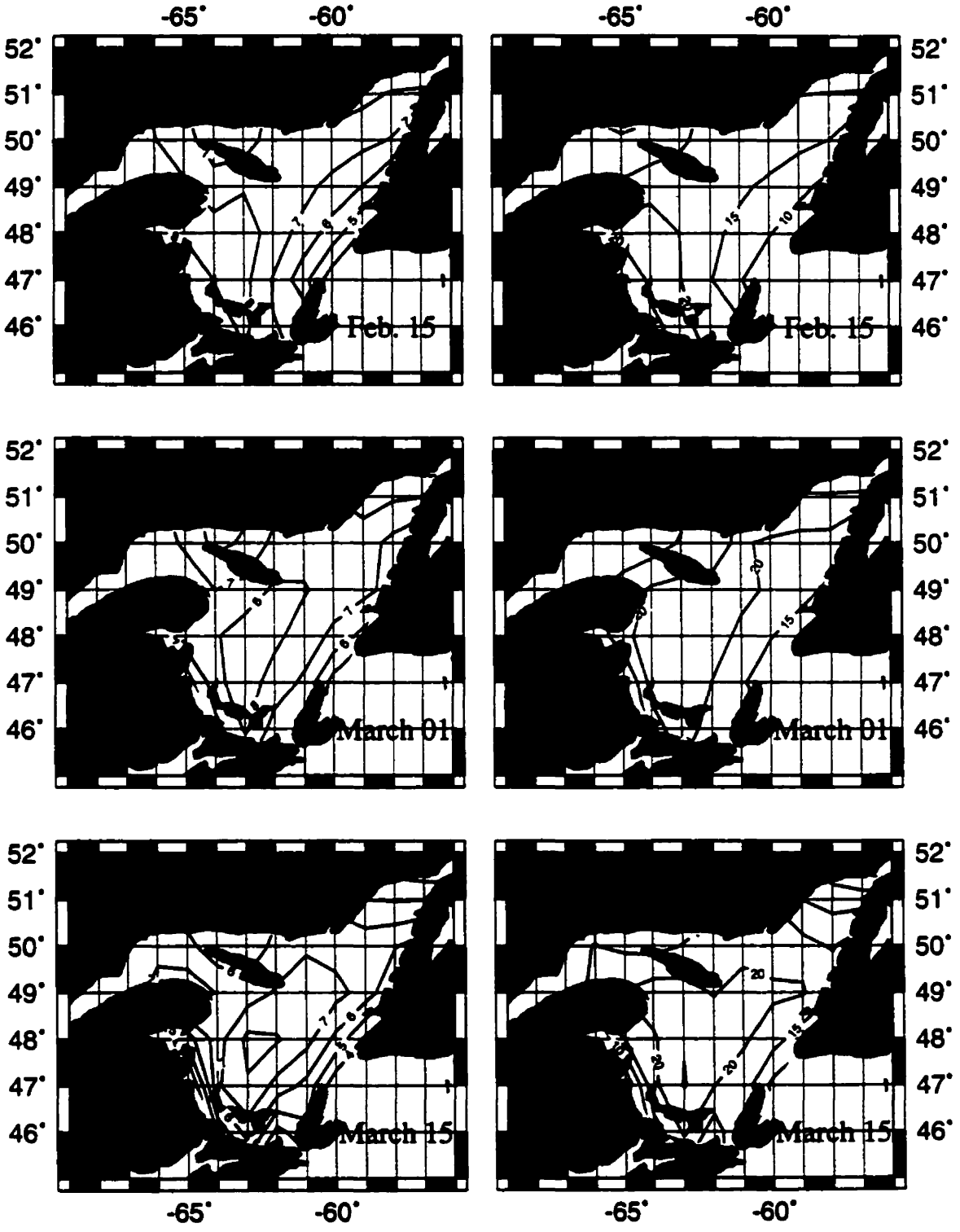

Figure 5.4 (Continued)

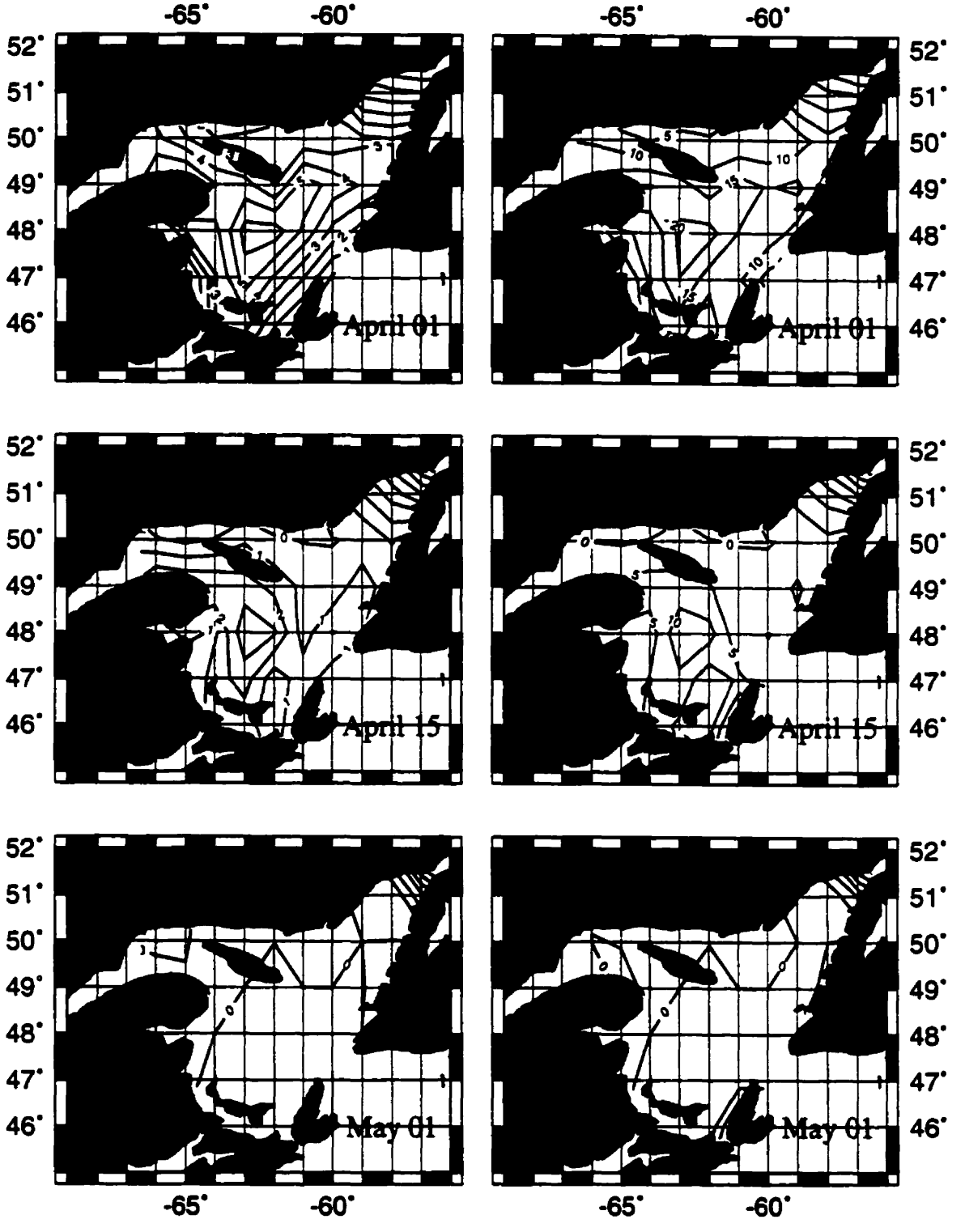

Figure 5.4 (Continued)

an interval of half a month and Figure 5.5 shows the comparison of modeled sea-ice cover averaged over the entire Gulf with observed long-term means (1963-96). Compared with observations (Figure 3.1), the model reproduced well the main features of annual variations of sea-ice cover over the Gulf of St. Lawrence for both spatial and temporal variations. Temporally, the model generated the seasonal cycle of sea ice variations fairly well, i.e., sea ice appears in late December, reaches maximum values in late February, and disappears by early April. Spatially, the model indicated that sea ice begins in the coastal regions, and later extends into the central Gulf, and that there is less sea-ice cover off southwestern Newfoundland and more ice cover in the Strait of Belle Isle region and southwestern Gulf, in agreement with the observations. However, there are some discrepancies between the model results and observations. For example, observations (Figure 3.1) indicate the largest sea-ice cover occurs off Cape Breton Island, between March 15 and April 15. However, the model shows maximum values in the southern-central Gulf. We believe this discrepancy is caused by the neglect of surface currents in the model, since they tend to be southeastward (El Sabh, 1976) and could advect sea ice from the southern-central Gulf to the areas off Cape Breton Island. In addition, the model produced slightly later sea ice appearance and earlier sea ice disappearance over the Gulf-wide scale, if 1/10 sea-ice cover is used as a criterion for sea ice appearance and disappearance (Figure 5.5). We also made comparisons of the time of first ice presence, the time of last ice presence, and mean sea-ice cover averaged over the December-June period with observations (Figure 5.6). The modeled time of first ice presence shows a spatial pattern consistent with the observations. For the time of last ice presence, the model results are similar to the observations in the northeastern Gulf. The

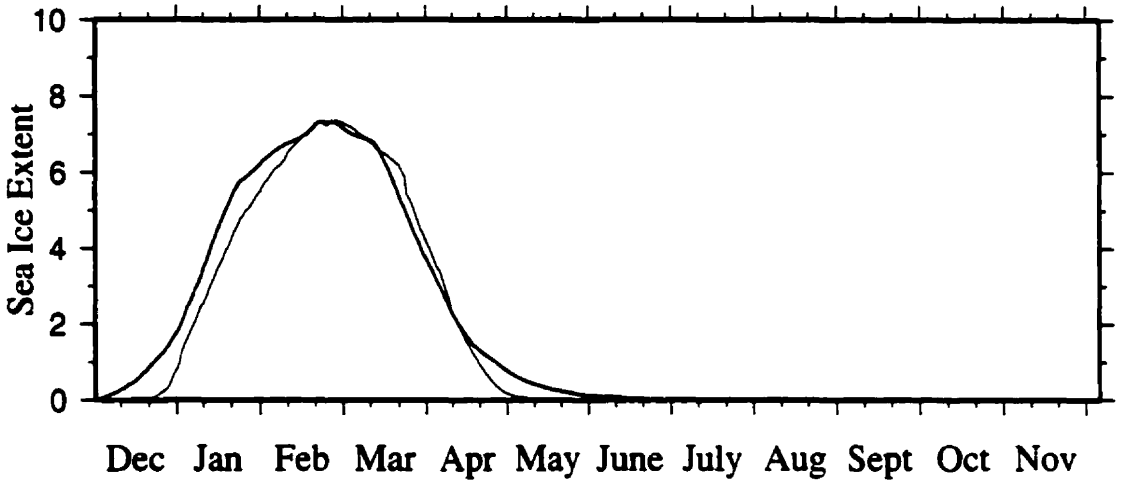

Figure 5.5 Comparison of model sea-ice extent climatology in tenths (thin line) averaged over the entire Gulf with observed long-term means (1963-96) of sea-ice extent (thick line).

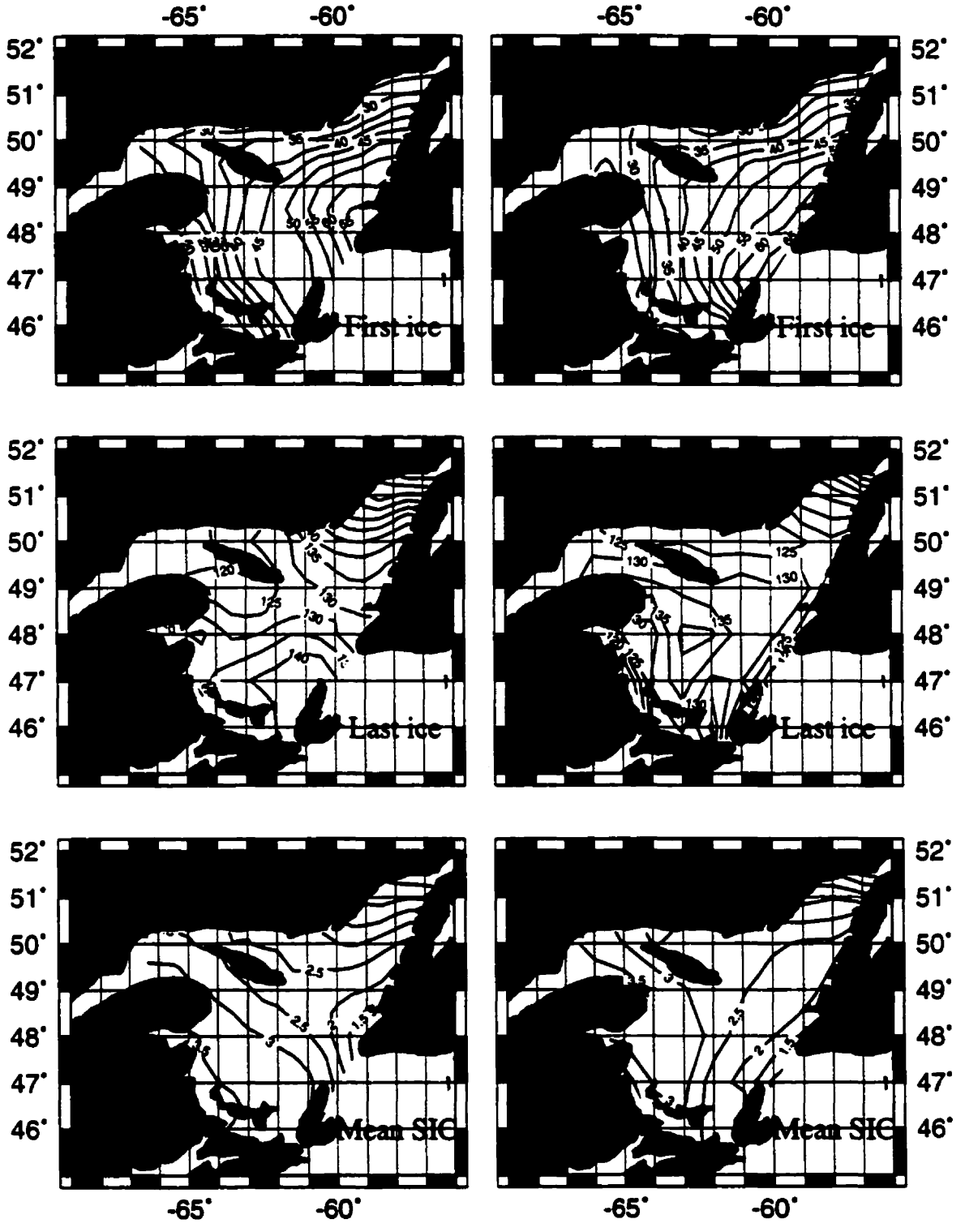

Figure 5.6 Comparison of modelled first ice, last ice, and mean sea-ice cover (right panels) with observations (left panels).

model indicates the sea ice lasts longest in the southern-central Gulf while observations indicate this occurs in the area off Cape Breton Island. This discrepancy is also believed to be caused by neglect of surface currents, as discussed previously. The modeled mean sea-ice cover is generally consistent with observations. Hereafter, we will refer to modeled sea-ice cover under climatological forcing (Figures 5.4–5.6) as the standard run.

5.4 Response of SIC, TFIP, and TLIP to anomalies of external forcing

In Chapter 4, we investigated the relationship between sea-ice cover, time of first ice presence, time of last ice presence and external forcing SAT, surface wind, and November SST. We also examined the relative importance of the forcing factors on interannual variability of sea-ice cover over the Gulf. In this section, these relationships are re-examined using our simple model.

Means and standard deviations of spatially averaged SAT, u-wind, and v-wind in the period of December-April were calculated using the daily NOAA-CDC data set (1958-97) and November SST from hydrographic observations (1962-96). The standard deviation for SAT is 1°C, for u-wind 0.74 m/s, for v-wind 0.60 m/s, and for SST 1.12°C. The model was run again using ± one standard deviation of December-April SAT, u-wind, v-wind, and November SST from their respective climatologies. The reason for this approach is two-fold. First, one standard deviation represents the typical variability of each forcing field. Second, it allows comparison of the relative importance of different forcing on sea ice variability.

Figure 5.7 shows the seasonal cycle of modeled anomalies of sea-ice cover from the standard run corresponding to a change of December-April SAT by ±1°C while keeping all the other forcing unchanged. As expected, a positive SAT anomaly yields negative anomalies of sea-ice cover and vice versa. Due to the accumulated effects of SAT anomalies on sea ice, the sea-ice anomalies increase with time. The sea ice anomalies caused by SAT originate in the coastal regions in early January and move to the central Gulf thereafter, indicating that the largest anomalies occurred in the regions of sea ice formation. This is because the change of SAT, which alters the surface heat flux, affects the freezing point of sea water initially in the coastal regions and later in the central Gulf. The largest anomalies occur in the southeast Gulf in February-March. By April, the largest anomalies occur in the central Gulf. Note there is asymmetry for the SIC anomalies caused by a change of ± one standard deviation of SAT before April 15, with a change of + one standard deviation producing larger SIC anomalies. This asymmetry is caused by the asymmetric change of latent heat flux since saturated vapor pressure in equation 5.18 increases faster with increasing temperature (Rogers and Yau, 1989). Figure 5.8 shows the anomalies of TFIP, TLIP, and mean SIC in December-June corresponding to a change of SAT by ± 1° C. As expected, lower (higher) SAT leads to earlier (later) sea ice formation, later (earlier) sea ice disappearance, and larger (smaller) mean sea-ice cover. The largest anomalies of SIC in the central Gulf are consistent with our previous SVD analysis. The largest mean sea-ice cover caused by a change of one standard deviation of December-April SAT is around 1/10. The largest TFIP anomalies in the southeast Gulf, around 6 days from climatologies, result from SAT in this region being smaller and the 1°C change of SAT in this area can cause relatively larger surface

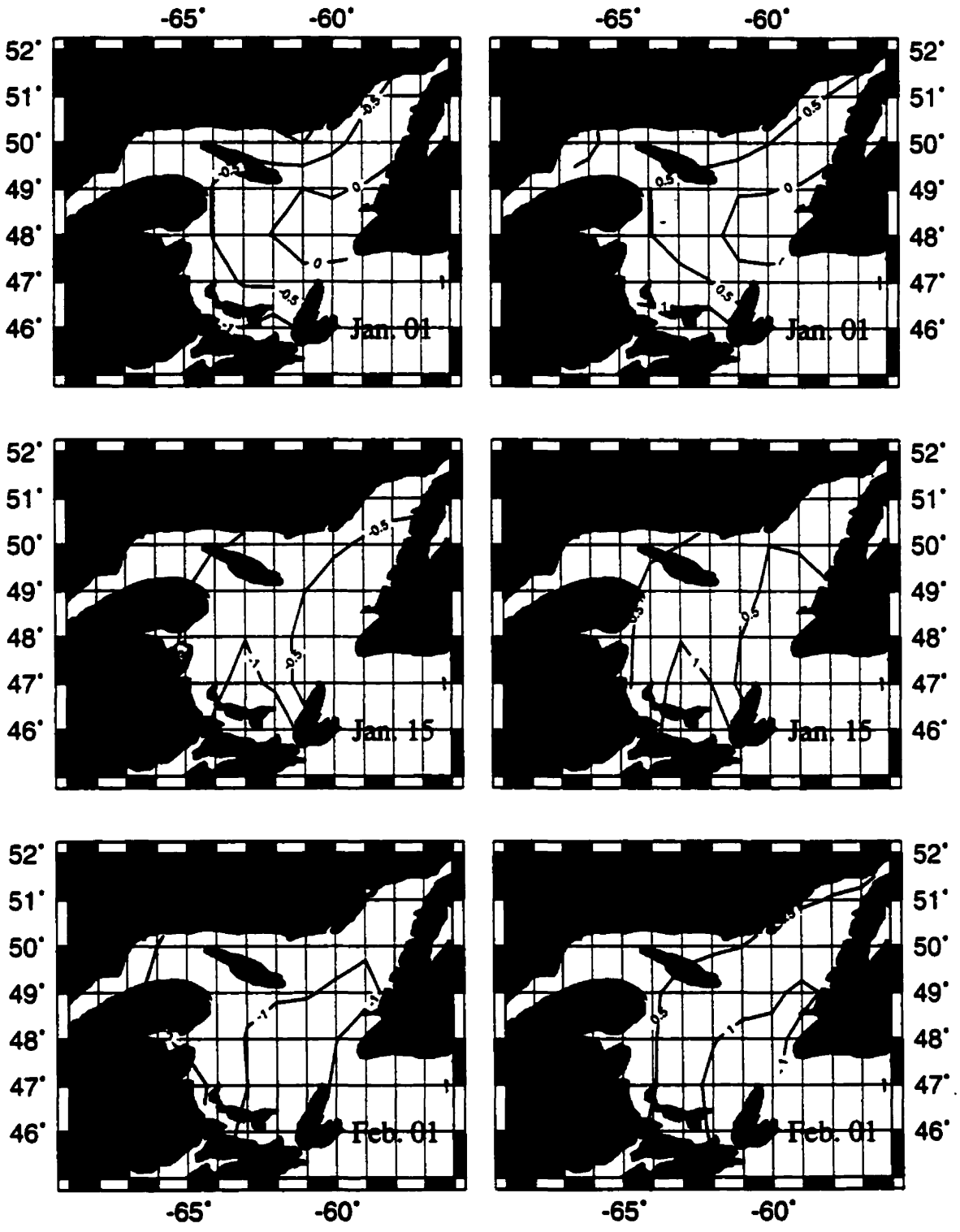

Figure 5.7 Modeled anomalies of sea-ice extent in tenths corresponding to change of SAT by +1°C (left panels) and -1°C (right panels)

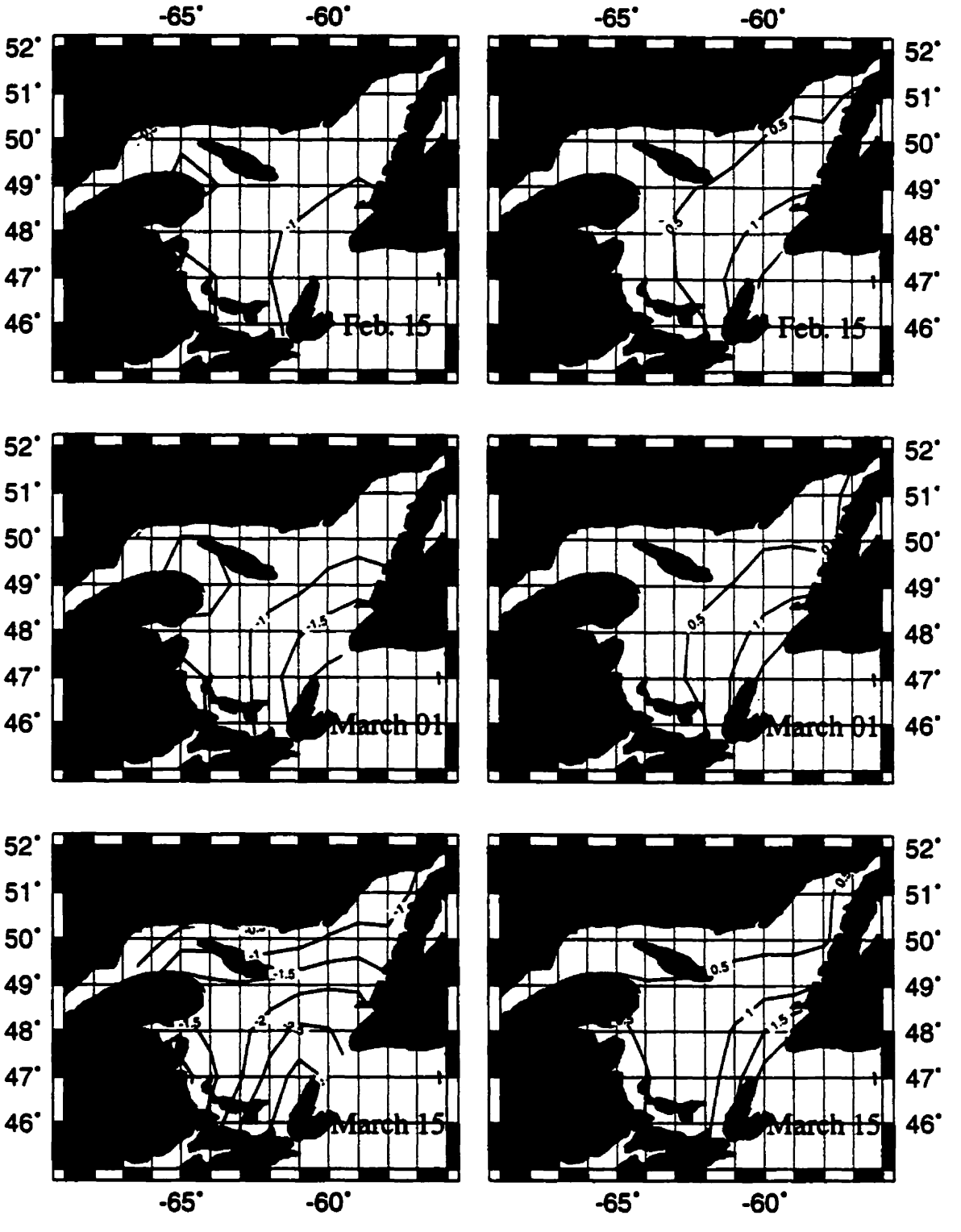

Figure 5.7 (Continued)

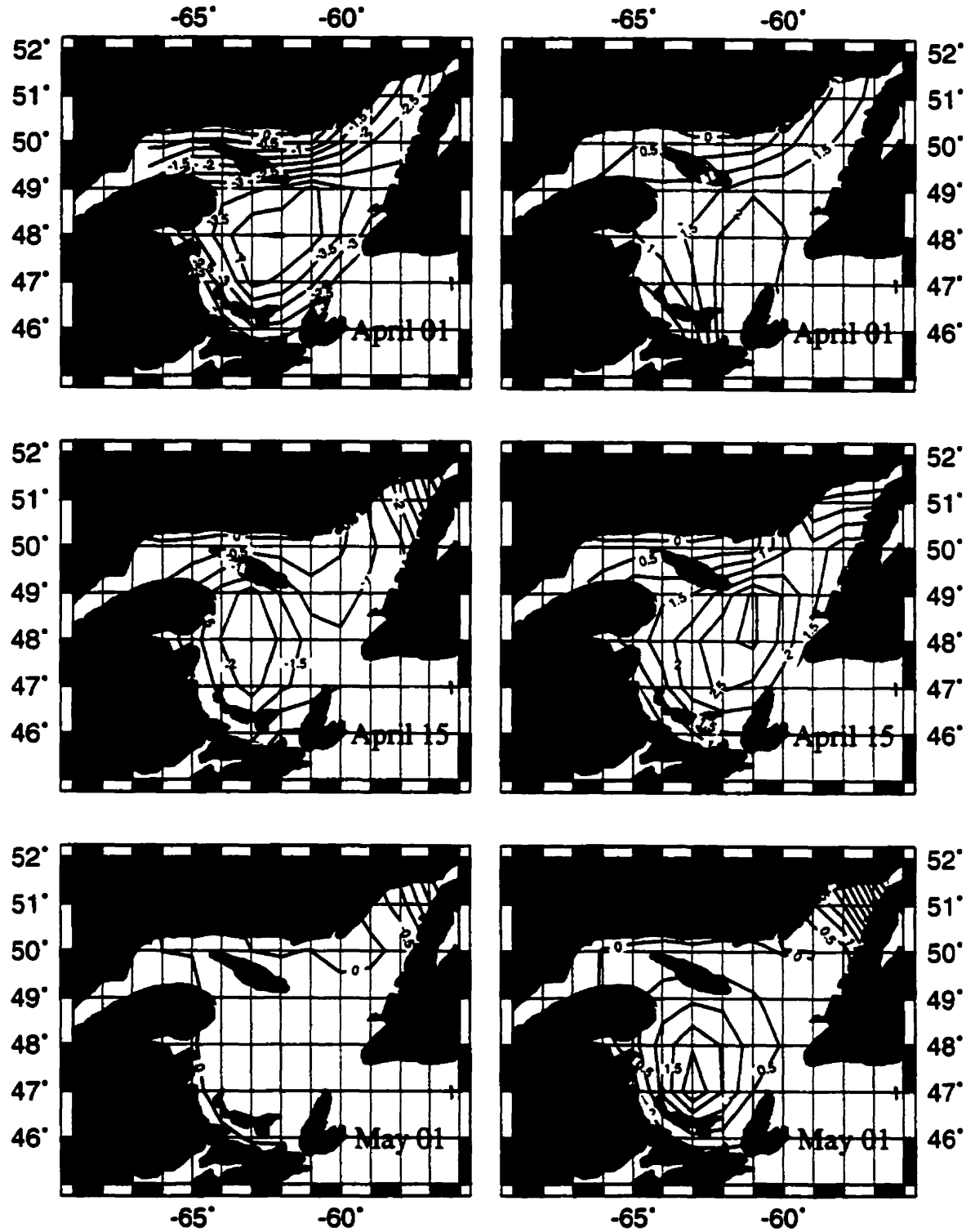

Figure 5.7 (Continued)

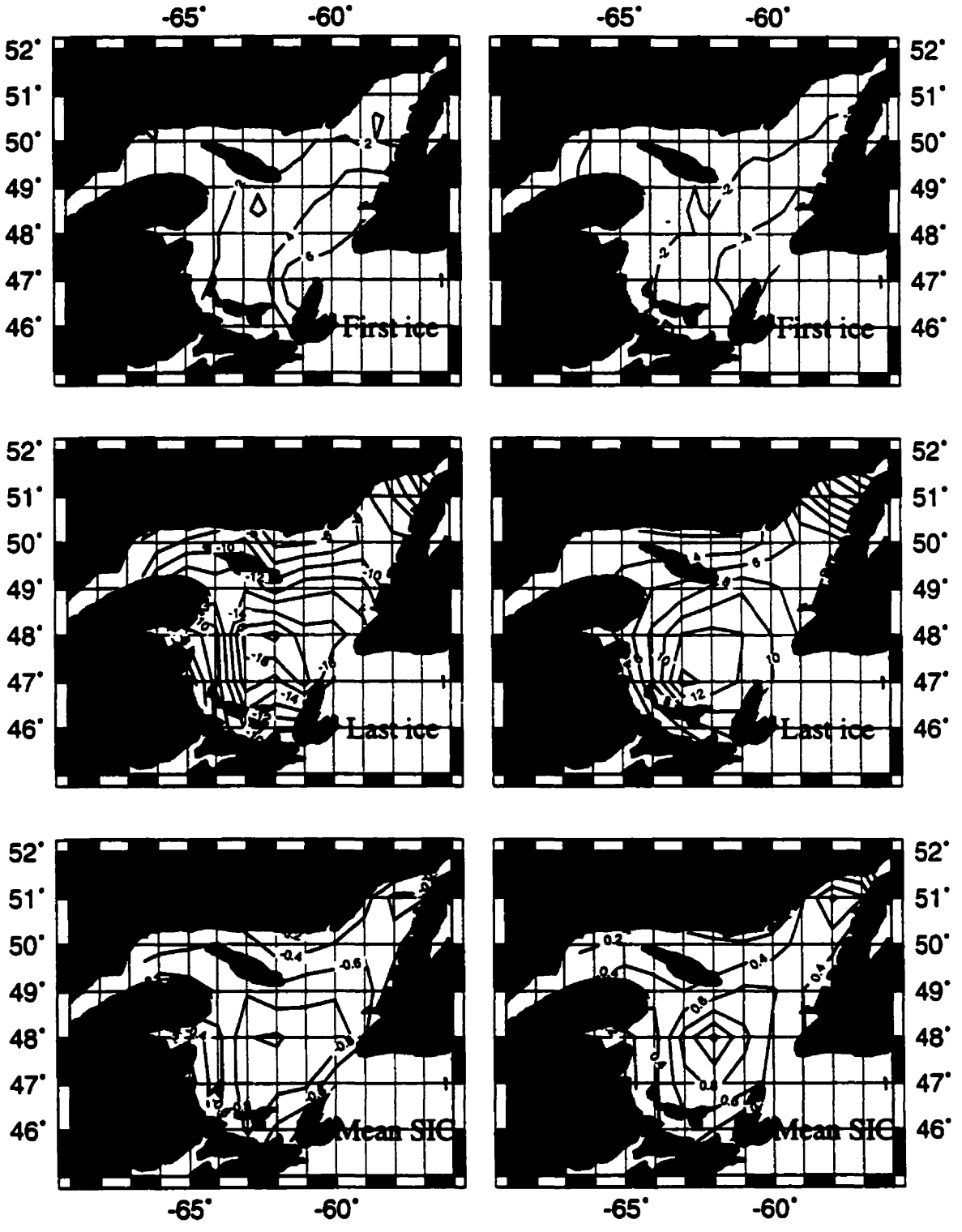

Figure 5.8 Modeled anomalies of TFIP, TLIP, and mean SIC corresponding to change of SAT by +1°C (left panels) and -1°C (right panels).

heat flux anomalies than in the other regions. The largest change in the time of sea ice disappearance caused by a change of one standard deviation of SAT is around 20 days.

Figure 5.9 shows the seasonal cycle of modeled anomalies of sea-ice cover from the standard run corresponding to a change of the December-April u-wind by ± 0.74 m/s, keeping all other forcing unchanged. As expected, a stronger (weaker) u-wind results in positive (negative) sea ice anomalies since stronger (weaker) u-winds can increase (decrease) heat flux and transportation of sea ice from the west to the east. As with the sea ice anomalies caused by the SAT anomaly, the sea ice anomalies caused by u-wind anomaly also increase with time. Again, changes in the sea-ice cover caused by the u-wind anomalies also originate in the coastal regions in early January and move to the eastern Gulf thereafter. The largest anomalies occur off Newfoundland in February-April. Figure 5.10 shows the anomalies of TFIP, TLIP, and mean SIC in December-June, corresponding to a change of u-wind by ± 0.74 m/s. Stronger (weaker) u-wind causes earlier (later) sea ice formation, later (earlier) sea ice disappearance, and larger (smaller) mean sea-ice cover. The largest anomalies of SIC in the eastern Gulf are consistent with our previous SVD analysis. This confirms the suggested importance of the u-wind component on sea-ice cover variability in Chapter 4. In addition, the largest TFIP anomalies occur off southwest Newfoundland. Note that the spatial patterns of sea-ice cover anomalies caused by stronger and weaker u-wind anomalies differ. The largest anomalies of sea-ice cover caused by the weaker u-wind anomalies are located off mid-Newfoundland while those associated with stronger u-wind anomalies are relatively spread out (Figures 5.9 and 5.10). Using the dynamic and thermodynamic equations,

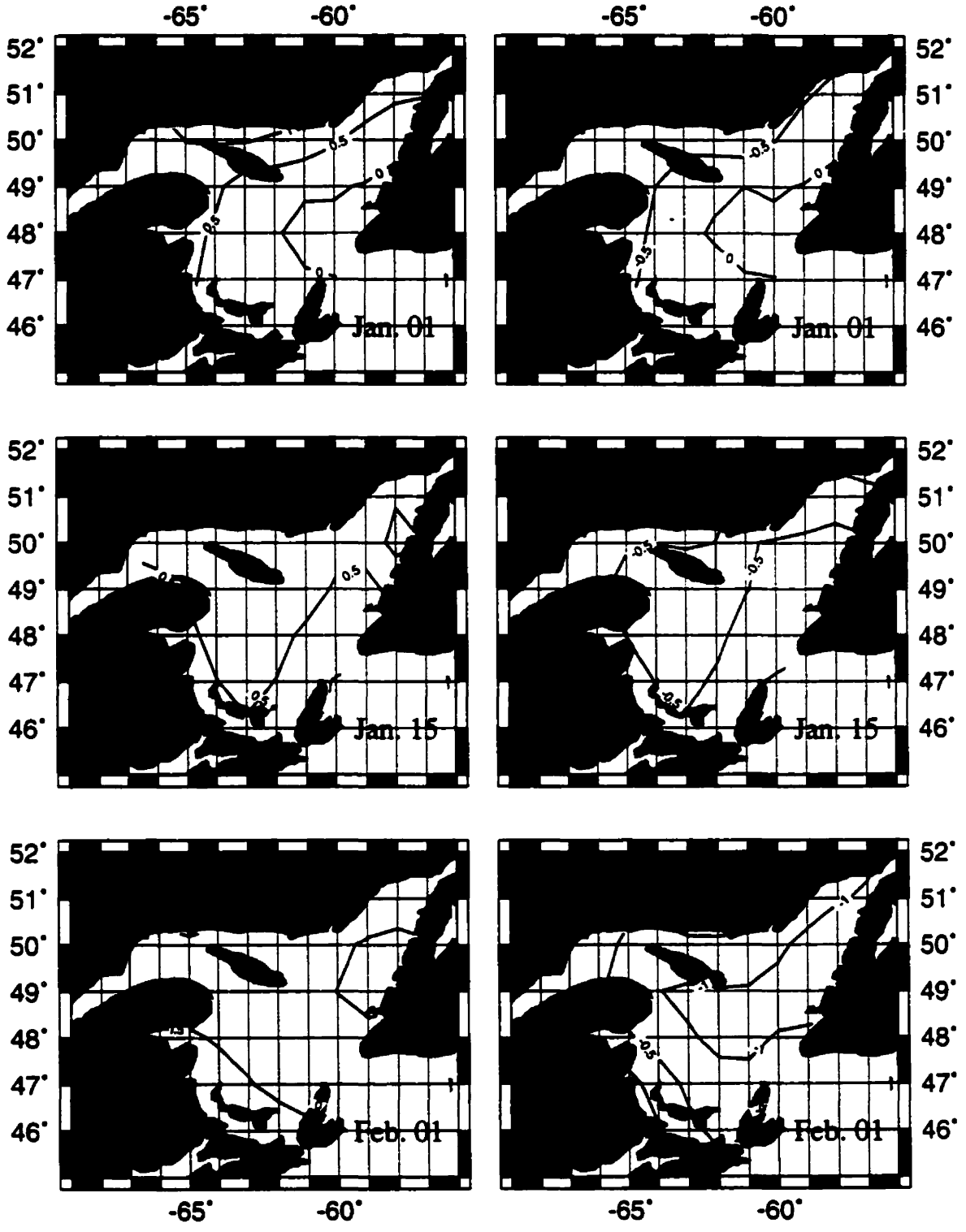

Figure 5.9 Modeled anomalies of sea-ice extent in tenths corresponding to change of u-wind by +0.74 m/s (left panels) and -0.74 m/s (right panels)

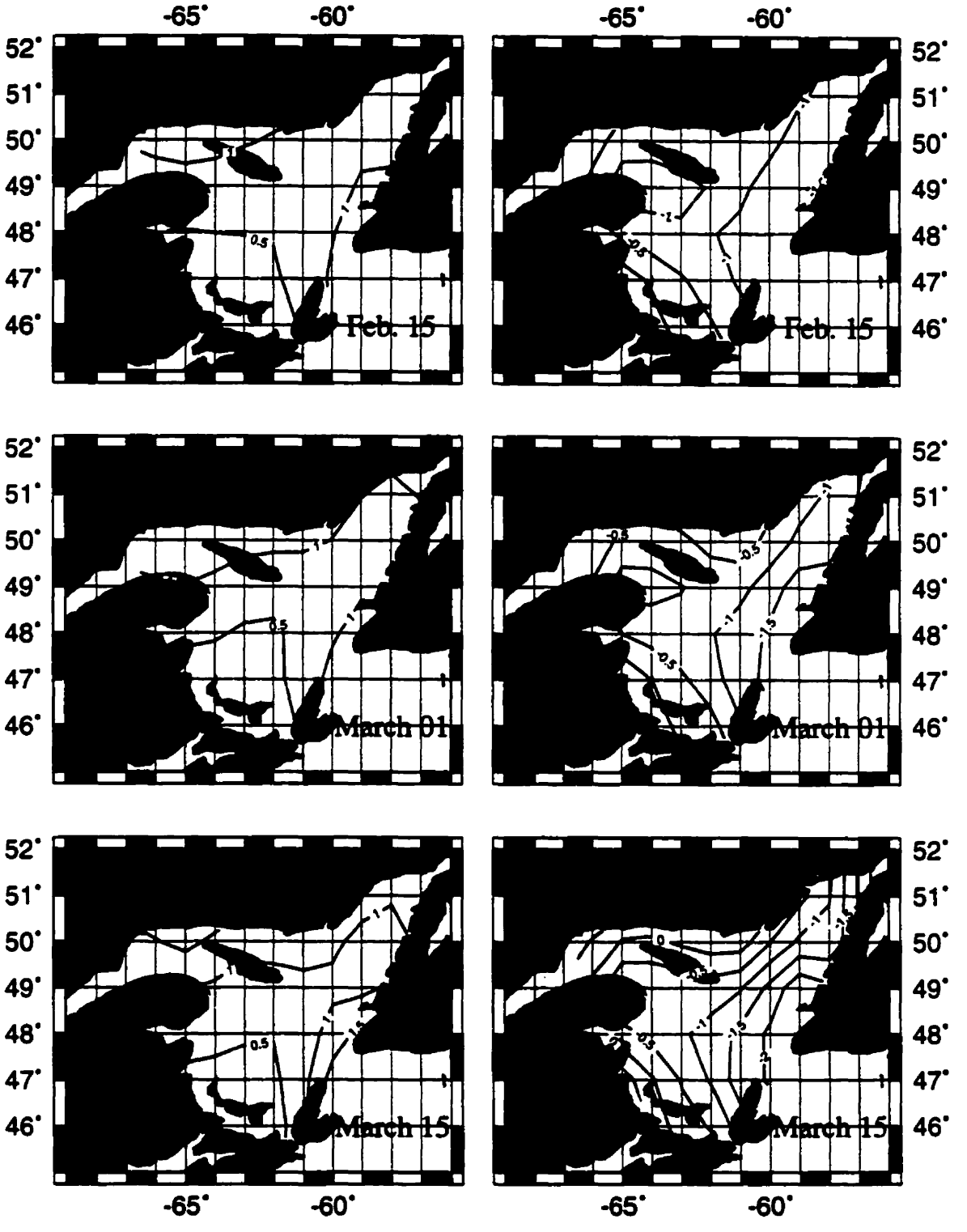

Figure 5.9 (Continued)

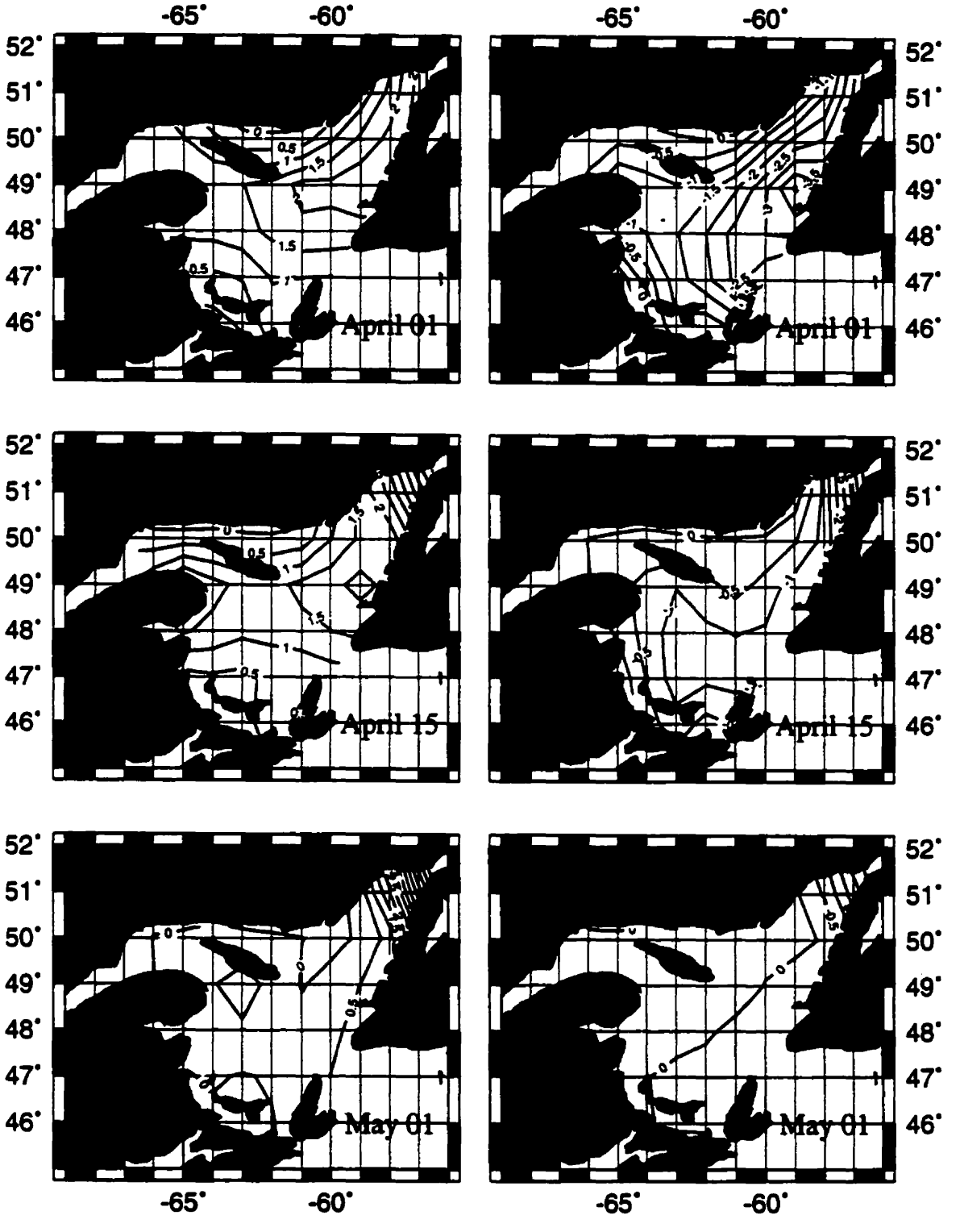

Figure 5.9 (Continued)

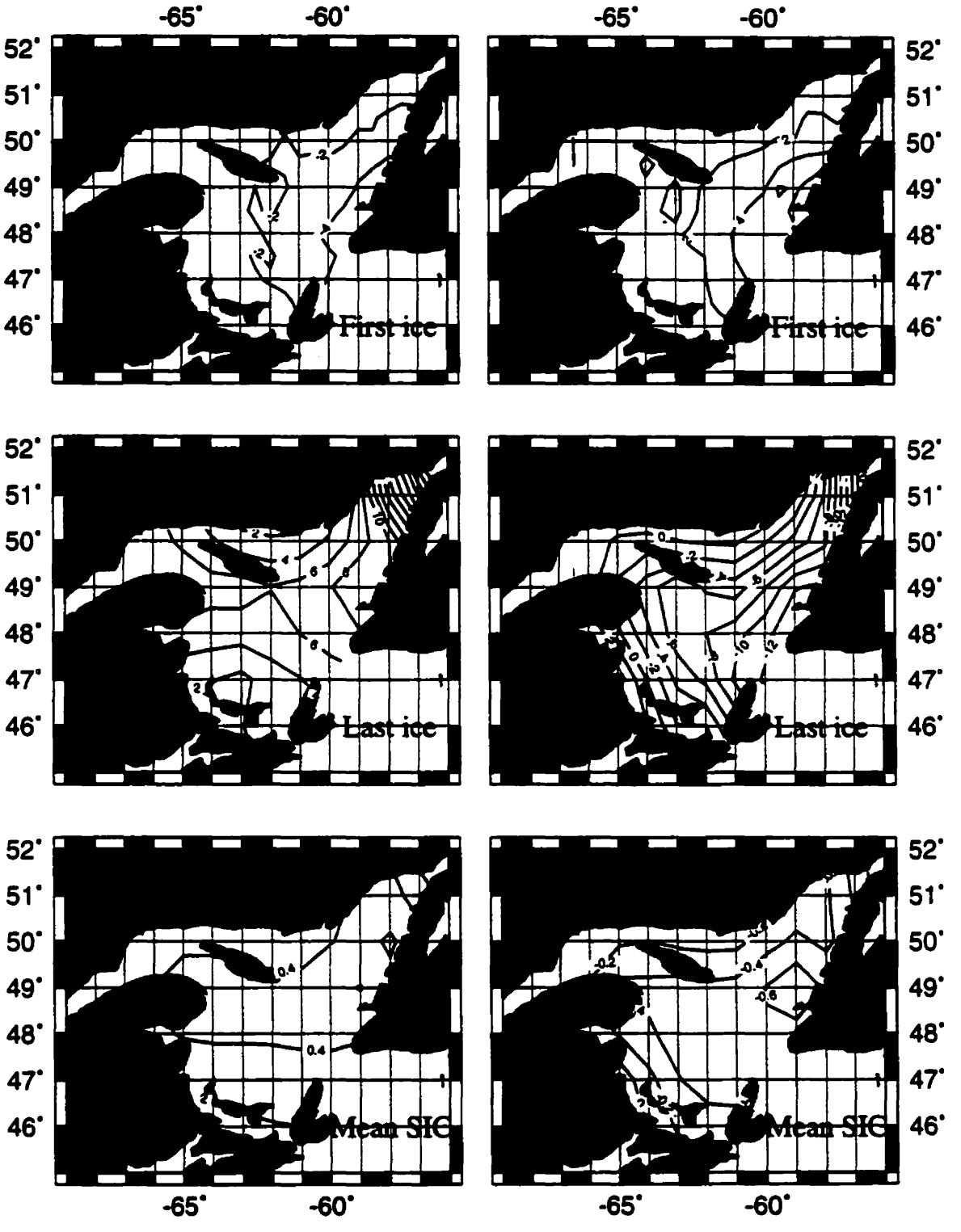

Figure 5.10 Modeled anomalies of TFIP, TLIP, and mean SIC corresponding to change of u-wind by +0.74 m/s (left panels) and -0.74 m/s (right panels).

One can see that a change of wind can cause a change in surface heat flux and wind-drag stress. The asymmetry of SIC anomalies with stronger and weaker winds suggests that for the weaker u-wind scenario wind stress is more important than the change of surface heat flux, while for the stronger u-wind scenario the opposite is true. Compared to the anomalies of TFIP, TLIP, and mean SIC caused by SAT, the resultant anomalies caused by u-wind are smaller. This indicates that December-April SAT plays a more important role than u-wind on sea ice variability.

Compared to the anomalies of sea-ice cover caused by SAT and u-wind, the anomalies caused by the v-wind anomaly are relatively featureless (Figure 5.11). The negative (positive) anomalies of sea-ice cover in January corresponding to changes of +0.60 m/s (-0.60 m/s) can be explained as follows. The mean v-wind in December-January is northerly (Figure 4.3). The 1 standard deviation change in v-wind of 0.60 m/s (-0.60 m/s) decreases (increases) the wind amplitude and the corresponding heat losses from the ocean, which in turn causes negative (positive) sea ice anomalies. The anomalies of sea ice cover in April are caused by the same mechanisms but the difference is that the v-wind in this month is southerly. The positive v-wind causes a larger heat flux (ocean receiving more heat), which in turn results in negative sea ice anomalies. Figure 5.12 shows the anomalies of TFIP, TLIP, and mean SIC in December-June caused by the v-wind anomaly. Compared to the anomalies caused by SAT and u-wind, these signals are small.

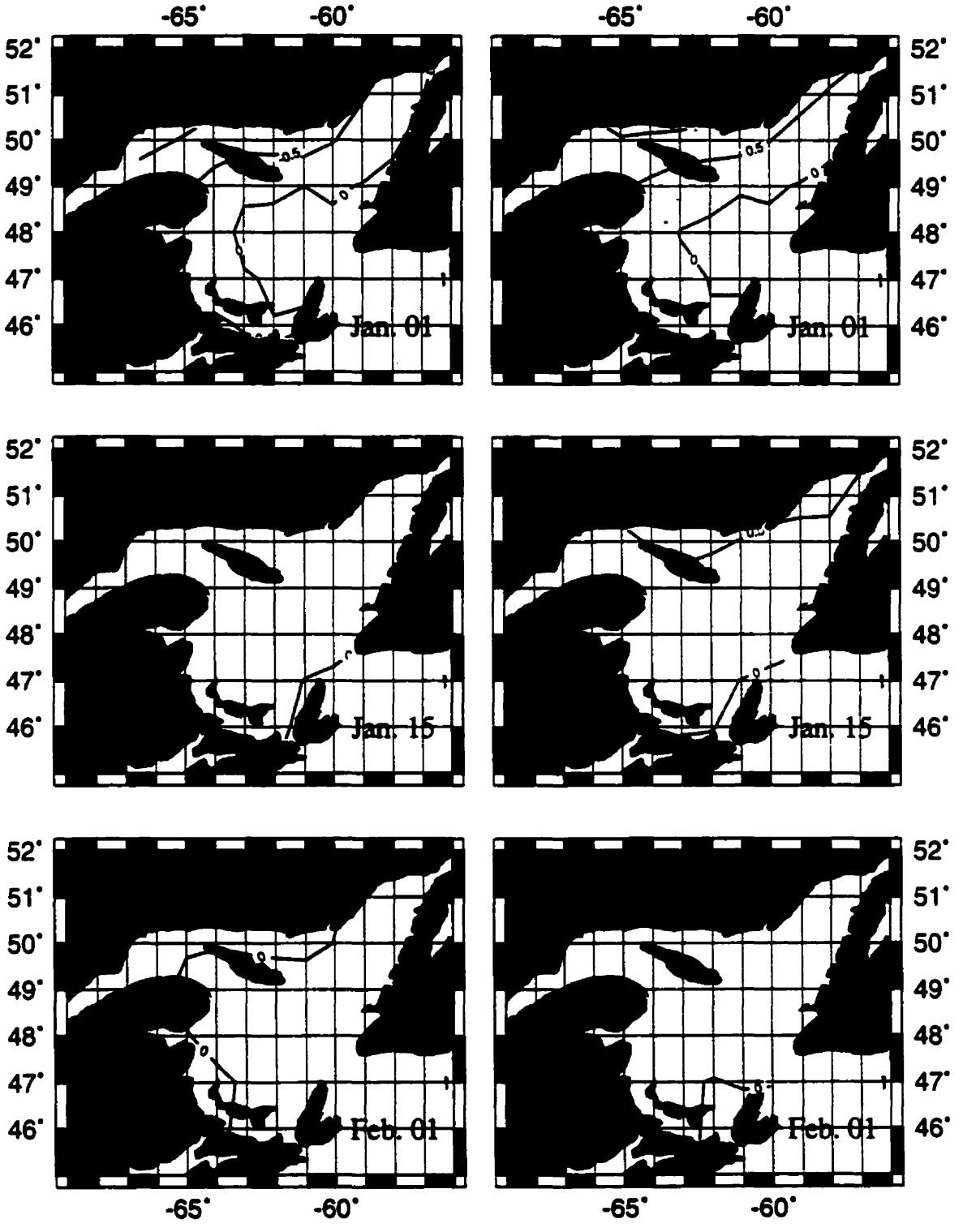

Figure 5.11 Modeled anomalies of sea-ice extent in tenths corresponding to change of v-wind by +0.60 m/s (left panels) and -0.60 m/s (right panels)

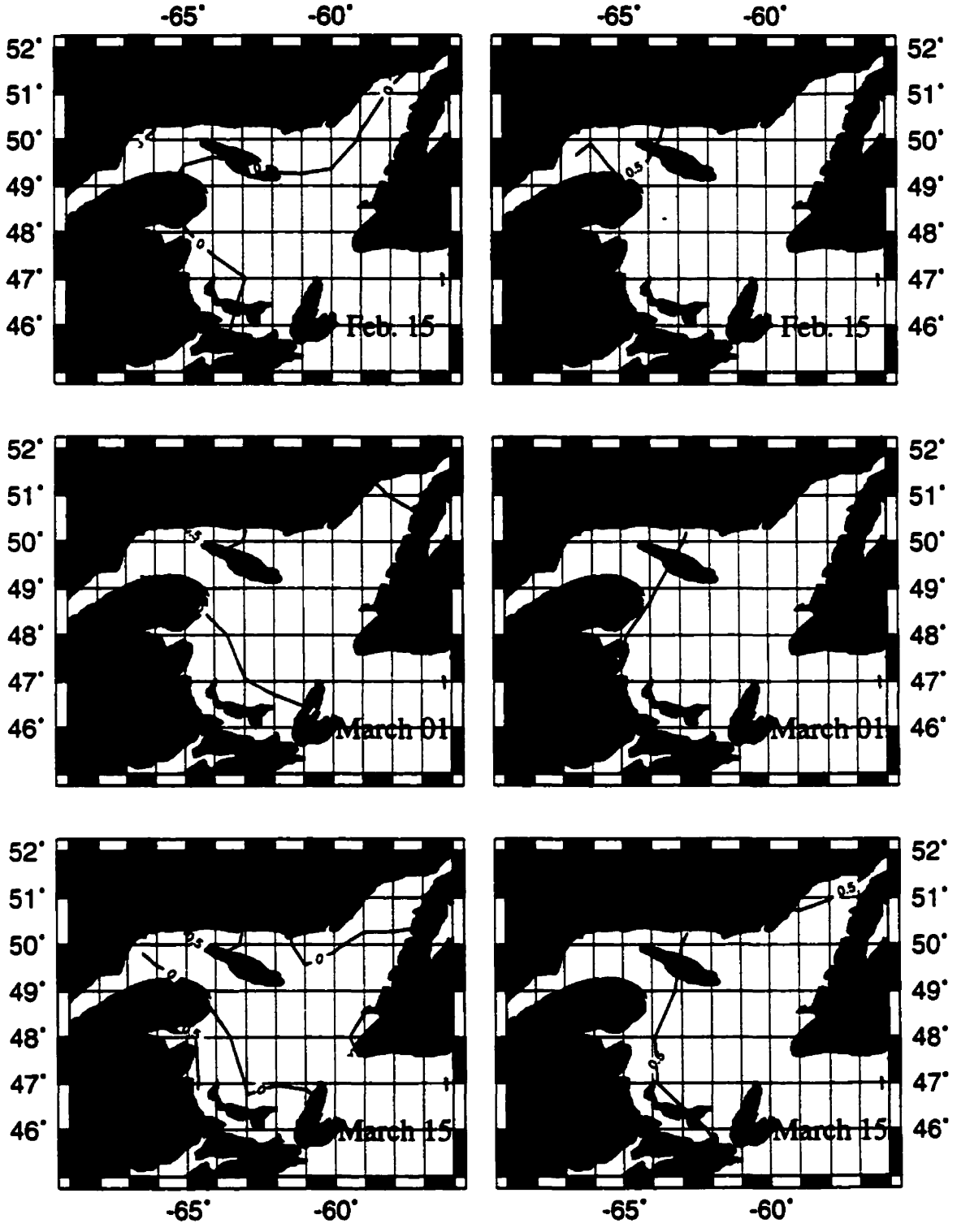

Figure 5.11 (Continued)

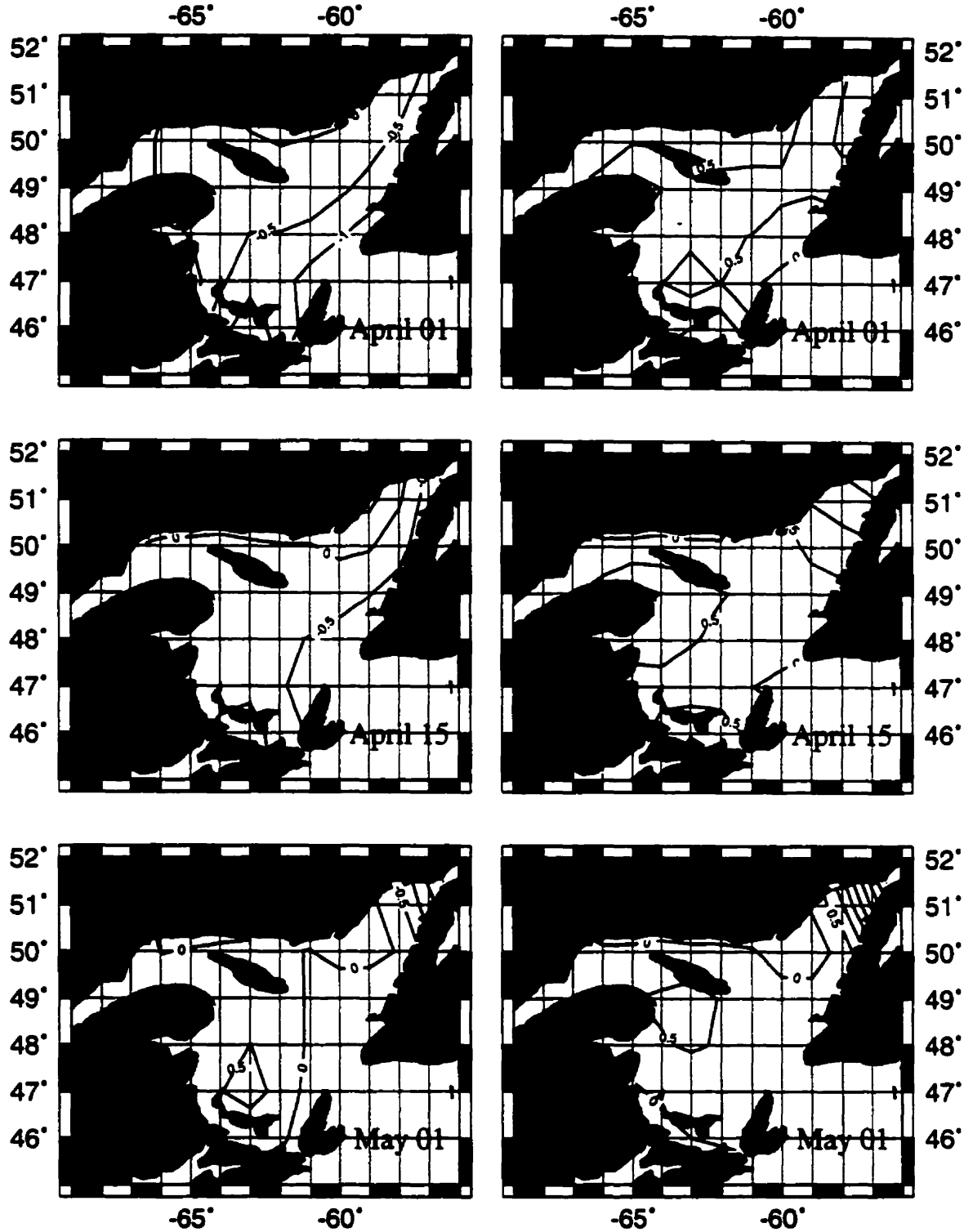

Figure 5.11 (Continued)

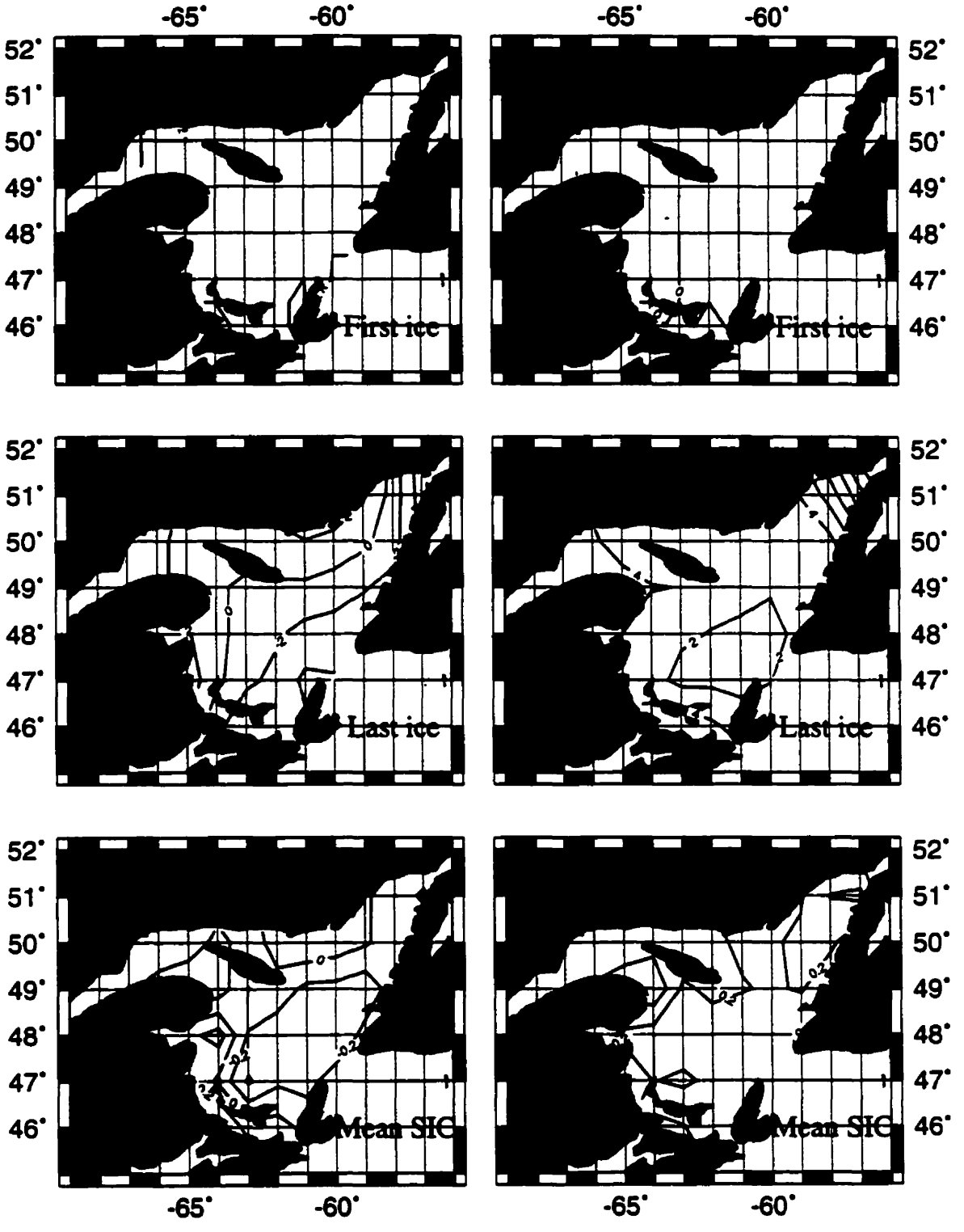

Figure 5.12 Modeled anomalies of TFIP, TLIP, and mean SIC corresponding to change of v-wind by +0.60 m/s (left panels) and -0.60 m/s (right panels).

Figure 5.13 shows the seasonal cycle of modeled anomalies of sea-ice cover from the standard run, corresponding to a change of November SST by ±1.12°C, while keeping all other forcing unchanged. The sea ice field changes caused by the November SST anomaly are the largest in early January, but decrease thereafter. This can also be seen from anomalies of TFIP (Figure 5.14), which are the largest changes caused by the forcing factors SAT, u-wind, v-wind, and SST in the northwest Gulf (Figures 5.8, 5.10, 5.12, and 5.14). This confirms the conclusion in Chapter 4 that the November SST plays a very important role on the TFIP field. The largest anomalies in the northwest Gulf occur because the mean SST is low there. After February, the largest anomalies caused by SST are in the eastern Gulf. Figure 5.14 also shows that the largest SIC anomalies caused by November SST are located in the northeast Gulf, which is consistent with the previous SVD analysis. In addition, it seems that November SST plays very little role in influencing TLIP.

Figure 5.15 shows comparison of sea-ice cover averaged over the entire Gulf for changes of ± one STD of December-April SAT, of u-wind, of v-wind, and of November SST, respectively, compared to the standard run. It can be seen that sea ice anomalies caused by SAT, u-wind, and v-wind tend to increase with time, while that caused by SST generally decrease with time from January to April. Among the four forcing factors, SAT causes the largest SIC anomalies, followed by u-wind, SST, and v-wind, in decreasing order. The SAT, SST, and u-wind fields play an important role in explaining TFIP, while both SAT and u-wind play an important role for TLIP. These conclusions can be also obtained by examining Figures 5.8, 5.10, 5.12, and 5.14.

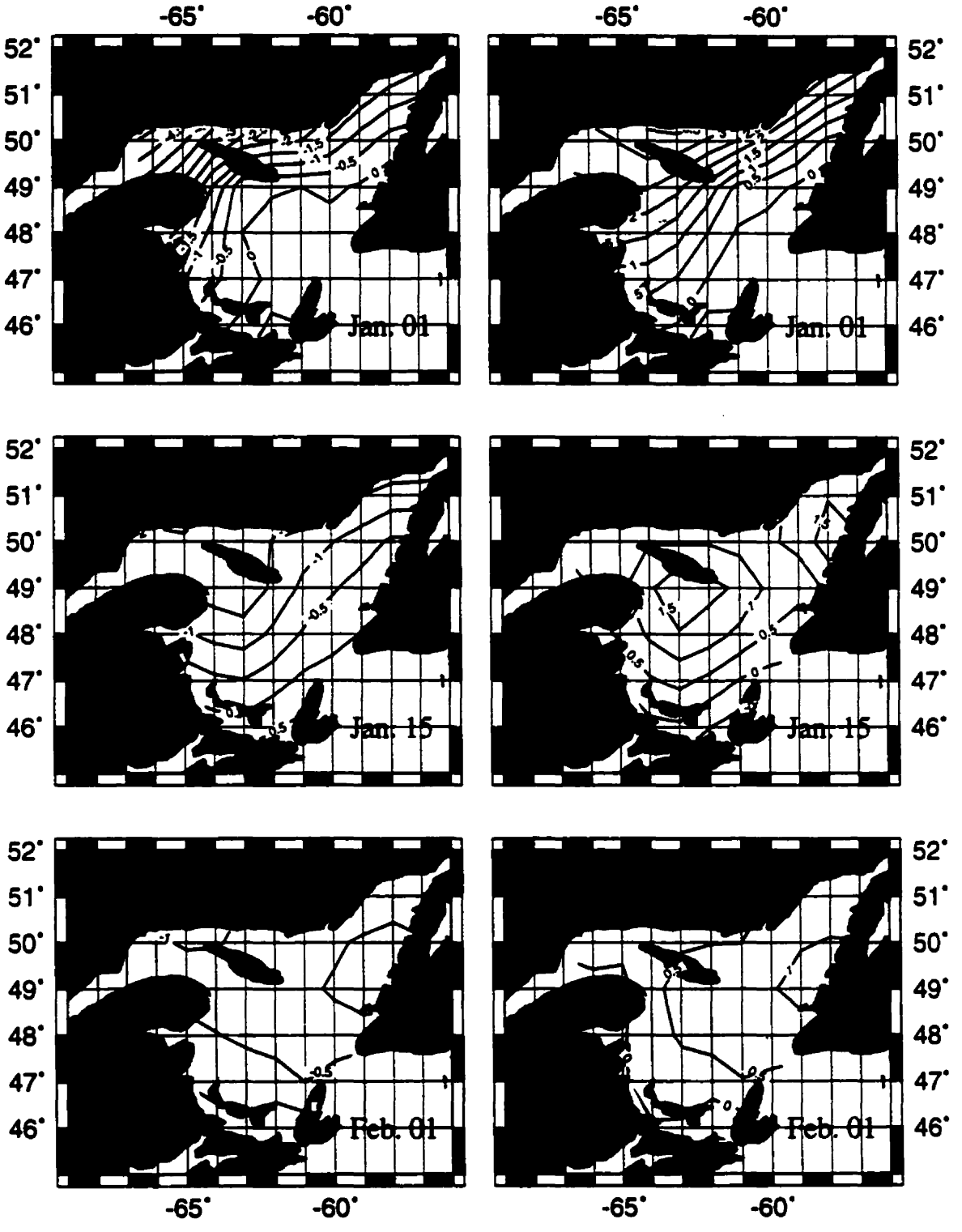

Figure 5.13 Modeled anomalies of sea-ice extent in tenths corresponding to change of SST by +1.12°C (left panels) and -1.12°C (right panels)

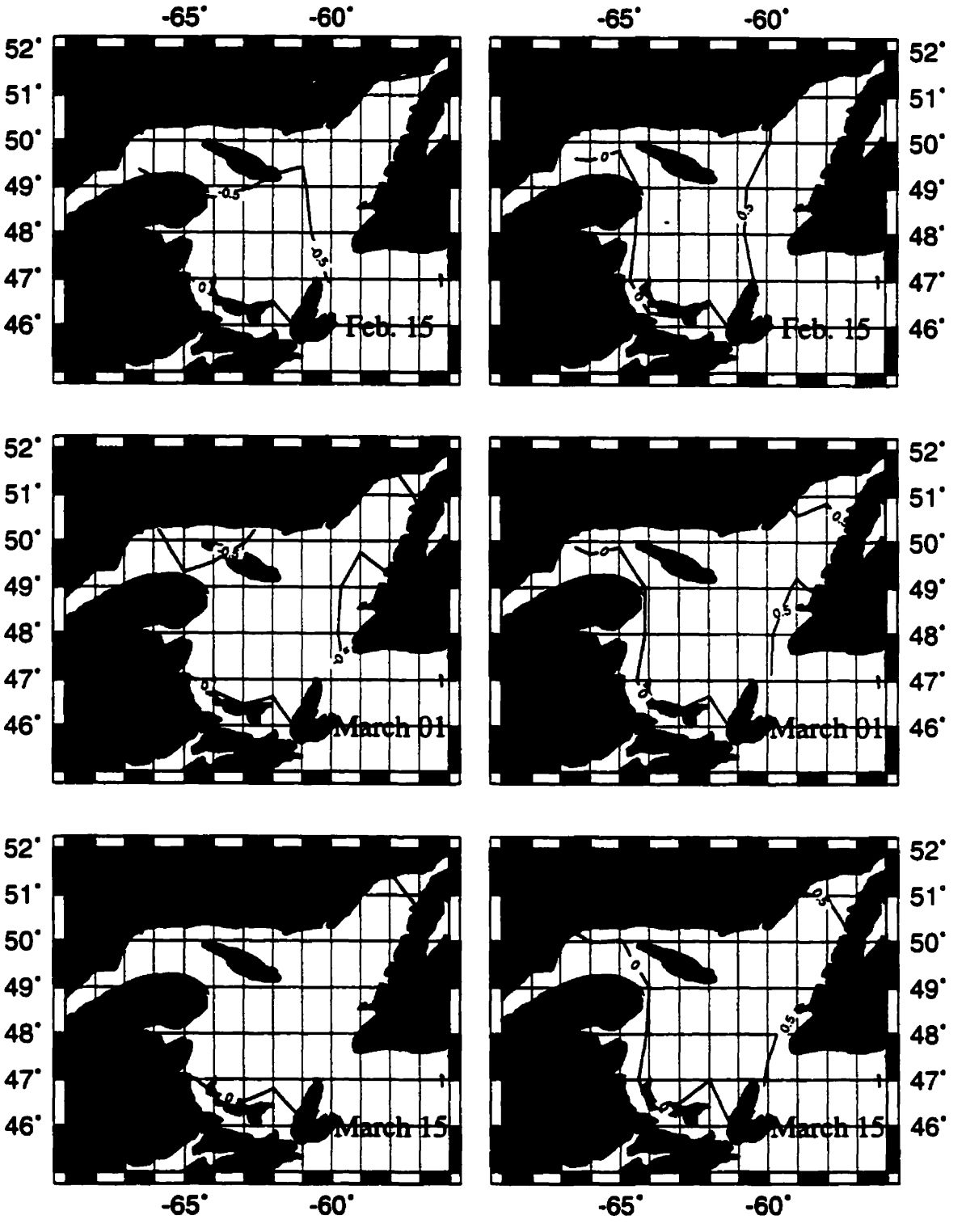

Figure 5.13 (Continued)

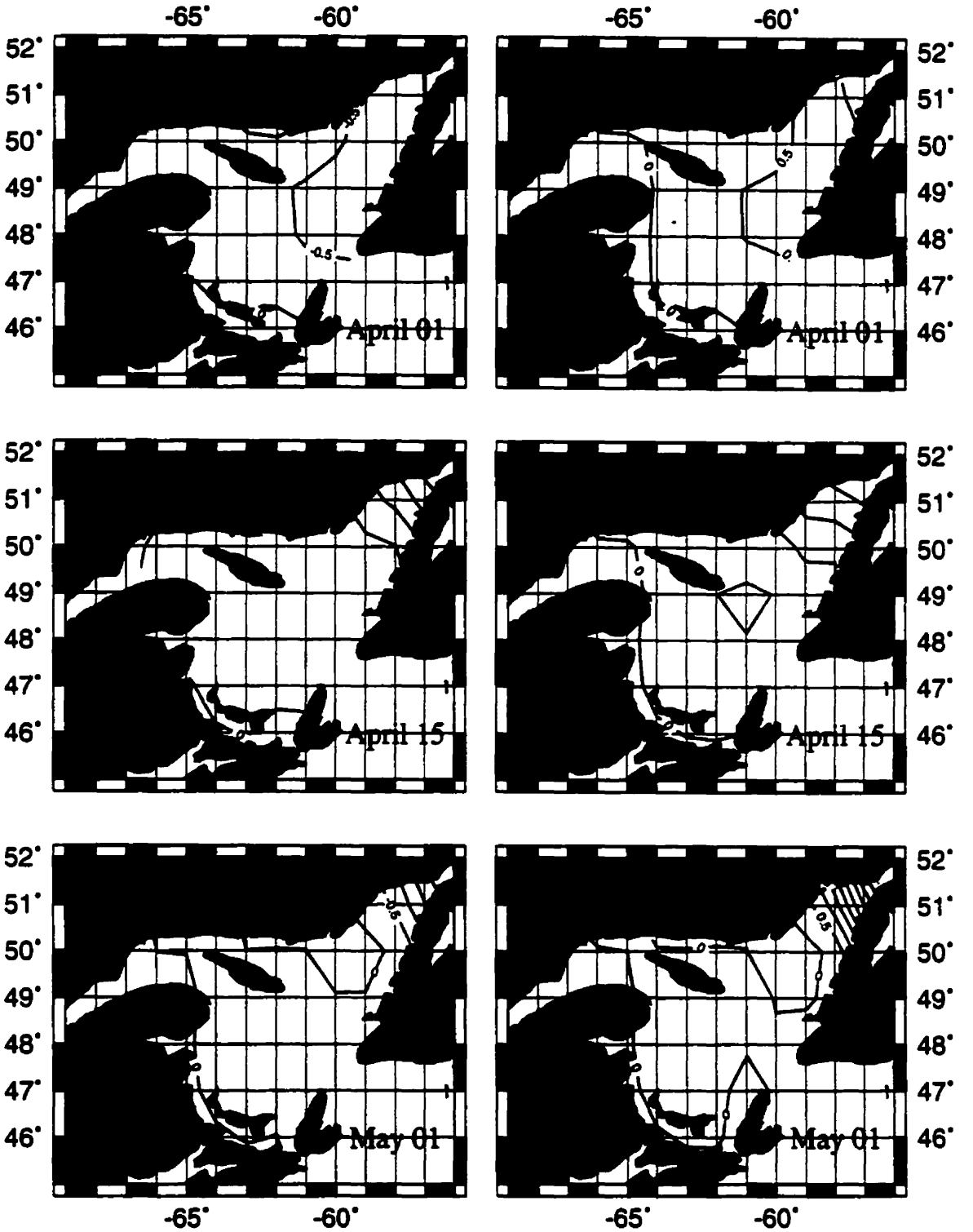

Figure 5.13 (Continued)

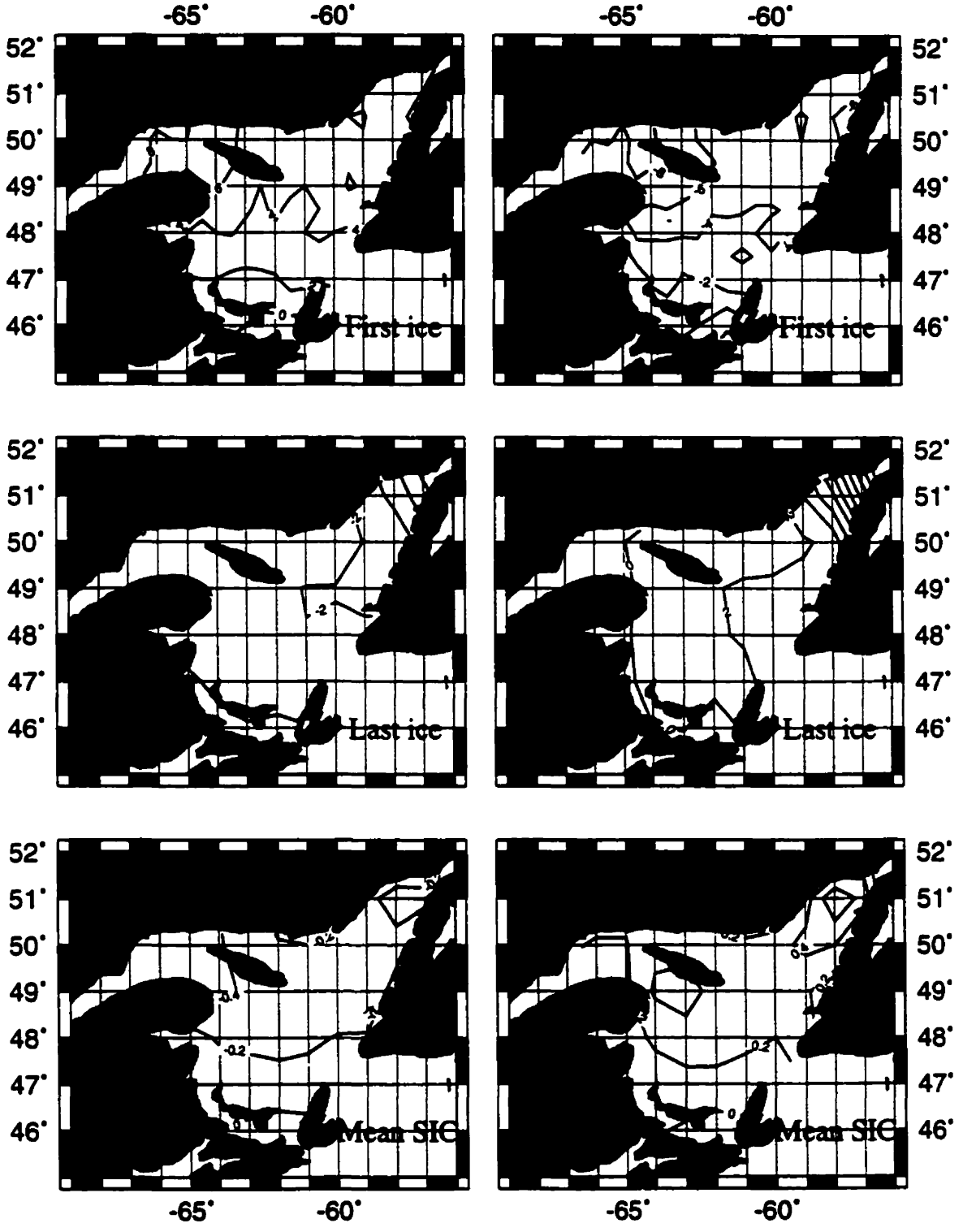

Figure 5.14 Modeled anomalies of TFIP, TLIP, and mean SIC corresponding to change of SST by +1.12°C (left panels) and -1.12°C (right panels).

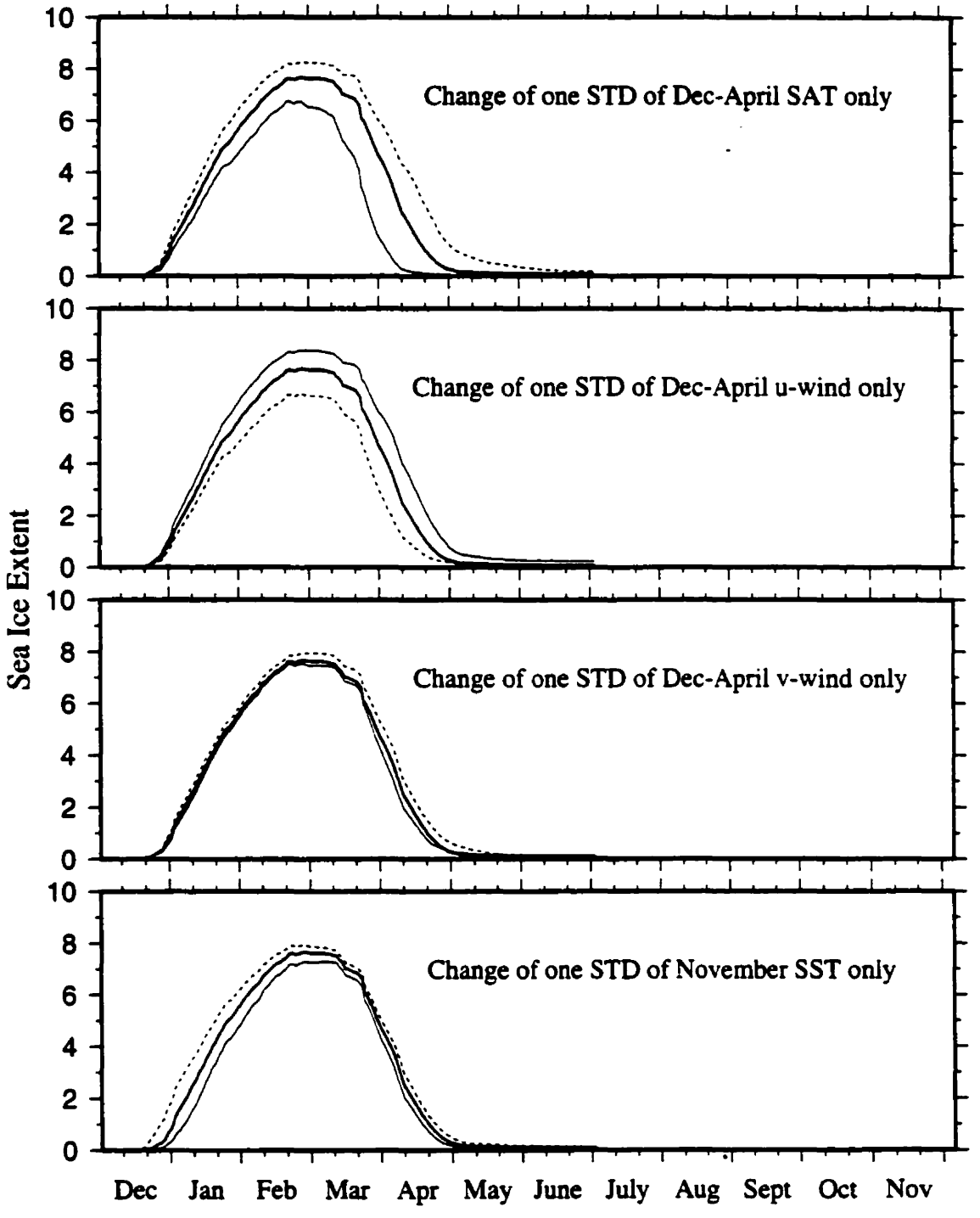

Figure 5.15 Comparison of sea-ice extent averaged over the entire Gulf under changes of one STD of December-April SAT, of u-wind, of v-wind, and of November SST, respectively, with standard run (thick solid line - standard run, thin solid line - by +1 STD, dashed line - by -1 STD).

5.5 Summary and conclusions

We simplified Hibler's (1979,1980) sea ice model to study the mechanisms of sea ice variability in the Gulf of St. Lawrence. First, we simulated annual sea ice variations for prescribed realistic climatological atmospheric and oceanic forcing. Then, we investigated the response of sea ice to changes in the external forcing factors. Given the typical variability for different forcing fields, we examined the relative importance of the different forcing factors on mean sea-ice cover, time of first ice presence, and time of last ice presence.

Our simplified model reproduced reasonably well the seasonal cycle of sea-ice cover in the Gulf of St. Lawrence in comparison with long-term observations. The model confirmed our findings from data analysis (Chapter 4) that SAT plays the most important role in controlling variability of sea-ice cover. The u-wind component and November SST values are also important, while the v-wind plays only a minor role. The model also verified that December SAT, November SST, and December u-wind play a key role in determining the time of first ice presence. For the time of last ice presence, the model indicated that December-April SAT and u-wind play the most important role. Thus, use of the model allowed an increased understanding of the important physical processes controlling sea ice variability in the Gulf.

The model used has some limitations. First, we did not consider internal ice stress, which may be a very important factor when sea ice becomes thicker or when ice floes collide with each other. Second, the sea ice advection term in the momentum equation was neglected. Third, sea surface circulation was not included because of a lack of observational data. Nevertheless, sea surface circulation is thought to be important in transporting sea ice within our study area. Fourth, the effect of river runoff was not taken into account. As a result of these limitations, there are discrepancies between the simulation results and observations. For example, the region of the highest sea-ice cover in April was not well reproduced. Furthermore, the advection of ice through the Strait of Belle Isle from the Labrador Sea to the Gulf is not reproduced although it is thought to be an important factor explaining sea ice variability in the northeast part of the Gulf, as suggested from data analysis in Chapter 4. These discrepancies can be eliminated only with the use of a fully coupled ice-ocean model including all of the major physical processes and additional observational data.

6. Summary and Discussions of Future Work

In this thesis, the intraseasonal and interannual variability of sea ice in the Gulf of St. Lawrence were examined using sea ice observations from 1963-1996. The mechanisms and relative importance of forcing factors in controlling sea ice variability in the Gulf were studied using statistical analysis and a simplified Hibler's model.

For the intraseasonal variations of sea-ice cover, the sea-ice cover over different sub-regions was found to display contrasting features. This study indicated that this is because the mechanisms responsible for sea ice variability over different sub-regions are not the same. The largest intraseasonal variations of sea-ice cover occur in the Strait of Belle Isle region and southwestern Gulf, where the mean sea-ice cover is largest and sea-ice duration is longest, exceeding 140 days for the former region. For the Strait of Belle Isle region, the lower SAT in December-April period, lower SST in November, and especially sea ice advection from the Labrador Sea can explain the higher SIC and longer SID in this region. In the southwestern Gulf, the shallower MLD in November, northwesterly winds, winter circulation patterns, and lower SSS in November all play very important roles in determining the ice distribution.

On the interannual scale, the sea-ice cover averaged over December-June and sea-ice duration displayed both interannual and decadal-scale variability, with the latter accounting for a large part of the total variance. The largest variability occurs in the area off mid-Newfoundland, where the mean sea-ice cover is small. This could be caused by

the following reasons. First, the MLD in this region is deeper and has a large interannual variability. A deeper MLD leads to a longer time to generate ice. Thus, the large interannual variability of MLD leads to substantial interannual variability of sea ice in this region. Second, the predominate westerlies can advect the sea ice from the western Gulf to the eastern Gulf. The large interannual variability of the u-wind component in this region can also cause large interannual variability of sea ice. Third, the large interannual variability of SST can also contribute to greater sea ice variability in this region. Fourth, SAT may also play a role in explaining the large sea ice variability in this region.

The time of first ice presence and the time of last ice presence displayed interannual-scale variability, with the largest variability in the area off Newfoundland for TFIP and along the northeast coast areas for TLIP. Similar to the SIC, the largest interannual variability of TFIP off Newfoundland can be explained by the deeper and large interannual variability of MLD in this region, u-wind, SST, and SAT. The biggest interannual variability of TLIP along the northeast coast areas can be explained by the large variability of SAT in this region and sea ice advection from the Labrador Sea.

In regard to severe ice years, the sea ice appeared 10 days earlier in the coastal regions and disappeared 10 days later over the entire Gulf. Sea-ice duration and sea-ice cover were longer and larger than normal over the entire Gulf, respectively, with more than 30 days longer for SID and 1/10 larger areal coverage for mean SIC in December-June for the area off mid-Newfoundland. In contrast, sea ice in light ice years appeared more

than 10 days later in the central and eastern Gulf and disappeared more than 30 days earlier in the eastern Gulf. Sea-ice duration and sea-ice cover were shorter and smaller than normal over the entire Gulf, respectively, with only 10 days duration and less than 1/10 in sea-ice cover for the area off mid-Newfoundland. The forcing fields in the extreme ice years were also examined. Lower (higher) SAT and stronger (weaker) u-wind component in December-April, and lower (higher) SST and lower (higher) SSS in previous November were found in years with severe (light) ice.

We examined the relationship between forcing factors and sea ice variability and explored the important physical processes controlling sea ice variability in the Gulf. We found that SAT, u-wind, SST, SSS, MLD, river runoff from the St. Lawrence River system, circulation pattern, and sea-ice advection from the Labrador Sea all play important roles in explaining sea ice variability. However, the contributions from these factors differ by subregions. On the interannual scale, the statistical analysis and a model study indicated that December-June averaged SAT, u-wind, November SST/SSS all contribute to the variability of sea ice in the Gulf, with SAT playing the most important role and u-wind and SST the second most important. The results also indicated that different forcing factors have contrasting geographic importance on sea ice variability. For example, SAT influences sea ice variability mainly in the central Gulf, while u-wind mainly effects the eastern Gulf. In addition, the linear regression between SIC and three independent variables SAT, SST, and SSS accounts for 81% of the total SIC variance.

The statistical analysis and model study also indicated that December SAT, u-wind, November SST/SSS, and MLD control the time of first ice presence, with SAT and SST playing the dominant role. The linear regression between TFIP and three independent variables u-wind, SST, and SSS accounts for 76% of the total TFIP variance. For TLIP, both SAT and u-wind play an important role. However, the variance accounted for by these two factors is not high, only about 40% of the total variance. In addition, this study shows that the v-wind component is unimportant in explaining sea ice variability in the Gulf.

The primary objective of this research was to examine the intraseasonal and interannual variability of sea ice in the Gulf of St. Lawrence and to understand the mechanisms of controlling sea ice variability in the Gulf. The results of this study are expected to be of importance to further research on sea ice variability in the Gulf and elsewhere. Additional work that could help improve our understanding of sea ice variability and the dominant mechanisms are as follows.

1. The mechanisms of controlling TLIP variability in the Gulf

We found in the present study that both SAT and u-wind play an important role in explaining variability of the time of last ice presence. However, the variance of TLIP accounted for by these two factors is not high (about 40% of the total variance). Thus, one open question is what other factors, not considered in the present study, are important in the variability of TLIP and what are the important physical processes controlling TLIP variability. Answering this question could help us to better understand mechanisms of

sea ice variability in the Gulf.

2. Intraseasonal and interannual variability of sea ice thickness in the Gulf

In the present study, intraseasonal and interannual variability of sea ice thickness in the Gulf was not investigated. Although Drinkwater et al. (1999) studied intraseasonal variations of sea ice thickness in the Gulf, their study was based upon some questionable assumptions. These included using an invariant mean thickness as a function of ice type, neglect of any ridging, no account for year-to-year differences in the thickness of the land fast ice, etc. In order to improve our understanding of sea ice variability in the Gulf, studies on intraseasonal and interannual variability of sea ice thickness and further sea ice volume in the Gulf are needed.

3. Field work in the Gulf of St. Lawrence

Ocean circulation and sea ice advection from the Labrador Sea were found to be important in controlling sea ice variability in the Gulf. Because of the lack of observational data, their role on generating sea ice variability was not considered. They were not included in the model either. In addition, hydrographic observations in the Gulf of St. Lawrence in winter months are rare. In this study, November SST/SSS and mixed layer depth were used to examine their effects on sea ice variability. To better understand mechanisms which control sea ice variability in the Gulf, observations of winter ocean circulation, sea ice advection from the Labrador Sea, and hydrographic conditions are required. Use of Radarsat imagery to track ice floes in the Gulf over the winter season and for different years may also allow us to generate a much improved record of sea ice

advection.

4. A coupled ice-ocean model

The simplified sea-ice model used in the present study did not consider internal ice stress, sea ice advection in the momentum equation, sea surface currents, river runoff, etc. In addition, the model is uncoupled with the ocean. Because of these shortcomings, we expect discrepancies between the simulation results and observations. These deficiencies can be eliminated only with the use of a fully coupled ice-ocean model including all of the major physical processes.

References

Bjornsson, H. and S.A. Venegas, 1997. A manual for EOF and SVD analyses of climate data. C^2GCR Report No. 97-1, McGill University, 52p.

Black, W.A., 1972. Sea-ice as an environmental factor, p. 3-18. In Coastal Zone, Seminar proceedings, Vol. 1. March 1972, Bedford Inst. Oceanogr., Dartmouth, N.S.

Bretherton, C.S., C. Smith, and J.M. Wallace, 1992. An intercomparison of methods for finding coupled patterns in climate data. Journal of Climate, 5: 541-560.

Brown, R. A., 1979. Planetary boundary layer modelling for AIDJEX. Proc. ICSI/AIDJEX Symp. On Sea Ice Processes and Models. University of Washington.

Bugden, G. L., 1981. Salt and Heat Budgets for the Gulf of St. Lawrence. Can. J. Fish Aquat. Sci. 38: 1153-1167.

Bunker, A. F., 1976. Computations of surface energy, flux and annual air-sea interaction cycles of the North Atlantic. Mon. Weather Rev. 104: 1122-1140.

Chapman W.L. and J.E. Walsh, 1993. Recent variations of sea ice and air temperature in high latitudes. Bull. Amer. Met. Soc. 74: 33-47.

Coté, P.W. 1989. Ice limits eastern Canadian seaboard. Environment Canada, Ottawa, 39 p.

Dery, F., 1992. Interannual and intraseasonal variability of the ice cover in the Gulf of Saint Lawrence, 1963-1990. M.Sc. Thesis. Department of Atmospheric and Oceanic Sciences, McGill University, 220p.

DeTracey, B., 1993: Modelling interannual sea ice variability in the Gulf of St. Lawrence. M.Sc. Thesis. Department of Atmospheric and Oceanic Sciences, McGill University, 108p.

Dickson, R.R., H.H. Lamb, S.A. Malmberg, and J.M. Colebrook, 1988. The "Great Salinity Anomaly" in the Northern North Atlantic 1968-1982. Progress in Oceanography 20: 103-151.

Doyon, P., 1996. Climatology and variability of the upper layer thermohaline fields in the Gulf of St. Lawrence. M. Sc. Thesis. Department of Atmospheric and Oceanic Sciences, McGill University, 165p.

Drinkwater, K.F. and G. L. Bugden, 1994. On the interannual variability of ice conditions in the vicinity of Cabot Strait. DFO Atlantic Fisheries Research Document 94/9: 1-11, Dartmouth, N. S.

Drinkwater, K. F., 1996. Atmospheric and oceanic variability in the Northwest Atlantic during the 1980s and early 1990s. J. Northw. Atl. Fish. Sci., Vol. 18: 77-97.

Drinkwater, K.F., E. Colbourne, and D. Gilbert, 1996. Overview of environmental conditions in the Northwest Atlantic in 1995. NAFO Scientific Council Studies, No. 27: 1-37.

Drinkwater, K.F., R. Pettipas, and L. Petrie, 1997. Overview of Meteorological and sea ice conditions off Eastern Canada during 1996. Department of Fisheries and Oceans, Canadian Stock Assessment Secretariat, Research Document 97/: 1-29, Dartmouth, N. S.

Drinkwater, K.F., R.G. Pettipas, G.L. Bugden, and P. Langille, 1999. Climatic data for the northwest Atlantic: A sea ice database for the Gulf of St. Lawrence and the Scotian Shelf. Can. Dept. Rep. Hydrogr. Ocean Sci. 199, 134p.

Dunbar, M. J. et al., 1980. The biogeographic structure of the Gulf of St. Lawrence. McGill Univ., Mar. Sci. Center, MS. Rep. 32: 142p, Montreal, Québec

Dunbar, M.J., 1980. The Gulf of St. Lawrence: physical constraints on biological production. In R. Lorimer and S. E. McMullin [ed.]. Canada and the Sea. Association for Canadian Studies, Canadian Issues, 3(1): 7-14.

El-Sabh, M., 1976. Surface circulation pattern in the Gulf of St. Lawrence. J. Fish. Res. Board Can. 33 (1): 124-138.

Fang, Z. and J. M. Wallace, 1994. Arctic sea ice variability on a timescale of weeks and its relation to atmospheric forcing. Journal of Climate, Vol. 7: 1897-1913.

Forrester, W.D., 1964. A quantitative temperature-salinity study of the Gulf of St. Lawrence. Rep. 64-11, Bedford Inst. Oceanogr., Dartmouth, Nova Scotia, 16p.

Forrester, W.D. and P.E. Vandall, Jr., 1968. Ice volume in the Gulf of St. Lawrence. Unpublished manuscript. Bedford Institute of Oceanography, Dartmouth, N. S.

Forward, C.N. 1954. Ice distribution in the Gulf of St. Lawrence during the break-up season. Geogr. Bull. 6: 45-84.

Garrett, C. and B. Petrie, 1981. Dynamical aspects of the flow through the Strait of Belle Isle. Journal of Physical Oceanography, 11 (3): 376-393.

Gilbert, D. and B. Pettigrew, 1997. Interannual variability (1948-1994) of the CIL core temperature in the Gulf of St. Lawrence. Can. J. Fish. Aquat. Sci., 54 (Suppl. 1): 57 - 67.

Gill, A.E., 1982. Atmosphere-Ocean Dynamics. Academic Press, Inc. 662pp, New York.

Hibler, W. D. III, 1979. A dynamic thermodynamics sea ice model. J. Phys. Oceanogr., 9: 815-846

Hibler, W. D. III, 1980. Modelling a variable thickness sea ice cover. Mon. Wea. Rev., 108: 1943-1973.

Hurrell, J.W. and H. Van Loon, 1997. Decadal variations in climate associated with the North Atlantic Oscillation. Climate Change 36: 301-326.

Ingram, R.G., J. Wang, C. Lin, L. Legendre, and L. Fortier, 1996. Impact of fresh water on a subarctic coastal ecosystem under seasonal sea ice (southeastern Hudson Bay, Canada). I. Interannual variability and predicted global warming influence on river plume dynamics and sea ice. Journal of Marine Systems, 7: 221-231.

Kalnay, E., et al., 1996. The NCEP/NCAR 40-year reanalysis project. Bulletin of the American Meteorological Society, 77(3): 437-471.

Koutitonsky, V.G. and G.L. Bugden, 1991. The physical oceanography of the Gulf of St. Lawrence: A review with emphasis on the synoptic variability of the motion. In J.C. Therriault [ed]: The Gulf of St. Lawrence: small ocean or big estuary? Can. Spec. Publ. Fish. Aquat. Sci. 113: 57-90.

Lauzier, L. 1957. The St. Lawrence spring run-off and summer salinities in the Magdalen Shallows. Bull. Fish. Res. Board Can. 111: 193-194.

Manak, D.K. and L.A. Mysak, 1989. On the relationship between Arctic sea ice anomalies and fluctuations in northern Canadian air temperature and river discharge. Atmosphere-Ocean 27:682-691.

Mann, M.E. and J.M. Lees, 1996. Robust estimation of background noise and signal detection in climate time series. Climatic Change 33: 409-445.

Markham, W.E., 1973. Ice conditions during severe winters in the Gulf of St. Lawrence, p. 56-72. In M. I. EL-SABH [ed.] Proceedings of Workshop on Physical Sciences in the Gulf and Estuary of St. Lawrence. 11-12 October 1973, Université du Québec à Rimouski, Rimouski, Québec.

Matheson, K.M., 1967. The meteorological effect on ice in the Gulf of St. Lawrence. Publ. In Meteorology No. 110, McGill University, Montreal, 107p.

McPhee, M., 1975. Ice-ocean momentum transfer for the AIDJEX ice model. AIDJEX Bull., 29: 93-111.

Mysak, L.A. and D.K. Manak, 1989. Arctic sea-ice extent and anomalies, 1953-1984. Atmosphere-Ocean, 27: 376-405.

Mysak, L.A., D.K. Manak and R.F. Marsden, 1990. Sea ice anomalies observed in the Greenland and Labrador Sea during 1901-1984 and their relation to an interdecadal Arctic climate cycle. Climate Dynamics, 5: 111-133.

Mysak, L.A. and S.B. Power, 1992. Sea-ice anomalies in the western Arctic and Greenland-Iceland Sea and their relation to an interdecadal cycle. Climatological Bulletin, 26: 147-176.

Mysak, L.A., R.G. Ingram, J. Wang, and A. van der Baaren, 1996. The anomalous sea-ice extent in Hudson Bay, Baffin Bay and the Labrador Sea during three simultaneous NAO and ENSO episodes. Atmosphere Ocean, 34(2): 313-343.

Petrie, B., 1990. Monthly means of temperature, salinity and sigma-t for the Gulf of St. Lawrence. Can. Tech. Rep. Hydrogr. Ocean Sci. 126, iv + 137 pp.

Power, S.B. and L.A. Mysak, 1992. On the interannual variability of Arctic sea-level pressure and sea ice. Atmosphere-Ocean, 30: 551-557.

Prinsenberg, S.J., I.K. Peterson, S. Narayanan, and J.U. Umoh, 1997. Interaction between atmosphere, ice cover, and ocean off Labrador and Newfoundland from 1962 to 1992. Canadian Journal of Fisheries and Aquatic Sciences, 54, Supplement 1: 30 -39.

Rogers, R. R., and M. K. Yau, 1989. A short course in cloud physics. Intl. Series in Natural Series, Pergamon Press, Oxford, 292pp.

Sciremammano, F., Jr., 1979. A suggestion for the presentation of correlations and their significance levels. Journal of Physical Oceanography, 9(11): 1273-1276.

Sinclair A. and L. Currie, 1994. Timing of cod migration into and out of the Gulf of St. Lawrence based on commercial fisheries, 1986-1993. DFO Atl. Fish. Res. Doc. 94/47.

Slonosky, V.C., L.A. Mysak, and J. Derome, 1997. Linking Arctic sea-ice and atmospheric circulation anomalies on interannual and decadal timescales. Atmosphere-Ocean, 35(3): 333-366.

Smith, W.H.F. and P. Wessel, 1990. Gridding with continuous curvature splines in tension. Geophysics, 55: 293-305.

Sowden, W.J. and F.E. Geddes, 1980. Weekly median and extreme ice edges for Eastern Canadian Seaboard and Hudson Bay. Unpublished manuscript. Ottawa, Ontario.

Sutcliffe, W.H. Jr., R.H. Loucks and K.F. Drinkwater. 1976. Coastal circulation and physical oceanography of the Scotian Shelf and the Gulf of Maine. Journal of the Fisheries Research Board of Canada 33: 98-115.

Thomson, D.J., 1982. Spectrum estimation and harmonic analysis. IEEE Proc. 70: 1055-1096.

Trites, R.W., 1972. The Gulf of St. Lawrence from a pollution point of view. P.59-72 in M. Ruivo [ed.] Marine Pollution and Sea Life. FAO, Fishing News Books, London.

Wallace, J.M., C. Smith, and C.S. Bretherton, 1992. Singular value decomposition of wintertime sea surface temperature and 500-mb height anomalies. Journal of Climate, 5: 561-576.

Walsh, J. and C.M. Johnson, 1979. An analysis of Arctic sea ice fluctuations, 1953-77. J. Phys. Oceanogr. 9: 580-590.

Wang, J., L.A. Mysak, and R.G. Ingram, 1994. Interannual variability of sea ice cover in Hudson Bay, Baffin Bay and the Labrador Sea. Atmosphere-Ocean, 32(2): 421-447.

Wessel, P. and W.H.F. Smith, 1991. Free software helps map and display data. EOS, 72: 441, 445-446.